

Some pages of this thesis may have been removed for copyright restrictions.

If you have discovered material in AURA which is unlawful e.g. breaches copyright, (either yours or that of a third party) or any other law, including but not limited to those relating to patent, trademark, confidentiality, data protection, obscenity, defamation, libel, then please read our [Takedown Policy](#) and [contact the service](#) immediately

SYNCHRONIZATION PROCESSES IN NONLINEAR SYSTEMS AND
THEIR RELATION TO CORTICAL OSCILLATORY DYNAMICS

AVGIS HADJIPAPAS

Doctor of Philosophy

ASTON UNIVERSITY

April 2005

This copy of the thesis has been supplied on condition that anyone who consults it is understood to recognise that its copyright rests with its author and that no quotation from the thesis and no information derived from it may be published without proper acknowledgement.

Aston University

SYNCHRONIZATION PROCESSES IN NONLINEAR SYSTEMS AND THEIR
RELATION TO CORTICAL OSCILLATORY DYNAMICS

Avgis Hadjipapas

Doctor of Philosophy

April 2005

This thesis was focussed on theoretical models of synchronization in relation to cortical dynamics as measured by magnetoencephalography (MEG). Dynamical systems theory was used in both identifying relevant variables for brain coordination and also in devising methods for their quantification. We presented a method for studying interactions of linear and chaotic neuronal sources using MEG beamforming techniques. We showed that such sources can be accurately reconstructed in terms of their location, temporal dynamics and possible interactions.

Synchronization in low-dimensional nonlinear systems was studied to explore specific correlates of functional integration and segregation. In the case of interacting dissimilar systems, relevant coordination phenomena involved generalized and phase synchronization, which were often intermittent. Spatially-extended systems were then studied. For locally-coupled dissimilar systems, as in the case of cortical columns, clustering behaviour occurred. Synchronized clusters emerged at different frequencies and their boundaries were marked through oscillation death. The macroscopic mean field revealed sharp spectral peaks at the frequencies of the clusters and broader spectral drops at their boundaries. These results question existing models of Event Related Synchronization and Desynchronization.

We re-examined the concept of the steady-state evoked response following an AM stimulus. We showed that very little variability in the AM following response could be accounted by system noise. We presented a methodology for detecting local and global nonlinear interactions from MEG data in order to account for residual variability. We found crosshemispheric nonlinear interactions of ongoing cortical rhythms concurrent with the stimulus and interactions of these rhythms with the following AM responses.

Finally, we hypothesized that holistic spatial stimuli would be accompanied by the emergence of clusters in primary visual cortex resulting in frequency-specific MEG oscillations. Indeed, we found different frequency distributions in induced gamma oscillations for different spatial stimuli, which was suggestive of temporal coding of these spatial stimuli. Further, we addressed the bursting character of these oscillations, which was suggestive of intermittent nonlinear dynamics. However, we did not observe the characteristic $-3/2$ power-law scaling in the distribution of interburst intervals. Further, this distribution was only seldom significantly different to the one obtained in surrogate data, where possible nonlinear structure was destroyed.

In conclusion, the work presented in this thesis suggests that advances in dynamical systems theory in conjunction with developments in magnetoencephalography may facilitate a mapping between levels of description in the brain. This may potentially represent a major advancement in neuroscience.

KEYWORDS: Magnetoencephalography (MEG); dynamical systems theory; chaotic synchronization; intermittency; Event-Related Synchronization (ERS) and Desynchronization(ERD);

Dedication
This thesis is dedicated
to my parents Christos and Vassilka,
and to my sister Sofia

Acknowledgement

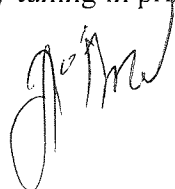
The work presented in this thesis was carried out by the author. Nevertheless, the following people from the MEG lab have contributed to the work presented in this thesis in terms of collaborative work with the author:

Chapter 2. Special thanks to Dr Arjan Hillebrand for providing the software for the forward source model, which was used as a part of the simulations presented and for valuable discussions on beamformer methodology. I want to thank Dr Ian Holliday, Dr. Krish Singh, Dr. Arjan Hillebrand and Dr. Gareth Barnes for helpful discussions.

Chapter 5. Special thanks to Dr. Michael Simpson, who collected the experimental MEG data and performed the dipole reconstructions. These data ultimately stimulated the development of the methods presented in this chapter. Also thank you Michael for your help (and your patience) with the implementation of these methods to the experimental data. Also, I want to thank both Dr. Caroline Witton and Dr. Michael Simpson for valuable discussions on auditory processing and for introducing me in the dark secrets of the auditory steady state response.

Chapters 6 and 7. Special thanks must go to Dr. Peyman Adjamian, who collected the experimental MEG data and performed the source reconstructions and time frequency analyses, from which the work presented in these chapters was inspired. Also, thank you Peyman for helpful discussions on the neural correlates of spatial frequency tuning in primary visual cortex.

Signed:



Supervisor:



Date: 03.08.2019

I have received many sources of support and assistance during my PhD at Aston. I want to particularly thank my supervisor, Dr. Gareth Barnes for his guidance and for his generosity to devote so much time and effort to provide valuable feedback, advice, unwavering encouragement and motivation throughout the years of my PhD.

Finally, I want to especially thank Dr. Ian Holliday, Dr. Krish Singh, Dr. Georgina Rippon and Dr. Gareth Barnes for their precious help with obtaining funding for my PhD, their unlimited academic and personal support throughout the years at Aston, their faith in me and my work and ultimately for providing me the opportunity to carry out the research presented in this thesis.

Table of Contents

Title page: ‘Synchronization Processes In Nonlinear Systems And Their Relation To Cortical Oscillatory Dynamics’	1
Thesis summary	2
Dedication	3
Acknowledgement	4
Table of contents	5-7
Figures and tables	8-10
Chapter 1. Theoretical frameworks for the binding problem and related coordination phenomena in the brain	11
1.1 Prologue.	11
1.2 The binding by convergence approach.	11
1.3 Dynamic binding and the temporal correlation hypothesis.	14
1.4 Beyond temporal correlation: metastability and coordination dynamics in complex nonlinear systems.	16
1.5 The need for a general framework of brain function	25
Chapter 2: Assessing interactions of linear and nonlinear neuronal sources using MEG beamformers	27
2.1 Background.....	27
2.2 Methods.....	29
2.2.1 Simulation of transiently correlated sources.....	29
2.2.2 Adaptive beamformer techniques.....	29
2.2.3 Measures of temporal performance of the beamformer.....	32
2.2.4 Reconstruction accuracy of source interactions.....	33
2.2.5 Measures of signal interdependency.....	33
2.2.5.1 Coherence estimation.....	34
2.2.5.2 Phase synchronization analysis.....	34
2.2.5.3 Assessment of event-related changes in measures of signal interdependency.....	36
2.2.6 Simulation of interacting nonlinear oscillators.....	37
2.3. Results.....	38
2.3.1 Spatiotemporal performance of the beamformer in the presence of correlated source activity.....	38
2.3.2 Reconstruction accuracy of simulated source interactions.....	43
2.3.3 Reconstruction of signal interdependencies by the beamformer.....	43
2.3.4 Reconstruction of interacting Rössler systems and their interdependence.....	45
2.4 Discussion.....	48

Chapter 3: Synchronization dynamics in low dimensional nonlinear systems.	52
3.1. Why study cortical synchronization and related oscillatory phenomena?	52
3.2 Why study synchronization in abstract models of nonlinear systems?	57
3.3 Chaos theory	59
3.3.1 Basic geometric concepts	59
3.3.2 Bifurcations and phase transitions	63
3.3.3 Periodic Vs Chaotic oscillations	65
3.4 Synchronization of mutually interacting chaotic oscillators	66
3.4.1 Phase and Frequency of a chaotic oscillator	66
3.4.2 Synchronization of chaotic systems	71
3.4.3 Symmetry condition: Synchronization of identical systems	71
3.4.3 Breaking the symmetry: Phase, lag and generalized synchronization of nonidentical systems.	79
3.4.4 Succession of qualitatively different synchronization regimes with increasing coupling	90
3.4.5 Chaos destroying synchronization and structural changes in attractor morphology	92
3.5 Concluding remarks	93
Chapter 4. Event Related Synchronization and Desynchronization and their relation to macroscopic spatiotemporal patterns in complex systems.	95
4.1. Objectives	95
4.2 Basic axioms of synergetics and pattern forming systems	95
4.3. The brain as a multiscale system	96
4.3.1 Microscopic and mesoscopic levels of description and network control parameters	97
4.3.2 Microscopic level: Mean field coupled network of nearly identical oscillators	100
4.3.3 Mesoscopic level: Locally coupled networks of nonidentical oscillators	107
4.4 Discussion	115
Chapter 5: Quantifying local and global nonlinear neural interactions from magnetoencephalographic data: application to an auditory AM task.	120
5.1 Background and rationale	120
5.2 Methods	121
5.2.1 Experimental Design	121
5.2.2. Recordings, Dipole Analysis	122
5.2.3 Time frequency analyses	122
5.2.4 Detection of signal interdependencies using the Hilbert transform	123
5.2.5 Detection of phase synchronization	124
5.2.6 Detection of interdependencies between instantaneous amplitudes.	127
5.2.7 Envelope versus phase interdependence	127
5.2.8. Detection of nonlinearity in signal interdependencies using surrogate data	128
5.2.9 Statistical comparison of signal interaction metrics between observed and surrogate data	129
5.2.10 Quantifying nonlinear interactions of envelope and phase dynamics in simulated datasets	130

5.3 Results.....	133
5.3.1 Results of dipole analysis for the time averaged AM following response.	133
5.3.2 Time-frequency analysis of the response to an AM stimulus and interhemispheric phase synchronization of the responses at the frequency of the stimulus.....	133
5.3.3. Quantifying the variance of instantaneous envelopes in the AM following response.....	136
5.3.4. Detection of local and global nonlinear interactions in continuous phase and envelope dynamics	138
5.3.4.1 Interactions of following AM response with ongoing rhythms in the same hemisphere.....	138
5.3.4.2 Interactions of following AM response with ongoing rhythms in the contralateral hemisphere.....	140
5.3.4.3 Interhemispheric interactions between ongoing rhythms in the same frequency range. .	142
5.4 Discussion.....	145
Chapter 6: The functional role of gamma oscillations in sensory coding- A complex systems approach.	150
6.1 Background and objectives	150
6.2 Methods.....	151
6.2.1 Subjects/Materials and Experimental procedures.....	151
6.2.2 Recordings	151
6.2.3 Source Reconstruction	152
6.2.4 Analysis of the frequency response in the primary visual cortex.....	152
6.2.4.1 Induced response.....	152
6.3 Results and Discussion	153
Chapter7.Quantitative investigation of the bursting behaviour of visually induced gamma oscillations.....	158
7.1 Rationale	158
7.2 On-off intermittency: phenomenology and quantification in abstract model systems	159
7.3 Detection of deterministic bursting in noisy magnetoencephalographic data	164
7.4 Statistical comparisons between distributions of interburst intervals in the real and surrogate data	170
7.5 Results of statistical testing and discussion	171
Chapter 8. Synopsis and general conclusions.....	175
8.1 Synopsis.....	175
8.2 General conclusions and implications	183
References.....	185-199
Appendix 1: Linear stability analysis and Lyapunov exponents.....	200-205

Figures and tables

Chapter 1

Figure 1. Schematic representation of the ‘binding by convergence’ approach.....	12
Figure 2. The Lorenz attractor	17

Chapter 2

Figure 1. Parameterisation of transient source correlation	31
Figure 2. Localization of the transiently correlated sources by the beamformer.....	39
Table 1. Coordinates of simulated sources and estimated source location.	39
Figure 3. Temporal performance of the beamformer in the presence of transient source correlation.	40
Figure 4. Reliability measure of the beamformer as a function of the relative duration of correlated source activity with respect to the length of the covariance time window	41
Figure 5. Relative Difference Measure as a function of the relative duration of transient source correlation with respect to the total duration of the covariance time window	42
Figure 6. Relative difference measures of the interaction measures as a function of the relative duration of source correlation with respect to the length of the covariance time window.....	42
Figure 7. Significant coherence and phase synchrony changes of the virtual electrodes	43
Figure 8. Detection of possible high order $n:m$ synchronization.	44
Figure 9A. Direct solutions of the integration of the Rössler systems	45
Figure 9B. Average wavelet time–frequency plots for the virtual electrodes time series corresponding to the two systems.	46
Figure 9C: The results of the cross frequency phase synchrony analysis of the two virtual electrode time series corresponding to the two Rössler systems	47

Chapter 3

Figure 1. Basins of attraction.....	60
Figure 2. Fixed (equilibrium) points in a 2-D state space.....	61
Figure 3. Nonchaotic attractors in 0, 1 and 2-D.....	62
Figure 4. The Rössler strange attractor described in equation [1].....	63
Figure 5. The bifurcation diagram of the logistic map.	64
Figure 6. Periodic (A and C) and chaotic (B and D) oscillations.	66
Figure 7. Schematic representation of the motion of an autonomous harmonic oscillator in polar coordinates.	68
Figure 8. (from Breakspear, 2004). Schematic representation of tangential and transverse dynamics	74
Figure 9. Almost identical synchronization in linearly coupled identical Rössler systems.....	76
Figure 10. State space portrait of coupled systems in almost identical synchronization shown in figure 9.....	76
Figure 11. Modulational intermittency before the transition to identical synchronization.....	78

Figure 12. The state space portrait of the two coupled systems in intermittent identical synchronization shown in figure 11.....	79
Figure 13. Nonidentical coupled systems possibly exhibiting generalized synchronization.....	81
Figure 14. State space portrait of the coupled systems plotted in figure 13.	83
Figure 15. Phase synchronization of nonidentical chaotic systems for low coupling strengths....	84
Figure 16. State space portrait of phase synchronized nonidentical systems plotted in figure 15.....	85
Figure 17. Intermittent dynamics in strongly coupled nonidentical systems.....	88
Figure 18. State space portrait of coupled systems exhibiting intermittent phase dynamics plotted in figure 17.....	89
Figure 19. Chaos destroying synchronization.....	93

Chapter 4

Figure 1. Schematic representation of the two levels of network descriptions that contribute to the generation of macroscopic signals.....	99
Figure 2. Power Vs time pattern across the array of ten mean-field coupled oscillators.	101
Figure 3. Interaction matrices for the array plotted in figure 2.	102
Figure 4. Power spectra of the individual units of the array shown in figure 2 for the precoupling and coupling time.....	103
Figure 5. Mean field signal of the integration of the system shown in figure 2.....	106
Figure 6. Lattice of locally coupled Rössler oscillators with a linear frequency detuning.	108
Figure 7. Interaction matrices for the lattice shown in figure 6.....	109
Figure 9. Effective interaction between lattice elements 1 and 3.	110
Figure 10. Interaction of lattice elements 4 and 5.	111
Figure 11. Power spectra of the χ variables of the individual units in the lattice of locally coupled oscillators.....	113
Figure 12. Mean field signal of the lattice of coupled oscillators.	114

Chapter 5

Figure 1. Quantification of nonlinear phase synchronization.....	131
Figure 2. Quantification of nonlinear envelope interactions.	132
Figure 3. Spatiotemporal dipoles for participant JS.	134
Figure 4. Non time-averaged narrow band filtered (30-34 Hz) AM following responses in each hemisphere for diotic and dichotic AM condition.	134
Figure 5. Distributions of relative phase differences between the responses in Figure 4.	135
Figure 6. Time frequency analysis (participant JS) in a virtual electrode at the source of the AM following response.....	135
Figure 7. Epochwise standard deviations of instantaneous envelopes in 30-34 Hz narrow band filtered signals for the two spatiotemporal dipoles for participant IEH and system noise.	137
Figure 8. Results for the interaction between the instantaneous envelopes between the AM following response and the ongoing rhythms in the right dipole time series, participant IEH....	138
Figure 9. Summary of results for the interaction of the left following AM response (30-34Hz) with ongoing rhythms in the same dipole for two participants.....	140

Figure 11. Nonlinear, crosshemispheric, n:m phase synchronization between the AM following response and ongoing rhythms in the contralateral hemisphere.....142

Figure 12. Summary results for crosshemispheric envelope interactions in the same frequency for all participants143

Figure 13. Significant cross-hemispheric interactions in the envelope dynamics of the ongoing beta rhythms during the presentation of the AM stimulus.144

Figure 14. Participant KDS. Summary of interhemispheric phase synchronization analysis.145

Chapter 6

Figure 1. Example of induced oscillatory change of the signal arising from the SPM peak voxel located in primary visual cortex (V1) for one subject at 3 c.p.d.153

Figure 2. Adapted from Adjamian et al, 2004a. Group-average magnitude of oscillatory power in primary visual cortex as a function of stimulus SF and cortical response frequency. .154

Figure 3. Stimulus-related changes in the spectral distribution as a function of temporal frequency for 0.5, 3, and 6 c.p.d. patterns.155

Figure 4. Significant differences between stimulus-related changes in the gamma frequency range (30-60 Hz) for 3 subjects for the induced and evoked response.156

Chapter 7

Figure 1. Adapted from Adjamian et al., 2004a. Wavelet time–frequency analysis of the activity in the SPM maximum located in primary visual cortex (participant SW).158

Figure 2. Adapted from Zhan, Wei, and Lai, 2002. Intermittent lag synchronization of coupled nonidentical Rössler systems, the coupling parameter is below the threshold for onset of lag synchronization.162

Figure 3. Adapted from Zhan, Wei, and Lai, 2002. Lag synchronization of coupled nonidentical Rössler systems, the coupling parameter is above the threshold for onset of lag synchronization.162

Figure 4. The top panel shows the band pass filtered time series of the SPM peak voxel located in the primary visual cortex for participant F.M after the appearance of a 3 c.p.d pattern at time 0.165

Figure 5. The data in figure 4 were rectified by taking the absolute values.165

Figure 6. The rectified data in figure 5 were transformed to z-scores and thresholded at $z > 3$. .165

Figure 7. Distributions of gamma interburst intervals pooled over all experimental trials for participant F.M. viewing a 3 c.p.d. grating.167

Figure 8. Log-log plots of the PDF's (probability density function) Vs the duration of interburst intervals for participant KDS and a 3 c.p.d. stimulus.169

Table 1. Results of the chi-square statistical analysis for all stimuli conditions and all participants.172

Figure 9. Results of chi-squared test between the real distribution of laminar phases and the distribution in surrogate data for participant F.M viewing a 3 c.p.d. stimulus.173

Chapter 1. Theoretical frameworks for the binding problem and related coordination phenomena in the brain.

1.1 Prologue.

Maybe the foremost challenge for contemporary neuroscience rests in the integration of findings coming from different levels of description within the brain and especially the neuronal, the network and the systems level. The integration of experimental findings from distinct subdisciplines such as single and multi unit electrophysiology, metabolic and neuroelectric neuroimaging techniques crucially depends on a generic theory of brain function, which has to account for the communication between levels of description. In the past two decades or so, this problem has been central to many subfields in neuroscience and a lot of effort has been put into integrating current knowledge into theoretical frameworks. Next, the most prominent of these frameworks will be introduced and discussed in the context of the binding problem and the general issue of coordinated brain activity.

1.2 The binding by convergence approach.

One of the key problems in contemporary neuroscience is how local sensory information corresponding to distinct stimulus features is integrated into a global coherent percept. Extensive research in the last century has argued the case of 'local' and 'modular' neuronal processing. This refers to strictly localized neurons, which seem to respond to specific stimulus characteristics preferentially; hence they are reactive to a specific range of stimulus parameters. The latter properties are commonly known as receptive fields and these are thought to be the fundamental functional units in sensory processing. This has been particularly observed for the early stages of the visual system, especially the primary visual cortex, (see the classical work of Hubel and Wiesel, for instance Hubel and Wiesel, 1962, 1968, 1972, Hubel 1982). Using mostly methodologies related to single cell electrophysiology, orientation (Hubel and Wiesel, 1968), direction (DeValois *et al.*, 1982, Livingstone, 1998) and even spatial frequency (Albrecht *et al.*, 1982, Foster *et al.*, 1985) 'selective' neurons have been found. The apparent 'modular' processing mode of these neurons was attributed to specific cellular properties or to specific input of these neurons and thus the somatotopically-organized pattern of afferent pathways. The idea of an ever-increasing degree of convergence of specific afferents into more and more specialized neurons has led to the formulation of the single cell doctrine. Followers of this doctrine have claimed that this mechanism of convergence is iterated many times in a perceptual system that exploits a serial processing hierarchy (for instance Felleman and Van Essen, 1991). Hence the neurons at the top of the hierarchy would receive highly specific afferents and would only

respond to a highly specific stimulus, such as one's grandmother (see figure 1). This idea of specifically tuned neurons has been meanwhile expanded to much higher levels of cognitive processing and hence to almost any area of brain function such as object (e.g. Kobatake and Tanaka, 1994) and face recognition (e.g Perret , Rolls and Caan, 1982) and even working memory (for a review see Goldman-Rakic, 1995).

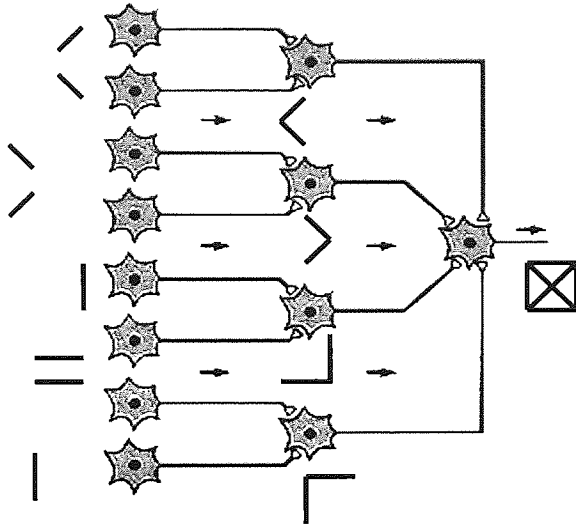


Figure 1. Schematic representation of the 'binding by convergence' approach. Many 'low-level', neurons with specific response properties, converge on a fewer 'higher' level neurons, which respond only to a certain combination of features. Note that the processing stream is strictly serial, feed forward and there are no connections between processing levels.

Immediately an obvious processing problem becomes apparent. If specific and thus distributed neurons (or even brain areas) respond to specific stimulus features, how does this information get integrated into a coherent pattern or percept? This is the core of what is referred to as the binding problem (von der Malsburg, 1981 and 1999, Singer, 1999 and 2001). This problem of course is not specific to the visual system. Similar problems arise not only in all other sensory systems but also in the motor system, where several muscle groups have to be coordinated to produce a coherent movement. At a higher level of processing, such as multisensory perception, cognition or sensorimotor coordination for example, this problem is even more apparent: sensory systems can code for several stimuli or stimulus characteristics simultaneously. The integration of this information practically means a disambiguation of these distinct codes, which has to occur rapidly so that action can be taken. The latter also entails that the sensory and motor codes have to be integrated, so that smooth and coherent sensorimotor behavior can be generated. However, these multimodal sensory and motor representations seem to be spatially distributed and have highly distinctive and specific response patterns. How can this information be integrated? The answer that the binding by convergence approach provides, is that there will always be a more specialized processing unit; call it a neuron or an area, where all this information will converge. This leads us to the idea of the central processor, an entity that combines all the pieces of

information and makes 'sense' of it. This argument reduces to another version of the older 'Cartesian Theatre' notion, where the sensory systems deliver a performance to a central 'homunculus' structure, which is the centre of the mind, or the 'seat of the soul' (Descartes, 1644).

There are further conceptual difficulties with the implementation of this approach. One major disadvantage is the difficulty of dealing with new representations and thus learning. The acquisition of a new concept automatically implies the possible combinations with all other already preexistent concepts. For example, as a child grows and acquires new concepts, the amount of representations would grow exponentially because of a combinatorial explosion. A modular representation mode is also not efficient in terms of information processing; huge problems arise when attempting to represent the degree of similarity or difference among such distributed informational items or for constructing new concepts from separated items of information. (Wickelgren, 1999)

Several empirical facts about the brain are also quite difficult to reconcile with the binding by convergence approach. For instance, there are about 10^{16} connections in a human brain (as opposed only 10^{11} neurons), that have a very specific multilevel spatial structure (see chapter 4). What is more, quantitative anatomical connectivity studies in the macaque have shown that there are about as many feedback as feed forward connections (Koetter and Stephan, 2003). This strongly questions models of serial and convergent processing. The huge amount of connections and the sophistication in the connectivity patterns strongly supports a very different view of the brain, namely that of a recurrent, distributed network.

Indeed, single cell studies have demonstrated a non-modular response properties and thus neurons that respond to several stimuli or stimuli combinations (see Sakurai, 1999 and references therein). This is consistent with the notion of overlapping receptive fields or possibly sparse coding (Wickelgren, 1999, Sakurai 1999) that are ubiquitous in the mammalian brain (Young and Yamane, 1992, Földiák, and Young, 1995, Rolls and Tovee, 1995).

The composition of the previous observations and conceptual arguments leads to the conclusion that the functional units of information processing in the brain, the receptive fields are very likely to reflect dynamic population codes (Sakurai, 1999) rather than isolated single neuron codes. Thus the receptive fields can be viewed as emergent network properties rather than deterministic properties of a hard-wired serial network hierarchy. Several processing

advantages arise through adoption of this notion of network representation (Wickelgren, 1999 and Sakurai, 1999). The next two sections will consider two such approaches.

1.3 Dynamic binding and the temporal correlation hypothesis.

This section, an approach to feature binding often referred to as the temporal correlation hypothesis will be discussed. This framework was first proposed by von der Malsburg (von der Malsburg, 1981 and 1999) and then operationalized by Wolf Singer's group. Singer (1999, 2001) proposes some kind of dynamic binding that involves processes of neuronal synchronization. He suggests that 'synchronicity serves as a tag of relatedness most likely because it causes a joint increase of the saliency of the synchronized responses, which in turn favours their joint evaluation (binding) at subsequent processing stages.' Two complementary binding mechanisms are proposed, which are sequentially iterated in a multistage processing system. Salient feature conjunctions corresponding to common stimulus features are implemented by specific 'conjunction' units and less ordinary, novel or contextual information is coded by dynamic grouping of the responses of distributed (feature detecting) neurons by means of spike synchronization. It is important to note, that the grouping criteria are specific to the level of processing. For early processing stages such as early vision they could just adhere to simple principles, such as co linearity or continuity of contours, at higher levels of processing the criteria can become more abstract, such as symmetry or pattern coherence for instance. This claim rests on two fundamental empirical observations about neuronal synchronization: the universal nature and the temporal precision of synchronous neuronal discharge and the greater sensitivity of neuronal mechanisms to synchronous as opposed to asynchronous input. The dynamic assembly 'code', which is dependent on processing level specific grouping criteria, enhances the probability of *joint* processing of the outputs of the synchronized neurons at *subsequent* levels of processing. At a next level of processing either a specific 'conjunction' unit or further dynamic grouping takes place in order to disambiguate these dynamic codes. The (perceptual or cognitive) grouping criteria, according to which neurons get to be dynamically bound, become more abstract, as one goes further up in the processing hierarchy. Dynamic grouping is especially advantageous when *distributed* representations have to be mapped on one another. This is particularly important in sensorimotor coordination. If these distributed representations are formed by synchronous discharges in both the sensory and the motor processing stream, a bottleneck problem can be easily circumvented, since these representations use the same format of 'code'.

At the microscopic neuronal level, there is meanwhile considerable evidence for the coding of global stimulus features in terms of consistent interneuronal timing rather than modulation of

the neuronal rate coding (Singer and Gray, 1995, Roelfsema *et al.*, 1997, Singer, 1999, Singer, 2001, Engel and Singer, 2001). That is, neurons tend to exhibit synchronized responses when coding for the same stimulus or holistic stimulus feature.

Stimulus or task specific synchronization processes could be also shown at higher levels of description of cortical networks (Varela *et al.*, 2001). There is meanwhile also considerable evidence for synchronization subserving *large-scale integration* in the form of transient and task-specific interactions between brain areas during various perceptual and cognitive tasks (Sarnthein *et al.*, 1998, Rodriguez *et al.*, 1999, Tallon-Baudry and Bertrand, 1999, review in Varela *et al.*, 2001).

Although, the temporal correlation approach is clearly more advantageous than the classical notion of 'binding by convergence', there are several problems and unclarified aspects in this theoretical framework. First of all, Singer's main argumentation concentrates on the idea that synchronization may help increase the salience of responses at a *subsequent* level of processing. This assumes that in every processing instance a multilevel process *has* to take place, even for simple stimuli. Most importantly, this approach does not explain what the actual *neuronal substrate* of this information processing might be. Saying that synchronized responses are more likely to be grouped at a subsequent level of processing does not solve this problem; it essentially postpones it until the next level of processing, which may eventually be more appropriate for the coding of a certain stimulus. The question that arises then is a very central one, not only to neuroscience but also to any science that deals with complex, multilevel systems. How can we tell, which level of processing is the most appropriate in a given experimental situation?

Most importantly, this framework does not include any description of the temporal or spatial dynamics of these synchronization processes and thus the dynamics of the putative representations. Thus, such an approach does not exploit the advantages of the population or network codes (see Sakurai, 1999). However, it is exactly the dynamic properties of population codes that underpin the adaptive and context sensitive nature of perception and cognition.

Finally, temporal correlations and especially long-term and stable correlations are not particularly efficient in terms of information theory (Friston, 2000a). This is purely because of poor and inflexible information transfer. However, transient and dynamic correlations are efficient and can be context sensitive. Thus, there is the additional possibility of coding of

some stimulus feature at the same processing stage. This 'code' can be implemented in terms of a collective but specific global network state (for example Freeman, 1992) such as a distributed cell assembly code. This state would result from a stimulus specific reorganization of the pattern of interactions in a given neuronal network. These global states are multidimensional and can exhibit complex spatial and temporal dynamics. Such transient network states can be sufficiently complex 'informational' entities in their own right, so that a 'next' level of processing may not be required.

The main value of Singer's approach lies perhaps not in a detailed account of the mechanisms underlying information processing but in the important general insight, that the stress in contemporary neuroscience should be placed on *collective and dynamical* neuronal behaviour rather than on specific and rigid properties of single neurons.

1.4 Beyond temporal correlation: metastability and coordination dynamics in complex nonlinear systems.

This theoretical framework is largely based on dynamical systems and deterministic chaos theory. In this section, solely the main concepts will be illustrated in a geometrical qualitative fashion. Furthermore, specific arguments in support of the validity of this approach as a framework for brain function and thus considering the brain as a complex nonlinear system will be provided in chapters 3 and 4. As in all novel theoretical frameworks, there is still a lack of consistency in the nomenclature and significant confusion may arise through the use of related but distinct concepts and a battery of interrelated terms. Often a single term is associated with somewhat different meanings and regularly different terms are used to refer to the same concept. This requires some clarifications, which will be briefly undertaken in this section.

The most fundamental concept therein is maybe the one of *state space* (see figure 2 for an illustration of the Lorenz attractor). The dimensionality of the state space is defined by the variables indispensable for the description of the system, also referred to as degrees of freedom or state variables. For a given set of initial conditions (for each one of the state variables), the system is said to follow a trajectory in the M multidimensional state space. An *attractor* is a subpartition of the state space where a lot of such trajectories will eventually *converge to* if the system evolves for a sufficiently long time. One core characteristic of chaotic system is the sensitivity to initial conditions. Thus different initial conditions may give rise to different long-term behaviour. The set of initial conditions that gives rise to a certain attractor (and thus a certain pattern of system dynamics) are referred to as *basins of attraction*. The geometric representation of an attractor also gives an intuitive impression

about the effective dimensionality of the system, which just corresponds to the geometric dimensionality of the manifold. Chaotic systems (see chapter 3), display complex geometric shapes that exhibit *fractal* (non integer) *dimensionality*, and are often referred to as *strange attractors*. The geometrical (hyper) surface of such an attractor is often referred to as the *manifold*. Possible subdivisions of the manifold are referred to as attractor wings or submanifolds. The parameters that govern the dynamics of the evolution of the state variables are called *control parameters*. Critical qualitative changes in system behaviour as such a control parameter is varied occur through *bifurcations*, which result in a change in the stability of the current system dynamics and thus give rise to qualitatively different system behaviour. This can be conceptualised geometrically as an abrupt change from one basin of attraction to another, giving rise to qualitatively different long-term behaviour (different state space attractors). These abrupt changes in system dynamics are called phase or state transitions and are per definition bound to a *slow* change of the control parameters.

However, it must be stressed that changes in system dynamics are not necessarily bound to changes in the control parameters. From Figure 2 it is easy to see that the system may occupy different wings of the attractor manifold and ‘switch’ between them even *without* any changes in the control parameters. This apparent ‘switching’ behaviour is referred to as *chaotic intermittency* (Manneville and Pomeau, 1979). In geometrically more complex manifolds that include many subpartitions a restless wandering of the system between these attractor wings is referred to as *itinerancy* (Tsuda, 1991, Kaneko and Tsuda, 2003, Tsuda and Umemura, 2003). Using this geometrical representation of dynamics, it is easy to conceptualise that such complex manifolds can pertain to interacting subsystems of a more global system.

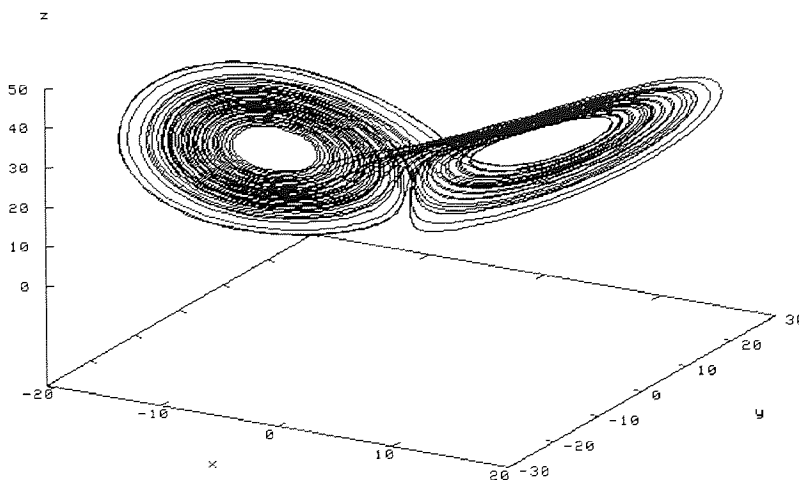


Figure 2. The Lorenz attractor is defined by a system of 3 coupled ordinary differential equations, describing the evolution of the x,y and z variables in time:

$$\begin{aligned} dx/dt &= \sigma(y-x) \\ dy/dt &= \rho x - y - xz \\ dz/dt &= \alpha y - \beta z \end{aligned}$$

where x,y, z are the state variables and sigma, rho and beta are the control parameters.

After the system has evolved for a sufficiently long time (transients are outlived) it tends to confine itself in a certain subpartition of the state space, called the attractor. The geometrical structure of the dynamics is often referred to as manifold. One can clearly see a subdivision of this manifold in two subpartitions. These are usually referred to as attractor wings or sub manifolds.

Overall, the dynamical approach views the brain as a complex multiscale system and considers brain function to be the product of a large assembly of coupled nonlinear dynamical subcomponents exhibiting transient and unstable coordination dynamics (Kelso, 1995, Friston, 2000b, Bressler and Kelso, 2001). From this perspective the brain is in an unstable (often referred to as metastable) regime due to the struggle of forces mediating *functional integration* on one hand and *functional segregation* of inputs on the other (Friston, 1997, Friston, 2000c, Bressler and Kelso, 2001). The former refers to a high degree of integration in the system with information exchange between subcomponents. This is characterized by high interdependency between so-called, *collective variables*; these are the relevant observables that capture the dynamics of the coordination between system subcomponents (Kelso, 1995, Bressler and Kelso, 2001). Such a collective variable can be for example the phase difference between two system subcomponents, as we shall see in greater detail and specific model systems in chapters 3 and 4, so that phase synchronization is the relevant mode of interaction. The other extreme case of coordination dynamics is functional segregation and thus low interdependency between system subcomponents and autonomous or self-sustained behaviour.

Because of the huge amount of different nomenclature in the literature and the often very different meanings attributed to the terms 'complexity' and 'metastability' and a significant conceptual overlap of these notions a short clarification of these notions is in place.

It must be stressed that both metastability and complexity refer to the same underlying dynamical state of affairs, namely a spatially extended dynamical system that 'lives' near a subtle balance between functional integration and functional segregation, but still they reflect different aspects of it. Metastability often appears in the framework of deterministic chaos and refers to a dynamic instability leading to what appears to be erratic switching between qualitatively different system behaviours, whereas complexity often appears in the context of information theory and refers to a composite emergent spatial pattern of the interactions between system subpartitions.

A first account of complexity is motivated from information theory. Complexity is defined as a compromise state of affairs, which lies between integration and segregation (Tononi, Sporns and Edelman, 1994 and 1996, Sporns and Tononi, 2002). Complexity is attributed to an underlying sparseness of connections between subcomponents in a system (Sporns and Tononi, 2002). A highly interconnected system, exhibits high degrees of integration and thus strong interdependency between system subcomponents but no local specificity. On the other hand a very poorly connected system exhibits locally specific behaviour but very little integration and thus weak interdependency between system subcomponents. A sparsely connected system on the other hand is somewhere in the middle of these two cases and exhibits specific patterns of integration and segregation. The emergent entities of specific integration are defined as the subset of elements that exhibit stronger mutual interactions than with the rest of the system elements. Tononi, Sporns and Edelman have proposed a quantification of this type of complexity, which essentially is a multivariate generalization of mutual information (Tononi, Sporns and Edelman, 1996). According to this notion, complexity is the emergent formation of specific spatial subgroupings of elements, to subserve diverse functions; therefore these are referred to as *functional clusters*. Complexity is a measure of this emergent *spatial* clustering behaviour. According to Sporns and Tononi 2002: 'Complexity captures the extent to which a system is both functionally segregated (small subsets of the system tend to behave independently) and functionally integrated (large subsets tend to behave coherently)'. Complexity can be quantified as the difference of two terms: the sum of the shared information between each individual element and the rest of the system minus the total amount of integration. Thus, complexity is greater if single elements are highly informative about the system to which they belong, while not being excessively similar.

The subtle and inherently unstable equilibrium arising in the struggle between those forces of integration and segregation can be approached from a different dynamic point of view, namely its stability (linear stability analysis in deterministic chaos theory, see Appendix 1). The term metastability as originally introduced in the field of neuroscience by the work of Scott Kelso (see for instance Kelso, 1995) refers to a situation where *global states of coordination* are not perfectly stable (and thus do not form an attractor in state space) but there is a tendency for the system to remain in a particular 'neighbourhood' of the state space. The notion of metastability is very much related to *chaotic intermittency* (see Manneville and Pomeau, 1979) and *itinerancy* (Kaneko 1990, Tsuda, 1991, Kaneko and Tsuda, 2003, Tsuda and Umemura, 2003) and more specific examples would be given throughout this work. As

we shall see later on, the term intermittency usually refers to *local* long-term dynamics with switching between (often) no more than two possible dynamic states whereas itinerancy refers to intermittent *global* dynamics with partial attraction to specific neighbourhoods, causing a restless wondering of the system from one subpartition of the state space to the next one. The quintessence of metastability is that there is a certain attraction to a stable state of coordination so that the system spends a lot of time in the neighbourhood of these stable states. However unexpectedly (and *without* change in the underlying control parameters) and in irregular intervals the system leaves the particular state of coordination to switch to a different state (often to a different neighbourhood in state space). Abrupt state transitions leading to *qualitatively* different *global* behaviour are common in such a dynamical scenario and can contribute significantly to a flexible and context sensitive information coding (Friston 1997 and 2000b, Bressler and Kelso 2001). Friston refers to this state of affairs as Type II complexity (Friston 2000b) in order to contrast it to Type I Complexity. The latter refers to complex behaviour that occurs *locally* in a distributed system. Such behaviour can be captured for example by analysis of a univariate time series of a relevant observable (e.g. one EEG electrode trace). Type II complexity refers to a situation where *global states of coordination* are not perfectly stable (and thus do not form an attractor in state space) but there is a tendency for the system to remain in a particular 'neighbourhood' of the state space. The term Type II complexity can thus be used interchangeably with the term metastability.

Nevertheless, as Friston himself remarks, the distinction between Type I and II complexity is predominantly a question of scale (Friston 2000b). Intermittency and thus dynamic instability can arise in a local system (or subsystem), when its control parameters are *static*. However, if the same system provides input to another local system, its input constitutes a *dynamic* control parameter for the second system in which a similar dynamic instability can arise. However, what could be considered as dynamic control parameter at a *local* scale could be viewed as a *state variable* on a more *global* scale. Thus this distinction is clearly dependent on where one places the boundaries of a system, a question that is not trivial for complex and spatially continuous systems such as the brain.

However it must be emphasized, that in simpler cases where such systems can be defined, for example the olfactory system, this approach yields very interesting empirical results and theoretical insights. Part of the classical and ingenious work of Walter Freeman is centred on explaining olfaction in terms of a multidimensional global attractor system, exhibiting many mutually interactive subpartitions (Freeman, 1992). The discrimination and categorization of odours is achieved through chaotic itinerancy through the submanifolds of the global system

dynamics. These submanifolds are thought to represent some sort of self-organized and dynamic memory constructs. This is a consequence of reinforcement learning and is due to the modification of synapses. That is the system has the *potential* (in terms of specific basins of attraction) to express certain dynamic patterns, which can be conceived as local interrelated neighbourhoods of a more global dynamical behaviour (in terms of submanifolds of a given attractor). According to the type of odour present in the olfactory input at a given time (and thus the set of initial conditions, which define a basin of attraction), the system continuously wanders through the state space and temporarily resides in a certain subdivision thereby expressing the categorization (in terms of similarity) of a certain odour. Thereby the system reconstructs a certain multidimensional dynamic state, which is very distinct for every odour and thus it comprises the relations between all the subpartitions of the system in euclidian feature space. Thus according to this model, the perception of odours is a process of *categorization* according to differences in multidimensional feature space. It must be noted that the implementation of this categorization process is using the chaotic construct model of Freeman (see for example Freeman and Barrie, 1994) is a self-organized dynamical process, that does not rely on any storage of particular bits of information in terms of representations, percepts or memory engrams, it just depends on the connectivity in the underlying network, that may or may not have undergone use dependent modification and the dynamics conditional upon it. Crucially, such a chaotic system can naturally create or destroy information (in terms bifurcations that give rise to stable or unstable states). A further extremely important aspect of this model of a global, multidimensional complex system is that it is inherently unstable and thus small changes in the stimulus or in the system itself can cause the system to engage in qualitatively different behaviour; that is the system can encode information in real time. Thus Freeman's conception of the olfactory system is one of a global pattern forming system that has a complex manifold subdivided into special neighbourhoods of dynamic behaviour. This clearly adheres to type I complexity as defined by Friston (Friston, 2000b) but is also consistent with a global, multicomponent system, which can exhibit type II complexity.

Although the main ideas within the supporters of the dynamical approach revolve around the same theme, there are some differences in their views, which will be shortly discussed. Furthermore, the relation of the dynamical approach to neuronal synchronization will be addressed.

Maybe the most influential notions behind the dynamical framework come from the field of synergetics, first proposed by the German physicist Herman Haken (e.g. Haken, 1983) and

then ingeniously applied and operationalized in the in the field of neuroscience by Scott Kelso and coworkers (see Haken, Kelso and Bunz, 1985 for a classical example of synergetic model applied to of human finger coordination and Kelso, 1995 for a number of theoretical and empirical explorations). This approach deals with complex systems that are inherently unstable. Such systems have a large number of degrees of freedom but their dynamics can be specified by a few *collective variables* or *order parameters*. The latter are defined as such by their ability to capture the dynamics of the interactions between subcomponents in a system. The core idea in synergetics is that the dynamics of a complex system can be specified by the utility of a few relevant collective variables. Because of the inherent instability of the system, it often undergoes non-equilibrium state transitions, which constitutes the core condition for pattern formation. Such macroscopic patterns are constantly created and destroyed by the system that continuously evolves in its coordination dynamics; that is the dynamics of system interdependencies, which are specified by the collective variables. This approach will be followed and exemplified many times throughout this work, since it constitutes its core ideological basis of dealing with neuroimaging data, which essentially provide a macroscopic description of an immensely complex system with microscopic and mesoscopic levels of description.

Friston and co-workers, although clearly adhering to the same framework, follow a somewhat different approach that explicitly addresses a *mesoscopic* rather than a *macroscopic* level of description. In the labile brain series, Friston proposes a full account of the taxonomy of cooperative brain behaviour and therefore of neural coding based on what he calls a fundamental equivalence (Friston, 2000a). The latter suggests that observing the relevant neuronal transients of two or more interacting systems provides the same information as a detailed, description of the system at microscopic levels. Thus by just knowing the recent history of inputs and outputs of a given neuronal system one can infer the essential function of the system. This can be achieved by using a system identification approach using Volterra Kernels. Thus the Volterra kernels are a polynomial, series of a time dependent parameters, which specify of how the input of a neuronal system is transformed in to an output. The kernels themselves inform about the function, which has been performed by the system. In a system with many subcomponents, these Volterra kernels (corresponding to neuronal transients) correspond to dynamic descriptions of the effective interactions. Thus the stress here is on the diversity of different interactions at a mesoscopic level as opposed to the global patterns controlled by a few collective variables at a macroscopic level as with synergetics. The Volterra kernels can be estimated from input output data using system identification techniques. This approach yields very informative results when applied to neural modelling

data but is less successful when applied to real neuroimaging data. The main reason for this is simply that most of the neuroimaging techniques provide macroscopic data and thus they do not provide direct access to system input and outputs. In other words, complex networks like the brain it is difficult to know, what the input and what the output is or more generally what is considered to be the system and where the borders the systems are. Many times what constitutes an input to a certain brain area is an output of another area. Macroscopic measurements provide the sum of such inputs to a certain area and it is therefore difficult to trace these inputs back to specific brain areas that provided them as outputs. Thus during a typical neuroimaging experiment it is hard to say, that area A has made the transformation X of the activity that it received from area B. Most of the time, the only definitive statement one can make is that area A and B seem to be interacting in the X dynamic fashion. This is a fundamental limitation, which Friston himself discusses extensively in (Friston, 2000a).

Maybe the most important implication of Friston's work is making explicit the idea of *dynamic neuronal transients* as the core entities of any effective neural code. Friston stresses the fact that any framework looking at information processing or even collective behaviour in the brain has to be a dynamic one, because neuronal networks always operate on the basis of their recent history of inputs and almost never isolated in time. Thus the neuronal moment is not an instant but a transient. Instantaneous codes and synchronous codes such as spike coincidences or spike cross correlations can be therefore considered merely as special cases of neuronal transients.

The second major distinction that Friston introduces is between synchronous and asynchronous codes (Friston, 2000a) and stresses the fact that asynchronous codes are more important and more salient than synchronous codes. According to this formulation, the most effective and the most salient regime of brain coordination is a nonlinear (asynchronous) coupling between nonlinear subcomponents. According to this view synchronous codes are linear and therefore essentially not dynamic. It should be noted that, synchronization as described by Friston, is essentially limited to the special cases of stable *linear resonance* phenomena involving processes that operate at the same frequency, such as the interactions, which can be captured by cross correlation techniques applied to spike trains or cross spectral analysis applied to EEG /MEG signals. Friston (2000a) then refers to a certain subtype of synchronization, namely cross frequency synchronization as 'asynchronous' and thus 'nonlinear' and claims that such asynchronous interactions are more salient than synchronous interactions in real brain coordination.

It has meanwhile become clear that several different types of synchronization may occur in nonlinear and even chaotic systems (Pikovsky, Rosenblum and Kurths, 2001). There is a vast amount of literature on synchronization in nonlinear systems (review in Boccaletti *et al.*, 2002) and some of these ideas have been also been applied to brain dynamics more specifically (Breakspear, 2002, Stam and Van Dijk, 2002, Stam, van Walsum, and Micheloyannis, 2002, Breakspear, Terry and Friston, 2003, Stam *et al.*, 2003, Breakspear, Williams, and Stam, 2004). This literature will be extensively reviewed in chapter 3 and 4. In spatially extended nonlinear systems processes of synchronization and desynchronization may even govern global system behaviour, which can be generally viewed as a process of pattern formation (see chapter 4 and references therein).

Hence synchronization of nonlinear systems is far from being just a trivial stable linear resonance process. Therefore, the original distinction between asynchronous and synchronous coupling introduced by Friston cannot be upheld in the face of the new findings in nonlinear science. However the most important implication in Friston's original argumentation is a methodological one. Linear and stable synchronization processes, i.e. similar to rigid resonance, of the type that is encountered in systems that are driven by strong forcing, are not particularly useful and moreover they are not commonly observed in the brain. Linear methods can only capture the linear parts of a certain interaction. Consequently, the latter are not of particular use for the study of brain function and of even lesser utility to the theory of brain coordination.

To sum things up, from the perspective of the dynamic approach, the brain evolves through a succession of global states determined by its coordination dynamics (Bressler and Kelso, 2001). These involve the emergent formation of transient functional clusters, which however are unstable in time, which means that even small and local system changes can lead to the dissolution of these functional groupings and the emergence of new groupings. There can be both local-interareal and global-intraareal constraints in the form of dynamic interactions and these will eventually determine the expression of global patterns. These global patterns constitute a real time collection of diverse salient informational entities, the functional clusters. Furthermore, these patterns also provide information about the relations between these clusters. Thus in every instant in time, information processing can be characterized as a self-organized global brain state, that exhibits local specificity and a certain pattern of interactions due to local and global constraints. However, these constraints are also dynamic and tend to reside near unstable equilibria, enabling flexible switching between different

global states according to small perturbations in the given internal or external context. The most fascinating aspect of this framework is its universality: both neuronal and behavioural processes exhibit phenomenology that can be accounted for. In the brain this involves nonlinear, nonstationary, transient and intermittent signal behaviour. What is more, these phenomena are scale invariant and thus can be observed at a neuronal, network and brain area level. Furthermore, these brain phenomena are consistent and probably causal to the dynamic, flexible, context sensitive and most of all adaptive nature of human cognition and behaviour.

1.5 The need for a general framework of brain function

This literature review stresses the point of how important a certain ideological framework is. This does not only apply to the interpretation of the experimental data but also in the guidance as to what experiments and what measures are to be used so that meaningful information with respect to brain function can be extracted.

The 'binding by convergence' approach does not attempt to explain the dynamics of perception and cognition, furthermore it does not provide with any concrete neuronal mechanisms that can account for the holistic, coherent and context dependent nature of information processing in the brain.

The temporal correlation approach clearly builds on a robust neurophysiological foundation and profits on marked empirical support. Although, this approach postulates synchronization as a *dynamic* binding mechanism, it does not provide any accounts for synchronization *dynamics*. Furthermore, although synchronization clearly plays a role in neuronal coordination, this approach does not specify how this relates to higher levels of organization in the brain such as large-scale neural networks and interareal coordination. Without such a formulation, there can be no relation to the resultant patterns of perception, cognition and behaviour, which are bound to be related to large-scale brain phenomena.

Although, the dynamical approach is currently still far from the status of a solid and formal theoretical framework, it seems to be the only approach, which is naturally concordant with the inherently dynamic, context sensitive and flexible nature of the brain and the mind. Kelso gives an extremely succinct but exact description for this state of affairs; he calls it a *dynamic isomorphism* of brain and mind (Kelso, 1995). Thus both brain and mind share the same dynamic principles and exhibit the same dynamic patterns.

Furthermore, the dynamic framework of all others can directly provide abstract but nevertheless sufficiently formal models of communication between different levels of brain organization, which in turn can be used for specifying *which* (of the many existent) experimental variables are of interest in the first place. It may additionally provide insights into *how* such variables should be measured and how these measurements are to be interpreted. These somewhat rhetoric formulations will become more clear in chapters 3 and 4, where we will examine such abstract models in more detail.

Chapter 2: Assessing interactions of linear and nonlinear neuronal sources using MEG beamformers.

2.1 Background.

One of the most active areas of research in contemporary neuroscience deals with the issue of functional connectivity and neural integration. At the microscopic level progressively more evidence has accumulated for distributed and transient cell assembly coding (Sakurai, 1996, Sakurai, 1998, Sakurai, 1999, Singer, 1999, Singer, 2001, Engel and Singer, 2001, Roelfsema *et al.*, 1997) with the possibility of partially overlapping cell assemblies contributing to different processes simultaneously at different frequencies (Sakurai, 1996, Sakurai, 1998, Sakurai, 1999) or even encoding information by manipulating the timing of their peak responses rather than the level of their mean activity (Roelfsema *et al.*, 1997, Singer, 1999, Singer, 2001, Engel and Singer, 2001). In particular, the latter phenomenon was proposed as a universal binding mechanism applicable to all levels of description of cortical networks and is referred to as the *synchronization hypothesis* in the neurophysiological literature (Roelfsema *et al.*, 1997, Singer, 1999, von Stein *et al.*, 2000, Singer, 2001, Engel and Singer, 2001, Varela *et al.*, 2001). At the macroscopic level of large-scale cortical networks, signals of interest such as the Electroencephalogram (EEG) and Magnetoencephalogram (MEG) are of an oscillatory nature and thus the phenomenon relevant to the coordination of the timing of the network's responses is phase synchronization (Varela *et al.*, 2001). Certainly, there is considerable experimental evidence in support of synchronization subserving large-scale integration in the form of transient and task-specific interactions between brain areas during various perceptual and cognitive tasks. This has been mostly demonstrated by coherence or phase synchrony analysis of scalp EEG recordings (Sarnthein *et al.*, 1998, Rodriguez *et al.*, 1999, Tallon-Baudry and Bertrand, 1999, review in Varela *et al.*, 2001). A second dynamical approach to functional connectivity (Kelso, 1995, Friston 2000c) considers the changes in dynamic emergence and disruption of synchronous and asynchronous (Friston, 2000a) coupling between brain regions as the substrates of the neural code. In this model the brain evolves through a succession of global states determined by its coordination dynamics (Bressler and Kelso, 2001). From this perspective, the brain is in a metastable regime due to the interplay of forces mediating functional integration on one hand and functional segregation of inputs on the other (Kelso, 1995, Friston 2000c, Bressler and Kelso, 2001), where abrupt state transitions¹ seem to be functionally significant (Kelso, 1995, Friston, 1997, Friston 2000b, Bressler and Kelso, 2001). In fact, such transient, mostly nonlinear,

¹ commonly referred to as phase transitions in dynamical systems theory

interdependences between brain areas have been demonstrated only recently in scalp EEG (Breakspear and Terry, 2002a, Breakspear and Terry, 2002b) and MEG sensor recordings (Stam *et al.*, 2003). Interestingly, nonlinear interdependence was more pronounced in MEG sensor data as compared to EEG scalp recordings (Stam *et al.*, 2003). Nevertheless, virtually all of the results at the macroscopic level described above were obtained by analysis of EEG/MEG sensor level data and therefore hindered by dispersion of the source signal in sensor space. This is particularly problematic when interdependencies are to be investigated (Nunez *et al.*, 1997, Nunez *et al.*, 1999, Lachaux *et al.*, 1999).

Ideally, in order to study neuronal interactions one has to go beyond the sensor level: first neuronal sources have to be identified and then their temporal activity has to be estimated before possible interdependencies can be investigated. In order to do this it is necessary to produce a solution to this inverse problem through the use of an appropriate assumption set. In this paper we use a variation of a nonlinear minimum variance beamformer (Robinson and Vrba, 1999) based on the assumption that no two distinct neuronal sources are perfectly linearly related (Van Veen *et al.*, 1997). Throughout this paper the terms correlation and coherence will be used to denote such strictly linear relationships between time series.

It has recently been demonstrated that MEG beamformers identified frequency specific and spatially selective task related changes in neuronal spectral power, which were spatially coincident with BOLD (Blood Oxygen Level Dependent) - fMRI responses for the same task (Singh *et al.*, 2002, Barnes *et al.*, 2003). Similarly, Hall *et al.*, 2005 have recently shown that beamformer estimates of human visual cortical gamma band activity concur spatially, temporally and functionally with local field potential recordings and BOLD-fMRI in the primate. This empirical evidence gives some initial confidence in the assumptions behind the beamformer. Most importantly, the temporal resolution of the MEG recordings is preserved in such reconstructions and the time series of specific regions of interest, usually referred to as a 'virtual electrodes', can be examined. Since MEG beamformer techniques have been shown to provide reliable estimates both of the spatial location and the time courses of activity of neuronal sources, a natural question would be whether these methods are suitable for the study of neuronal interactions. A pioneering technique of imaging coherent brain sources using MEG beamformer methods was introduced recently (Gross *et al.*, 2001). Nonetheless, there is a potential pitfall in this approach, namely that the MEG beamformer methodology is based on the underlying assumption that no distinct neuronal sources are perfectly linearly related (Van Veen *et al.*, 1997, Robinson and Vrba, 1999, Sekihara *et al.*, 2002). In fact, both deterioration of the 'virtual

electrode' signal intensity and temporal distortion in the presence of high, long-lasting, source correlations have been reported in the literature (Sekihara *et al.*, 2002). One mitigating factor is that we typically use beamformer analysis over relatively long time periods (seconds). From an information-theoretical point of view, such long-term cortico-cortical correlations are not efficient in the healthy brain (Friston, 2000a) because context-dependent information transfer is necessarily more *transitory*. Furthermore empirical studies show that neuronal synchrony seems to be a very transient phenomenon (see Singer, 1999 and Varela *et al.*, 2001 for a review).

In the first section of this paper we describe a simulation study and examine the effects of transient source correlation on the spatial and temporal performance of the MEG beamformer. In the second section we show that for a typical time window of beamformer analysis the interdependencies of the simulated sources are preserved. In the third section we simulate two interacting nonlinear oscillating systems representing neuronal sources and show that the MEG beamformer method in conjunction with a phase synchronization detection method based on Mutual Information are suitable for characterizing the phase interdependencies of these systems.

2.2 Methods.

2.2.1 Simulation of transiently correlated sources.

Two distant dipolar neuronal sources were simulated over 100 epochs (see Table 1 for coordinates). The time courses of the simulated dipoles consisted of uncorrelated (one predominantly at 20Hz, the other at 40Hz) and correlated signal segments (predominantly at 20 Hz, see figure 1, the top panel shows the two time courses superimposed). Both sources were of 2nAm peak amplitude with additive Gaussian ($\sigma = 1\text{nAm}$) white noise. The correlation coefficient between the two correlated signal segments was $r = 0.666$ ($p < 0.01$, $N=687$).

Forward solutions of the induced magnetic field in the sensor space, the lead field, were calculated using a single sphere model (Sarvas, 1987) and 3rd order gradiometer configuration (151 channel OMEGA MEG system, CTF Systems Inc., Canada). Sensor white noise at 10fTesla/ $\sqrt{\text{Hz}}$ over a 0-80Hz bandwidth was added to the signals.

2.2.2 Adaptive beamformer techniques.

Adaptive beamformer techniques are spatial filtering methods for localizing sources of brain electrical activity from EEG/MEG sensor recordings. As the details of these techniques are beyond the scope of this paper, we will only concentrate on some essential qualitative characteristics of the beamformer techniques. Detailed and formal descriptions of the method can

be found in (Van Veen *et al.*, 1997, Robinson and Vrba, 1999, Sekihara *et al.*, 2002, Barnes and Hillebrand 2003, Hillebrand *et al.*, 2005) and experimental imaging applications in (Singh *et al.*, 2002 and Singh *et al.*, 2003). MEG data is collected over a *number of epochs*, each containing a stimulus or task window and a rest period. Some time and frequency range within each epoch is used to define a *covariance time window* (Tcov). The choice of covariance window ultimately determines the spatial filter properties of the beamformer (Barnes and Hillebrand, 2003). For each possible source a weight vector or spatial filter is calculated. The output of this spatial filter, when applied to the MEG data, gives an estimate of the electrical activity, $y(t)$, termed the *virtual electrode* output, given by:

$$y(t) = (\mathbf{L}_\theta^T \mathbf{C}^{-1} \mathbf{L}_\theta)^{-1} \mathbf{L}_\theta^T \mathbf{C}^{-1} \mathbf{m}(t) = \mathbf{W}_\theta^T \mathbf{m}(t), \quad [1]$$

where $\mathbf{m}(t)$ is a column vector of N MEG channels at a single time instant t , \mathbf{W}_θ^T is a weight vector for the source θ . \mathbf{L}_θ is the lead field vector for source θ and \mathbf{C} is the data covariance matrix computed over time window Tcov.

A contrast window consisting of a pair of time (or time-frequency) segments, say Tactive and Tpassive, can be defined, and for each voxel in a pre-defined source space, a statistical parameter can be computed from measures of spectral power change across all pairs of contrast windows. We used the standard pseudo-t measure from the CTF SAM software, given by:

$$T_\theta = \frac{\overline{P_\theta^{\text{active}}} - \overline{P_\theta^{\text{passive}}}}{\overline{N_\theta^{\text{active}}} + \overline{N_\theta^{\text{passive}}}}, \quad [2]$$

where \overline{P} refers to average source power and \overline{N} is an estimate of the power of the projected sensor noise (Vrba and Robinson, 2001). A volumetric Statistical Parametric Map (SPM) can subsequently be obtained by estimating this index of change in neuronal activity (equation 2) for each voxel in the source space sequentially (using a grid of 5mm in this study).

The sources were first spatially localized by the beamformer formulation using an approximately 1.4s long covariance time window, which in this case contained transient correlated source activity amounting up to 23% of its total length. The following contrast time windows were used

for the localization of the sources (see figure 1): Tactive (0.0 to 0.87s) and Tpassive (-0.5 to 0.0s). The spatial location of the two sources was estimated from the two largest peak values of the SPM in the 0-80Hz-frequency range (see figure 2 and table 1).

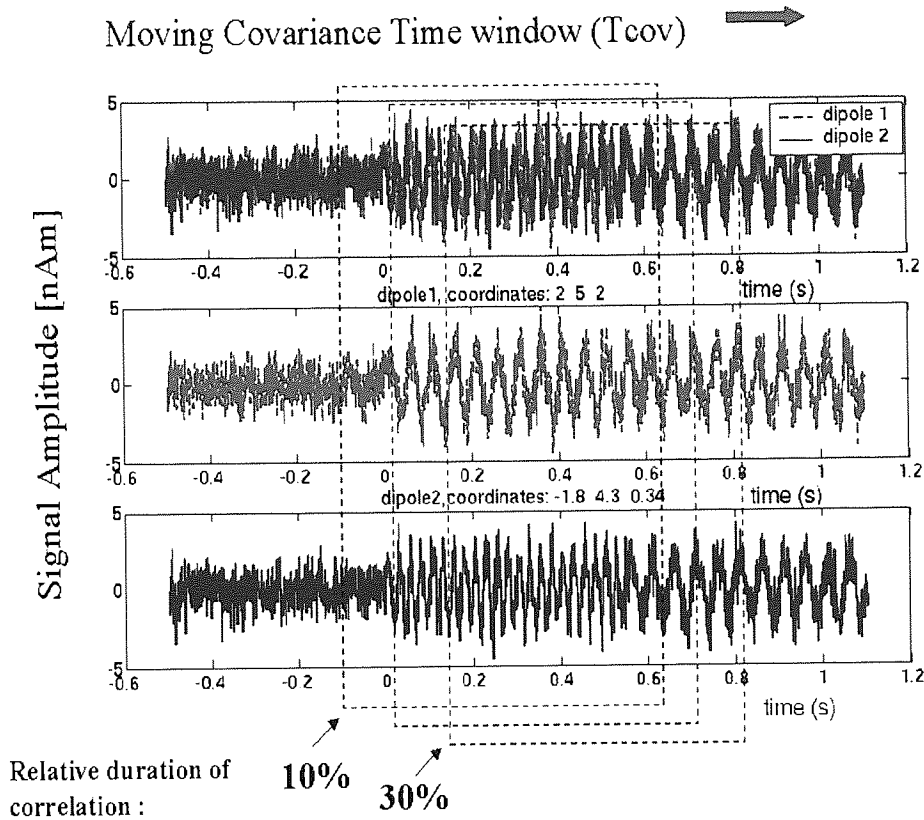


Figure 1. Parameterisation of transient source correlation: The time courses of the simulated sources consisted of a segment of white noise in both simulated dipoles (time: -0.55 to 0.0s), then a segment of noisy different frequency oscillations (20 Hz and 40 Hz dipole 1 and 2 respectively; time: 0.0 to 0.55s) and finally a segment of noisy 20 Hz oscillations in both dipoles (time: 0.55 to 1.1s). The progressive shift of the covariance time window by 10% of its length across the data allowed for a parameterisation of the relative duration of the correlated source activity with respect to the length of the covariance time window. The bottom two panels show the time courses of the two simulated sources and the top panel shows their superimposed time courses.

Since the covariance window completely determines the spatial filter (equation 1), an easy way to parameterize the effect of transiently correlated source activity is to introduce a segment of bivariate data containing correlated source activity and then just move the covariance window across the data allowing for increasingly longer correlated segments. The next step was therefore to estimate the time series of electrical activity in the two voxels while varying the relative duration of correlated source activity with respect to the total duration of the covariance time window (T_{cov}). For this purpose the beamformer was formulated over a 0.6s long moving covariance time window. T_{cov} was progressively shifted by 10% of its length across the data towards the segment containing correlated source activity and thus allowed for a parameterisation of correlated source activity with respect to the duration of the covariance time window (see

figure 1). Note that each of the covariance time windows represents a new beamformer spatial filter because a new set of beamformer weights is determined. The time series of the two voxels at the same location was then computed for each new set of weights.

2.2.3 Measures of temporal performance of the beamformer.

Two summary measures were computed for the quantification of the beamformer estimates as a function of the relative duration of correlated source activity:

1. A *reliability measure* corresponding simply to the mean correlation coefficient between the simulated time series and its beamformer estimate (the virtual electrode time series) across 100 epochs.

$$r = \frac{1}{Nepochs} \sum_j \left\langle \frac{p \sum_i est_{ij} sim_{ij} - \sum_i est_{ij} \sum_i sim_{ij}}{\sqrt{\left[p \sum_i (est_{ij})^2 - \left(\sum_i est_{ij} \right)^2 \right] * \left[p \sum_i (sim_{ij})^2 - \left(\sum_i sim_{ij} \right)^2 \right]}} \right\rangle \quad [3]$$

where i is an index for data points, $i=1 \dots p$, p the total number of data points in each epoch of data, j is an index for epochs of data, $j=1 \dots Nepochs$, and $Nepochs$ is the total number of epochs of the dataset, sim_{ij} is the simulated time series and est_{ij} is the estimated time series of the virtual electrode. Here est_{ij} is given by the virtual electrode output at the SPM maximum see equation [1].

2. A pointwise *relative error measure* between the simulated time series and its beamformer estimate. We used the relative difference measure (RDM- see Meijjs *et al.*, 1989).

$$RDM = \frac{1}{Nepochs} \sum_{j=1}^{Nepochs} \left\langle \frac{\sqrt{\sum_{i=1}^p (est_{ij} - sim_{ij})^2}}{\sqrt{\sum_{i=1}^p (sim_{ij})^2}} \right\rangle \quad [4]$$

The symbols and indices are the same as in equation [3]. The mean correlation coefficient and the RDM were computed separately for each source.

2.2.4 Reconstruction accuracy of source interactions.

When the reconstruction of the time series of true sources is imperfect, this can have a larger, supralinear, effect on measures of source interactions, since these measures are based on a *pair* of such reconstructed time series. Since the temporal performance of the beamformer is likely to deteriorate in the presence of long-lasting correlations, it would be useful to know the degree of deterioration in measures of signal interdependency as a function of the relative duration of correlated source activity. In order to parameterize this effect, relative difference measures (RDM_interaction, see below), were computed for three relevant measures of signal interdependency for beamformer reconstructions corresponding to different durations of source correlations. Details of the measures of signal interdependency (i.e. coherence and synchronization indices) employed are provided in the following section; however the RDM measures for the interactions were generally defined as follows:

$$\text{RDM_interaction} = \frac{1}{\text{Nepochs}} \sum_{j=1}^{\text{Nepochs}} \left\langle \frac{\sqrt{\sum_{i=1}^p (Mreconstr_{ij} - Mtrue_{ij})^2}}{\sqrt{\sum_{i=1}^p (Mtrue_{ij})^2}} \right\rangle \quad [5]$$

with i, p, j and $Nepochs$ defined as above, $Mtrue_{ij}$ is the true measure of signal interdependency (as calculated between the simulated signals) and $Mreconstr_{ij}$ is the reconstructed measure of signal interdependency (as calculated for the virtual electrode outputs of the beamformer). We used 3 signal interdependency measures here, the coherence function, defined as the average value over a broad frequency band (0-80Hz), the synchronization index at 20 Hz (based on narrow band filtered data, here a 10 Hz wide band pass filter centred at 20 Hz was used) and the synchronization index between source1 and 2 at 20 and 40 Hz respectively (the data was band pass filtered using a 10 Hz wide filter centred at 20 and 40 Hz respectively).

2.2.5 Measures of signal interdependency.

All of the following measures discussed were applied to the virtual electrode time series.

2.2.5.1 Coherence estimation.

Coherence as a function of frequency ($\hat{\gamma}_{a,b}^2(f)$) is estimated as the magnitude-squared cross spectrum divided by the power spectra of both time series, that is

$$\hat{\gamma}_{a,b}^2(f) = \frac{|\hat{G}_{a,b}(f)|^2}{\hat{G}_a(f)\hat{G}_b(f)} \quad [6]$$

where $\hat{G}_{a,b}(f)$ is the cross-spectral density functions of time series recorded in virtual electrodes a and b and $\hat{G}_a(f), \hat{G}_b(f)$ are the auto spectra of the time series in virtual electrodes a and b.

Coherence is an indirect measure of phase concentration: it evaluates the strictly linear relationships between a pair of signals at a given frequency. If coherence ~ 1 this indicates a perfect linear relationship, if coherence ~ 0 , then no linear relationship can be assumed for the signals in question.

2.2.5.2 Phase synchronization analysis.

This section comprises a brief review of the broader topic of phase synchrony. Recently two methods for detection of phase synchrony in brain signals were proposed independently (Tass *et al.*, 1998, Lachaux *et al.*, 1999, for a comparison see Van Quyen *et al.*, 2001). The second one is based on convolution with Morlet wavelets, whereas the first one involves narrow band filtering and utilizes the analytic signal concept (Gabor, 1946) and thus the Hilbert transform, in order to obtain *uniquely* defined estimates of the instantaneous phase and instantaneous amplitude. In Tass *et al.*, 1998, the variable of interest is the univariate instantaneous phase difference of paired signals and a synchronization index (SI) is proposed on the basis of either Shannon Entropy or conditional probability. In this study we adopted a very similar approach but we treated the bivariate instantaneous cyclic phases (the instantaneous phases of the signals were wrapped in the interval $[0, 2\pi]$, that is $\phi_k \bmod 2\pi$ and $\phi_l \bmod 2\pi$) of paired signals as the variables of interest and calculated a phase synchrony index based on Mutual Information (MI). A similar method was proposed for detecting phase locking from experimental data but it was not applied specifically to brain signals (Palus, 1997).

The Shannon Entropy of a given univariate probability of a distribution of the phase angle in a given time series can be easily estimated using histogram based methods (Van Quyen *et al.*, 2001) according to:

$$H(\phi_k) = - \sum_{k=1}^{Nbins} p(\phi_k) \ln p(\phi_k) \quad [7]$$

where $Nbins$ is the number of bins in the histogram and $p(\phi_k)$ is the relative frequency of finding the phase in the k -th bin. The number of bins was determined as the cubic root of the number of data points in the distribution. The binned distribution was then evenly spaced between its maximum and minimum.

The joint entropy can be estimated analogously as:

$$H(\phi_k, \phi_l) = - \sum_{k=1}^{Nbins} \sum_{l=1}^{Mbins} p(\phi_k, \phi_l) \ln p(\phi_k, \phi_l), \quad [8]$$

where $Nbins = Mbins$ are the number of bins in the univariate phase distributions ϕ_k, ϕ_l respectively and $p(\phi_k, \phi_l)$ is the relative joint frequency of finding the phase ϕ_k and phase ϕ_l in the k -th and l -th bin respectively.

Mutual Information (MI) between the instantaneous phases of two signals is then:

$$MI(\phi_k, \phi_l) = H(\phi_k) + H(\phi_l) - H(\phi_k, \phi_l) \quad [9]$$

We used a histogram-based method to assess Mutual Information. With this method the maximal MI is a function of the number of chosen histogram bins. The MI measures we present here have been normalized by the maximal possible MI.

Explicitly:

$$SI = \frac{MI}{MI_{\max}}, \quad SI \in [0, 1] \quad [10]$$

where MI is the observed Mutual Information and $MI_{max} = \ln(Nbins)$.

In this way we obtain a synchronization index, SI , between 0 and 1, where $SI = 0$ represents no synchronization and $SI = 1$ represents perfect synchronization.

An important feature of the synchronization index based on MI is that it can identify interdependence between phase at different frequencies and thus n: m phase locking² according to

$$|n\phi_k - m\phi_l| \leq c \quad [11]$$

where ϕ_k, ϕ_l are the instantaneous phases of the two frequency signals, c is a constant and n, m are integers defining the frequency ratio of the signals. If the analysis is done across the entire combination space in terms of all possible cross frequency interactions, n and m can be explicitly set to the mean frequency of the frequency range on which the analysis is being conducted. Explicitly, if two signals of interest are narrow band filtered at two different frequency ranges, say $range_1 = f_1$ to f_2 for signal 1 and $range_2 = f_3$ to f_4 for signal 2 and ϕ_k and ϕ_l are the instantaneous phases of the narrow band filtered signals 1 and 2 respectively, then [11] can be used in the following way:

$$\left| \frac{f_3 + f_4}{2} \phi_k - \frac{f_1 + f_2}{2} \phi_l \right| \leq c \quad [12]$$

That is, $n = \frac{f_3 + f_4}{2}$ and $m = \frac{f_1 + f_2}{2}$.

The products $n\phi_k$ and $m\phi_l$ are then substituted in place of the instantaneous phase angle values (ϕ_k and ϕ_l) in equations [7]- [10] and then the cross frequency, high-order synchronization index SI is computed for every possible frequency combination.

2.2.5.3 Assessment of event-related changes in measures of signal interdependency.

In most experimental cases it is useful to assess an (event-related) modulation in some signal quantity during the experimental condition ('active state') with respect to some baseline ('passive state') rather than just the raw values. Although the distinction between 'active' and 'passive' states is clearly an oversimplification, since there are no true 'passive' brain states, we used this

distinction for simplicity, while we would practically expand this terminology to denote a more general distinction between different brain states, defined as states that are subject to *differential* experimental manipulation. In our study the white noise signals segment was chosen as baseline. The epoch-wise differences of ‘active state’ and ‘passive state’ in coherence and in the phase synchronization index based on MI described above were then subjected to non-parametric permutation testing, implicit in which was a correction for multiple comparisons. The ‘event-related’ differences were then thresholded at a given significance level (in this paper $\alpha=0.01$ unless otherwise stated) and only significant results are displayed.

2.2.6 Simulation of interacting nonlinear oscillators.

Phase synchronization is essentially a nonlinear phenomenon defined as the adjustment of the rhythms of two or more self-sustained oscillating systems due to *weak interaction* (Pikovsky, Rosenblum and Kurths, 2001). Self-sustained oscillators are systems that have their own *independent and autonomous* oscillatory activity. In other words, in order to study synchronization, one has to measure systems whose parameters and nature of coupling are known. We accomplish this by simulating two coupled Rössler systems (identical to those in Tass *et al.*, 1998) as active neuronal sources at distinct locations using the same spatial coordinates as in the simulation study above. The main point in this particular part of the study implementing the Rössler oscillators as neuronal sources was *not* to parameterize the effect of the correlation between them, but test *if* interactions between nonlinear systems could be identified under realistic measurement conditions. The Rössler systems are defined by a system of 6 ordinary differential equations:

$$\begin{aligned}
 \dot{\chi}_{1,2} &= -\omega_{1,2}\psi_{1,2} - z_{1,2} + \xi_{1,2} + \varepsilon(\chi_{2,1} - \chi_{1,2}), \\
 \dot{\psi}_{1,2} &= \omega_{1,2}\chi_{1,2} + 0.15\psi_{1,2}, \\
 \dot{z}_{1,2} &= 0.2 + z_{1,2}(\chi_{1,2} - 10).
 \end{aligned} \tag{13}$$

where the parameters $\omega_1 = 1.015$, $\omega_2 = 0.7\omega_1$ represent the natural frequencies of the two systems and govern their initial frequency mismatch ($\delta\omega = |\omega_1 - \omega_2|$); ε is the parameter governing the coupling strength of the two systems and $\xi_{1,2}$ are two Gaussian delta correlated noise processes.

² n: m phase locking refers to high order, cross frequency phase synchronization, where n and m are integers and determine the ratio of frequencies of the two synchronized processes (see Pikovsky *et al.*, 1999 and Pikovsky, Rosenblum and Kurths, 2001).

The integration of the above systems was realized in MATLAB using the Runge-Kutta technique. The step of integration was set to $2\pi/1000$. We varied the coupling strength ε and obtained phase synchronization indices based on MI for two levels of coupling, namely $\varepsilon = 0.0$ or ‘no coupling’ corresponding to autonomous oscillation and $\varepsilon = 0.17$ or ‘moderate coupling’. From a dynamical systems point of view, this constellation corresponds to a *linear*, symmetrical, bi-directional coupling of two non-identical *nonlinear* systems.

The solutions of the $\chi_{1,2}$ oscillatory variables of the Rössler systems were then resampled at 1250Hz for a total duration of 1s and their forward solutions were computed over 100 epochs. Sensor white noise at 10fTesla/ $\sqrt{\text{Hz}}$ over a 0-80Hz bandwidth was added to the signals. Subsequently we applied the same methods described above in order to obtain the beamformer reconstruction of the spatial location and the time series of the Rössler systems.

Additionally, in order to study the spectral and temporal dynamics of the Rössler systems as reconstructed in the virtual electrode time series, multiresolution time-frequency analysis was performed using Morlet wavelets. Then the average spectral power across epochs was plotted for both virtual electrode time series.

Although the Rössler systems do not directly relate to ‘brain-like’ models, we chose to implement them because they possess the essential and universal features and mechanisms of coordination of oscillatory behavior (Pikovsky, Rosenblum and Kurths, 2001). Two of the basic features shared by interacting Rössler systems and interacting neuronal networks are that both show nonlinear and nonstationary oscillatory time courses and their interactions near equilibrium (after initial transients have died off) are specified by a two-opponent gradient interplay. Specifically, both neural and abstract (model) oscillators express characteristic frequencies forcing them to autonomous oscillation on one hand and bi-directional coupling of their instantaneous activities obliging them to cooperation and integration on the other.

2.3. Results.

2.3.1 Spatiotemporal performance of the beamformer in the presence of correlated source activity.

The results of the simulation of transiently correlated sources are summarized in Table 1 and Figures 2 and 3. Figure 2 shows the results of the spatial localization of the sources and coordinates are given in

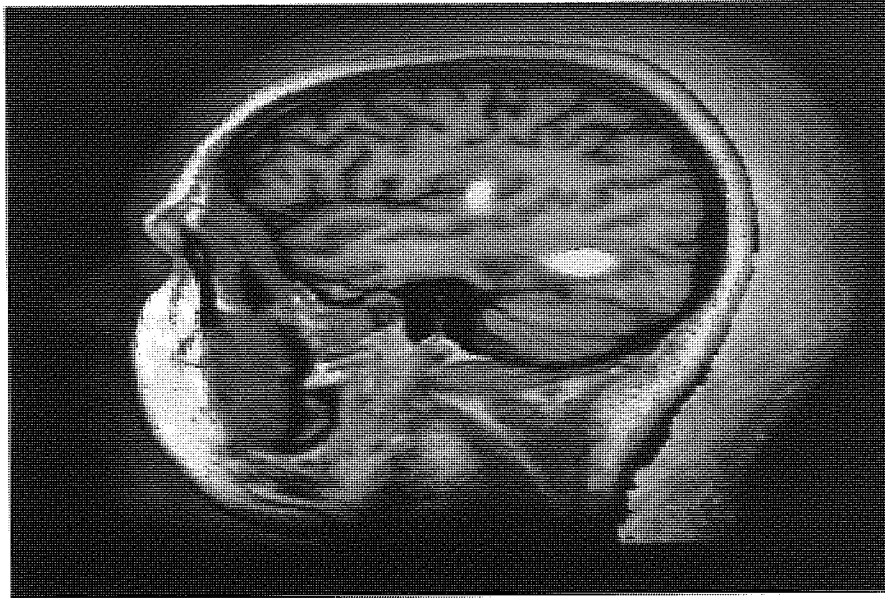


Figure 2. Localization of the transiently correlated sources by the beamformer. The beamformer was formulated over a covariance time window that contained transient correlated source activity over 23% of the total duration. The image shows the SPM of the pseudo-t measure as in equation [2] over a bandwidth of 0-80Hz using the contrast time windows T_{active} (0.0 to 0.87s) and $T_{passive}$ (-0.5 to 0.0s), see figure 1.

Simulated cortical sources	Coordinates of simulated sources (mm)	Coordinates of estimated source location (mm) and associated peak T-values of the SPM
Source 1	[2,5,2]	[2,5,2] T=27.2
Source 2	[-1.8,4.3,0.34]	[-2,4.5,0.5] T=13.8

Table 1. Coordinates of simulated sources and estimated source location. T denotes the pseudo-t values as in equation [2], calculated over a bandwidth of 0-80Hz using the contrast time windows T_{active} (0.0 to 0.87s) and $T_{passive}$ (-0.5 to 0.0s). Note the close correspondence between the coordinates of the simulated sources and the coordinates of the estimated source locations given the 5mm grid.

Table 1. As is evident, although the sources were highly correlated over 23% of the duration of the covariance window, the localization errors are negligible (given the 5mm grid spacing). Figure 3 shows a qualitative description of the temporal performance of the beamformer in the presence of correlated source activity. Examples of the reconstructed time series, the ‘virtual electrode’, (shown in blue) are plotted together with the simulated time series (shown in red) for low, medium and very high correlation levels (from top to bottom). It is evident that the beamformer can tolerate duration of transient correlations as high as 30% of the

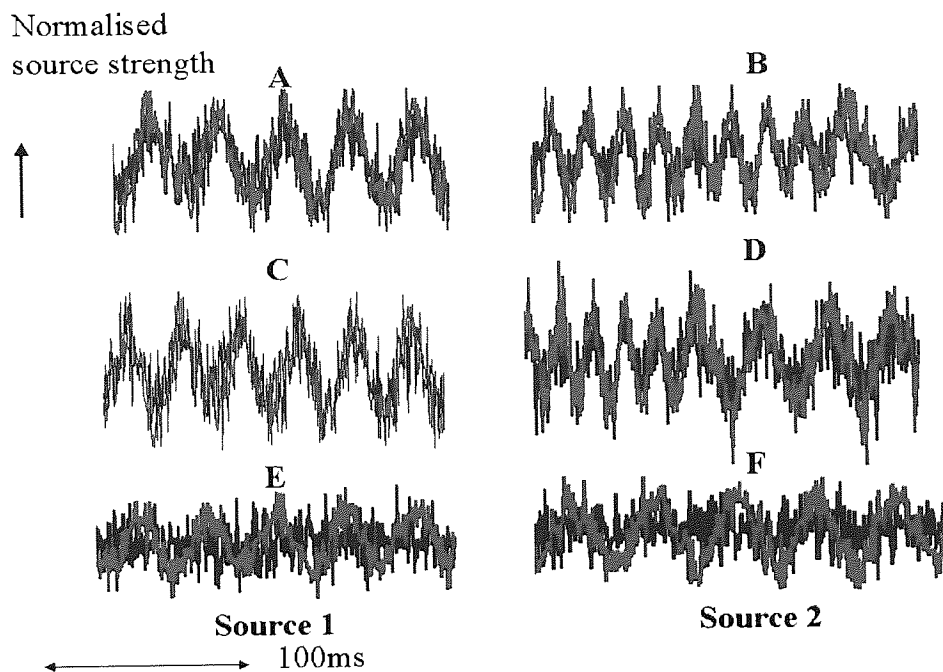


Figure 3. Temporal performance of the beamformer in the presence of transient source correlation. From top to bottom, low (10 % of the covariance time, A and B), moderate (30 % of the covariance time, C and D), and high duration (90 % of the covariance time, E and F), of correlated source activity. The simulated time series for the two simulated sources is shown in red; the corresponding reconstructed virtual electrode time series is plotted in blue. Note the accurate reconstruction of the source time series for low (A and B) and moderate (C and D) duration of correlated source activity. At very high durations of correlated source activity (E and F) the temporal performance of the beam former deteriorates and the signal intensity is clearly reduced.

covariance window over 100 epochs. Nevertheless the effects of temporal distortion demonstrated for long-term, high correlations in Sekihara *et al.*, 2002 are also evident in the bottom panel. At high durations of source correlation, here 90% of the covariance time window, the temporal resolution of the beamformer deteriorates and the reconstructed source intensity is clearly reduced. These results are quantified in Figures 4 and 5 by means of reliability and

relative error plots. In Figure 4 the reliability measure of the temporal performance of the beamformer is displayed. It is quite evident that the reliability of the beamformer estimates, that is the correlation between simulated data and the beamformer estimates, drops monotonically with the relative duration of the source correlation with respect to the covariance window but it is nevertheless quite reasonable for beamformer formulations including less than 40% correlated activity in the covariance window. Figure 5 shows the Relative Difference Measure (RDM) as a function of relative duration of the source correlation. This plot is consistent with the reliability plot since for durations of source correlations higher than 40% of the covariance window, there is a steep increase of the RDM.

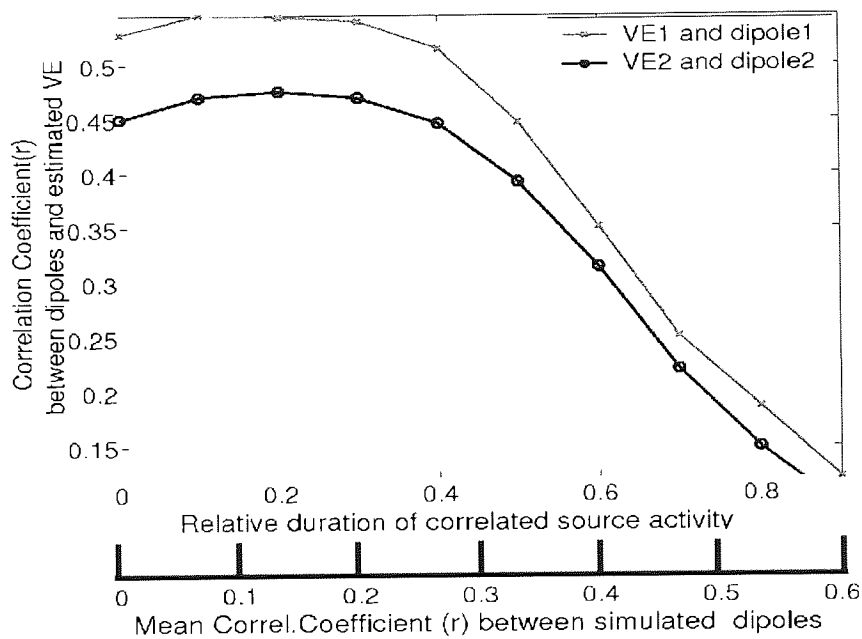


Figure 4. Reliability measure (see methods, equation [3]) of the beamformer as a function of the relative duration of correlated source activity with respect to the length of the covariance time window and the mean correlation coefficient between the simulated sources (the mean is taken across 100 epochs). Note the monotonic decrease of the reliability measure with increasing durations of correlated source activity. The reliability measure is nevertheless reasonable for beamformer formulations including less than 40% correlated activity in the covariance window.

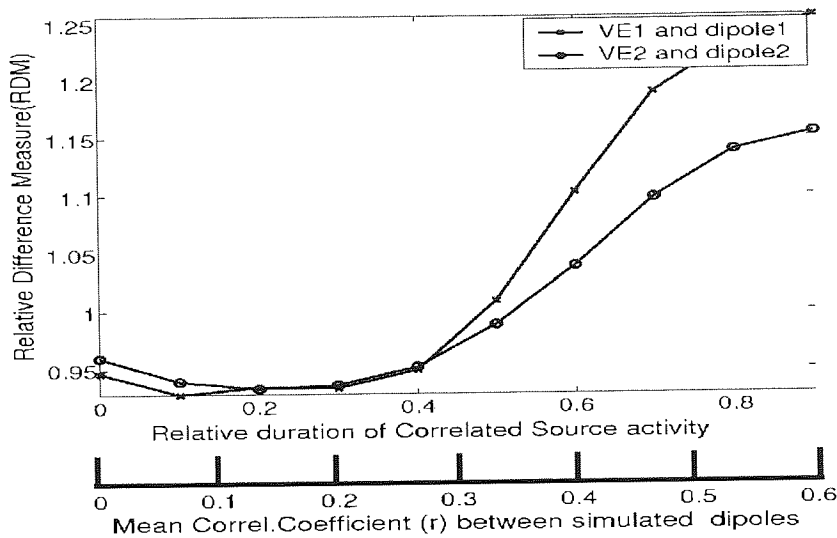


Figure 5. Relative Difference Measure (see methods- RDM, equation [4]) as a function of the relative duration of transient source correlation with respect to the total duration of the covariance time window and the mean correlation coefficient between the simulated sources. Note the monotonic increase of the RDM measure with increasing durations of correlated source activity. The RDM measure is relatively low for beamformer formulations including less than 40% correlated activity in the covariance window.

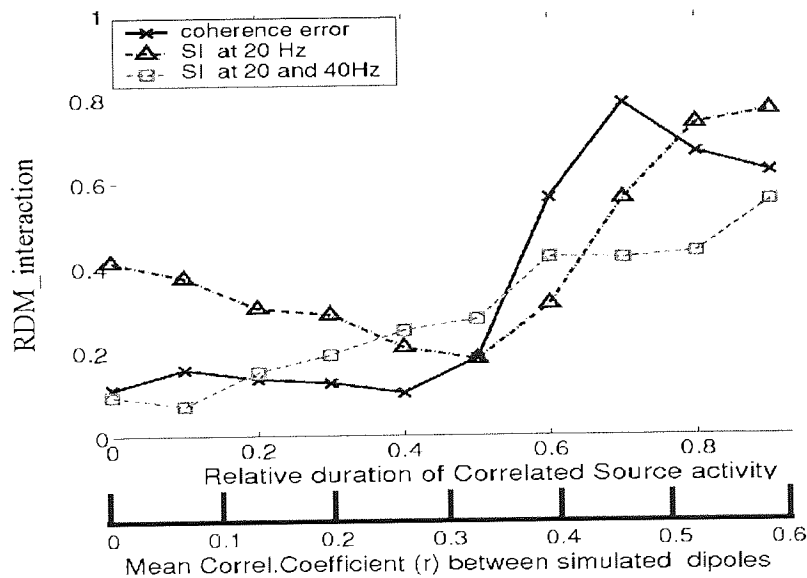


Figure 6. Relative difference measures of the interaction measures (these are the errors of the interdependency reconstruction, see methods, RDM_interaction in equation [5]) as a function of the relative duration of source correlation with respect to the length of the covariance time window. The y-axis shows the errors for three measures of source interdependence, that is the coherence error, the synchronization index error at 20 Hz (abbreviated as SI at 20 Hz) and the synchronization index at 20 and 40Hz (abbreviated as SI at 20 and 40Hz). Note that the errors are relatively small for shorter durations of source correlation, however they increase monotonically for durations of source correlation, which exceed 40% of the covariance time window. This consistent with the reliability and RDM measures of the temporal performance of the beamformer in figures 4 and 5.

2.3.2 Reconstruction accuracy of simulated source interactions.

Figure 6 demonstrates the results of the relative different measures of the interaction metrics, which is the interaction errors, as a function of the relative duration of source correlation. Essentially two of the three measures, the relative difference measures for coherence and the synchronization index at 20 and 40 Hz (see methods) show similar behaviour, they increase almost monotonically with increasing durations of source correlation. Source correlations that extend over 40% of the time window of beamformer analysis are associated with higher errors in the measures of source interactions. However the errors are relatively small for shorter durations of source correlation. The error measure for the synchronization index (SI) at 20 Hz is originally high, it decreases for moderate durations of source correlations and then increases again for longer durations. The initial high values are possibly due to the fact that the sources are not synchronized at 20 Hz to begin with, so the absolute values of the SI are very small. Hence small errors in the reconstructed time series will cause large errors in the SI. Eventually, as larger portions of the signal become synchronized the error seems to be reasonably sized and then with increasing source correlation the errors are similar to the 20 and 40 Hz case.

2.3.3 Reconstruction of signal interdependencies by the beamformer.

Since both the spatial localization and the temporal reconstruction of the simulated sources were

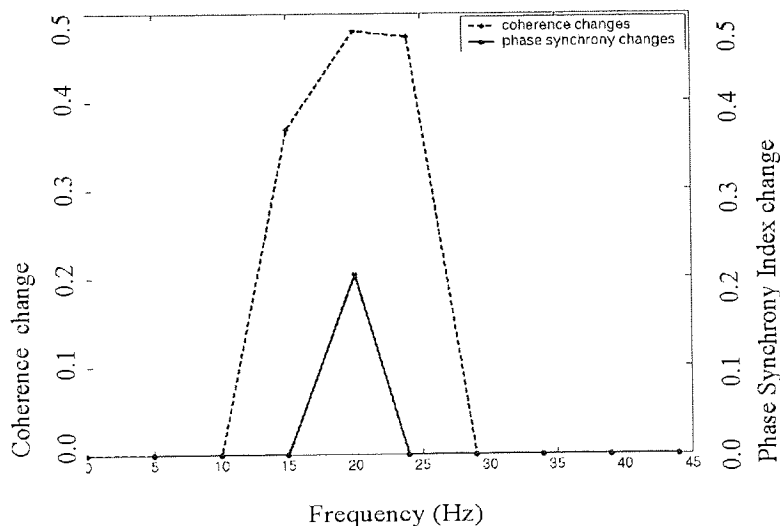


Figure 7. Significant coherence and phase synchrony changes of the virtual electrodes at 20 Hz over the time window 0.55-1.00s. The simulated sources contain correlated 20 Hz noisy oscillations for this particular segment of data (Figure 1, time: 0.55 to 1.1s). The segment of data that contains white noise in both sources serves as baseline (compare Figure 1, time: -0.55 to 0.0s). The coherence analysis quantifies the increase of the linear relationship between the two simulated sources at 20Hz. The phase synchrony analysis also correctly identifies the increase of the 1:1 phase interdependence between the two sources.

very good for moderate durations of *transient* source correlation the next step is to explicitly raise the question whether source interdependencies are preserved in the beamformer estimates. For this purpose the beamformer was formulated over a time window, which contained a *transient* source correlation for 20% of the covariance time window. The time series of the sources were reconstructed and then coherence and phase analysis was performed on the particular segment of data containing correlated, noisy 20Hz oscillations as the ‘active state’ (Figure 1, time: 0.55 to 1.1s) and the white noise data as baseline (Figure 1, time: -0.5 to 0.0 s). Figure 7 shows an estimate of the statistically significant coherence and phase synchrony index changes between the reconstructed time series as a function of frequency. Coherence analysis identifies correctly the presence of a significant change in the linear relationship between the two sources at 20Hz. Note the ‘frequency leakage’ to neighboring spectral bins at 15 and 24 Hz due to the small number of data samples in the cross-spectral analysis. The phase synchrony index change metric based on Mutual Information is shown on the same figure. The analysis correctly identifies the 1:1 phase interdependency at 20 Hz.

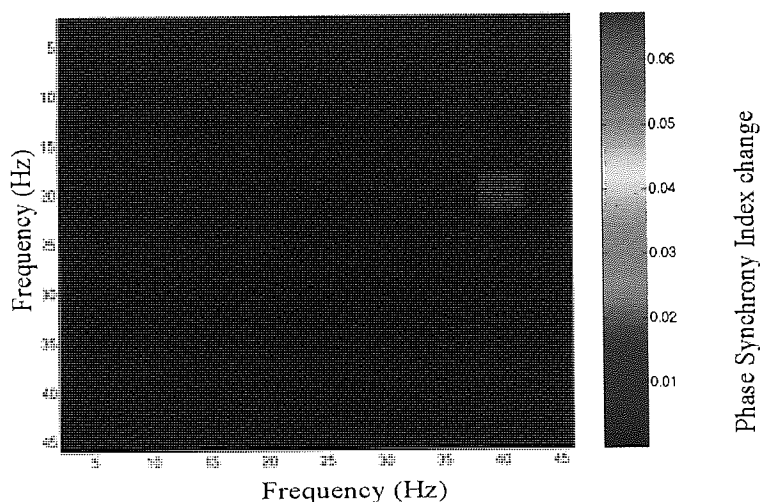


Figure 8. Detection of possible high order $n:m$ synchronization. The figure represents the cross frequency phase synchrony analysis between the time courses of a two simulated neuronal sources. The x and y axes represent frequency in the first and second source respectively. The colour code represents a significant event-related change in the phase synchrony index in some ‘active’, experimental state with respect to some baseline (see methods section) as a function of the frequency of the two sources. Warm colours (e.g. red) indicate an increase; cold colours (e.g. blue) indicate a decrease of the phase synchrony index with respect to baseline. Here the phase synchrony analysis is done on the particular segment of simulated data that contains 20 Hz and 40 Hz noisy oscillations in source 1 and 2 respectively (Figure 1, time; 0.0 to 0.55s). The segment of data that contains white noise in both sources serves as baseline (Figure 1, time: -0.55 to 0.0s). The analysis correctly identifies an increase of the phase synchrony index with respect to the baseline between 20 Hz oscillations in the first source and 40 Hz oscillations in the second source.

Figure 8 shows the results of phase synchrony analysis for a segment of simulated data that contains 20 Hz and 40 Hz noisy oscillations in source 1 and 2 respectively (Figure 1, time: 0.0 to 0.55s) with respect to white noise data serving as a baseline (Figure 1, time: -0.5 to 0.0 s). Since the simulated sources are periodic and stationary, a 1:2 stable relationship exists between their phases. The analysis of the virtual electrode time series accurately reconstructs this relationship suggesting that nonlinear high order phase interdependencies can be detected in the estimated time series.

2.3.4 Reconstruction of interacting Rössler systems and their interdependence

Figure 9 illustrates the results for the simulation of two Rössler systems serving as neuronal sources. For clarity of illustration of the effects of coupling on the amplitudes and phases of the Rössler systems, the original time series (the direct solutions of the integration) are shown here and not the reconstructed virtual electrode time series. Essentially, the reconstructed time series exhibit the same spectral and phase changes in the transition from ‘no-coupling’ to the ‘moderate-coupling’ as the original solutions except for the presence of additional strong simulated white noise that was projected from the sensors. Nonetheless the time-frequency and

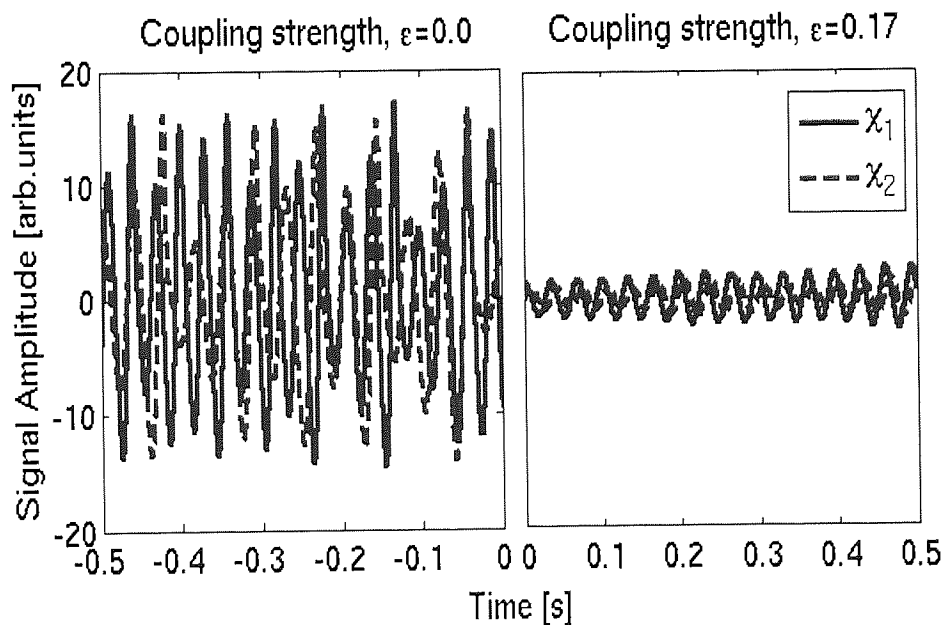


Figure 9A. Direct solutions (the $\chi_{1,2}$ oscillatory observables) of the integration of the Rössler systems for no coupling (left) and moderate coupling (right) between the two systems. Note the decrease in amplitude from the uncoupled to the coupled case and the appearance of consistent timing between the peaks.

phase analysis described below concerns the reconstructed virtual electrode time series.

Figure 9A shows the direct solutions of the integration of the Rössler system. On the left, the $x_{1,2}$ oscillatory observables are plotted for the ‘no coupling’ case and thus the autonomous oscillation and the respective $x_{1,2}$ time series for the ‘moderate coupling’ case are plotted on the right. Note the decrease in amplitude from the uncoupled to the coupled case and the appearance of consistent timing between the peaks. It is obvious that in the ‘no-coupling’ case the two systems exhibit autonomous oscillation with different principal frequencies. Also note the approximately stable time lag of the peaks for the two signals in the ‘moderate coupling’ case. This suggests a regime of phase synchronization between the systems.

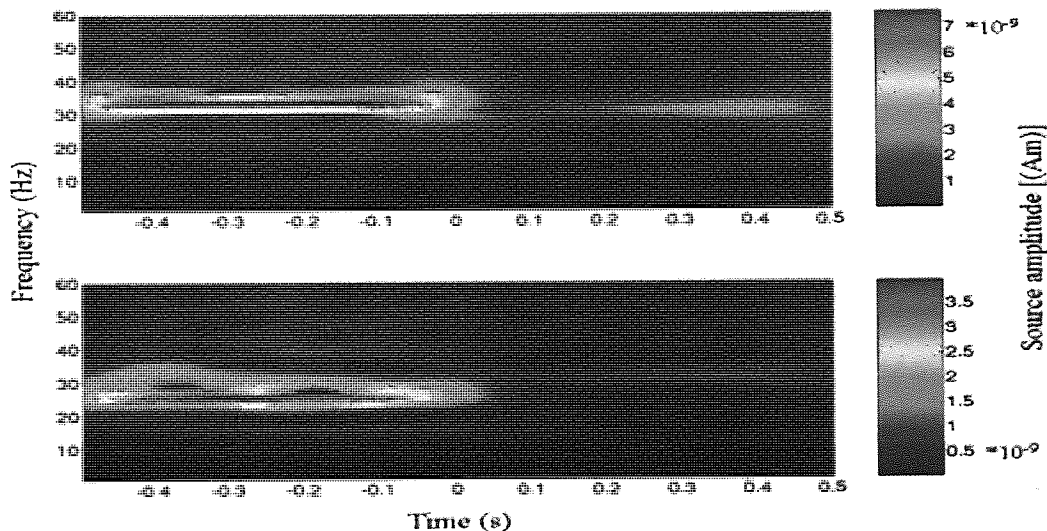


Figure 9B. Average wavelet time–frequency plots for the virtual electrodes time series corresponding to the two systems. The colour code represents signal amplitude of the virtual electrode time series. The time -0.5 to 0.0 s corresponds to autonomous oscillation and thus no coupling between the systems and 0.0 to 0.5 s corresponds to moderate coupling between the systems. Note the marked overall decrease in amplitude in the coupled case with respect to the autonomous case. In the case of moderate coupling between the systems the only visible peak lies at approximately 30 – 32 Hz in both systems and corresponds to a ‘compromise’ *beat frequency* lying somewhere in between the frequencies of the two systems in the autonomous case.

Figure 9B shows the average wavelet time–frequency plots for the virtual electrode time series corresponding to the two systems. The time -0.5 to 0.0 s corresponds to autonomous oscillation and thus no coupling between the systems and 0.0 to 0.5 s corresponds to moderate coupling between the systems. Note the marked overall decrease in amplitude in the coupled case with respect to the autonomous case. In the case of moderate coupling between the systems the only noticeable peak lies at approximately 30 – 32 Hz in both systems and corresponds to a ‘compromise’ frequency lying somewhere in between the frequencies of the two systems in the autonomous case.

Figure 9C shows the results of the phase synchrony analysis of the two virtual electrode time series corresponding to the two Rössler systems. The ‘no coupling’ time during which the systems oscillate autonomously (-0.5 to 0.0s) served as baseline. The phase synchronization index increases significantly between the two systems at 28-35 Hz in the coupled case indicating phase and frequency locking of the two systems at these frequencies. Additionally the phase synchronization index decreases between the 30-35 Hz oscillations in the first virtual electrode and the 25-30 Hz oscillations in the second virtual electrode, which correspond to the main frequencies of oscillation in the uncoupled case as evident in Figure 9B. These results portray the transition to synchronization in the form of adjustment of both the phases and the frequencies of the coupled systems. The transition to synchronization in this case is not smooth as it is reflected in the concurrent considerable spectral power drop observed in the time frequency plots. Coupling of the systems forces them to adjustment of their rhythms. However, due to the great initial frequency detuning of the two systems this ultimately leads to an additional dissipation of energy. This spectral power drop bears striking phenomenological resemblance to an event related decrease in the spectral power of ongoing brain rhythms as recorded by EEG/ MEG, known as ERD (Event Related Desynchronization, Pfurtscheller and Lopes da Silva, 1999).

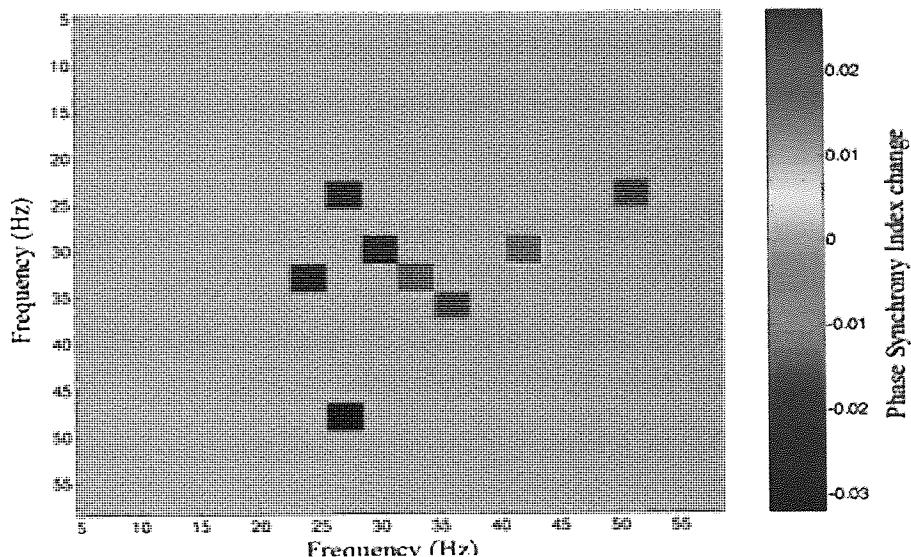


Figure 9C: The results of the cross frequency phase synchrony analysis of the two virtual electrode time series corresponding to the two Rössler systems. The x and y axes represent the estimated virtual electrode time series for systems 1 and 2 respectively. The colour code represents a significant change in the phase synchrony index with respect to baseline as a function of the frequency of the two sources. Warm colours (e.g. red) indicate an increase; cold colours (e.g. blue) indicate a decrease of the phase synchrony index with respect to baseline. Here the ‘no coupling’ time, that is the time when the two systems oscillate autonomously (see figure 8A, time: -0.5 to 0.0s) serves as baseline. The phase synchrony index increases significantly with respect to baseline at 28-35 Hz in the coupled case (figure 8A, time: 0.0 to 0.5s) indicating phase and frequency locking

of the two systems at these frequencies. Additionally the phase synchrony index decreases between the 30-35 Hz oscillations in the first virtual electrode and the 25-30 Hz oscillations in the second virtual electrode, which correspond to the main frequency of oscillation in the uncoupled case as evident in the spectrograms. These results portray the transition to synchronization in the form of adjustment of both the phases and the frequencies of the coupled systems.

2.4 Discussion.

In this paper we have shown that MEG beamformers can accurately reconstruct the spatial location and the time series of simulated neuronal sources that exhibited a *transient* correlation. In our simulation study the reconstruction of the time series was not affected if the duration of the transient correlation in source activity did not exceed 30 to 40 percent of the total duration of the covariance time window, that is the period over which the beamformer weights are computed. At longer durations, effects of temporal distortion and signal cancellation were observed, a finding which is consistent with previous literature (Van Veen *et al.*, 1997, Gross *et al.*, 2001, Sekihara *et al.*, 2002). This would suggest that if the beamformer is formulated using covariance time windows that are long relative to the duration of any transient linear (and zero phase lagged) interactions, it could provide us with accurate estimates of both the spatial and temporal aspects of neuronal source activity. The trade off is that the longer the covariance window, the smaller the portion of stimulus related activity relative to baseline state, and hence a decrease in overall SNR resulting in a loss of spatial resolution (Van Veen *et al.*, 1997, Gross *et al.*, 2001).

In our simulations we have shown that even source coherence, corresponding to correlation in the frequency domain, is preserved and can be assessed using the beamformer methodology. In addition, a method for detecting phase synchronization in the time series of neuronal sources was introduced. The method is based on Mutual Information and is a modification of previously proposed methods (Tass *et al.*, 1998, Pikovsky *et al.*, 2000, Van Quyen *et al.*, 2001). It allows for detecting and quantifying both simple and high order n : m phase locking and returns a synchronization index that can be assessed statistically by non-parametric permutation testing. Using the beamformer methods in conjunction with this approach, both frequency and high order n : m phase locking between simulated periodic, oscillatory sources could be correctly quantified. Our approach to the detection of phase synchronization of neuronal sources is comparable to a method proposed recently in Tass *et al.*, 2003. The main difference of the two methods lies in the algorithm for the reconstruction of neuronal sources from MEG sensor data: our approach is based on adaptive beamformer techniques, whereas in Tass *et al.*, 2003, Magnetic Field

Topography (Ioannides *et al.*, 1990) is utilized for the estimation of cerebral current source density from sensor data.

Current thinking in theoretical neuroscience considers brain function to be the product of a large assembly of coupled nonlinear dynamical subcomponents exhibiting transient and inherently metastable dynamics (Kelso, 1995, Friston, 1997, Friston, 2000a, Friston, 2000c, Friston, 2000b, Bressler and Kelso, 2001). Recent fascinating developments in nonlinear science have provided a more specific framework for understanding coordination phenomena and especially synchronization in weakly coupled nonlinear oscillating systems (Rosenblum *et al.*, 1996, Pikovsky *et al.*, 1999, Pikovsky *et al.*, 2000, Pikovsky, Rosenblum and Kurths, 2001), stressing the significance along with the universality and scale invariance of *phase synchronization* in the coordination of oscillatory activity. As a first step towards investigating coordination phenomena of brain sources, in this study we simulated two coupled nonlinear Rössler oscillators, reconstructed their activity using beamformer methods and looked at their phase interdependencies. By doing so we wanted to test whether the interactions of such nonlinear systems serving as neuronal sources can be detected by the beamformer methods in conjunction with the phase synchronization analysis described above. The prediction was that by increasing the coupling of the systems, phase synchronization³ would occur, which would result in an increase of the MI based synchronization index. By introducing a large initial frequency mismatch between the systems, and thus making the synchronization transition less smooth (Pikovsky, Rosenblum and Kurths, 2001), we were aiming to imitate conditions that are more likely to occur in real mesoscopic and macroscopic cortical network interactions. Macroscopic cortical networks can oscillate at quite distinct frequencies (Pfurtscheller and Lopes da Silva, 1999) and might even exhibit nonlinear high-order, cross-frequency (n: m) synchronization (Schack *et al.*, 2002). Another important prediction was that although the phases of the two systems may be bounded and interdependent, the amplitudes might still be chaotic in time and not strongly interdependent, especially since the systems were expected to undergo a 'rough' synchronization transition. In our simulation study, with just two coupled nonlinear oscillating brain sources, we replicated these predictions for *phase synchronization* of chaotic oscillators reported previously in a totally different context (Rosenblum *et al.*, 1996, Pikovsky *et al.*, 1999, Pikovsky *et al.*, 2000, Pikovsky, Rosenblum and Kurths, 2001). These interactions of nonlinear

³ Phase synchronization in chaotic systems: The phases of the systems are bounded for some region of the system parameters and strongly interdependent, whereas the amplitudes may remain chaotic in time and independent. Complete Synchronization in chaotic systems: both phase and amplitudes are bounded and the systems follow an identical trajectory in state space. For an exhaustive discussion see Pikovsky *et al.*, 1999 Pikovsky, Rosenblum and Kurths, 2001.

oscillating systems could be identified by a combination of the beamformer methods and our phase synchrony analysis based on Mutual Information.

Recently, it has become increasingly clear that phase synchronization is not by far the only relevant or quantifiable nonlinear coordination phenomenon in the brain. One major conceptual problem is that phase synchronization is a phenomenon which can be observed between so called 'phase coherent' oscillators, that is oscillators that exhibit more or less a *singular* approximate periodicity, so that phase can be clearly defined (Boccatelli *et al.*, 2002). The Rössler attractors display such a phase coherent behavior but this *not* typical for healthy brain signals, which tend to exhibit multiple and sometimes interrelated periodicities. The phase synchronization approach is strictly speaking only valid if applied to narrow-band filtered signals, which in the optimal case will be centered on one of the present system periodicities. Of course several problems arise, which are related to the choice of filtering parameters and the possibility of partial destruction of otherwise present nonlinear structure, which might involve more than one periodicity. Several authors have stressed the importance of generalized synchronization (first described by Rulkov., 1995) as a putative mode of interaction in the brain and have proposed methods for quantification of this phenomenon (Stam and van Dijk, 2002, Breakspear and Terry 2002a, Quiroga *et al.*, 2002, Stam *et al.*, 2003, David *et al.*, 2004). Generalized synchronization refers to a more general class of nonlinear interdependence between dynamical systems, in which trajectories in one system can be directly mapped to a second system by means of a deterministic functional relationship. Various methods have been developed to quantify this phenomenon; most of them involve time-delay embedding algorithms with the reconstruction of a multidimensional state space. The majority of these methods take advantage of the fact that the local structure, the relationships between neighboring data points in state space, will be functionally related in two interacting systems, if such a direct mapping function exists. The main benefit of these methods over the ones quantifying phase synchronization is a conceptual one. These methods do not require an arbitrary partition of the signal in to frequency bands and can therefore quantify a broader range of coordination phenomena, especially metastable and nonstatic nonlinear phenomena, which cannot be captured by phase synchronization based metrics. These phenomena arise through transient and weak coupling and seem to be very important from a theoretical point of view (Friston 1997 and 2000c). In fact, a study testing the performance of several interdependence measures, found generalized synchronization metrics to be more sensitive than phase synchronization metrics, especially when the coupling was weak (David *et al.*, 2004). Nevertheless both kinds of metrics seem to be qualitatively equivalent in realistic measurement

conditions (Quiroga *et al.*, 2002) and seem to be comparable in terms of their ability to capture nonlinear components in a certain interaction (David *et al.*, 2004). The disadvantages of the generalized synchronization based methods is that they require long computation times, they are sensitive to noise and to nonstationarity of the data, they involve several parameters for the time-delay reconstruction and most importantly, their computation requires a large number of data samples which limits their effective temporal resolution. Methods quantifying phase synchronization on the contrary can potentially offer very good temporal resolution, which can be of great importance considering the transient nature of real brain interactions.

In summary, we have presented a general framework for the identification of macroscopic interactions across active brain regions. MEG beamformer methods in conjunction with phase synchronization analysis based on Mutual Information provide accurate spatial and temporal descriptions of the simulated interactions between linear and nonlinear neuronal sources. The practical utility of these methods will be established through applications to experimental Neuroimaging data.

Chapter 3: Synchronization dynamics in low dimensional nonlinear systems.

3.1. Why study cortical synchronization and related oscillatory phenomena?

A vast amount of experimental evidence has been collected over the last two decades in support of the functional role of macroscopic cortical oscillations, which in all probability result from collective synchronization phenomena occurring at the microscopic level. Specifically, stimulus, event -and task- related changes in the ongoing cerebral rhythms in terms of spectral power of macroscopic integral signals such as the EEG and MEG have been the main focus of research. These commonly, frequency-specific spectral power changes referred to as Event Related Desynchronization (ERD) and Event Related Synchronization (ERS) for power decreases and power increases respectively seem to be fairly universal as they were found to be contingent and to co vary with functional changes in almost every area of human behaviour (reviews in Pfurtscheller and Lopes Da Silva, 1999 and Basar *et al.*, 2001) including perception (Tallon-Baudry *et al.*, 1996 and 1998 Keil *et al.*, 1999, Fell *et al.*, 2003), memory (Klimesch ,1996 and 1999, Burgess and Gruzelier, 2000, Jensen and Tesche, 2001, Klimesch *et al.*, 2001, Raghavachari *et al.*, 2001, Sauseng *et al.*, 2002, Jensen *et al.*, 2002, Tesche and Karhu, 2002) language processing (Krause *et al.*, 1996 and 1999, Pulvermüller *et al.*, 1995 and 1997 , Karrasch, 1998, Rohm *et al.*, 2001), movement (Neuper and Pfurtscheller, 1996, Pfurtscheller *et al.*, 1997, Pfurtscheller, Neuper, Krausz, 2000) and motor control/ movement imagery (Leocani, Magnani, Comi, 1999). Furthermore recent advances in Magnetoencephalography (MEG) have made it possible to spatially map the cortical sources underlying these phenomena (Singh *et al.*, 2002).

The foremost consequence of this line of research was a resulting concept -change with respect to the notion of brain activity in neuroelectric and neuromagnetic imaging studies. Explicitly, the signal plus noise concept implicit in the Event Related Potential (ERP) literature was at least to some extent replaced with a more plausible concept of brain function, namely the notion of event related modulation of the ongoing cortical activity in terms of event related rearrangement of the phases of ongoing rhythms into resonant frequencies (Basar, 1980 and 1992) or frequency specific power changes (Pfurtscheller and Lopes Da Silva, 1999). Although ERP research has been applied successfully to many different experimental paradigms and especially in the case of sensory evoked potentials it has additionally proven clinically very useful (chapter 5 and references therein), there are some

fundamental theoretical difficulties implicit in the ERP concept. Some of these problems will be discussed next.

The ERP concept implies that in the absence of a stimulus or an experimental task demand, there is no relevant activity in the brain area under consideration, apart from random neuronal discharges. The latter can be therefore considered as noise and therefore discarded by signal averaging. According to this concept, stimulus (or task-) specific neurons are recruited in a given location and at a specific time. The spatial and temporal summation gives rise to a specific signal of a fixed latency and polarity. This leads to the notion of signal averaging, and thus averaging across trials to 'increase' the signal to noise ratio. Thus, the assumption is that the exact same process will occur on every trial, so that averaging the signal across trials would enhance the contribution of time locked (or phase locked) components. Hence, the implicit assumption is that the brain activity, which precedes the stimulus, does not in any way influence the activity following the presentation of a stimulus. To summarize, the ERP concept is based on these two core assumptions:

1. There is no ongoing activity in the brain, which is not due to the stimulus other than noise
2. After the presentation of a stimulus, specific *additional* activity is generated, which is superimposed on the ongoing brain 'noise', without the former interacting with the latter in any way.

Clearly, these assumptions are simplifications of brain function. The first one is perhaps justified for early sensory processing occurring in the peripheral nervous system and to some extent in the spinal cord and subcortical nuclei. There, the main functional objective is secure information transfer and feature-detecting mechanisms might be at play. The ordered and strictly anatomically separated structure of afferent nerve fibres supports this view. Thus peripheral coding may well utilize, the 'labelled line' or serial processing mode, discussed in chapter 1. However, even in the simplest cortical systems such as the olfactory, this strict anatomical separation of projections is not given (Freeman, 1975 and 1992, Freeman and Barrie, 1994). Quite, the opposite is actually the case, a series of vastly divergent and recurrent projections transmit the information to every part of the cortical structure. This functionally corresponds to spatial and temporal integration. Thus the objective of the cortical networks seems to be a very different one, namely to integrate information. The second assumption is also largely unjustified. Cortical networks are never silent, as is sometimes the case in peripheral networks. This perhaps ensues from the divergent anatomical connectivity. Therefore, there is always ongoing 'spontaneous' network activity, which has been even documented to be dynamically more complex than the activity during

the presence of a stimulus (Freeman, 1992). This is a clear statement against the notion of spurious noisy ongoing activity, the fundamental assumption of the ERP concept. The fact, that the ongoing activity has a complex dynamic structure, taken together with the robust findings of stimulus and task specific modulations of the ongoing activity, also clearly contradicts the second assumption behind the ERP concept, namely that ongoing and stimulus related activity do not interact.

The classical work of Basar and coworkers (Basar 1980, 1992, Basar and Schurmann, 2001) considers evoked potentials as superpositions of induced rhythms or as resonance phenomena in the brain. Indeed several studies, suggest that the stimulus locked responses, might be attributed to either phase locking of ongoing ('induced') cortical rhythms (Basar *et al.*, 1997, Quiroga *et al.*, 2000, Basar and Schurmann, 2001) and even multiple, spatially distributed generators (Makeig *et al.*, 2002). These papers show that the 'evoked' response represents a rearrangement (Makeig uses the term partial phase resetting) of the phases of non-phase locked 'induced' rhythms. Thus, the time-locked, so called 'evoked' activity could be just a (somewhat artificial) subpartition of the overall cortical response, which results from signal averaging. The evoked response may therefore accurately reflect basic neurophysiological properties of the cortical response to a sensory stimulus, such as the underlying anatomical network wiring but may be deprived (because of the averaging process) of any additional specific information regarding the nature of this response.

In addition, a lot of evidence at the microscopic level points to a role of synchronization between neurons to achieve perceptual binding, which gives rise to macroscopically measurable oscillations (Gray and Singer, 1995, Koenig, Engel, Singer, 1995, Traub *et al.*, 1996, Nase *et al.*, 2003). Thus certain macroscopic patterns of oscillatory activity can be regarded as functional 'modes' of the brain dynamics. This view will be illustrated with experimental data from the visual modality in chapter 6. ERP's in contrast are not related to any coordination phenomenon grounded at the microscopic level and thus the axioms of Neuroscience, rather they are empirical observations contingent with certain behavioural tasks. Further, ERD/ERS phenomena typically display very large effect sizes (the changes are in the order of 50-300% of the baseline signal). In contrast ERP's are an order of magnitude smaller than the raw signal and exhibit relatively small modulations.

Finally, on a more intuitive psychological note, the ongoing 'spontaneous' activity of the cortex is a reflection of some intrinsic action (self-organization). It is almost trivial to say, that the perception of a stimulus is a function of the state of the brain at the time of perception,

which varies from time to time and from individual to individual and is furthermore subject to learning. However, according to the ERP concept, this spontaneous activity would not influence the perception of a certain stimulus. This rules out any context or learning effects, something that is incongruent with the marked context sensitivity of perception and memory.

Thus a number of arguments support the idea of ongoing cortical activity providing the internal 'context' of a stimulus. This ongoing activity can be specifically modulated by the stimulus, in the sense of a reorganization process. These 'induced' changes in ongoing brain rhythms were often operationalized in terms of the task and frequency specific spectral changes (ERD/ERS, Pfurtscheller and Lopes Da Silva, 1999).

Nevertheless as commonly encountered in the field of functional neuroimaging the origin and the nature of such macroscopic, functional activity is fuzzy, resulting in a definition of activity in phenomenological terms. The reason for that is that functional neuroimaging techniques such as the EEG and MEG measure the integral activity of many thousands of interconnected neurons constituting large-scale networks, however very little is known about the function and the underlying dynamic patterns of these networks. The names ERD and ERS imply that these phenomena might be caused by processes of desynchronization or synchronization in the pool of interconnected neurons at the microscopic level resulting in either decreases or increases of the macroscopic mean field (Lopes Da Silva and Pfurtscheller, 1999, Pfurtscheller and Lopes Da Silva, 1999).

Although this simple model is plausible and intuitive at first sight, it fails to explain central issues about the very nature of these macroscopic oscillatory phenomena. As a result a lot of interesting dynamic phenomena of ERD/ERS have remained unexplained. One crucial issue refers to the debated frequency invariance vs. frequency specificity dichotomy. The original concept of frequency invariant ERS and ERD corresponding to 'cortical idling' for instance (Klimesch, 1996, Pfurtscheller, Stancak and Neuper, 1996, Pfurtscheller, and Lopes Da Silva, 1999, Pfurtscheller, 2001) and 'cortical activation' (e.g. Pfurtscheller, and Lopes Da Silva 1999, Pfurtscheller, 2001) respectively seems to be an oversimplification, since ERS phenomena in the theta (4-7 Hz) range and the broad gamma range (30-70 Hz) seem to be contingent with states of cortical activation. In fact gamma power increases (ERS) were observed during tasks that require visual short term memory (Tallon –Baudry *et al.*, 1998), object recognition, (Tallon –Baudry and Bertrand, 1999), language processing (Pulvermueller 1995, 1997) and theta ERS's were consistently observed and even functionally modulated by task demands in the field of memory research (Klimesch, 1996 and 1999, Jensen and Tesche,

2002, Jensen *et al.*, 2002). Thus increases of power in the gamma and theta ranges are compellingly contingent with cognitive, perceptual and linguistic tasks. Even the legendary example of 'cortical idling' the occipital alpha rhythm, was recently found to covary and increase in terms of its spectral power with increasing task demands during a working memory task (Jensen *et al.*, 2002) and a phonological encoding task (Krause *et al.*, 1996).

Furthermore, a considerable paradox arises when comparing experimental evidence from microscopic (invasive recordings) and macroscopic levels (scalp EEG or MEG). ERS *cannot* be a correlate of cortical idling especially if it reflects synchronization of neurons at the microscopic level, since the latter is considered to subserve perceptual or cognitive binding (see chapter 1 and references therein). However, as we have seen above this is a commonly held view and used in the interpretation of experimental results. Some explanations have been attempted in terms of the frequency specificity of ERS and ERD; for instance an ERS in the alpha band may be interpreted as cortical idling whereas an ERS in the gamma range may imply cortical activation. Although this general statement is true it does not provide any theoretical insights why this should be the case. A theoretical model (Lopes DaSilva *et al.*, 1976) using a simulated neuronal network showed that the power of the signal increases with the number of the oscillators whereas the frequency decreases. Thus for lower frequencies higher signal power is to be expected. Based on this interpretation a further dichotomy is introduced in terms of the frequency content of the power changes: high amplitude low frequency oscillations are seen as the product of a spatially extensive 'idling' network in contrast to spatially-circumscribed, high frequency oscillations interpreted as a specific 'activated' network (Pfurthscheller and Lopes Da Silva, 1999). However, at least in the case of theta oscillations, the latter is clearly not the case; theta oscillations are evidently contingent with sustained attention, memory and cognition. Furthermore, concurrent ERD and ERS phenomena have been reported for the broad alpha band (Klimesch *et al.*, 2000). Based on the interpretations illustrated above, this finding implies simultaneous synchronization and desynchronization within the same cortical rhythm, which was deemed as a paradox.

To conclude, neither the relation between neuronal synchronization and desynchronization and macroscopic ERD/ERS patterns nor the temporal dynamics of the ERD/ERS phenomena are sufficiently elucidated by existing models to allow data interpretations beyond phenomenology.

3.2 Why study synchronization in abstract models of nonlinear systems?

It is clear that although ERD and ERS phenomena are very reactive with respect to virtually almost every behavioural paradigm and thus extremely motivating to neuroimaging research, basic characteristics and dynamic patterns of ERD and ERS still constitute a 'black box'. The reason for that is that understanding ERD and ERS beyond the phenomenological level is ultimately tightly bond to the understanding of the dynamics and the functional organization of the underlying large –scale neuronal network.

Considering the diversity of neurons, neurotransmitters, synaptic mechanisms at the microscopic level and the complexity of network architectures at a mesoscopic and macroscopic level, one can almost say, that understanding large-scale network function is a challenging enterprise.

Nonetheless, recent developments in nonlinear science have provided substantiation for the universality and scale invariance of the dynamics and the mechanisms underlying synchronization phenomena in a range of physical, engineering and biological nonlinear systems (a comprehensive review can be found in Pikovsky, Rosenblum and Kurths, 2001). Furthermore, coordinative phenomena such as synchronization of nonlinear systems can now be adequately understood in terms of a simple two-opponent gradient interplay between forces subserving integration on one hand and forces subserving autonomous oscillation on the other. The universality and scale invariance of these mechanisms provides us with the motivation to abstract ourselves from the complexity and diversity of a realistic description of a large-scale cortical network and just concentrate on the essential mechanisms, directly responsible for a network's dynamics.

Thus the justification for the use of abstract models of coupled systems for the study of synchronization in the brain is mainly centred on the established nonlinear nature of brain systems and thus the capability to exhibit chaotic dynamics. A brief (and by far non exhaustive) depiction of a few fundamental facts to support this nonlinear approach to brain dynamics is in order. Nonlinearity seems to be a universal feature in the brain and can be encountered at all levels of description. Firstly, on a microscopic scale the main phenomena related to neural transmission and thus to collective neural behaviour are evidently nonlinear. The interplay of two opponent biophysical gradients governs transmembrane ion flow; the osmotic gradient causing ion diffusion and the electric gradient of charged particles. Reversal potentials resulting from the voltage sensitive nature of ion channels ensure unstable and highly nonlinear equilibrium dynamics for transmembrane ion fluxes. Subsequently, neuronal

firing, thus the effective output signal of a neuron, is determined by a sigmoid-shaped relationship between soma membrane potential and mean firing rate (Freeman 1975, 1992, Freeman and Barrie, 1994, Breakspear and Terry, 2002a). At the next level of description and thus that of a neural assembly the input to output conversions are again distinctly nonlinear. Thus the mean local field of a population of neurons (reflecting the collective local neural activity, which is approximated by the recorded EEG in the vicinity) is nonlinearly (sigmoidally) related to the mean pulse density as estimated from multiple intracellular recordings (Freeman, 1992). The above introduce nonlinear terms into all major models of ion channels, single neural firing and population activity (Breakspear 2004). On a macroscopic level of description involving the integral activity of large-scale neuronal aggregates, such as reflected in human EEG, the evidence for *weak nonlinearity* has been consistent (see Breakspear and Terry, 2002a, Stam *et al.*, 2003, Breakspear, 2004 and references therein). To conclude, both from a phenomenological and a theoretical point of view (Friston 2000a, b, chapter 1), the brain can be regarded as a global system consistent of interacting nonlinear systems.

The above motivate the study of coupled nonlinear systems. In this chapter we examine synchronization dynamics in the simplest case possible that of two mutually coupled nonlinear oscillators. This study might potentially provide us with insights about generic mechanisms and dynamic patterns associated with synchronization phenomena in nonlinear systems in general. This approach also yields insight about potential metrics of quantification of such synchronization dynamics. Hence, the logic for studying synchronization phenomena in simpler systems is centred on the idea that the mechanisms and the dynamics of the collective coordination process will be *universal* and also *primarily causal* for the appearance of macroscopic order in the brain (or in fact any other complex system). Therefore all the fine detail regarding the constituent microscopic units of a system become secondary. In addition, even the simplest coupled (nonlinear) dynamics give rise to extraordinarily rich and complex synchronization behaviours; consequently their study is justified in its own right. In this chapter we will therefore focus on the essential mechanisms and associated dynamics within generic synchronization processes. In the next chapter, we will extend the study to more complex systems that have an explicit spatial structure in order to study the resultant collective patterns. This approach may facilitate the understanding of macroscopic spatiotemporal patterns in the brain, such as ERD and ERS. In chapter 6, we will test some of the predictions of these models with experimental MEG data. The next section of this chapter, introduces some basic concepts of nonlinear dynamics and chaos theory, which are essential for the description of chaotic synchronization.

3.3 Chaos theory

3.3.1 Basic geometric concepts

In chapter 1, the basic concepts of dynamical systems and chaos theory were introduced, to facilitate understanding of the theoretical frameworks. Here a more detailed description will be undertaken.

The central characteristic of chaotic systems is the sensitivity upon initial conditions in the state space. Recall from chapter 1, that the set of initial conditions for a given system has a value for each state variable (degree of freedom). Thus for a multivariate system, one speaks of a 'cloud' of initial conditions. The sensitivity of chaotic systems on these initial conditions, means that trajectories (evolutions of the system when started from a certain set of initial conditions) that are initiated in nearby points in this M dimensional state space (nearby implies a small Euclidian distance in state space) will eventually diverge and disembark at very different parts of the state space.

If the system is asymptotically converging to a certain part of the statespace (and thus a certain dynamic pattern) then one speaks of an attractor. This means that on long-term (thus after initial transients have died off) the dynamics will be concentrated or attracted to a certain subpartition of the state space. This is referred to as an attractor. Thus the system does not explore the whole state space but 'contracts': it confines itself to a certain subpartition. In fact this entails a dimensional reduction, the system has on the long-term fewer effective degrees of freedom than at the time it originated (then the degrees of freedom are equal to the dimensionality of the state space and not the dimensionality of the attractor). The state space is organized in terms of *basins of attractions* (see figure 1). The latter correspond to subpartitions of the state space that will give rise to a long-term behaviour, which leads to a certain attractor. Different basins of attraction give rise to different attractors, or otherwise stated, if the system is initiated in two points in state space that belong to different basins of attraction, its behaviour will converge onto different attractors. The basin boundaries have often-complex (fractal), geometrical shapes thus often the surfaces are intertwined. This geometric representation is very illustrative for the notion of sensitivity to initial conditions. Because of the intertwined basins of attraction, nearby points can give rise to extremely different long-term behaviours (attractors). Actually, the more these surfaces are intertwined in the M dimensional state space and thus the basin boundaries are fractal, the more 'chaotic' the system will be. A quantitative measure of sensitivity to initial conditions, the Lyapunov exponent exploits exactly this fact, namely the divergence of nearby trajectories.

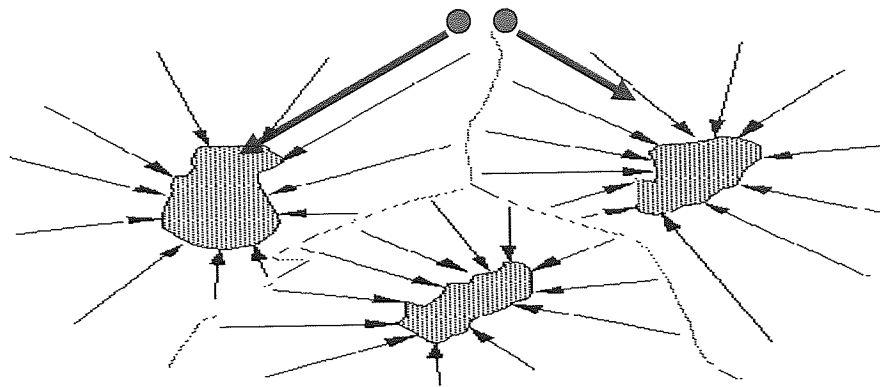


Figure 1. Basins of attraction. If a trajectory is started in any point within a basin of attraction (displayed as dotted contours) it will end up (in the long term) in a certain attractor (shown as grey surfaces within solid contours). However, trajectories started from different basins of attraction will end up in different attractors. Note, that neighbouring sets of initial conditions as shown in red, will diverge on the long term as shown by the blue arrows.

It should be noted, that the existence of attractors is not given. The opposite can also be true. Thus a system, can diverge in its long-term behaviour, and would not settle down to a certain pattern of dynamics. This is the notion of a repellor, which is an antonym for attractor. Essentially, the absence of an attractor means that the system is expanding, thus its dimensionality increases, until it occupies the entire state space. The other (theoretical) possibility is that the system is conservative, thus it neither grows nor contracts. One speaks then of neutrally stable behaviour.

Attractors and repellers can be considered in all possible dimensions depending each time on the degrees of freedom of the system under study. In figure 2, a 2-D representation is shown, the leftmost panel shows an attracting point, also known as stable fixed point and spiral point. Here we can see a trajectory spiralling into the stable fixed point. On the middle panel a repellor or unstable point is shown, here a trajectory spirals out of the unstable point. The rightmost panel shows a so-called saddle point. Here we have an unstable steady state solution (e.g. a point or a cycle) that repels in some directions of the state space and attracts in others. Saddles are extremely important in organizing the state space in terms of basin boundaries. For example in figure 2 we can see that the middle part of the state space is attracting and the outer parts are repelling. The repelling directions form a complex geometrical structure called the *unstable manifold*, which is invariant upon the system dynamics. The attracting directions form a complex invariant manifold called the *stable manifold*. Trajectories cannot cross these boundaries. Therefore, the invariant manifold, which

is formed in the presence of such saddles, is called a *separatrix*. The basin boundaries are formed by the insets of saddle points.

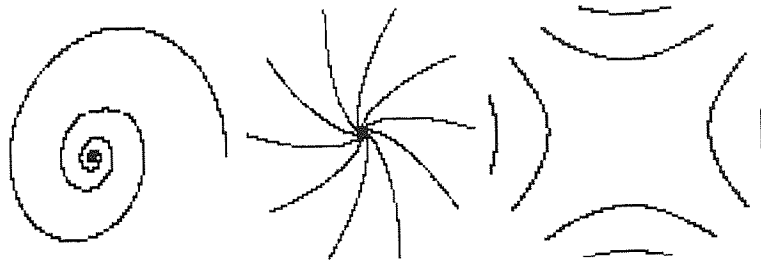


Figure 2. Fixed (equilibrium) points in a 2-D state space. On the left panel, we can see a stable fixed point (a point attractor), and a trajectory that spirals on to it. In the middle, an unstable point is shown. The trajectory spirals out as it is repelled by it. On the right a saddle point is shown, here the inset forms the basin boundaries for each one of the four attractors in state space. This can thus be considered a separatrix as it organizes the state space. The main characteristic of a saddle point, is that it attracts in some direction of the statespace and it repels in others, thus in terms of linear stability analysis (see Appendix 1) we have a negative and a positive eigenvalue.

The stability of attractors of a given dynamical system can be formally assessed using linear stability analysis with the calculation of Lyapunov exponents. Lyapunov exponents are generally defined as the exponential rate of divergence of two trajectories initiated at two neighbouring points (sets of initial conditions). Chaotic systems exhibit positive Lyapunov exponents meaning that two (initially) nearby trajectories will exponentially diverge. For reasons of limited space linear stability analysis and Lyapunov exponents are presented in Appendix 1.

Next some forms of attractors in different dimensions will be presented. Figure 3 shows some examples of non-chaotic attractors. On the top left, we can see the meanwhile familiar point attractor. The dynamics here is reduced to an asymptotically stable and constant motion. On the top right, we can see a limit cycle attractor. Essentially, this corresponds to a harmonic oscillation. On the bottom right, we can see a 2-D torus. Motion along the two main radii of the torus corresponds to a 2-frequency periodicity and is contingent on a rational ratio ($n:m$) of these two frequencies. The two radii correspond to the two frequencies involved. This 2 frequency behaviour is often referred to as $n:m$ phase locking if we are considering two interacting systems or mode locking if we are considering two subcomponents of the same system. The motion of such a system (or two coupled systems) is essentially periodic, with period 2 and thus *nonchaotic*. Another possible motion here is *quasiperiodic*, which corresponds to an irrational frequency ratio. The trajectory of the system in this case fills the entire surface of the torus.

We should also comment upon the fact that these nonchaotic attractors can exist in nonlinear systems for a range of control parameters. However, when varying control parameters transitions to chaos can occur. This will be shown schematically in the example of the logistic map. For example, slow variation of a control parameter can lead to a phase (or state) transition, which can occur through a so-called Hopf bifurcation. The latter can lead the system from a point attractor to a limit cycle. A subsequent Hopf bifurcation can lead the system to a second limit cycle at a harmonic frequency and thus motion on a 2-D torus. Eventually, a succession of such bifurcations can lead to chaos. This commonly known as the period doubling route to chaos (originally discovered in the logistic map, see May, 1974 and 1976). In other systems, which tend to exhibit 2-D tori attractors, the appearance of a third frequency often leads the transition to chaos. This is referred to as the quasiperiodic route to chaos (Ruelle and Takens, 1971).

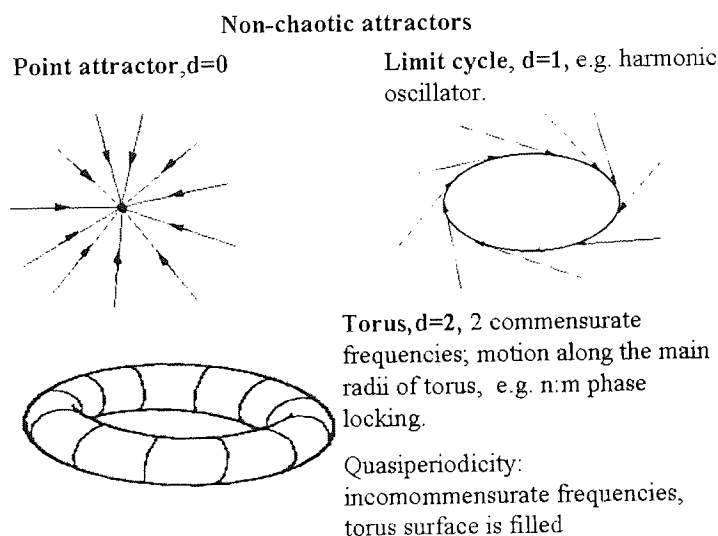


Figure 3. Nonchaotic attractors in 0,1 and 2 D. Note that d refers to the *topological* dimensionality of the geometric object.

Figure 4, shows a state space plot of a chaotic Rössler system. This is probably the simplest system, which can produce chaotic behaviour. The attractor here appears less regular and has a more complex geometrical structure than the ones shown in figure 3. Such chaotic attractors are often referred to as strange attractors, thus geometrical objects whose dimensionality is noninteger but *fractal*.

The Rössler system is of the general form:

$$\begin{aligned}\dot{X} &= -(Y + Z), \\ \dot{Y} &= X + aY, \\ \dot{Z} &= b + XZ - cZ.\end{aligned}\tag{1}$$

where X, Y, Z are the 3 state variables and a, b and c are the control parameters. For a range of parameters and initial conditions, the typical attractor is obtained. Here we used $a=0.45, b=2.0$ and $c=4.0$. The presence of the third equation introduces a quadratic nonlinearity. This effectively imposes a constraint on the system, which introduces a folding of the flow apparent on figure 4. However, the bottom part of the attractor still resembles a limit cycle oscillator. Stretching and folding behaviour is fairly typical for chaotic systems. Stretching results in divergence of trajectories while folding causes mixing – ultimately these phenomena are due to sensitivity to initial conditions. In the Rössler attractor, stretching and folding is largely confined to trajectories radiating outward from the saddle focus at the centre of the disk (see figure 4). It follows that the motion is phase coherent (Boccaletti *et al.*, 2002), which is to say that there is very little divergence, even though trajectories are thoroughly mixed radially. Coherence in the phase space is reflected in the power spectrum by the presence of sharp rather than broad peaks. The Rössler chaotic attractor can be considered as a prototype of a low dimensional chaotic flow, which exhibits such a phase coherent behaviour and will be widely used in our simulations.

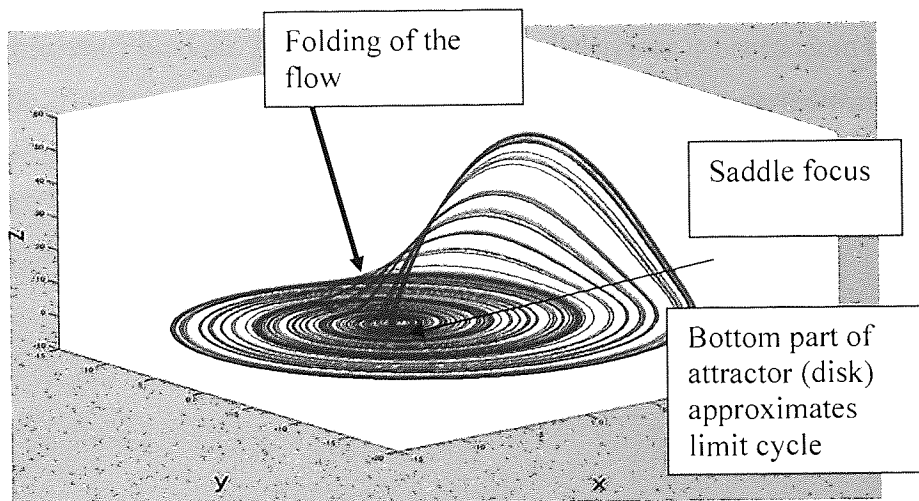


Figure 4. The Rössler strange attractor described in equation [1].

3.3.2 Bifurcations and phase transitions

In general, a bifurcation represents the sudden appearance of a qualitatively different solution (state) for a nonlinear system as some parameter is slowly varied. The phenomena associated with bifurcations are called phase (or state) transitions. These are particularly important in dissipative (non –equilibrium) complex systems and in the theory of synergetics (Haken, 1983). A bifurcation implies that the long-term dynamics (the attractor of a system) changes

abruptly as a parameter is *slowly* varied. This enables flexible switching between very different behaviours. Complex systems are thought to 'live' close to such unstable equilibria, where phase transitions are common (Haken, 1983). Figure 5 shows a so-called *bifurcation diagram* for the logistic map. This is just a plot showing the system state variable that undergoes qualitatively different behaviour as a function of the relevant control parameter. The logistic map is a discrete, recursive, iterated map of the form:

$$X_{n+1} = AX_n(1 - X_n) \quad [2]$$

Where n represents the number of iterations, X_n , is the value of X at the n th iteration, and A is a control parameter. Despite the simplicity of this equation, which essentially involves one variable (X), one parameter (A) and a quadratic nonlinearity, the logistic map can generate quite complex behaviour. Figure 5 shows, that to begin with (for low values of $A \sim 2.9$), X is a constant, this implies the presence of a point attractor. After a while an abrupt change, takes place with emergence of two symmetric values of X and thus a limit cycle oscillation. This is called a Hopf bifurcation, and it is a universal dynamic mechanism, which characterizes the phase transition from a point attractor (the fixed point becomes unstable) to a limit cycle. If A is varied further and around $A \sim 3$, a second Hopf bifurcation takes place, with the appearance of another limit cycle (another frequency). This happens once more, with the appearance of a third frequency and then at a *critical* value of A , the behaviour seems to become apparently random. As a matter of fact, this behaviour is not random but deterministic and chaotic. This signifies the transition to chaos. If A , is further varied windows of periodic behaviour seem to be randomly interleaved with periods of chaos.

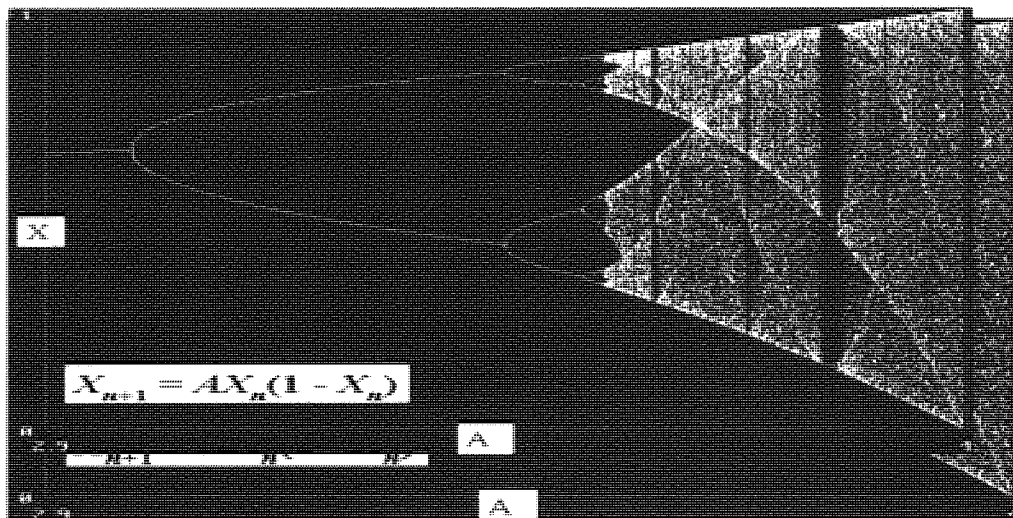


Figure 5. The bifurcation diagram of the logistic map. Note the abrupt changes in the behaviour of X as A is slowly varied. These are called phase transitions and rely on certain dynamical mechanisms, referred to as Hopf bifurcations (see text for details).

3.3.3 Periodic Vs Chaotic oscillations

An important feature of chaos is its *aperiodicity*. Thus a trajectory in a chaotic system, never *exactly* repeats it self. On the other hand, there is a certain structure in the chaotic time series; it is not random. As a result, chaotic oscillation, can be placed somewhere in between periodic and noisy oscillation. This becomes very clear in a visualization of chaotic Vs a periodic time series, such as in Figure 6. In panel A, the regular oscillation comes from a Rössler system with adjusted parameters, so that it produces limit cycle behaviour, here the time course of the x variable is plotted. On the right hand side (B), we have the typical time course of a chaotic Rössler attractor. Note the difference in the peak amplitudes. This leads to the difficulty of defining a period, since the system never repeats itself completely. However, note that there is some regularity in the behaviour, one can think of an average periodicity. In C and D the respective 3 D plots, are shown for a periodic limit cycle oscillation (C) and chaotic oscillation (D). These are essentially the plots of variables X against Y as a function of time. In C one can clearly see, how after an initial transient the system gets ‘trapped’ in a stable harmonic oscillation. In D, the system still exhibits somewhat regular behaviour but it seems to be reinjected in *close vicinity* to the limit cycle but never quite on the limit cycle it self. This general property of chaotic systems is known as *recurrence*. In this particular case, the phase coherent Rössler attractor the system recurs to a more or less regular orbit, which on its side implies, that on average there should be a characteristic periodicity. As a consequence, a sharp peak in the power spectrum of the system can be observed. Actually, the existence of such an average ‘period’ enables such chaotic systems to synchronize their phases, as we shall see in the next section.

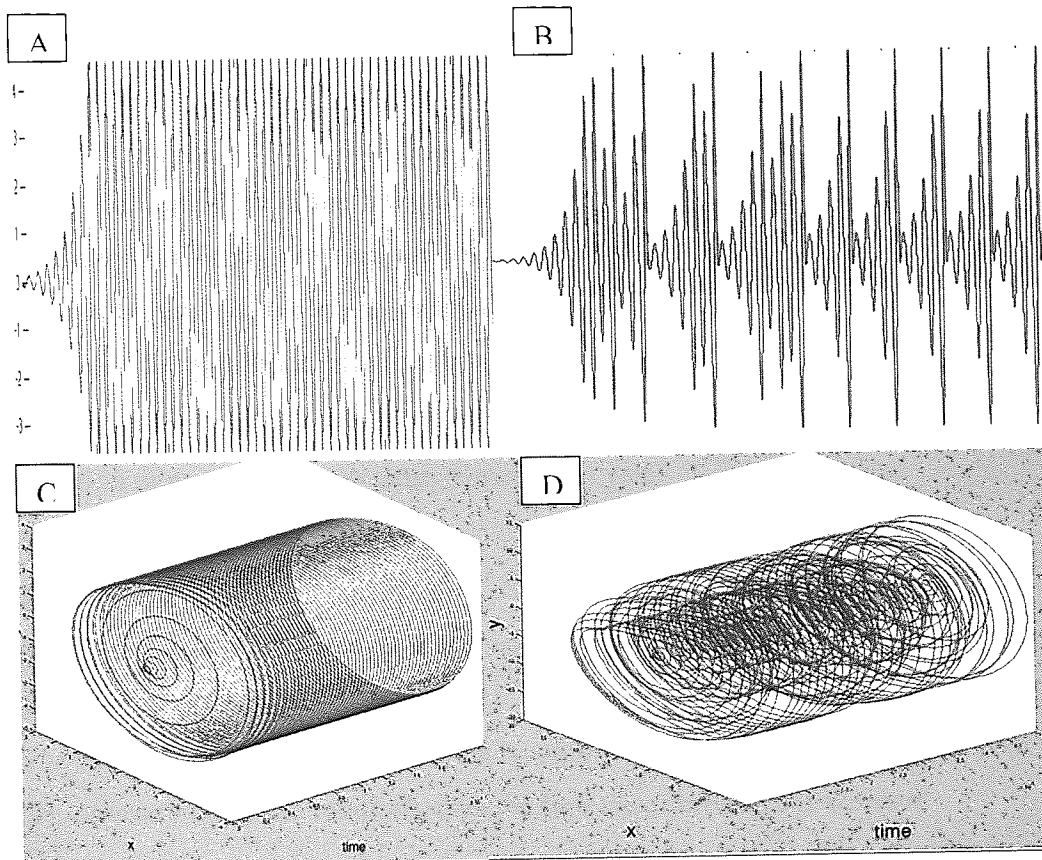


Figure 6. Periodic (A and C) and chaotic (B and D) oscillations. Parameters for limit cycle behaviour (A and C) according to the equations in [1] are $a=0.2$, $b=0.2$, $c=2.5$. For chaotic behaviour (B and D) the parameters were $a=0.45$, $b=2$, $c=4$. In both cases the systems were set off with the same initial conditions $[X=0; Y=0.01; Z=-0.01]$.

3.4 Synchronization of mutually interacting chaotic oscillators

3.4.1 Phase and Frequency of a chaotic oscillator

Synchronization of chaotic systems seems counterintuitive at least at first glance. This is essentially because the frequency of a chaotic system is constantly changing and therefore phase cannot be unambiguously defined. It is difficult to imagine synchronization between systems, whose frequency varies and thus the growth of the phase decelerates and accelerates continuously. Nonetheless, as we have seen in the previous section, chaotic systems are characterized by some degree of periodicity. Strictly speaking, one should speak of recurrence rather than periodicity, due to the fact that the system never repeats itself exactly but it may well return to points neighbouring to ones previously visited by a trajectory. Thus one can intuitively conceive an approximate period and frequency of a chaotic process if the latter is observed for a sufficiently long time to capture such a recurrent behaviour. If the frequency and thus the phase of a chaotic system can be defined then chaotic systems can be synchronized in terms of phase and frequency locking as in linear/noisy systems. The latter is meanwhile established and in fact phase synchronization of chaotic systems is a very active

research area. Here, we will briefly examine the basis on which this is possible. More comprehensive and detailed treatments can be found in Rosenblum et al, 1996, Pikovsky, Rosenblum and Kurths, 2000 and 2001.

The definition of the phase in (*autonomous*) periodic systems is a basically one of a neutrally stable and uniformly growing variable. This is demonstrated in figure 7.

Let's consider an autonomous periodic system in polar coordinates by creating two new variables, the amplitude and the phase of the oscillator. The radius of the cycle corresponds to the amplitude A . The phase ϕ can be defined as a cyclic variable that rotates uniformly in the direction of motion in the system, namely the cycle.

$$\phi = 2\pi N, \quad [3]$$

where $N=1,2,3,\dots$ is an integer that specifies the number of times the system has rotated by 2π or a full cycle.

The rotation of the phase on the cycle is uniform in time for a periodic system (it grows by 2π on every complete rotation), thus the first time derivative is constant

$$d\phi/dt = c \quad [4]$$

The velocity of the phase rotation is defined as the angular frequency ω and is a function of the period T , that is the time between two subsequent rotations along the cycle.

$$\omega = 2\pi/T \quad [5]$$

Thus from dynamical systems point of view, the phase growth corresponds to a *trajectory along the motion* of the system. In the case of a harmonic oscillator this is a limit cycle and the growth is uniform. This means that perturbations along the cycle are neutral to the system, thus phase can be considered *stable*. All, perturbations *transversal* to the motion and thus *amplitude* perturbations are however unstable (thus the system undergoes a relaxation back to the cycle).

As we can see from [4], the evolution of the phase in autonomous harmonic oscillators generally corresponds to a zero Lyapunov exponent in the direction of the motion, and evolution of the amplitude (in transversal direction to the motion), corresponds to a negative Lyapunov exponent (see Appendix 1). From this it becomes clear, that the notion of phase

may well be generalized to chaotic systems. There the phase can be defined as the growth *along the direction of the flow* and all other directions are defined as amplitude.

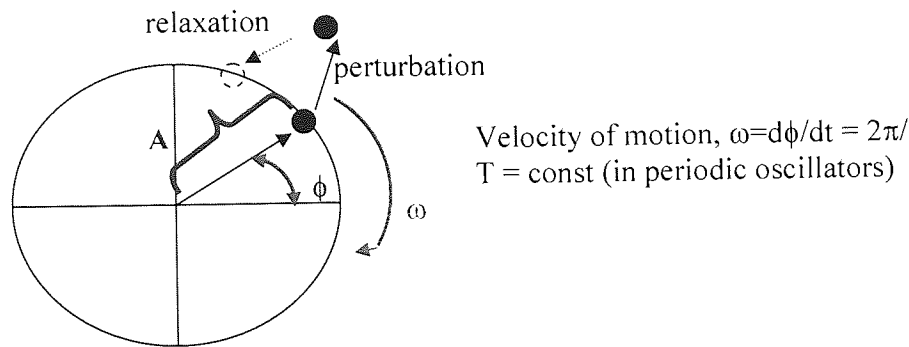


Figure 7. Schematic representation of the motion of an autonomous harmonic oscillator in polar coordinates. The motion is confined on a cycle, whose radius is the amplitude (indicated by a blue A) and the angle is the phase (indicated by a red ϕ). The rotation of the phase is uniform along the cycle and its velocity corresponds to the angular frequency $\omega = 2\pi/T$, where T is the period of the oscillation. Perturbations in the phase direction, which is the direction of motion are thus neutrally stable (no relaxation required). In contrast, perturbations of the amplitude (transversal to the direction of motion) are unstable and lead to relaxations back to the limit cycle.

In [5] we observe that the angular frequency and thus the velocity of the phase rotation depends on the period T. The latter is invariant for periodic systems but in chaotic systems it varies. This implies that the equality in [4] does not hold anymore, and thus the phase growth is not uniform: there can be accelerations and decelerations. However, chaotic systems do exhibit some kind of repeatability (recurrence), thus one can consider the times between two subsequent similar events as *instantaneous* periods T_i . Thus, we can conceptualise phase as a variable that grows *uniformly* by 2π on every 'cycle'. This 'cycle' can be viewed as an instantaneous period, defined as the time passed between two *maxima* of a system observable, or the time elapsed between two subsequent piercings of a Poincaré secant surface (Pikovsky, Rosenblum and Kurths, 2001). Thus we can use the *return times* (the times between subsequent crossings of the Poincaré section) as a measure of the instantaneous periods. Ofcourse it should be also noted that the return times and thus the instantaneous periods, crucially depend on the choice of the Poincaré section, which is *transversal* to the flow. Therefore the instantaneous periods depend on the amplitude. However, often the construction of an appropriate Poincaré map can facilitate the definition of phase as a variable that grows by 2π at each return time and thus between two subsequent piercings of the Poincaré secant surface. Similarly to [3] we have:

$$\phi = 2\pi \frac{t - t_n}{t_{n+1} - t_n} + 2\pi N, \quad t_n \leq t < t_{n+1} \quad [6]$$

where $N=1,2,3,\dots$ is the number of piercing of the Poincarè surface, t_n is the time of the n-th crossing and so on. We observe that if the denominator of the first term is zero and thus subsequent instantaneous periods are equal, the phase becomes equal to $2\pi N$ and thus [6] is reduced to [3] meaning that the above general definition holds for periodic systems, where the instantaneous periods are all equal. Furthermore, because the Poincarè surface is transversal to the flow, the phase defined in this way corresponds to a rotation along the flow and thus to a zero Lyapunov exponent.

From the above definition follows that an average period can be defined, which is equal to the total time elapsed divided by the total number of crossings of the Poincarè surface or simply equal to the average return time:

$$T_p = \frac{t_{total}}{N} = \frac{1}{N} \sum_{i=1}^N t_i - t_{i-1} \quad [7]$$

where t_{total} is the total time elapsed, $i=1 \dots N$, denotes the 1st to the Nth crossing, the subscript p indicates that this period is dependant on the choice of the Poincarè section.

The average frequency is then:

$$\nu_p = \frac{1}{T_p} \quad [8]$$

Thus even with this nonunique definition of phase on board one can examine if a chaotic sytem can be synchronized in terms of adjustment of its *average frequency*.

Following Pikovsky, Rosenblum and Kurths, 2001, one can write the following two formalisms for the Poincarè map for amplitude,

$$A_{n+1} = M(A_n) \quad [9]$$

and phase dynamics,

$$\frac{d\phi}{dt} = \omega(A_n) \equiv \omega_0 + F(A_n) \quad [10]$$

where M is a transformation that defines the Poincarè map, $\omega(A_n)$ is the instantaneous angular frequency, ω_0 denotes the time averaged angular frequency and $F(A_n)$ denotes some diffusion (variance) in the velocity of phase rotation.. The latter can be expressed as 'effective' noise of purely *deterministic* origin.

This means that the phase will diffuse according to the perturbations of the amplitude, which is chaotic and governed by positive Lyapunov exponents transversal to the flow. Two important remarks are in place. Firstly, it is clear that the phase diffusion will broaden the spectral peak of the system and the degree of this diffusion will be proportional to the *width* of the spectral peak. The latter can be used as an indicator of whether a system is likely to exhibit a coherent phase. Thus in the case of the Rössler system described above the spectral peak is narrow and thus phase synchronization is easily achieved. For systems exhibiting a broader spectral peak, such as the Lorenz system for instance, phase synchronization is not smooth (Pikovsky, Rosenblum and Kurths, 2001 and Boccaletti *et al.*, 2002). Note that the phase diffusion discussed here is of purely deterministic origin, namely it corresponds to the positive transversal Lyapunov exponents. Secondly, equation [10] is very similar to the one obtained in linear systems in the presence of noise:

$$\frac{d\phi}{dt} = \omega_0 + \xi_t \quad [11]$$

where ξ_t is a stationary random process.

There the phase diffuses according to the strength of the noise. The only difference is that in chaotic systems the 'noise' is not of stochastic origin and may be (more or less) bounded depending on the system under consideration.

To conclude, one should note that there clearly are limitations of this approach. Most importantly, many systems do not exhibit a phase coherent attractor, therefore an appropriate Poincarè section, one that transversally intersects all the trajectories, cannot be found. This concerns predominantly systems with multiple frequency ranges. On the other hand, often one can decompose these systems into different subsystems, which then exhibit a more or less phase coherent behaviour. This is sometimes particularly helpful in the case of multistable systems such as the brain. As a consequence the global behaviour can be treated as an interaction between *modes*. Alternatively, if one wishes to treat the system dynamics as a whole, one should adopt a more general approach (beyond phase synchronization), within the framework of generalized synchronization (Rulkov *et al.*, 1995).

Despite its limitations the approach discussed in this section leads to an extremely important conclusion: synchronization of noisy and chaotic systems can (under certain conditions) be treated in the same way (Rosenblum *et al.*, 1996, Tass *et al.*, 1998). In both cases the detection of synchronization can be formulated in a statistical sense, namely exploiting the appearance of a preferred value in the distribution of the phase difference. Note, that this *does not* in effect eliminate the distinction between interactions of deterministic and stochastic

origin. These issues can be addressed through the use of appropriate surrogate data, where all possible nonlinearities have been destroyed. This approach will be illustrated in chapter 5. Another important issue relating to the generalization of the concept of phase to autonomous chaotic oscillators is that, similar to the case of periodic oscillators, the phase of these oscillators is free (neutrally stable) and can be therefore easily adjusted. Consequently, phase synchronization may be an efficient mechanism for emergence of macroscopic order in multidimensional systems. This issue will be addressed in a forthcoming section.

3.4.2 Synchronization of chaotic systems

Synchronization phenomena in chaotic systems were first reported by Fujisaka and Yamada in 1983 but did not attract much attention until the early 90's. The study of synchronized chaos was grounded by a pioneering paper by Pecora and Carroll (1990) and since then there is an ever-growing growth of both empirical findings and theoretical insights. This enormous amount of significant literature cannot be done justice here. A comprehensive and formal review of the field is not only a challenge in its own right but is also beyond the scope of this thesis. The interested reader should refer to Boccaletti *et al.*, 2002 for a comprehensive formal review of the field and related generalizations. A recent book by Pikovsky, Rosenblum and Kurths (2001) provides the reader with both qualitative and formal accounts for a range of synchronization phenomena and underlying dynamic mechanisms. The scope of the following sections will be merely to introduce the basic concepts in the field of synchronization in chaotic systems by virtue of simple numerical simulations and to emphasize *qualitative* differences between different forms of synchronization and mechanisms of coupled dynamics. We will be particularly focussing on phenomena and mechanisms that we consider to be of direct relevance to collective behaviours occurring in the brain. The discussion will be centred on identifying (whenever this is possible), *which* regimes of synchronization may be feasible in the brain and under what circumstances they may occur. The main concept is that neuronal networks may exhibit a range of synchronization phenomena, which might subserve different functions. An intriguing possibility is that different synchronization regimes may not be mutually exclusive but *complementary* modes of collective brain behaviour. In case of dynamic, time-varying coupling parameters (as this is very much expected in the brain) different synchronization regimes may even reflect transient and successive stages of global spatiotemporal coordination dynamics.

3.4.3 Symmetry condition: Synchronization of identical systems

The simplest case of coordination comes about with the interaction of identical systems. Although, this state of affairs is very unlikely to be observed in any real experimental

situation it is very important theoretically, since it constitutes the limit of coordination behaviours and will be discussed below.

More formally, the dynamic evolution of a global system comprising of two coupled subsystems with n degrees of freedom each thus x^n and y^n can be expressed by a system of coupled differential equations of the general form:

$$\frac{dx^n}{dt} = f_a(x^n) + h(x^n, y^n) \quad [12]$$

$$\frac{dy^n}{dt} = f_b(y^n) + h(y^n, x^n)$$

The functions f_a and f_b specify the form of the local dynamics in terms of point attractors, limit cycles, tori or strange attractors as governed by intrinsic local parameters. The function h is considered extrinsic to the local dynamics and specifies the form of the coupling between x^n and y^n . The simplest case arises when the system is symmetric and thus the transformations $x^n \rightarrow y^n$ or $y^n \rightarrow x^n$ leave the system dynamics invariant. Obviously, the extreme case of coordination in the symmetric case corresponds to *identical evolution* of the two subsystems in time, and thus

$$x^n(t) = y^n(t) \quad [13]$$

The latter has been termed *identical synchronization* (IS), however the term *complete synchronization* (CS) is also widely used. The identity function in [13] has been referred to as the synchronization manifold (SM). SM in the case of identical systems is often supported on the invariant *symmetry manifold*, which has a simple geometry, namely that of a (hyper) plane. The synchronization manifold represents motion of the system confined on this hyperplane. Thus for identical systems the synchronization manifold coincides with the symmetry manifold. It is useful to differentiate between directions of motion, which are restricted to the symmetry manifold (these are commonly referred to as *tangential*) and those that are not confined on the symmetry manifold (referred to as *transverse*). This is illustrated schematically in figure 8 (adapted from Breakspear, 2004), which shows a two dimensional invariant plane (N), which we can think of as the symmetry manifold, and a one-dimensional transverse subspace T. In the case of two coupled 3-D systems (such as the Rössler attractors) the symmetry manifold would correspond to the hyperplane $x_1 = x_2, y_1 = y_2, z_1 = z_2$. Motion confined on the plane is *tangential* or normal (N) to the manifold. The motion on this plane in figure 8 corresponds to a stable limit cycle. Here two trajectories originated from different points on this plane converge on a limit cycle. The Lyapunov exponents (see Appendix 1) associated with this motion are referred to as *tangential*; in this case they will be negative since the trajectories converge. Perturbations tangential to N will decay

exponentially and converge back onto the limit cycle. Thus, in the case of two coupled systems, such motion would represent synchronous periodic oscillation. However, if the tangential exponents were positive then synchronous chaotic motion would be observed on the symmetry manifold and thus identical (chaotic) synchronization (IS). The stability of IS (or the synchronization manifold) would be determined by the *transverse* Lyapunov exponents. The direction T depicts *transverse* directions to the symmetry manifold. In panel a, transverse perturbations are attracted to the manifold (the transverse Lyapunov exponents would be negative) and thus the *motion on the symmetry manifold is stable*. In panel a, the scheme implies stable synchronous periodic oscillations. In panel b however, transverse perturbations point away from the symmetry manifold (the transverse Lyapunov exponents are positive), which means that synchronized motion on the symmetry manifold will become unstable.

We can see that the above geometrical criteria for the stability of synchronous dynamics are very powerful. Perturbations of the dynamics can therefore be expressed in terms of Euclidean distances from the synchronization manifold. In case of a stable chaotic synchronization manifold and thus identical synchronization the Euclidean distances will decay exponentially. In case of an unstable manifold the perturbations will increase exponentially and thus the synchronization manifold will become unstable.

We illustrate this with an example of two coupled Rössler systems:

$$\begin{aligned}\dot{\chi}_{1,2} &= -\omega_{1,2} \psi_{1,2} - z_{1,2} + \xi_{1,2} + \varepsilon (\chi_{2,1} - \chi_{1,2}), \\ \dot{\psi}_{1,2} &= \omega_{1,2} \chi_{1,2} + 0.15 \psi_{1,2}, \\ \dot{z}_{1,2} &= 0.2 + z_{1,2} (\chi_{1,2} - 10).\end{aligned}\tag{14}$$

where the parameters $\omega_{1,2}$ govern the initial frequency mismatch of the two systems, ε is the parameter governing the coupling strength of the two systems and $\xi_{1,2}$ are two Gaussian delta correlated noise processes. In the case of two mutually coupled

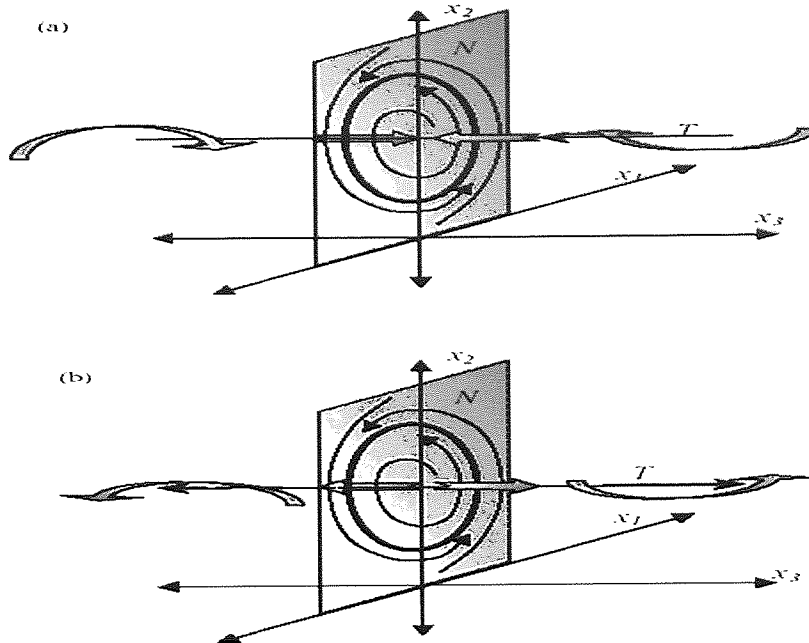


Figure 8 (from Breakpear, 2004). Schematic representation of tangential and transverse dynamics. In both panels the motion is confined on the vertical plane (N) and corresponds to an attracting limit cycle. Any perturbations on the N manifold are referred to as tangential and will exponentially decay. Thus in both cases the tangential Lyapunov exponents are negative. Perturbations vertical to N here denoted as T and curved arrows are referred to as transverse perturbations. These are likely to affect the stability of the N manifold. In panel a these perturbations are in converging direction to the manifold, meaning that they will eventually decay and the manifold will remain stable. This implies a negative transverse Lyapunov exponent. Thus in this case the limit cycle is an attractor in the full state space. In panel b the opposite is the case, the transverse perturbations will increase and eventually the manifold will become unstable. Thus here a positive transverse Lyapunov exponent can be implied. This means that the limit cycle is a saddle on the full state space.

Rössler systems these are firstly the coupling strength parameter ε which forces the systems to uniform synchronization behaviour and secondly an antagonistic parameter $\delta\omega$ which refers to the initial frequency mismatch between the natural frequencies $\omega_{1,2}$ of the coupled systems, which forces the systems to autonomous oscillation close to their natural frequency and thus to lower levels of interdependence of the systems' output.

A few words with respect to the nature of the coupling are in order here. In terms of equation [12] the coupling term h is a function of the instantaneous difference and thus

$$h_1 = \varepsilon(\chi_1 - \chi_2) \quad [15]$$

$$h_2 = \varepsilon(\chi_2 - \chi_1)$$

This means that the coupling aims to reduce the difference between the two variables but it vanishes when their instantaneous values are equal, namely when $\chi_1 = \chi_2$. This constellation is referred to as *diffusive coupling*. Thus the coupling term in equation [14] is symmetric and diffusive. The latter form of coupling is very common in a variety of physical systems (Pikovsky, Rosenblum and Kurths, 2001) and is therefore of primary interest here.

First, we consider a case of identical systems and thus $\delta\omega = \omega_1 - \omega_2 = 0$. The coupling parameter ε is set to 0.15. The resultant dynamics are displayed in figures 9 and 10. Figure 9 qualitatively describes the interaction of the two systems. Panel A shows the superimposed time courses of the $\chi_{1,2}$ variables. We observe almost coincidence of their time courses. This is further seen in the instantaneous difference $\chi_1 - \chi_2$ plotted in panel B. The latter does not significantly deviate from 0 (taking into account the stochastic noise components). This plot can be considered as a univariate approximation of the Euclidian distance, which additionally involves the differences of the y and z variables. Panel C depicts a scatterplot of the χ_1 Vs the χ_2 variable. This plot can be considered as a *linear subspace* of the symmetry manifold, which in the case here is a hyperplane defined by $\chi_1 - \chi_2$; $\psi_1 - \psi_2$; and $z_1 - z_2$.

We observe that the motion is confined on the diagonal $\chi_1 = \chi_2$. For the sake of completeness and consistency with subsequent sections, we also present the phase dynamics here. Panel D and E depict the time course and the distribution of the instantaneous cyclic phase difference of the $\chi_{1,2}$ variables respectively. The phases are obtained from the Hilbert transform (see chapters 2 and 5 and references therein) of the $\chi_{1,2}$ variables and the phase difference is wrapped modulo 2π . Here the phase difference is essentially constantly 0, when disregarding some of the wrapping artifacts giving peaks around 0 and 2π . This becomes clear if the phase is ‘unwrapped’ and thus not defined on the circle $[0, 2\pi]$ but on the full line (not shown here).

Figure 10 depicts the state space portrait for the two-coupled systems; we observe almost complete overlap. Thus, we conclude, that the two systems are in a regime of identical synchronization (IS).

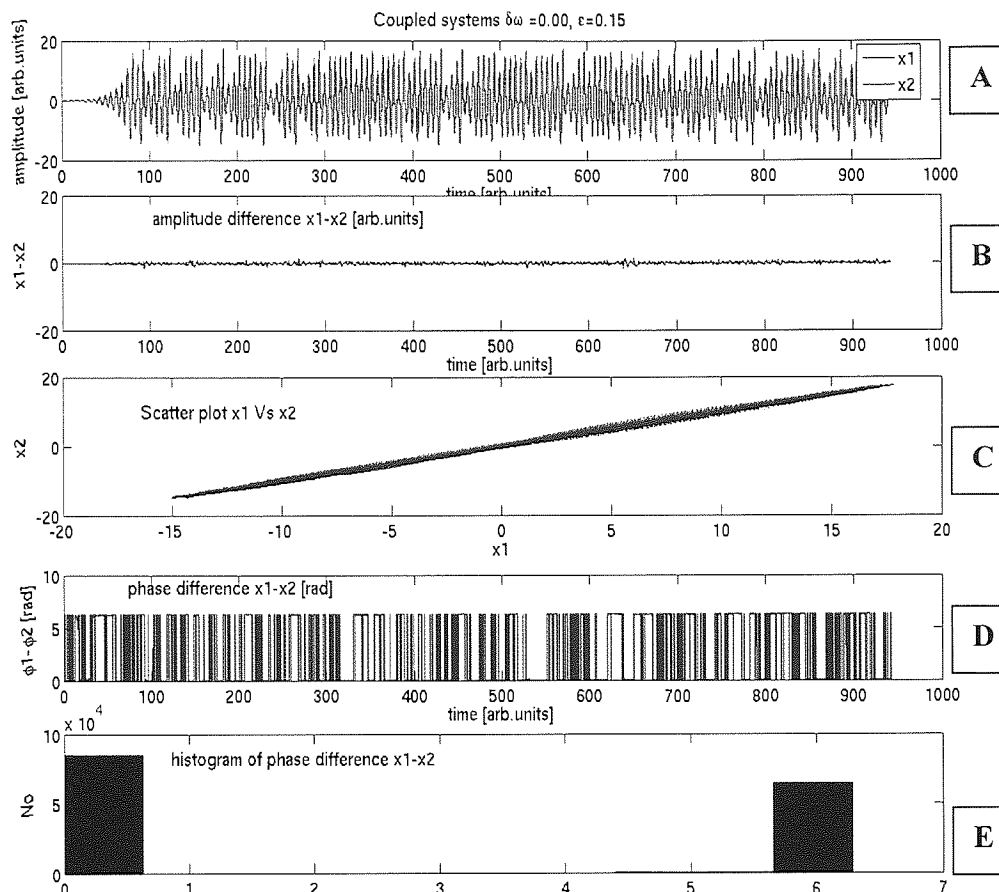


Figure 9. Almost identical synchronization. Linearly coupled identical Rössler systems as in [14], the frequency mismatch $\delta\omega$ is 0 and the coupling strength ε is 0.15. Panels from top to bottom: A: superimposed time courses of the $x_{1,2}$ variables, B: difference $x_1 - x_2$, C: x_1 Vs x_2 , D: time course of cyclic instantaneous phase difference $\delta\phi$ of $x_{1,2}$ variables mod 2π . The phase of each signal was extracted by means of the Hilbert transform (see chapters 2 and 5 and references therein) E: Distribution of instantaneous phase difference $\delta\phi$ mod 2π in radians.

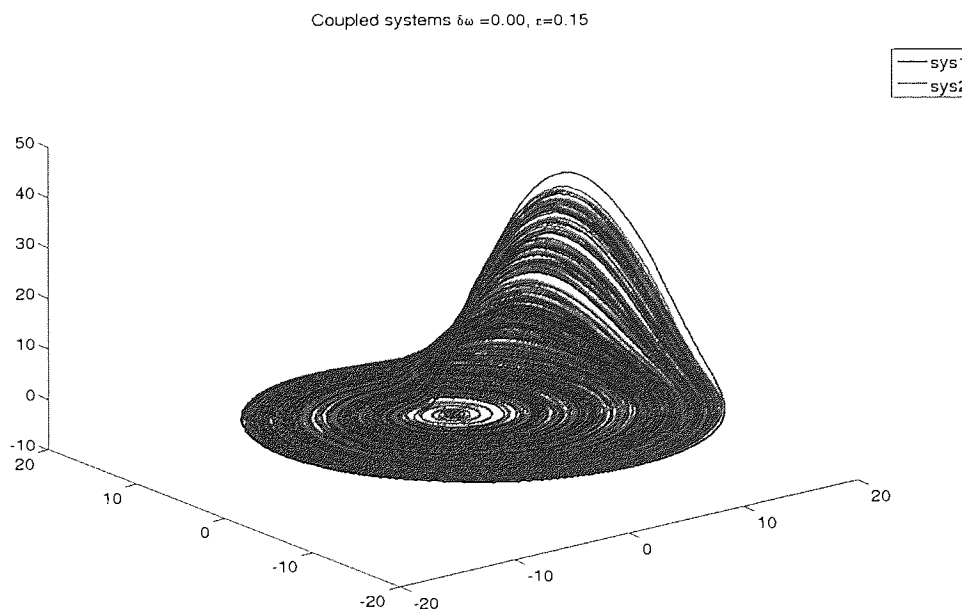


Figure 10. State space portrait of coupled systems in almost identical synchronization shown in figure 9. Note the almost identical evolution.

As previously illustrated, the stability of IS can be assessed in terms of the Lyapunov spectrum (see Boccaletti *et al.*, 2002, Breakspear, 2004) and more concretely in terms of the transverse Lyapunov exponents. These are the ones that correspond to the directions x_1-x_2 , y_1-y_2 and z_1-z_2 . A positive transversal exponent would mean that any perturbations along the corresponding direction will increase exponentially and thus the particular subspace of the synchronization manifold will become unstable. One can also think of the transverse Lyapunov exponents as the *slopes* of the instantaneous differences, such as the one plotted in figure 9B. If the slope is zero (the instantaneous difference remains flat) then a negative transverse Lyapunov exponent can be assumed.

The symmetry condition allows a powerful detailed study of the stability of coupled dynamics in geometrical terms. Indeed work by Pecora and Carroll and others has demonstrated that even for systems with complex spatial structure, analytical master stability functions can be derived (Pecora and Carroll, 1998). Generally, the stability of the synchronized state is a function of the coupling strength; stronger coupling generally ensures stability of the synchronization manifold in symmetric linearly coupled systems. However, exceptions exist when the coupling occurs through only one variable (Boccaletti *et al.*, 2002) or in the case of nonlinear coupling (Breakspear, 2002). The study of the dynamics of identical synchronization has shed also some light on desynchronization phenomena, common in coupled chaotic systems. In the symmetry condition, these are generally due to positive transverse Lyapunov exponents. They give rise to so-called ‘blow out’ bifurcations (Ott and Sommerer, 1994). In these cases the coupled dynamics are no longer confined on the synchronization manifold but become abruptly independent in a much higher dimensional space. Interestingly blow out bifurcations can be found above the critical coupling strength for which the transverse Lyapunov exponents are not positive. It has been shown, that these desynchronization bifurcations are due to unstable periodic orbits of low order (period -1 and -2), which are dense on the chaotic manifold. Thus, although a trajectory converging on the chaotic attractor may have an (average) negative transverse Lyapunov exponent, it may briefly ‘shadow’ the orbit of a nearby unstable periodic orbit embedded on the attractor. This gives rise to desynchronous bursts of *intermittent* character, thus involving a collection of time scales (Pikovsky and Grassberger, 1991, Rulkov and Sushchik, 1997, Maistrenko *et al.*, 1998, Heagy *et al.*, 1998, Breakspear, 2002 and 2003).

These effects can be studied by slowly decreasing the coupling parameter of the system in [14]. The transition to identical synchronization occurs through such a state, which is often referred to *modulational intermittency* (Pikovsky, Rosenblum and Kurths, 2001) or *on-off intermittency* (N. Platt, Spiegel and Tresser, 1993). This is illustrated in figure 11. The coupling parameter ϵ is set to 0.08 this time. We observe intermittent dynamics indicating a transverse instability. This can be indeed observed in panel B in terms of the instantaneous difference of the variables x_1, x_2 . Epochs of IS are irregularly disrupted by brief epochs of desynchronization and thus perturbations from the synchronization manifold. This can be indeed observed in panel C, now the

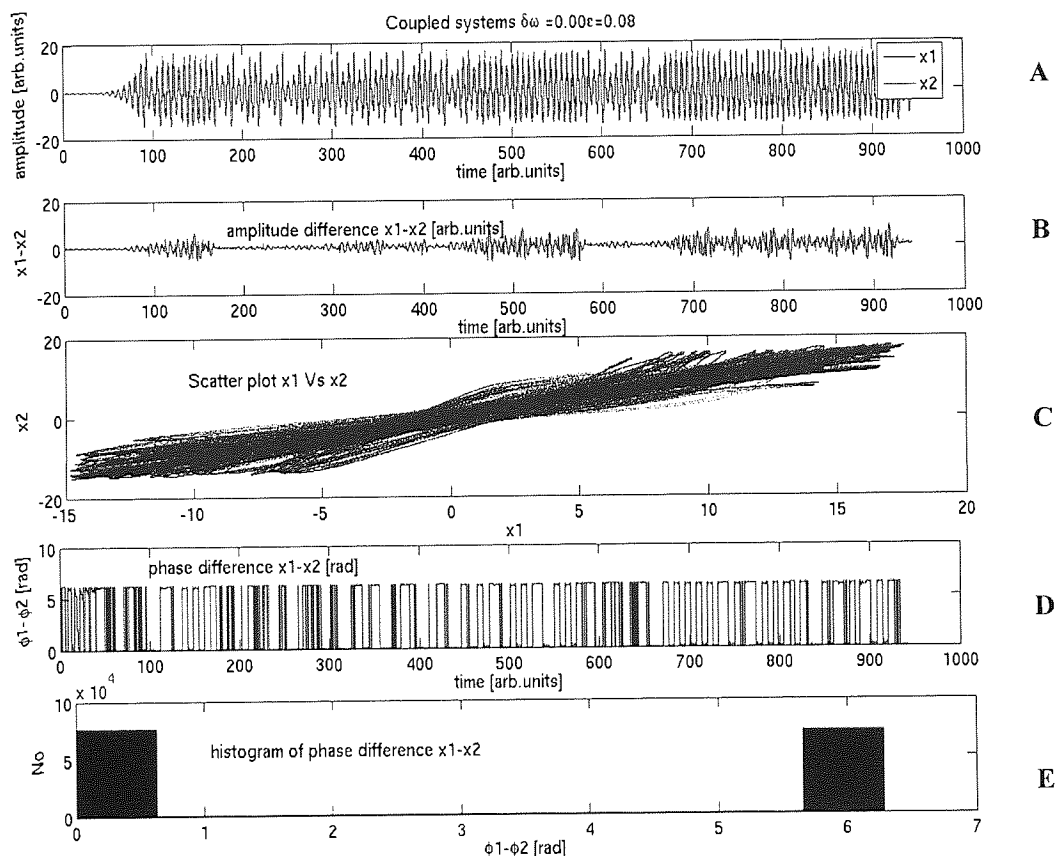


Figure 11. Modulational intermittency before the transition to identical synchronization. The figure has the same format as figure 9. The coupling parameter ϵ is set to 0.08. We can see that periods of identical synchronization are alternated with brief periods of desynchronization. These are evident as increases of the instantaneous difference plotted in panel B. In panel C we see that the coupled systems are no longer confined on the synchronization manifold. The phase difference is however relatively stable.

system is not confined along the diagonal but shows irregular perturbations away from it. However on average, the attractors (the long term dynamics) of the two systems almost completely overlap as evident in figure 12, which shows the state spaces of the coupled systems. As discussed above, the apparent irregular switches between IS and desynchronization are not random but may be due to *unstable periodic orbits* of higher order, and may therefore exhibit complex temporal structure. Similar bursting behaviour will be explored in chapter 7 with the example of MEG data during a visual experiment. Intermittent

behaviour in general has several advantages in terms of coordination dynamics in the brain; they will be discussed later with the example of intermittent phase dynamics.

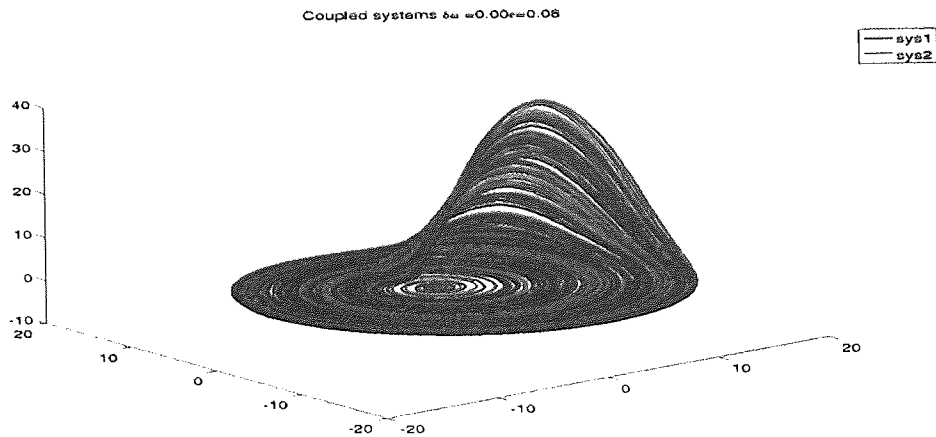


Figure 12. The state space portraits of the two coupled systems in intermittent identical synchronization shown in figure 11. Note the almost perfect coincidence of the attractors despite the intermittent bursts shown in figure 11B.

3.4.3 Breaking the symmetry: Phase, lag and generalized synchronization of nonidentical systems.

Until now we have considered synchronization of identical systems in terms of the synchronization manifold, which was supported on the invariant symmetry manifold. However, it is difficult to imagine that the symmetry condition will be met in the brain and thus that any two interacting neuronal systems will be identical. Actually, there is quite compelling evidence that this symmetry is not given. Such ‘broken symmetry’ conditions in the brain are thought to arise through a multitude of factors including asymmetric anatomical coupling between and within brain areas, differences in ‘characteristic’ oscillation frequencies of coupled neuronal networks, delays in neurotransmission in extended networks and differences in dendritic integration times (see Bressler and Kelso, 2001 for a comprehensive discussion of broken symmetry in brain dynamics). Furthermore, scale specific symmetry relations maybe the hallmark of the multiscale nature of the brain. Thus at microscopic levels of coordination – e.g. within cortical columns- a higher degree of symmetry might exist than at microscopic levels and thus interactions between such cortical columns (Mountcastle, 1997). The latter line of arguments will be pursued in chapter 4. For the current purposes we need only establish that broken symmetry conditions are especially relevant for the brain and thus the nature of the resultant coupled dynamics is of particular importance.

The broken symmetry condition can be understood in the general context of coupled dynamics and thus equation [12]. Recall that the functions f_a and f_b specify the form of the local dynamics. In the symmetry condition we dealt with the special case of $f_a = f_b$ and thus the two systems expressed the *identical* (autonomous) local dynamics. Also recall that this was the basis for the existence of an invariant set; the symmetry manifold, on which the (identical) synchronization manifold was supported. Breaking the symmetry means that f_a and f_b are no longer equal. Based on the geometrical framework underlying the concept of the synchronization manifold, research was centered on how the latter was effected by symmetry breaking. Two main scenarios seem to have been notable: small and large departures from symmetry lead to qualitatively different dynamics sometimes referred to as *weak* and *strong* generalized synchronization respectively (Pyragas, 1996). In the first case and especially when the synchronous dynamics are strongly stable (when the coupling is strong) a small symmetry breaking ‘lifts’ the resultant synchronization manifold smoothly ‘off’ the symmetry manifold (Josic, 1998, Kocarev *et al.* 2000). However, the synchronization manifold may still be attracting and hence synchronization will still occur (Kocarev and Parlitz, 1996, Breakspear, 2004). The trajectories of the two-coupled, nonidentical systems x^n and y^n will no longer be identical but will be instead related by a differentiable one-to-one functional relationship,

$$x^n(t) = \psi(y^n(t)) \quad [16]$$

Equation [16], simply states that there exists a smooth one to one correspondence between in the systems x^n and y^n at each time point t . Thus there is a deterministic function ψ , which maps the first system to the second one. This regime was first studied in unidirectional coupling (driver-response) schemes and is referred to as *generalized synchronization* (GS, Rulkov *et al.* 1995). The existence of ψ implies that the evolution of one system can be predicted by knowledge of the evolution of the second system. At weaker coupling strengths and thus less stable dynamics the dynamics, the synchronization manifold may become nondifferentiable (Hunt *et al.* 1997). The complex geometry of the synchronization manifold may mix features of the individual coupled nonidentical attractors or change strongly with only small modifications of asymmetry (see Breakspear, 2004 and references therein). This result has the important implication that stability of the synchronization manifold can not be assessed by virtue of tangential or transverse Lyapunov exponents, since there will be no *unique* tangential and transverse directions at every point on the manifold. However, the complex geometrical manifold ψ will remain *continuous*. This means that neighborhoods in one system can be mapped into neighborhoods of the other. As we have seen in chapter 2, this property was exploited in several methods in order to detect *nonlinear interdependence* (see

Shiff *et al.*, 1996, Breakspear and Terry, 2002a, Stam and Van Dijk, 2002). It is important to note that the latter detection exploits the similarity of local neighborhoods in isochronously occurring points in two systems to infer some interaction. Thus it does not specify the nature of the functional relationship in ψ , rather than it just postulates that such a relationship may exist.

We illustrate this state of affairs qualitatively in two interacting Rössler systems [14] when the frequency mismatch parameter $\delta\omega$ is no longer zero and thus the systems are nonidentical. Here $\omega_1 = 1$ and $\omega_2 = 0.85$ and thus $\delta\omega$ is set to 0.15. If the coupling parameter is set below the threshold range for identical synchronization here $\epsilon = 0.3$ a different pattern of synchronized behaviour results. Intermittent behaviour is no longer present but IS is not detectable either. Figure 13 illustrates the results. We can see that the two systems are not confined on the diagonal and their transversal variables do not approach zero. Thus we do not observe IS. Panel B shows the instantaneous difference and thus the transverse variable.

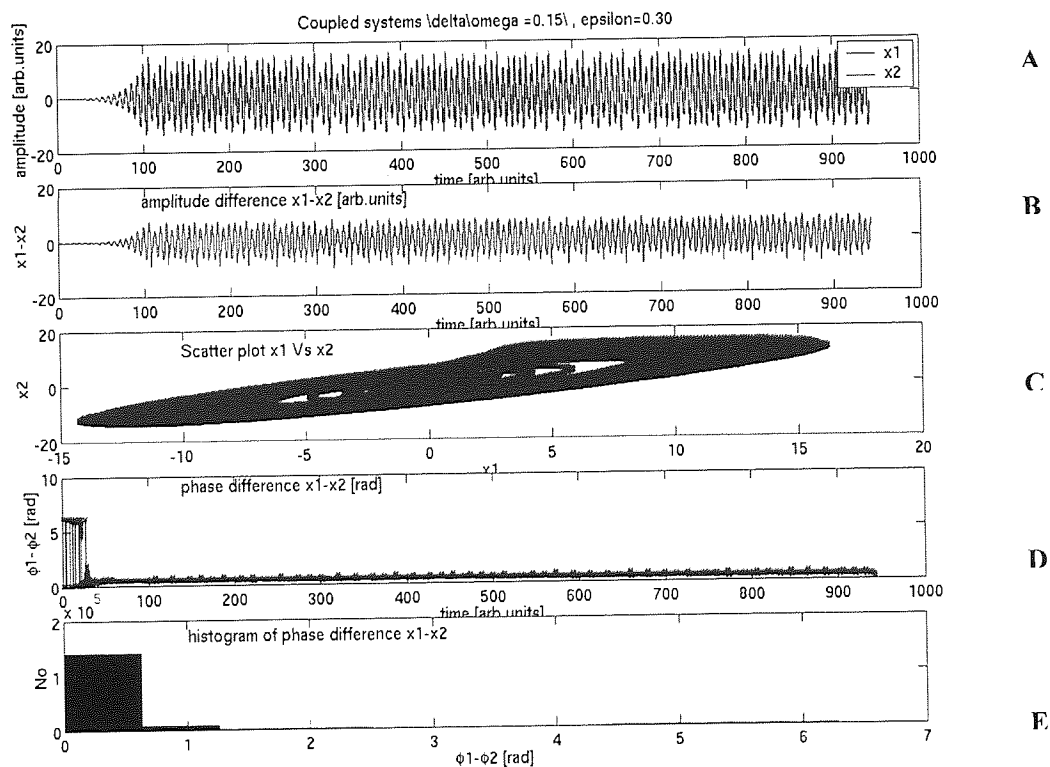


Figure 13. Nonidentical coupled systems possibly exhibiting generalized synchronization. Same format as figure 9. Panel B and C show the characteristic deviations of the synchronization manifold from the symmetry manifold. The instantaneous difference in B is of the same order as the signals themselves. Panels D and E show that phase synchronization is also present and supported on a more general synchronization manifold.

We can see that it is in the same order as the oscillatory variables of the attractors. However non-random structure is evidently present in the scatterplot shown in panel C. Thus the synchronization manifold is no longer supported on the symmetry manifold. Figure 14 shows the state space portraits of the coupled systems, this is consistent with panel C in figure 13:

nonidentical attractors, which however seem to be related, are observed. A look at panels D and E in figure 13 shows a bounded phase difference. Nevertheless, the classical notion of phase synchronization in chaotic systems implies that the amplitudes of the synchronized systems are not correlated, whereas the phases of the two systems are strongly interdependent (Rosenblum *et al.*, 1996). However, this is not the case here, as there seems to be strong correlation between the amplitudes of the interacting systems (panel C). Thus neither identical nor phase synchronization is observed in this case. Therefore generalized synchronization (GS) may be assumed (GS is not formally quantified). Interestingly, we see that in this particular situation the phase synchronization manifold seems to be supported on a more general manifold (panel C), or in other words the latter subsumes the former.

Several central comments are in order. Generalized synchronization is extremely relevant to coordination dynamics in the brain by virtue of the fact that it is a likely resultant form of dynamic interdependence when interacting systems are *not* identical. Strong generalized synchronization bearing marked resemblance with IS may result with small departures from symmetry as this may occur in microscopic networks of functionally interrelated neurons such as *within* a cortical column (chapter 4 and references therein). The synchronization manifold then may simply be a smooth displacement of the symmetry manifold and thus collective activity may reflect to a great extent merely an amplification of the behaviour of individual units. The latter may prove useful for achieving an effective signal to noise ratio in order to warrant successful neural transmission. Thus at the level of the cortical column this strong interdependence may underpin secure message transfer. However, excessive stability of such states may lead to self-sustained identical synchronization and be spread to a large array of units. This stereotype behaviour can then no longer be considered useful in terms of information processing since the entropy of the signal will remain low both in the temporal and spatial domain (Breakspear, 2002). Such states are typical of epilepsy and in fact metrics of generalized synchronization have shown increases before and during the onset of seizures in the EEG of epileptic patients (for instance Altenburg *et al.*, 2003). Perhaps on the opposite end of the continuum, a loss of synchronization can have dramatic consequence to memory and cognition. Using metrics based on the concept of generalized synchronization, Stam *et al.*, 2002 and Pijnenburg *et al.*, 2004 have found an overall decrease in gamma and beta band synchronization in the EEG of cognitively impaired Alzheimer patients. These two observations taken together show how important an 'appropriate' level of synchronization is for normal brain function.

As discussed above, a weaker form of generalized synchronization may come about when the coupling is not strong and the coupled systems are rather dissimilar. In this case the

synchronization manifold is not just a shifted version of the symmetry manifold but it may be a *mixture* of the effects of the two contributing attractors. Therefore, this kind of interdependence is inherently more integrative. Such a state of affairs, namely weaker coupling and larger departures from symmetry are likely to occur at mesoscopic scales in the brain for instance including interactions of neurons *between* cortical columns (chapter 4 and references therein). Thus it is interesting to explore the idea that weak generalized synchronization (together with phase synchronization as we shall see below) may be one of the common modes of coordination at such scales. This will be a sufficient way to produce a common signal (the synchronization manifold), which is a *mixture* of the dynamics of the contributing systems and not merely an *amplification* of the individual system dynamics (such as the synchronization manifold supported on the symmetry manifold). By small manipulation of the symmetry breaking parameters, macroscopic order may arise through mixing of nearby elements in to novel emergent structures and thus yield clustering behaviour. The latter will be illustrated extensively in chapter 4 by means of numerical simulations of spatially extended nonlinear systems. The symmetry breaking condition may also yield a multitude of interesting dynamic behaviours and phenomenology, which constitute global bifurcations. These include among others the emergence of periodic behaviour by increasing the coupling strength of chaotic systems a phenomenon known as chaos destroying synchronization and oscillation death by virtue of increased coupling (Pikovsky, Rosenblum and Kurths, 2001). Furthermore, these phenomena often lead to metastable intermittent behaviours, which are particularly favourable in terms of information processing and stability of the brain states. This will be next discussed using the example of phase synchronization in nonidentical systems.

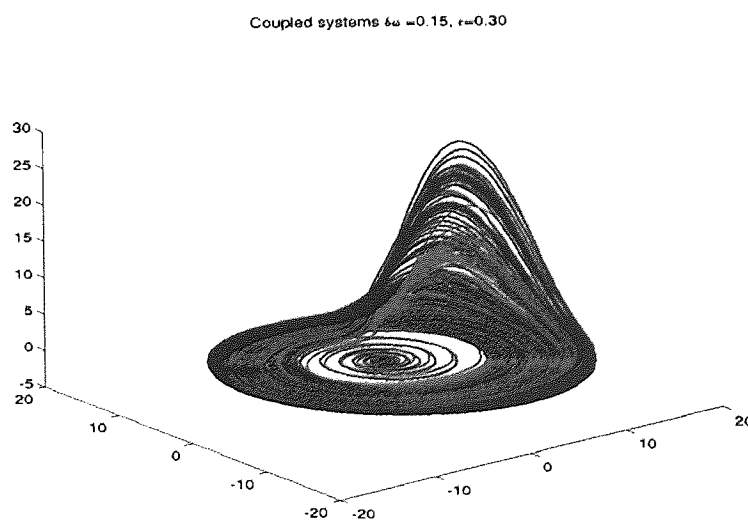


Figure 14 shows the state space of the coupled systems plotted in figure 13. We observe that the systems exhibit different but related long term attractors. Note, the difference between form of synchronization shown here and identical synchronization as shown in figure 10. Although no identical synchronization exists the two systems seem to exhibit some form of general interdependence.

In section 3.41 we have already suggested that in some cases an appropriate phase can be defined for a chaotic system. We have also seen that the synchronization occurs through the adjustment of the *average* frequency of the interacting systems. The existence of a mean period of oscillation and a bounded distribution of instantaneous periods around the mean has the consequence that the instantaneous phase difference between two interacting systems is bounded. The main implications of this approach is that chaotic systems can be treated in the same way as noisy systems: synchronization can be defined in a statistical sense, thus as a process with some mean value and an amount of phase diffusion about that mean (equations [10] for chaotic and [11] for noisy systems). As we have already seen in chapter 2, the sufficient condition for phase synchronization is:

$$\delta\phi = [n\phi_k - m\phi_l] \bmod 2\pi \leq c \quad [17]$$

where ϕ_k, ϕ_l are the *instantaneous* phases of two systems k and l , c is a constant and n, m are integers defining the frequency ratio of the systems. The instantaneous phase difference $\delta\phi$ is wrapped in the interval $[0, 2\pi]$.

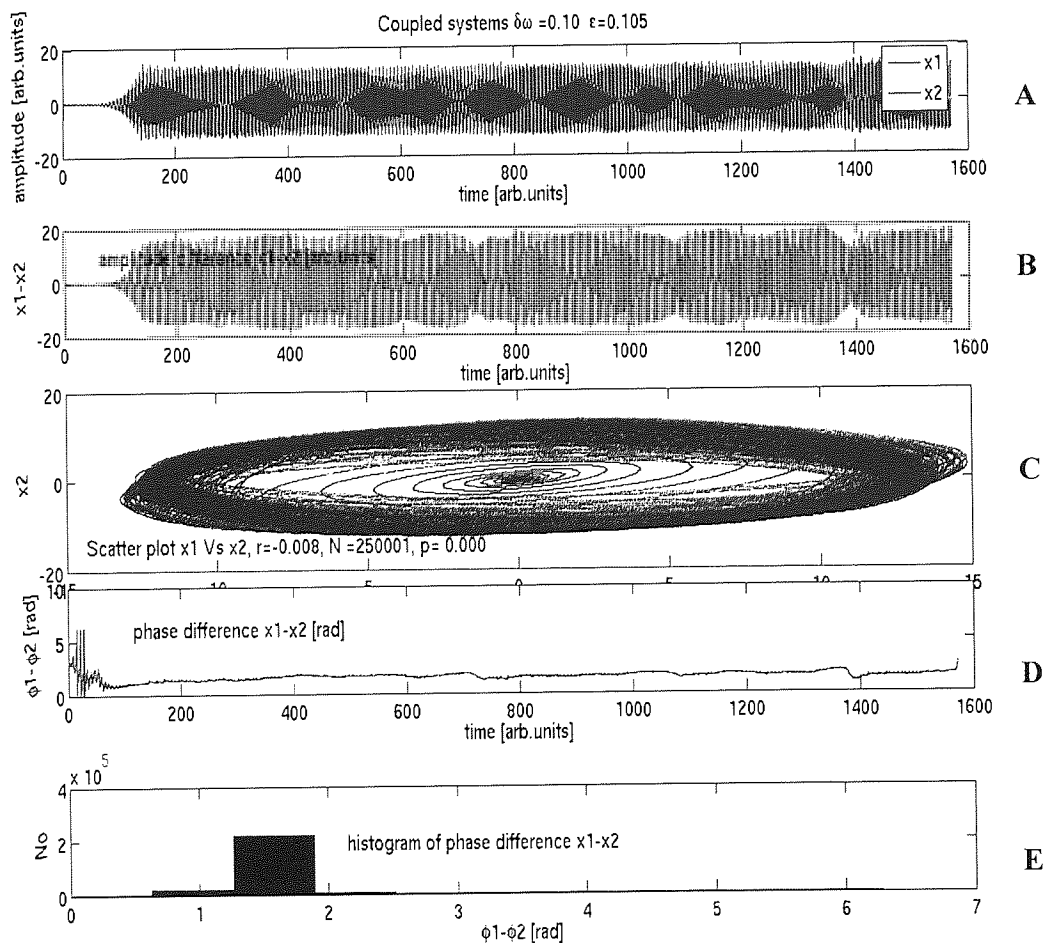


Figure 15. Phase synchronization of nonidentical chaotic systems for low coupling strengths. Same format as figure 9. The phase difference of the two systems is bounded (panel D) and its distribution is normal

around a preferred value of 1.5 radians (panel E). At the same time the amplitudes of the systems are not strongly related (panels A and C).

Rosenblum *et al.*, 1996 have shown for the first time that phase synchronization of mutually coupled chaotic systems is possible by itself and thus unaccompanied by identical or generalized synchronization. The hallmark of phase synchronization in chaotic systems seems to be that although the phase difference of two coupled systems is bounded, the amplitudes may remain chaotic and uncorrelated. Phase synchronization in nonlinear systems is of theoretical importance because it represents the weakest form of interdependence; it does not require adjustment of the systems' manifolds but merely adjustment of their time scales *on average*.

Two theoretical points make phase synchronization relevant for the brain. As we shall see below phase synchronization can occur in the presence of very *weak* couplings even between considerably *dissimilar* systems. Thus phase synchronization requires neither similarity of the interacting systems nor strong coupling to come to pass. In addition, phase synchronization between dissimilar systems and weak couplings is often intermittent, which might prove of adaptive importance for brain function. Further, interacting systems exhibiting phase synchronization can demonstrate lag, generalized and identical synchronization with increasing levels of coupling (Boccaletti *et al.*, 2002).

We briefly illustrate the typical phenomenology related to phase synchronization with the system in [14] in figures 15 and 16. The systems are not identical, $\omega_1 = 1$ and $\omega_2 = 0.9$ and thus $\delta\omega$ is set to 0.1. The coupling parameter is set to $\varepsilon = 0.105$. Panel A in figure 15 shows the $x_{1,2}$ variables. We observe little relation between the amplitudes but some regularity in

Coupled systems $\delta\omega = 0.10$ $\varepsilon = 0.105$

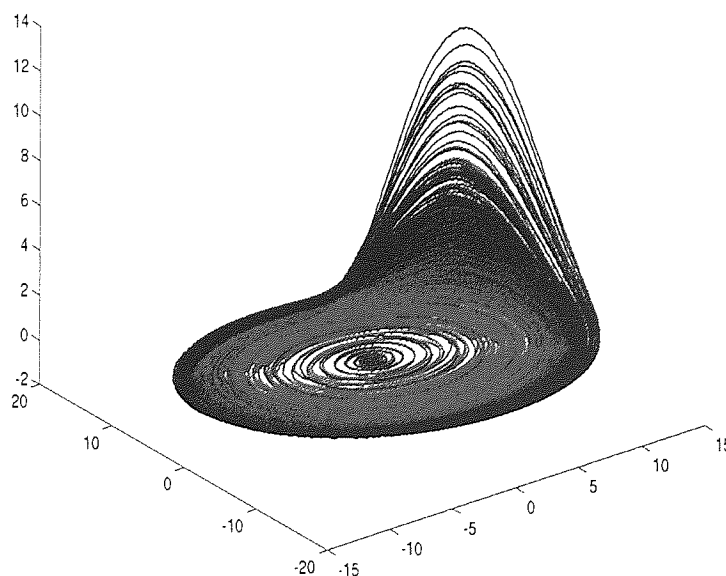


Figure 16. State space of phase synchronized nonidentical systems plotted in figure 15. Note that the systems are not supported on a common manifold.

the relation of the time scales of the two systems. The instantaneous amplitude difference in B is of the same magnitude as the variables themselves and thus the synchronization manifold is not supported on the symmetry manifold. This is evident also in C where we see that the system is not confined on the main diagonal and the correlation between the amplitude of the variables is lower than 0.01. However there is some ellipsoid structure here corresponding to the adjustment of the time scales. The latter is observed in panel D, which shows a bounded phase difference as a function of time. Panel E shows the distribution of the phase difference. We observe a narrow normal distribution centred around 1.5 radians. Thus *phase synchronization* is observed in the absence of *amplitude correlation*. The state space plots of the two coupled systems are shown in figure 16. We see that the systems exhibit different attractors; even a weak form of a relationship is difficult to infer. In other words, the interacting systems seem to preserve their overall differences in terms of long-term dynamics but at the same time merely adjust their phases. This weak interaction can be captured in the spectrum of Lyapunov exponents, where the onset of phase synchronization is marked by a (previously zero) Lyapunov exponent becoming negative (Rosenblum *et al.*, 1996). This exponent corresponds to the direction in state space related to the phase difference. A negative exponent means that perturbations along the direction of the phase will exponentially decay and thus the phase difference will remain bounded. We should note the difference to the case of identical synchronization. In identical synchronization strong criteria were imposed on the transverse Lyapunov exponents to ensure stability of synchronization. Here the adjustment of merely one of the previously zero Lyapunov exponents (corresponding to the direction of the flow and thus of the phase) to negative values is sufficient to ensure stability.

It should be noted that phase synchronization occurs also in identical systems for low levels of coupling, however then it is supported on the symmetry manifold. Thus substantial correlations of the amplitudes will be expected even at low levels of coupling.

If the detuning of the systems in terms of the frequency difference $\delta\omega$ is increased phase synchronization may become unstable. This can be understood in terms of equation [10], where this would correspond to a growing phase diffusion term of deterministic origin. For a range of parameters intermittent phase synchronization occurs. This illustrated in figure 17. The two systems exhibit a regime of intermittent oscillations and apparent silence, a phenomenon known as on-off intermittency (Platt, Spiegel and Tresser, 1993). Similar to the case of modulational intermittency, which occurred for low coupling in identical systems,

here the instantaneous difference varies as a function of time. The instantaneous difference mimics the time course of the variables and is close to zero, only when the amplitude in both systems diminishes. This is not a simple short-lived digression from the symmetry manifold. Indeed, in panel C we observe a less regular synchronization manifold. In panel D we see that the phase difference remains stable for longer epochs but this is interrupted by irregularly occurring short desynchronization bursts. The distribution of the phase difference still shows a preferred value but the entropy of the distribution is now larger. Figure 18 shows the state space for the coupled systems. Note that the typical Rössler attractors have collapsed and we observe a *structural* change resulting to a remnant of the chaotic dynamics. This is often referred to as a *chaotic ruin* (Boccaletti *et al.*, 2002). Thus the strong coupling between dissimilar oscillators that causes the instability of the phase also causes the dissipation. Oscillation death a consequence of the strong coupling and the frequency detuning contributes to the dynamic ‘shrinkage’ of the coupled systems.

Two aspects of these interactions are of main interest here. The first one is related to the implications of intermittent phase dynamics for the stability and the information capacity of a given interaction. The second aspect relates to the observation of oscillation death (or quenching), which is observed during desynchronised epochs.

Firstly, the behaviour of the phase difference is very important. It captures the hallmarks of what Kelso refers to as *metastability* (Kelso, 1995, Bressler and Kelso, 2001). The phase difference is the collective variable, which specifies the interaction between the two systems. In the case of intermittent dynamics the phase difference alternates between periods of stability and periods of instability. Thus the phase difference is stable in relative terms (metastable). Thus for the *same* configuration of control parameters the coupled system will be asymptotically confined on the phase synchronization manifold. However, departures from the manifold will occur and will ensure for entropy. As previously discussed, this itinerant type of behaviour may be useful for brain systems because of the need for context sensitivity and constant updating of information. Thus the intermittent wondering of the system off the phase synchronization manifold (and thus the epochs of phase desynchronization) might constitute some search process and the reinjection to the manifold might subservise some ‘updating’ process. Moreover, the importance of intermittency in such an ‘updating’ process manifests itself in extensive network of coupled elements: synchronization may lead to formation of clusters; spontaneous desynchronization may lead to dissolution of these clusters and formation of different clustering configurations. If synchronization is too stable, then these configurations will be rigid and thus non adaptive. Thus intermittent behaviour of phase

synchronization is deemed functional by virtue of its instability (*metastability*). The latter however also ensures higher entropy (uncertainty) of the signal.

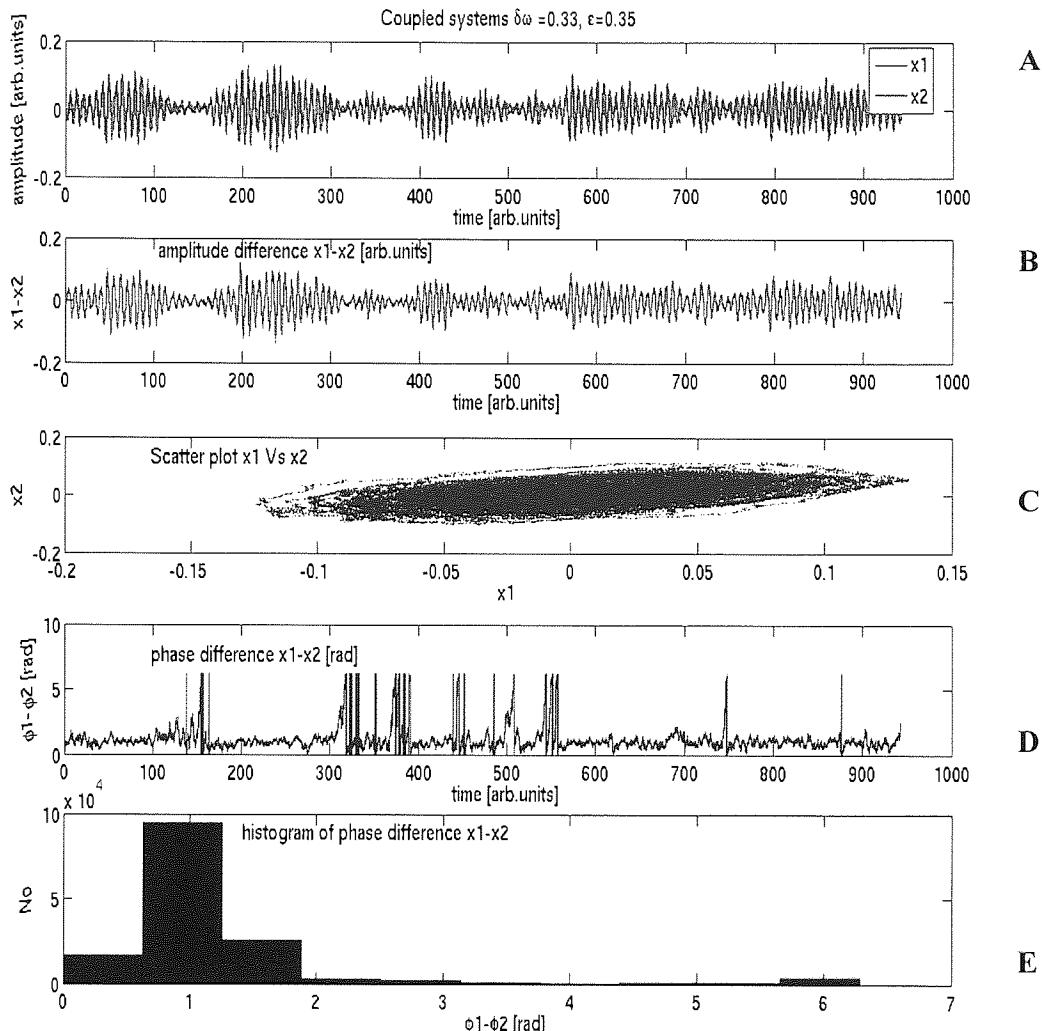


Figure 17. Intermittent dynamics in strongly coupled nonidentical systems. Same format as figure 9. Note the bursting oscillations in the two coupled systems (panel A). Also note that the instantaneous amplitude difference is itself bursting (panel B). However the phase difference for the coupled systems is bounded for long periods of time, which are alternated by periods of phase desynchronization (panel C). These desynchronizing bursts seem to occur irregularly and coincide with amplitude minima (panel A). However, on the whole the phase difference distribution is normally distributed and peaks around 1 radian, suggesting phase synchronization.

It has been proposed (Breakspear, 2002 and 2004,) that a signal composed of epochs of alternating phase synchronization and desynchronization has a very high information capacity (Galtin, 1972). Simply stated, synchronous epochs ensure secure message transfer and desynchronous epochs warrant sufficient message entropy. Thus intermittent phase dynamics maybe beneficial both in terms of its adaptive and flexible nature and also because of its high information capacity (Breakspear, Terry and Friston, 2003, Breakspear, Williams and Stam, 2004). Intermittent synchronization and desynchronization and spatial clustering behaviour has been indeed observed in realistic models of coupled cortical columns (Breakspear, Terry and Friston, 2003). Furthermore, evidence for unstable synchronized clusters in the spatial

and temporal domain has been obtained in scalp EEG recordings (Breakspear, Williams and Stam, 2004). Unstable and rapidly fluctuating synchronization levels have also been experimentally observed in spontaneous MEG activity (Stam *et al.*, 2003) and task-related EEG recordings (Stam, van Walsum and Micheloyannis, 2002).

The second interesting observation here refers to the phenomenon of oscillation death or ‘quenching’. This phenomenon of amplitude deterioration often occurs in situations where diffusive coupling is introduced between inherently dissimilar systems. In the case presented here the dissimilarity is expressed in terms of frequency detuning. The phenomenon of oscillation death was observed in a number of diverse physical and biological systems. It seems to be a particularly frequent phenomenon in coupled oscillatory systems that exhibit a continuous spatial coupling pattern in the presence of spatial gradients in the natural frequency (Pikovsky, Rosenblum and Kurths, 2001). The biophysical mechanism of the phenomenon is simple. The mismatch of the frequency of coupled elements leads to an ever-growing phase difference. On the other hand the (diffusive) coupling tends to reduce the phase difference.

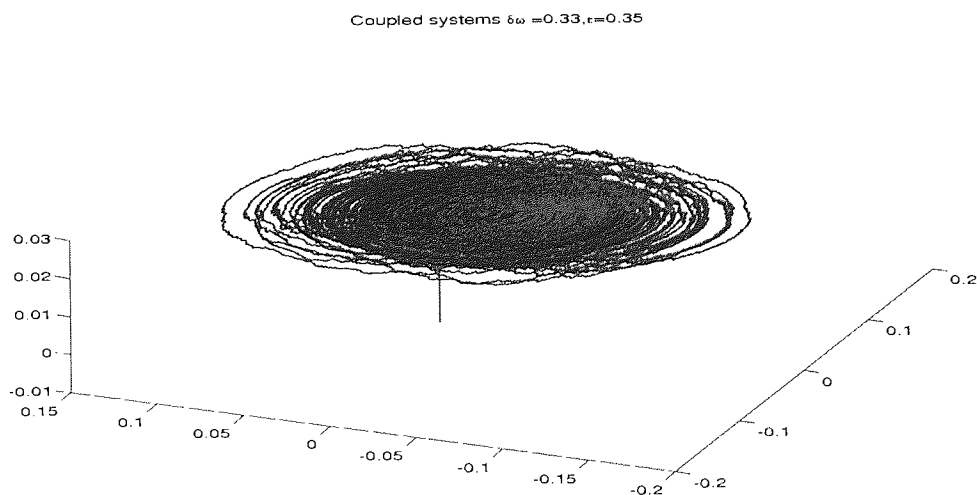


Figure 18. State space of coupled systems exhibiting intermittent phase dynamics, see figure 17 and text. Note that the typical Rössler attractors have collapsed and we observe a structural change resulting to a remnant of the uncoupled dynamics. This is often called a chaotic ruin. The synchronization manifold is difficult to define in this case.

The only way these things can be compromised, so that an energetic (short wavelength) catastrophe can be avoided, is for the amplitude to strongly diminish, in which case the phase cannot be defined. This results in the appearance of *space-time defects* (Pikovsky, Rosenblum and Kurths, 2001). The appearance of oscillation death through such space-time defects can be viewed as a mechanism for effective ‘restarting’ of the system. Ermentrout and Koppel (1984) have shown that oscillation death occurs in mammalian intestine at the border of functional clusters of smooth muscle tissue. The clusters are defined as muscle tissue segments, which show the same characteristic frequency of excitation. An oral to aboral

frequency gradient is utilised to achieve peristaltic motion. Thus the frequency gradient has to be maintained despite the *local* coupling of the smooth muscle cells occurring through direct electrical contacts (gap junctions). Oscillation death is a mechanism that helps maintaining this gradient in the presence of coupling. In chapter 4 we will argue that maybe similar gradients are at play in the brain, in order to achieve functional separation (possibly again through a characteristic distribution of frequencies) in the presence of strong influences towards integration. Oscillation death may therefore contribute to the separation of dynamic synchronized clusters. It should be also stressed that oscillation death does not only occur at specific parameter configurations but for a wider range of parameters.

3.4.4 Succession of qualitatively different synchronization regimes with increasing coupling

Phase synchronization of chaotic systems seems to be one of the most common forms of interaction; it can be observed for a range of control parameters and it is possible for relatively dissimilar systems and weak couplings strengths. Meanwhile a series of related phenomena have been reported, for reasons of limited space we will not present detailed examples. However a depiction of how these phenomena relate to each other and how they depend on the coupling strength may be useful.

When the coupling is not sufficiently strong *or* the frequency detuning (or any other parameter contributing to symmetry breaking) is relatively large with respect to the coupling strength, phase synchronization in the sense of equality in equation [17] may not be possible. The common denominator in these situations is the existence of a *rather broad* distribution of time scales in the behaviour of the *coupled* system. This reminds us of section 3.4.1 and the distinction of phase coherent and non-coherent attractors of individual systems. For instance a Lorenz attractor exhibits a broader distribution of time scale and it is thus difficult to synchronize perfectly and thus so that the phase difference with some driving force remains stable. In such cases the phase difference shows periods of rather bounded acceleration and deceleration excursions. Furthermore phase slips of 2π may occur but the phase difference remains relatively bounded when defined not on the full line but on the circle $[0, 2\pi]$. Note that this is not the same as intermittent phase dynamics where epochs of stable phase difference and epochs of apparently random behaviour were alternated. Here the phase difference is *never* quite stable but because it remains bounded, the distribution of the phase has a preferred value. This regime has been termed *imperfect phase synchronization (IPS)*. For a discussion see Boccaletti *et al.*, 2002 and references there in. In broader sense IPS may be considered as

another case of relative coordination (Kelso, 1995) other than the one arising from intermittency.

A second phenomenon related to phase synchronization of nonidentical systems occurs when the coupling is increased but is not sufficient to instate generalized or identical synchronization. Then the interesting phenomenon of *lag synchronization* occurs (Rosenblum *et al.*, 1997). This can be considered as a compromise situation between phase and identical synchronization. Essentially, in lag synchronization a signal $x_1(t)$ is approximately equal to a shifted version of another signal x_2 with some time lag τ :

$$x_2(t + \tau) \approx x_1(t) \quad [18]$$

Thus if one plots the two signals against each other one will obtain concentration along a straight line as in the case of identical synchronization. The phase difference will be constant but different than zero corresponding to some phase lag. Thus the lag synchronization (LS) manifold can be considered to be an (asymmetrically) shifted version of the symmetry manifold. Rosenblum *et al.*, 1997 proposed a method of detection of LS from data using a similarity metric. As we have seen in the previous section phase synchronization of nonidentical systems was accompanied by a change of one of the previously zero Lyapunov exponents that corresponded to the autonomous phases of the system. In phase synchronization one of these exponents becomes negative. When a second exponent becomes negative with increasing coupling either (strong) generalized or almost identical synchronization will occur. The regime of lag synchronization is situated somewhere in-between these two states. The transition from phase to lag synchronization occurs through a regime of intermittent lag synchronization. Analogously to intermittent IS here epochs of lag synchronization are alternated with epochs of unbounded errors in the similarity metric (Boccaletti *et al.*, 2002). An example of this will be shown in chapter 7 in the context of on-off intermittency.

To sum up, the interaction of nonidentical chaotic systems may result in a number of qualitatively different but interrelated synchronization phenomena. Which particular form of synchronization will occur crucially depends on the coupling parameter. For low levels of coupling phase synchronization occurs, with increasing coupling lag, generalized and almost complete synchronization may occur. The degree of total interdependence increases with the coupling (provided the systems are not too dissimilar to be synchronized). The transition regions between these regimes may be pinpointed by intermittent dynamics of the phase

difference, the amplitude at a certain lag or the combined amplitude and phase dynamics. Thus, once more we note that for a range of parameters intermittent coordination dynamics (metastability) are present. It is tempting to postulate that time dependent coupling parameters, as they may occur in the brain in terms of neuromodulators stemming from arousal systems (Breakspear, Terry and Friston, 2003) or indeed common influences of third parties on to two interacting sites, may provide us with brain dynamics, which exhibit such a rich spectrum of synchronization phenomena as the ones depicted here. Furthermore, these phenomena once expressed may subserve different functions.

To conclude, we have seen that inherently dissimilar systems, (thinking back to the breaking symmetry condition) can exhibit synchronization but they require higher coupling strengths and dissipate energy to do so. However, this is due to their tendency to preserve their autonomous dynamics. The coordination scenarios, which arise, are likely to involve intermittent coordination dynamics. If such processes were to occur in the brain, they may often concur with energy dissipation (oscillation death) and could be thus captured as amplitude changes in metabolic and electric measures of mean neuronal activity. Oscillation death when occurring on the basis of intermittent phase dynamics might be a phenomenon related to resetting the subtle equilibrium dynamics between different oscillatory processes (segregation) and inherent structural coupling (functional integration).

3.4.5 Chaos destroying synchronization and structural changes in attractor morphology

An interesting situation arises, when distinctly dissimilar chaotic systems are strongly coupled in terms of diffusive coupling (equation [15]). An example is illustrated in figure 19A. The systems are initiated with frequency detuning $\delta\omega=0.30$ and the coupling strength is set to $\epsilon=0.35$. The coupling is transiently introduced between roughly around 300 and 900 time units (shown by red vertical lines on the top panel). The bottom panel shows the phase difference defined on the real line (unwrapped). We observe that the phase difference remains constant during the coupling, while before and after the coupling it accelerates due to the frequency detuning. However the most striking effect is a decrease of the mean power and a regularization of the oscillation. Panel B on the right shows a detail of the time around which the coupling is switched on. Before the introduction of the coupling the systems exhibit independent chaotic oscillations. After the coupling is switched on an abrupt transition occurs, which leads to a state of almost periodic synchronous oscillation in both systems. Thus the systems are synchronized but no longer chaotic. This phenomenon is known as chaos destroying synchronization (Pikovsky, Rosenblum and Kurths, 2001) and seems to occur through a global bifurcation, where several Lyapunov exponents become abruptly negative

resulting to low dimensional periodic dynamics (Boccaletti *et al.*, 2002). Similar phenomena can be observed when chaotic systems are driven by a periodic force of a sufficiently different characteristic frequency (not shown here).

This phenomenon may be of considerable theoretical interest. In many experimental paradigms in traditional neurophysiology, 'driving' stimuli are presented. These stimuli (either visual or auditory) are periodic and often seem to be faithfully transmitted to the brainstem nuclei as such (for example Rees and Moller, 1987). It has been also repeatedly argued that similar behaviour occurs even at higher processing stages, namely at the cortical level. Hence, the sensory cortex is thought to closely follow the periodic dynamics inherent in the stimulus in terms of a steady state response (for example see Picton *et al.*, 1987). One should note the similarity of this scenario to the theoretical example of chaos destroying synchronization given above. Thus if these regular stimuli give rise to a strong periodic input from the brain stem to the sensory cortex, this may under circumstances cause a 'regularization' of the previously 'irregular' spontaneous activity in the cortex. Thus by introducing salient and artificially regular stimuli, one may enforce stable periodic dynamics upon the sensory cortex, which however may be *uncharacteristic* for the spontaneous cortical dynamics. This will be illustrated with the example of the auditory steady state response in chapter 5.

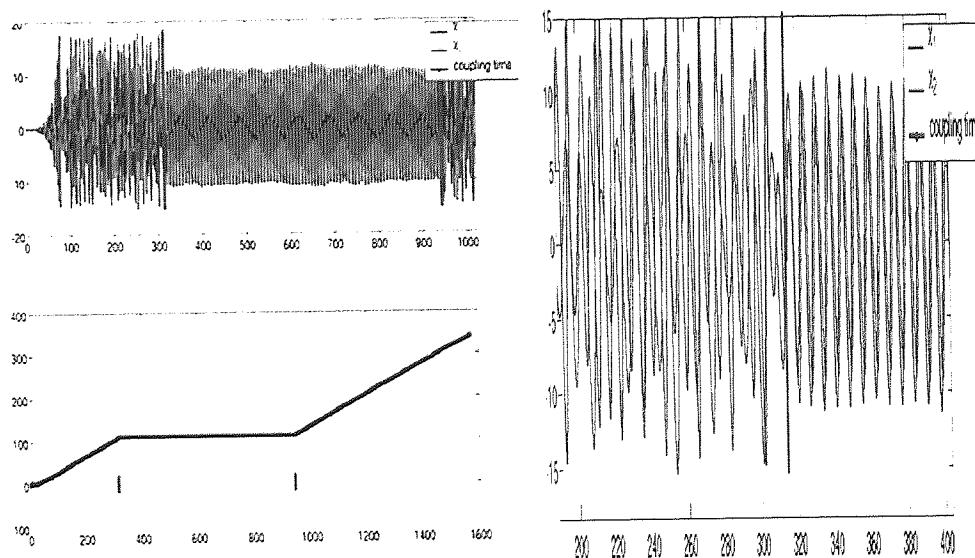


Figure 19 A (left) and B right. Chaos destroying synchronization. See text for details.

3.5 Concluding remarks

In this chapter we have examined the simplest case of dynamics governed by a two opponent gradient interplay of forces subserving integration on one hand and forces seeking segregation on the other (Friston, 2000 b, c). In the simple models of coupled chaotic oscillators we examined here, the coupling was the force seeking functional integration of the dynamics and

the frequency detuning (the non-identity of the oscillators) was the force that tended to keep the dynamics segregated. Although we realize the limitations of this simple approach, we are intrigued by the rich diversity of dynamics that can be generated by such simple models. Even in such simple models, a variety of qualitatively different synchronization and desynchronization behaviours occur. Here an attempt is made to *specify* which mechanisms and which of the synchronization/desynchronization regimes may underlie the generic process of functional integration and segregation (Friston 2000, b, c). This is clearly a difficult but nevertheless extremely important step towards understanding the exact dynamic substrates of functional integration and segregation (Breakspear, 2004). The work presented here is by no means exhaustive nor conclusive, which is not surprising considering that the literature centred on this issue is limited to a few pioneering papers, that have been published in the recent couple of years (Breakspear, 2002 and 2004, Breakspear, Terry and Friston, 2003, Stam *et al.*, 2003, Breakspear, Williams and Stam, 2004). However the stress in this work will be on identifying patterns of phenomenology, specifically related to these dynamic scenarios, so that these can be tested using experimental data arising from macroscopic brain signals. Intermittent bursting, oscillation death and chaos destroying synchronization are key phenomena occurring in abstract models of coupled chaotic oscillators exhibiting complex synchronization dynamics. These will be further pursued in simulations of spatially extended systems in chapter 4 and also potential links to experimentally observed MEG data will be attempted in chapters 5, 6 and 7.

Chapter 4. Event Related Synchronization and Desynchronization and their relation to macroscopic spatiotemporal patterns in complex systems.

4.1. Objectives

We have seen in the previous chapter that even the coordination of merely two coupled nonlinear systems can produce a multitude of distinct synchronization regimes and associated phenomenology. In this chapter we will investigate coordination phenomena in multidimensional systems, which exhibit an explicit spatial structure. The scope of this work is not so much to review the existent body of literature but rather to focus on specific configurations relevant to the functional organization of the brain. The main objective here is to identify the relationship between spatiotemporal macroscopic patterns formed through specific interactions in the system to the observed changes in the mean field signal. Thus, essentially we will attempt to address yet another inverse problem: Can the changes in the mean field signal tell us anything about the coordination process that is occurring in the underlying network? Explicitly, we are very much interested to test the ERD/ERS model (Pfurtscheller and Lopes Da Silva, 1999). Event related desynchronisation (ERD) and synchronisation (ERS) are thought to reflect processes of desynchronization/synchronization of interconnected neurons at the microscopic level resulting in decreases or increases of the macroscopic (MEG/EEG measured) mean field respectively. Therefore, according to this model, a power decrease is interpreted as a loss of synchronization and a power increase as an increase in local synchronization.

4.2 Basic axioms of synergetics and pattern forming systems

The basic theoretical framework we adhere to is *synergetics* (Haken, 1983). The field was founded by the German theoretical physicist Hermann Haken and deals with complex systems, defined as systems with several interacting subcomponents, which 'live' far from thermal equilibrium and therefore often undergo (non-equilibrium) phase transitions. The latter framework applies to a multitude of physical systems but also subsumes all biological systems including brain and behavioural systems (Kelso, 1995). Perhaps the most central concept in synergetics is the one of *circular causality*. The latter states that macroscopic variables are formed through interactions of microscopic system subcomponents, but when created they in turn specify the behaviour of the global system and thus *constrain* the activity of each and every microscopic subcomponent. Hence, we identify two main characteristics in this framework: there are more than one (at least two) levels of description: a microscopic one and an *emergent* macroscopic level. However, no level is more important than another because they are mutually interactive in terms of circular causality. Thus interactions in the microscopic level give rise to a lower dimensional macroscopic order state (often these states are spatiotemporal patterns), which is in turn specified by only a few variables, termed as *collective variables* or *order*

parameters. Once such macroscopic patterns are formed, they are governed by the order parameters and they in turn influence and *constrain* the activity of individual subcomponents at a microscopic level. Thus, the system exhibits self-organization by virtue of circular causality and the concurrent existence and interaction of multiple levels of description. One of the simplest forms of such a self-organization will be demonstrated in a network of globally coupled oscillators (termed as Kuramoto self-organization, see Kuramoto, 1975, 1984 and Strogatz, 2000). The beauty of synergetics is that in a complex system with an infinite number of degrees of freedom, only a few order parameters are sufficient to entirely specify the system. Thus the system undergoes a dimensional reduction through interaction. Therefore if one can specify the collective variables, the ones that specify the interactions of system subcomponents, one can specify the system. As a control parameter is varied slowly, such systems undergo abrupt changes in their behaviour; these are referred to as *phase transitions*. By virtue of the fact that such systems 'live' far from equilibrium, phase transitions are common for a range of parameters, and thus the resultant macroscopic activity continuously changes. This results to spatiotemporal pattern formation.

The scope of our work will be to explore some potential collective variables that lead to macroscopic patterns and how they change with respect to global system parameters. Since the brain is a multiscale system, we should identify *scale-specific* order parameters and see how they may contribute to the macroscopic patterns. Explicitly, we view ERD/ERS as macroscopic spatiotemporal patterns resulting from neuronal interactions in a spatially-extended, multiscale network and we want to know the collective variables and the resultant coordination dynamics, which may have produced these patterns. We also, address the viability of the model for microscopic and mesoscopic levels of description and discuss possible models of interpretation of macroscopic mean field signals.

4.3. The brain as a multiscale system

There are two characteristics that are sufficient for synergetic coordination dynamics to come about in an arbitrary system: the system has to be nonlinear and its units have to be coupled (Jirsa and Haken, 1996). The brain clearly fulfils both of these criteria. A third common characteristic of synergetic systems is complexity, a hallmark of which is the existence of multiple spatial and temporal scales. The brain is perhaps the prime example of a highly ordered multiscale system. Furthermore, temporal and spatial scales are not independent; for each spatial scale there are characteristic temporal scales. There are at least three discernible levels of brain organization; they are very much reflected in the spatial differentiation of the brain (Breakspear, Terry and Friston, 2003, Breakspear, 2004 and Breakspear and Stam, 2004). These are a microscopic level, which involves coordination of neurons that belong to the same

functional unit, such as the cortical column (Mountcastle, 1997 and 2003). The next level, to which we will refer to as *mesoscopic*, involves interactions between neurons belonging to different functional units, thus interactions of neurons between cortical columns. The interactions at the mesoscopic and microscopic levels produce a ‘macroscopic’ signal reflecting the collective activity of many cortical columns. This macroscopic signal is thought to reflect the collective activity happening at the level of a brain area. We should stress, that here we use the term ‘macroscopic’ for the activity of a functional *brain area* rather than the activity of the entire brain system. Such a definition of macroscopic activity is helpful in the interpretation of brain signals such as the EEG and the MEG, which probably arise at this level. However, we understand that ‘functional’ brain activity may well involve the coordination of several brain areas and subcortical regions. Thus the macroscopic signal arising from a brain area may reflect only a part of the total brain activity subserving a certain function.

The differentiation into the above levels of description essentially comes about through the interplay of two key factors, which in terms of synergetics can be considered as *control parameters* for the activity occurring at the macroscopic level: the *connectivity pattern* between neurons and the (spatiotemporal) *patterning* of the ‘*inputs*’ that these neurons receive through afferents. We regard these parameters as indispensable for the description of collective dynamics and we will next describe how they can be operationalized in terms of abstract modelling of coupled systems.

4.3.1 Microscopic and mesoscopic levels of description and network control parameters

We define the microscopic level, as the one that concerns the most elementary functional unit. The cortical column is most likely to embody this role in the vertebrate brain. According to Mountcastle (1997, 2003) the basic unit of the neocortex is the minicolumn. Neurons within one minicolumn possess a common embryological origin and develop in unison. As a consequence, neurons in minicolumns possess a certain set of properties in common, responsible for their collective activity. Minicolumns are linked into columns, which contain a limited number of minicolumns. Columns seem to vary in size by a factor of one to two in brains, which vary in total surface area by several orders of magnitude. Empirical evidence suggests that cortical columns are modular, thus for instance in primary visual cortex, they may code for a certain orientation of a bar stimulus (e.g. Hubel and Wiesel, 1962). In the somatosensory cortex columns may code for place or modality of a tactile stimulus (Mountcastle, 1997). Following Mountcastle (1997) ‘A cortical column is a complex processing and distributing unit that links a number of inputs to a number of outputs via overlapping internal processing chains’.

Mountcastle’s generalization after reviewing evidence from a range of brain regions and associated behaviors is that ‘*the effective unit of operation in such a distributed system is not the*

single neuron and its axon, but groups of cells with similar functional properties and anatomical connections’.

Simply put, at the microscopic level of a cortical column, nearby neurons tend to receive the same afferents and also tend to receive synchronized input. The latter deems global collective behaviour more likely. Indeed spike synchronization was observed in orientation columns experimentally (Gray and Singer, 1989) and theoretically (Çürüklü and Lansner, 2001). In the latter theoretical study, a realistic model of an orientation column was fed with a drifting bar stimulus. Synchronization between neurons in different minicolumns was observed and depended on the existence of horizontal connections. Interestingly, synchronization also occurred between minicolumns that were not mutually connected, stressing the effect of the collective network state on the individual elements.

Synchronization between individual neurons is known to give rise to mean field oscillations at well defined and discrete frequency ranges (Gray and Singer, 1995, König, Engel and Singer 1995, Traub, Whittington, Stanford, and Jefferys, 1996).

Quantitative studies of cortical connectivity (e.g. Braitenberg and Schüz, 1998, Hellwig, 2000) have shed some light on the dependence of the strength of neuronal connections on the spatial separation between the neurons. Following Hellwig (2000), who studied connectivity of neurons in primary visual cortex in the macaque, the strength of connectivity falls nearly exponentially as a function of distance: connection probabilities range from 50% to 80% for directly adjacent neurons and from 0% to 15% for neurons 500 μm apart. The latter scale exceeds somewhat the upper size limits of a cortical column. Thus, connectivity *within* minicolumns and to some extent within columns can be considered dense. However, connectivity *between* columns is sparse and of nearest neighbour type. The latter is also true for larger spatial scales for example considering the connectivity between cortical areas (e.g. Young, 1992, Sporns and Tononi, 2002). With the risk of oversimplifying things, one may say that cortical connectivity is roughly local at all spatial scales, excluding the microscopic scale of the cortical column, where the connectivity may be roughly considered as global. Clearly, these anatomical facts reflect some fundamental functional difference, which will be discussed with the example of numerical simulations.

To conclude, the above suggest that at least two network scales can be distinguished, microscopic and mesoscopic. The control parameters we consider indispensable for the description of a network dynamics are merely two: the *connectivity pattern* and the *dynamic diversity* of its units. This is illustrated schematically in figure 1. The microscopic level of cortical columns can be abstractly modelled as a *globally coupled* network of *nearly identical* oscillators. With ‘nearly identical’ we state that the dynamic diversity in the autonomous

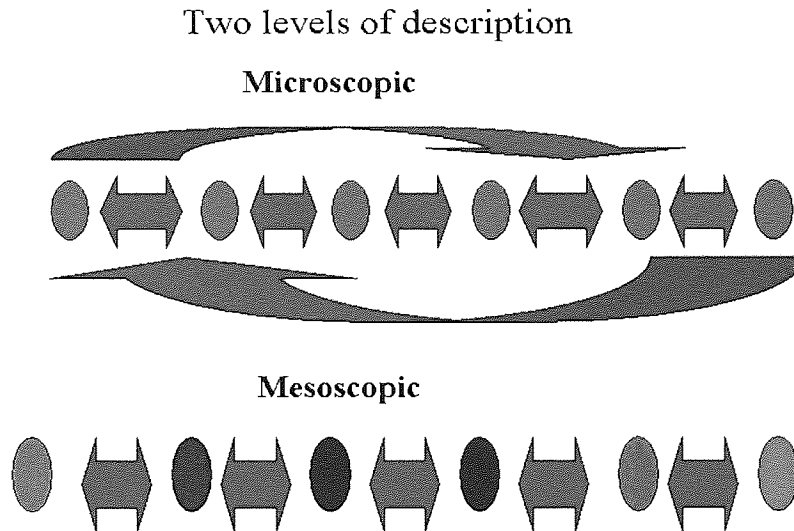


Figure 1. Schematic representation of the two levels of network descriptions that contribute to the generation of macroscopic signals. The microscopic level refers to interactions *within* a cortical column. The units are homogeneous (cell properties, inputs), as indicated by green circles and the coupling is global, thus each unit interacts mutually with all other units in the array (indicated by the arrows). The mesoscopic level refers to interactions *between* cortical columns. The units here are not homogeneous (neurons have different phenotypes and receive different inputs) and the coupling is local, thus each unit interacts only with its nearest neighbours.

(isolated) constituent units in the array will be limited. Here this will be modelled by means of a globally coupled network of chaotic oscillators exhibiting *similar* characteristic frequencies. The mesoscopic level can be modelled as a lattice of *nonidentical* chaotic oscillators where only *nearest neighbours* interact. The lack of identity in the oscillators implies that the constituent units are markedly diverse in terms of their autonomous dynamics. The latter is modelled by employing differences in the characteristic frequencies of each unit. The sensitivity of each unit to initial conditions and the difference in the average time scale grants a certain dynamic diversity to the mesoscopic array. Although, reducing the dynamic diversity to merely difference in the characteristic timescale is a simplification of the real network diversity, we consider it an appropriate one. It follows partly from the fact that neurons in different cortical columns are likely to receive different afferent signals at different times and moreover the internal processing of the inputs will vary between cortical columns (Mountcastle, 2003). This may result to expression of different preferential frequencies of oscillation in the mean field, a notion close to that of ‘resonant’ or characteristic frequencies.

Frequency gradients have been indeed experimentally observed along the sensorimotor strip, indicating that discrete areas may generate distinct rhythms upon sensory stimulation or voluntary movement (Neuper and Pfurtscheller, 2001). Furthermore, it is meanwhile well documented, that several distinct alpha rhythms may coexist in the spontaneous EEG (Basar *et al.*, 1997, Nunez, Wingeier and Silberstein, 2001). Moreover, a mean field signal arising from a mesoscopic level typically extends across several frequency ranges.

4.3.2 Microscopic level: Mean field coupled network of nearly identical oscillators

An array of globally coupled Rössler oscillators was simulated according to:

$$\begin{aligned}\dot{\chi}_i &= -\omega_i \psi_i - z + \xi_i \\ \dot{\psi}_i &= \omega_i \chi_i + 0.15 \psi_i + \varepsilon \Psi \\ \dot{z}_i &= 0.2 + z_i (\chi_i - 10)\end{aligned}\tag{1}$$

Where $i=1\dots N$, is an index specifying the number of the oscillator in the array, ξ_i are additive Gaussian noise components, ω is the characteristic frequency of the oscillator, ε is the coupling constant and $\Psi = \frac{1}{N} \sum_{i=1}^N \psi_i$, is the instantaneous mean field. A linear gradient

for the characteristic frequency can be introduced as:

$$\omega_i = \omega_1 + \delta (i - 1)\tag{2}$$

Where ω_1 and ω_i are the characteristic frequencies of the 1st and i^{th} oscillator respectively.

From [1] we observe that the oscillators are coupled through the ψ variable by the instantaneous mean field. This is equivalent to global (all to all) coupling (Pikovsky, Rosenblum and Kurths, 2001).

The first dynamic scenario of interest is when nearly identical oscillators are weakly coupled.

For the first simulation we used the following parameters, $N=10$;

$\omega_1 = 10$; $\delta = 0$; $\varepsilon = 0.3$. Thus the oscillators are not (frequency) detuned and weakly coupled; however note that the stochastic ξ component is different for each one of the units.

Given the sensitivity to initial conditions the latter means that the individual systems are nearly but not quite identical.

Homogenous elements transient coupling

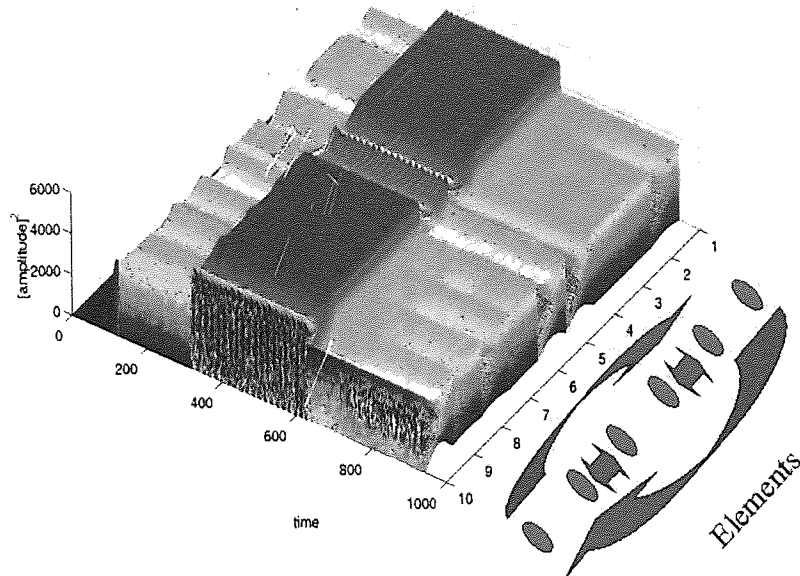


Figure 2. Power Vs time pattern across the array of ten mean-field coupled oscillators. The oscillators are not detuned but have different additive noise components. The right diagonal axis indicates the number of the unit in the array, the left diagonal axis indicates time and the vertical axis indicates the squared amplitude of each system. The coupling is introduced between 100 and 200π thus roughly between 300 and 600 time units. Two main effects are observed: the array appears more coherent and uniform during the coupling time and the power increases.

Figure 2 shows the results of the numerical integration of [1]. The integration was performed using the Runge Kutta technique with a step of $2 \pi/1000$. The left diagonal axis shows the time and the right diagonal shows the number of the unit in the array. The vertical axis shows the squared amplitude of each unit at each time. The coupling is transiently introduced between roughly 300 and 600 time units (100 - 200π). We observe two main effects: the power pattern in the array appears to be more regular and 'coherent' during coupling and also the power increases in most of the units (units 5 and 10 show somewhat irregular behaviour). As stressed in the beginning of this chapter, the main interest here is not primarily to study the details of the coordination effects, rather than to identify the main collective variables contributing to the observed macroscopic patterns and see whether they can be characterized by some parameter of a signal with low spatial resolution, such as the mean field signal, which is an instantaneous spatial ensemble average. Next we examine the synchronization index between all possible combinations of the units in the array. This 'interaction' matrix can inform as to which units are 'effectively' coupled. For simplicity here we use a

synchronization index based on mutual information of the instantaneous phases as in chapter 2. This is a means to quantify merely *phase* synchronization although here stronger interdependencies are to be expected such as strong generalized or identical synchronization.

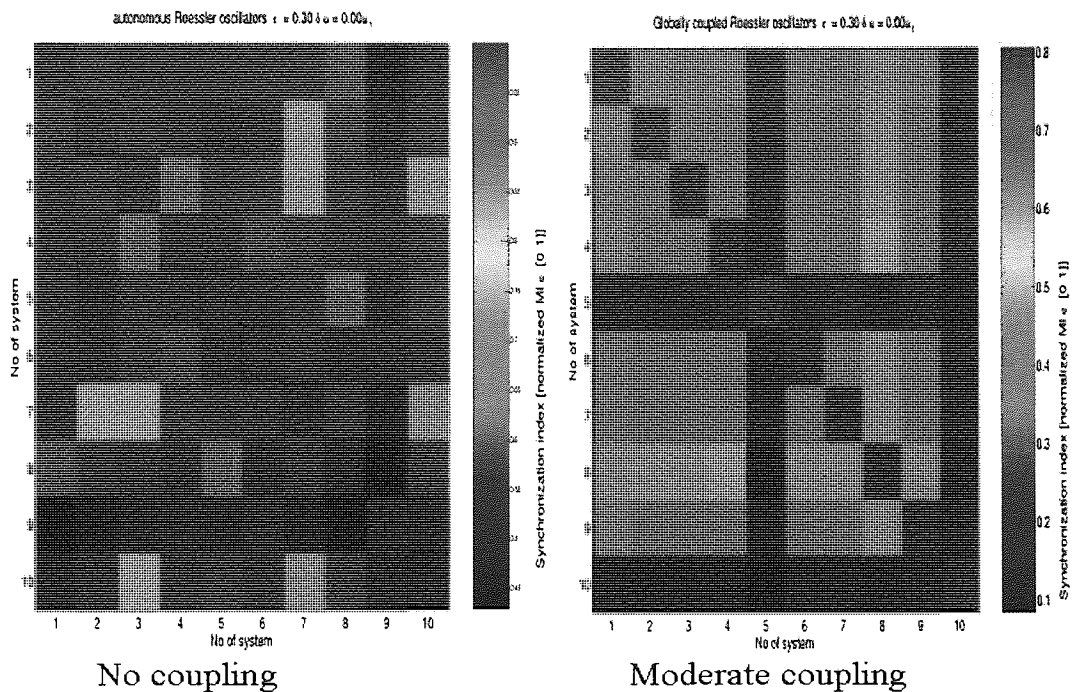


Figure 3. Interaction matrices for the array during the time of no coupling (left) and moderate coupling (right). Axes x and y specify the pair of systems tested for interaction and the colour bar indicates the strength of the (phase) synchronization index (see text for details).

Figure 3 shows the interaction matrix for two time windows: on the left we examine the time before the coupling is introduced ($0-100 \pi$) and on the right the time during coupling ($100-200 \pi$). We observe only spurious and weak synchronization indices for the time when the coupling is absent. When the coupling is introduced pronounced synchronization sets in between almost all units. Nevertheless, note the asymmetries present, especially unit 5 and 10, which are not synchronized with the rest of the array. Units 5 and 10 exhibit a very interesting phenomenon, namely the emergence of two additional frequencies in their power spectra; these are shown in figure 4. This genuine nonlinear effect is probably due to a bifurcation and is related to the size of the array and is in itself very interesting, however it will not be discussed in detail here.

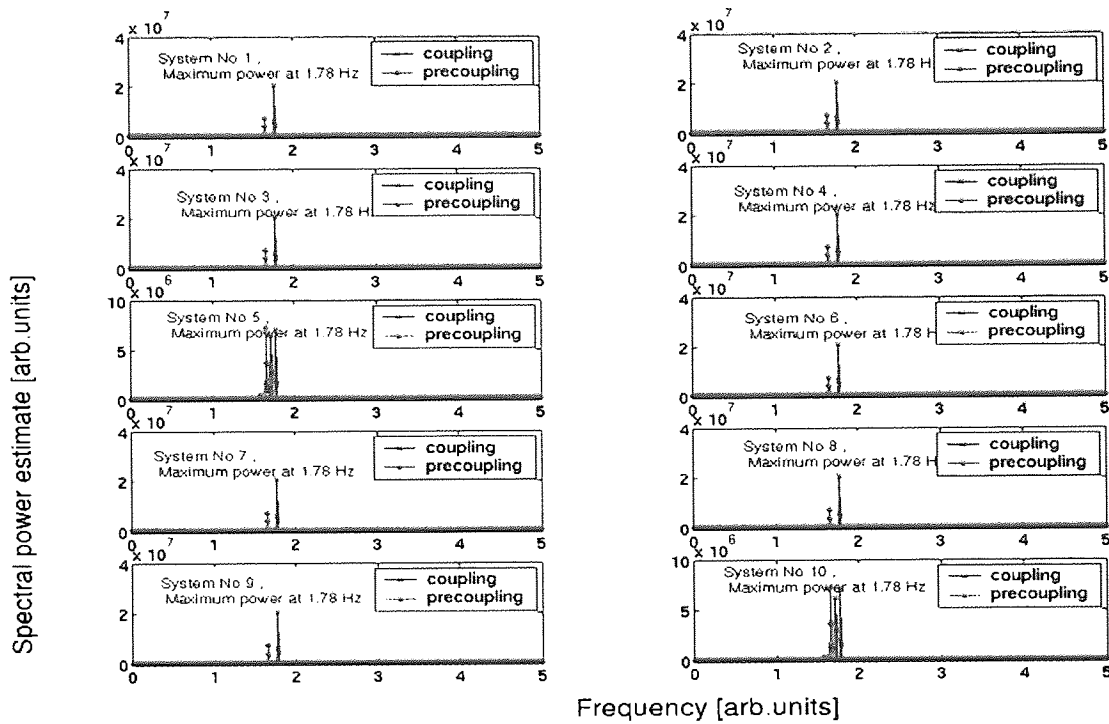


Figure 4. Power spectra of the individual units of the array in [1] for the precoupling (blue) and coupling time (red). Note that the transition to synchronization is accompanied by emergence of the same spectral peak for all systems after the coupling. This is also the peak frequency of the mean field signal (see figure 5). However note that for systems 5 and 10 complex behaviour occurs with the emergence of two additional modes in the spectrum.

Thus for this coupling strength we observe partial synchronization in the array; nevertheless the bulk of the units in the array are mutually synchronized. What we observed here is similar to the well-known Kuramoto transition expected in arrays of globally coupled phase oscillators (Kuramoto, 1975 and 1984, Strogatz, 2000). Qualitatively this can be described as follows. Below a critical coupling strength there is no synchronization between the units and thus the mean field is practically zero. However, if the coupling strength is sufficiently large to synchronize merely two oscillators, the mean field will increase. By virtue of the fact that the units are globally coupled and thus dependent on the mean field, increases in the latter will ‘pull’ further units towards the synchronization region. This effect will be potentiated further with increasing numbers of in-phase units. The synchronization region can be considered as a (spatially) global synchronization manifold, which in many cases is manifest in the frequency domain for a range of coupling strengths. If the coupling strength exceeds some critical value, all of the units will be eventually synchronized. It can be shown both analytically and numerically that the synchronized solution is stable (see Strogatz, 2000) and

thus the array undergoes a transition from quasiperiodic to synchronized motion. This essentially constitutes an extreme dimensional reduction, since the degrees of freedom are essentially reduced to those describing the singular motion on the global synchronization manifold. For very small coupling strengths, no synchronization is observed and the motion in the array is quasiperiodic, thus each system rotates with its own 'characteristic' frequency. If the coupling strength is somewhat larger but does not exceed the critical value, then clusters of synchronized units are observed. This effectively means again a dimensional reduction, however less extreme as in the case of complete synchronization of the array. In this case there is coexistence of several synchronization (sub) manifolds. The mechanism of emergent and self-sustained synchronization through the mean field is fairly universal and has been termed as Kuramoto self-organization (Kuramoto, 1975 and 1984). This phenomenon has been widely studied both analytically and numerically in phase, linear weakly nonlinear and recently also in chaotic oscillators (see Pikovsky, Rosenblum and Kurths, 2001, Boccaletti *et al.*, 2002 and Strogatz, 2000 for extensive reviews and formal treatment). Although the nature of the constituent units of a given system may contribute some differential variability, the global system behaviour and the main effects related to the transition to synchronization are similar across a range of different system classes, as long as the coupling is global. In oscillator models the completely synchronized solution implies motion at a compromise frequency, which roughly approximates the average characteristic frequency of the oscillators in the array.

A few conceptually important remarks are in order. In any globally coupled system, and for a range of coupling strengths, there exists a stable solution for either partial or complete synchronization of the array. The synchronization manifold in turn attracts the individual units and constrains their dynamic range. This is a prime example of circular causality in terms of synergetics, where an emergent macroscopic parameter, here the frequency of the mean field, specifies global system behaviour. This has the important consequence that no unit can be observed in isolation, since their behaviour is at least partially specified by the mean field. Thus in terms of cortical columns in the brain (which can be approximated by globally coupled arrays), the rationale of sampling *individual* neurons and then attributing functional 'receptive field' properties to them is not theoretically feasible. If anything, these receptive fields reflect collective network modes, such as the global synchronization manifold shown in this simulation. Recently Breakspear, Terry and Friston, 2003 have studied biologically plausible models of coupled cortical columns. For varying coupling strength they could observe effects of partial and complete array synchronization. Partial array

synchronization, i.e. clustering, was contingent with intermittent phase dynamics. Complete array synchronization was contingent with identical synchronization.

Undoubtedly, there is a multitude of interesting coordination effects arising in such networks many of which can be readily observed even in simple simulations as the ones shown here. The work of Breakspear, Terry and Friston, 2003 and Breakspear, Williams and Stam, 2004, Breakspear and Stam, 2004 provide prime examples of the applications of the concepts of spatially extended nonlinear systems to realistic brain models. However, we will not extend this discussion further in this direction since our main objective here is not to study the nature of coordination phenomena in systems, which are known (or predefined) but examine the inverse problem. Namely, if one does not know the system (in terms of a comprehensive model) but only has access to gross (mean field -like) observable, what can one infer about the collective process.

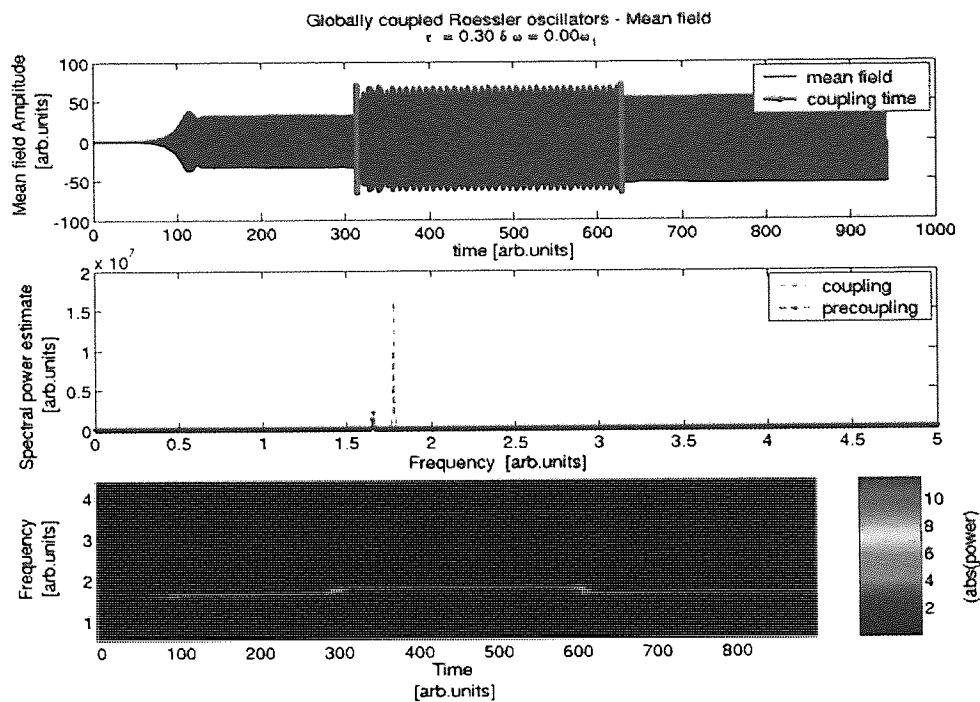
The mean field signal of the system in [1] is computed as the instantaneous spatial average of the solution of the χ variable across all of the systems in the array. Thus let $\chi_i(t)$ be the solution for the χ state variable of the i -th oscillator, then the mean field signal mf is:

$$mf(t) = \frac{1}{N} \sum_{i=1}^N \chi_i(t) \quad [3]$$

where t is time, and i and N are as in equations [1-2].

This is shown in figure 5. Thus the emergence of synchronization in the array is accompanied by a regularization of the mean field signal and an increase of its amplitude (top panel). It is instructive to examine the power spectrum of the mean field signal before and after the onset of the coupling. This is shown in the middle panel of figure 5, where we observe a power increase at a very discrete frequency. The existence of a spurious spectral peak in the mean field prior to the onset of the coupling is due to the inherent similarity of the systems in the array. The bottom panel of the figure shows a moving FFT spectrogram of the mean field signal. During the coupling time we observe a very discrete and temporally sustained frequency peak. Recall that from the interaction matrices in figure 3, we know that almost complete synchronization has occurred in the array and frequency analysis of the individual oscillators shows convergence towards a singular frequency (see figure 4), identical to the one in the spectrum of the mean field signal. Therefore the global synchronization manifold can be observed through the emergence of a singular and discrete spectral peak in the mean field signal. Thus when tackling the inverse problem, one can claim that if there is a power increase at a discrete frequency in the spectrum of the mean field signal this may denote the onset of

synchronization in the array. Note that this is in essence the ERD/ERS model (Pfurtscheller and Lopes Da Silva, 1999).



Mean field signal

Figure 5. Mean field signal of the integration of the system in [1] shown in figures 2 and 3 and 4. The units in the array are not detuned and globally coupled at a moderate coupling strength. The top panel shows the mean field signal as the spatial ensemble average. The coupling is introduced between $100-200\pi$ indicated by the red bars. We observe an oscillatory patterning and an increase in the amplitude. The middle panel shows the power spectrum of the signal before (blue) and after the coupling (red). We observe an emergence of a discrete spectral peak during coupling and a small, possibly spurious peak before the coupling. The bottom panel shows a moving window FFT spectrogram of the signal. Time and frequency are on the x and y axes respectively, the colour code indicates spectral power. We observe that during the coupling the activity is sustained at a discrete frequency.

However, we see that two fundamental assumptions in the model, which may generate this behaviour, are not feasible for the large scale networks, which supposedly generate the macroscopic mean field signals: the homogeneity of the units and the global coupling. The EEG and MEG are believed to be generated by summed postsynaptic currents arising from thousands and even millions neurons, stretching across entire centimetres of cortical surface (Nunez, Wingeier and Silberstein, 2002). Thus many thousands of cortical columns are sampled by a single macroscopic electrode or sensor. As discussed previously, under these circumstances the cortical units contributing to the macroscopic signal can be considered neither homogeneous nor globally coupled. Quite the opposite is true; the units of interest are inhomogeneous and predominantly coupled to their nearest neighbours. However, the clear cut one to one mapping of microscopic synchronization resulting to a power increase at a

discrete frequency is only given when these assumptions hold. This is however only the case for the microscopic level of description. Neurons that belong to the same cortical column may well generate mean field signals, which have more or less singular frequencies. Next we shall see that the relaxation of the homogeneity and the connectivity assumptions (from global to nearest neighbour coupling) destroys this mapping completely and might even reverse it in the sense that microscopic synchronization may even result in power decreases in the mean field signal.

4.3.3 Mesoscopic level: Locally coupled networks of nonidentical oscillators

An ideal and comprehensive model of the generation of macroscopic patterns, would involve a combination of the globally coupled network of identical units at small distances and a nearest neighbour model of nonidentical units at larger scale. However the complexity involved in the simulation of such nonlinear models with embedded spatial and temporal scales and long computation times make this quite a prohibitive task. The reader can refer to Jirsa *et al.*, 2002, Wright *et al.*, 2003 and Breakspear, Terry and Friston 2003, Breakspear and Stam, 2004 for excellent examples of continuum and discrete multiscale neuronal models respectively. We have seen in the previous section that globally coupled nearly identical oscillators can generate mean field signals with fairly discrete characteristic timescales (frequency content). Thus, one can consider a mesoscopic model, where the elementary units have different characteristic time scales, which can be thought to *emerge* through the interactions in the (globally-coupled) microscopic network. Thus the simplest possible model, describing the emergent mesoscopic level is one of nonidentical locally coupled elements.

Here we used a lattice of nonidentical (frequency detuned) Rössler oscillators:

$$\begin{aligned}
 \dot{\chi}_i &= -\omega_i \psi_i - z + \xi_i \\
 \dot{\psi}_i &= \omega_i \chi_i + 0.15 \psi_i + \varepsilon (\psi_{i+1} + \psi_{i-1} - 2\psi_i) \\
 \dot{z}_i &= 0.2 + z_i (\chi_i - 10)
 \end{aligned}
 \tag{4}$$

Where $i=1 \dots N$, is an index specifying the number of the oscillator in the array, ξ_i are additive Gaussian noise components, ω is the characteristic frequency of the oscillator and ε is the coupling constant. Note that the coupling here is linear and of diffusive type, thus it is proportional to the instantaneous difference of the activity in the i -th unit with its nearest neighbours. For simplicity, we did not use a parametric boundary condition and thus the first

and last unit were not coupled. As with the mean field model, a linear gradient for the characteristic frequency is introduced as:

$$\omega_i = \omega_1 + \delta (i - 1) \quad 5]$$

Where ω_1 and ω_i are the characteristic frequencies of the 1st and ith oscillator respectively.

The parameters used where $N=10$; $\omega_1 = 1$; $\delta = 0.05$; $\varepsilon = 0.15$.

Figure 6 shows the power Vs time pattern across the units in the array, which is formatted analogously to figure 2. In contrast to figure 2, we observe that during the coupling time the power in the array is redistributed between two maxima at the edges and a big power drop off in the middle. This pattern implies some sort of clustering behaviour. On the whole the power seems to be somewhat reduced during the coupling time. Figure 7 shows the interaction matrices, which are formatted exactly as with figure 3.

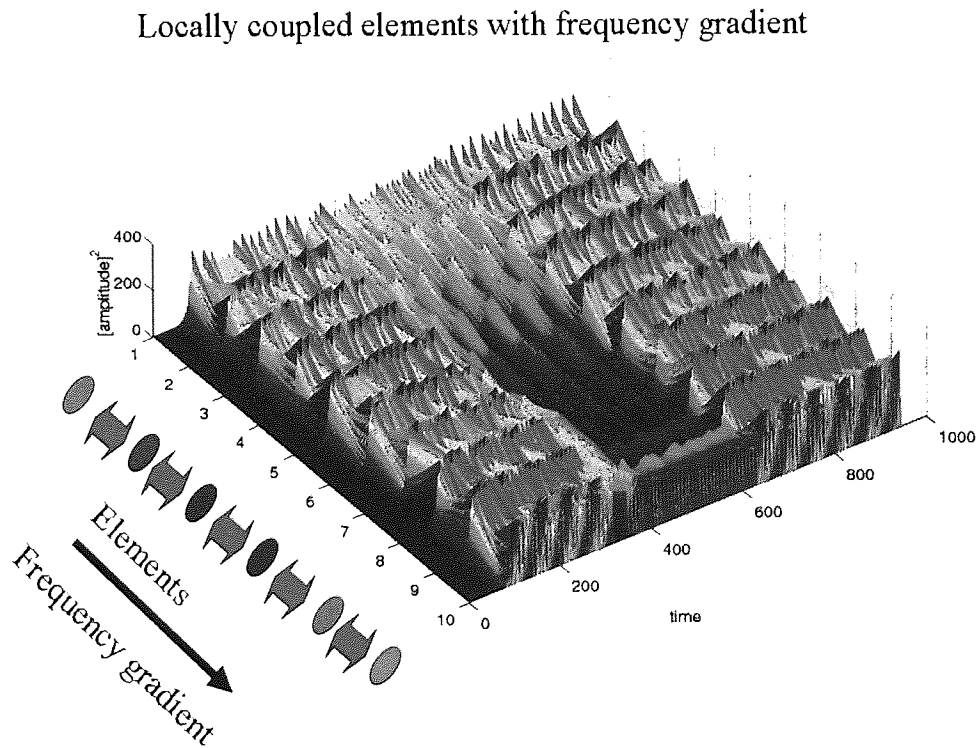


Figure 6. Lattice of locally coupled Rössler oscillators (see equation [4]) with a linear frequency detuning (equation [5]) with parameters $N=10$, $\omega_1 = 1$; $\delta = 0.05$; $\varepsilon = 0.15$. The format of the figure is similar to figure 2. Here the left diagonal axis indicates the unit in the lattice, the right diagonal axis is time and on the vertical axis squared amplitude is plotted. Coupling is introduced between $100-200\pi$ (roughly 300-600 time units). We observe that during the coupling time the power in the array is reordered in to two power maxima at the edges of the array and a large power drop in the middle.

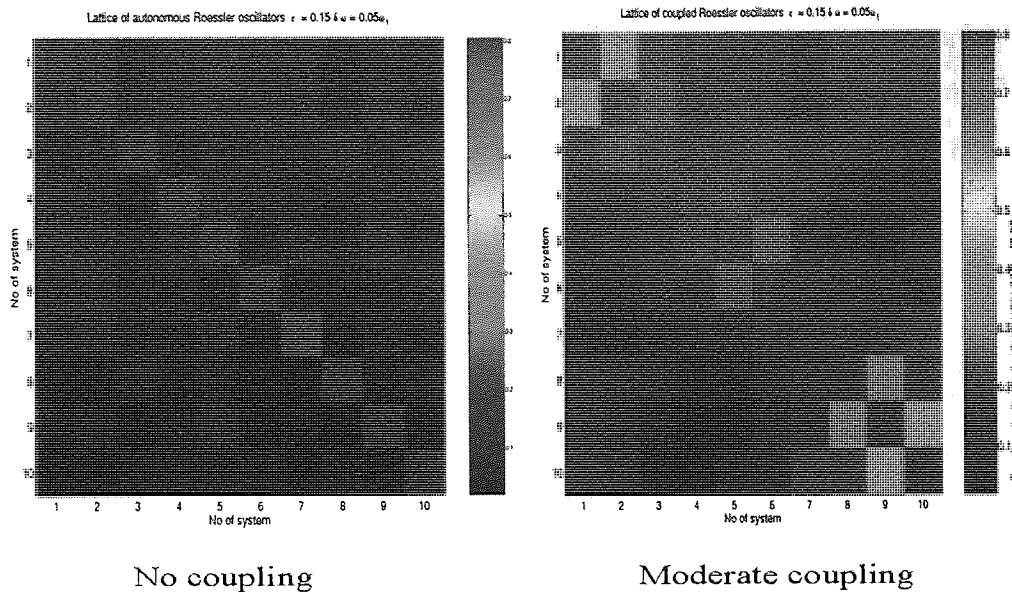


Figure 7. Interaction matrices for the lattice shown in figure 6. Same format as figure 3. Here we observe that during the coupling time several phase synchronized clusters are formed, see text for details. The frequencies of the 3 synchronized clusters are different, as this can be seen in figure 8, that shows the spectra of the individual units. The three synchronized clusters are also evident as distinct peaks in the power spectrum of the mean field signal in figure 9.

We observe that during the coupling time several clusters are formed. Units 1, 2 and 3 for instance are strongly interactive between them but less interactive with the rest of the elements. The same goes for units 8, 9 and 10. A smaller and weaker cluster also seems to exist in the middle of the lattice involving units 5, 6 (and partly unit 4). Units 1, 2 and 3 for instance are strongly interactive between them but less interactive with the rest of the elements. The same goes for units 8, 9 and 10. A smaller and weaker cluster also seems to exist in the middle of the lattice involving units 5, 6 (and partly unit 4). Note that the units that are not *physically* coupled are effectively strongly interactive, such as units 1 and 3 and units 8 and 10. This is a genuine self-organization effect arising through the dynamic interaction of the whole lattice; the position and extent of the clusters results from the nearest neighbour connectivity. Thus the formation of clusters can be viewed as a reduction of the effective degrees of freedom in the system. It is important to note that the relevant coordination phenomenon here is indeed phase synchronization, which makes the phase difference the relevant collective variable (order parameter) at the mesoscopic level. The latter can be seen by sampling two of the possible pairs of interaction.

Figure 9 shows the effective interaction between units 1 and 3. Note that these units are not *physically* coupled but both of them interact with unit 2. From the amplitude difference shown in B and the scatterplot of the amplitudes shown in C it is obvious that there is little correlation between the units; thus neither identical nor (strong) generalized synchronization is observed.

However as evident in panel D, the phase difference, which decelerates before the coupling (according to the frequency gradient) is introduced, remains bounded for the entire duration of the coupling. This is also reflected in the phase difference distribution shown in E, which shows a preferred value around 5 radians. Thus phase synchronization is observed.

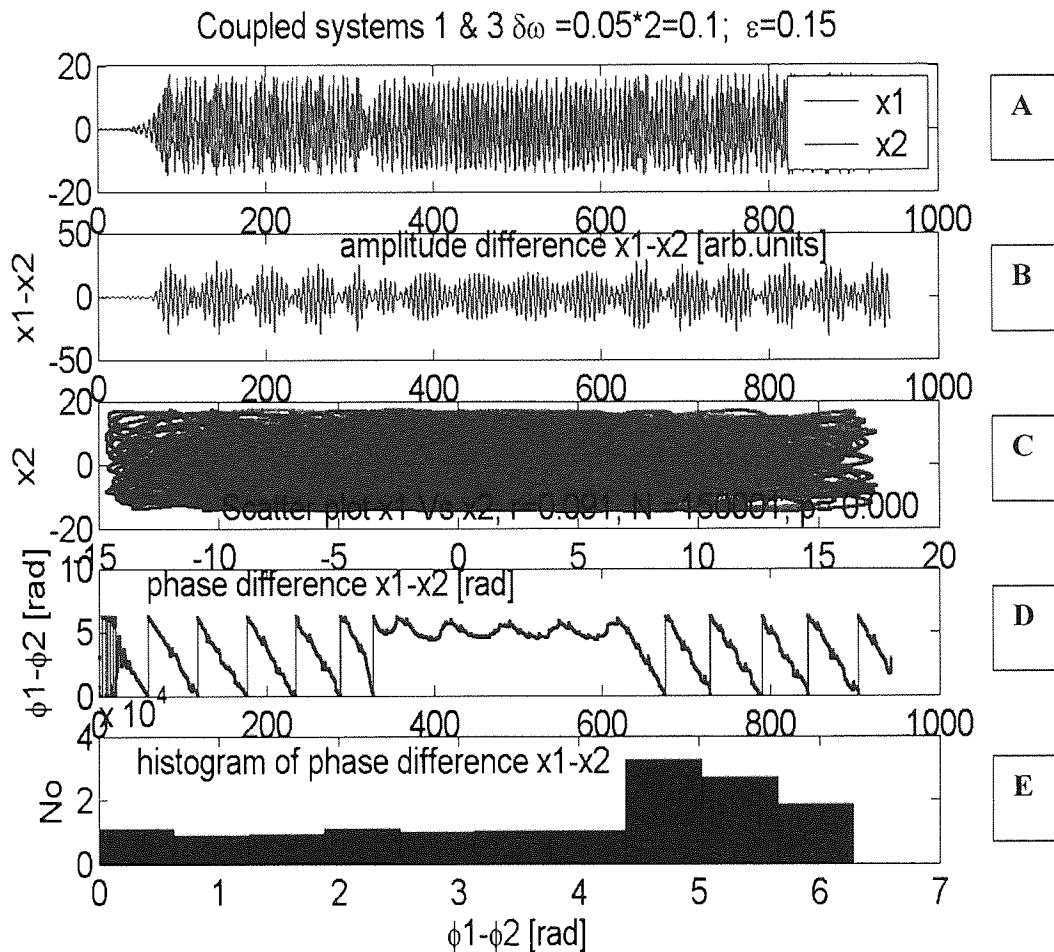


Figure 9. Effective interaction between elements 1 and 3. Note that these elements are not physically coupled. Panel A shows the two time courses superimposed; the coupling is introduced between roughly 300-600 time units. B shows the amplitude difference. Note that it is different from zero and fluctuates. C shows the scatter plot of the x variables. Note the low correlation coefficient, no systematic relationship is evident. D shows the time course of the phase difference wrapped mod 2π . During the coupling time (roughly between 300-600 time units) the phase difference remains bounded. This is also evident in the phase difference distribution shown in E, which shows a preferred value around 5 radians. Thus imperfect phase synchronization is observed.

Figure 10 shows the interaction between elements 4 and 5 and is formatted exactly as Figure 9. Note the intermittent amplitude dynamics shown in A and B and the lack of correlation between the amplitudes in C. In E we observe that the phase difference is bounded for most of the coupling time (roughly between 300-600 time units) but occasionally (probably) intermittent phase slips occur as evident in D. Another interesting effect is the marked

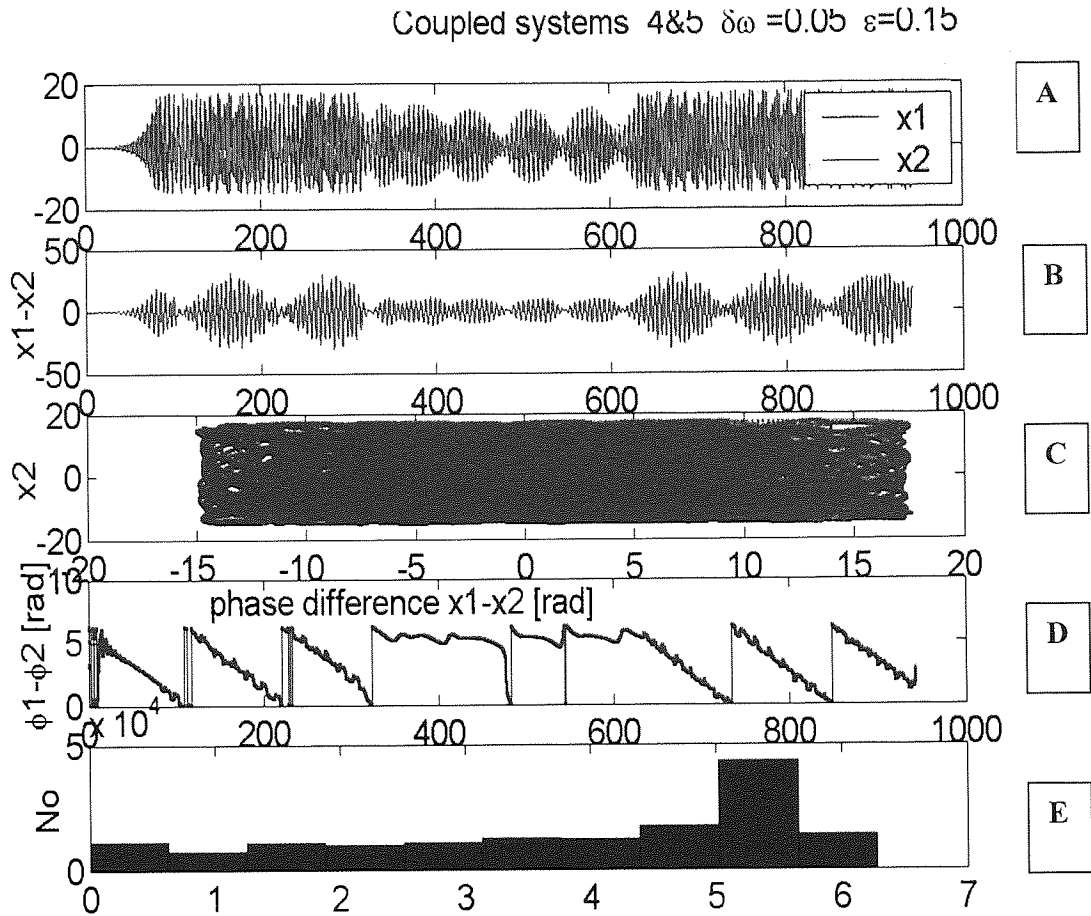


Figure 10. Interaction of units 4 and 5. Same format as figure 9. Note time intermittent phase difference dynamics in panel C and oscillation death in panels A and B during the coupling.

decrease in amplitude during the coupling time. This is consistent with the intermittent phase dynamics. This phenomenon is oscillation death and the phase slips observed here are attempts of the global system to ‘reset’ the phase difference by minimizing the amplitude.

The latter is evident from the temporal coincidence of the phase slips in panel C with local amplitude minima in panel A. Thus the observed phenomenology here is intermittent phase synchronization accompanied by quenching.

Coming back to the global behaviour in the lattice, we would like to examine the differences between the emergent clusters more closely. The main effect regards the frequencies of the synchronization processes in the 3 clusters, which are slightly different. This can be seen in figure 11, which shows the spectra of the individual units; the two strong edge clusters exhibit singular peaks with 0.17Hz (unit 1,2,3) and 0.23Hz (units 8,9,10). The weaker cluster in the

middle exhibits frequencies around 0.17-0.19Hz. We can see that the units within the clusters adjust their frequency during the coupling time; at the same time the units belonging to different clusters express different frequencies. These also correspond to the three main spectral peaks that can be observed in the mean field signal in figure 12. Interesting effects can be observed for the units in the middle of the cluster, namely units 4, 5, 6 and to a lesser extent the marginal units 3 and 7. Apart from the main frequencies these units display an appearance of a second spectral peak. This is particularly evident for unit 4. These two frequencies are likely to represent two competing modes of behaviour for the units in the middle of the lattice. While the units adjacent to the proximal end of the lattice (i.e. unit 3) exhibit a stronger peak in the lower frequency and a lesser peak in a higher frequency, the situation is inverted abruptly in unit 4 where the exact opposite is the case. Thus the higher frequency peak is more pronounced. In unit 5 a singular peak occurs at a somewhat higher frequency. The latter is preserved in unit 6 but an auxiliary peak occurs here. In units 5 and 6 and 7 the units tend to approach slowly the (higher) frequency of the distal cluster but this is not possible. At the same time, oscillation death occurs for the units exhibiting the competing frequency modes. Thus the two edge clusters are clearly defined by high power at a certain frequency and the middle part of the lattice seems to reflect a cluster boundary with possibly extremely complex dynamics, which involve the abrupt creation and destruction of frequency modes. The latter constellation is very important from a theoretical point of view. The two edge clusters maintain their separation in terms of frequency by virtue of these abrupt boundaries. Thus oscillation death, supported by local intermittent phase synchronization and the lack of global synchronization in the array contribute to the segregation of separate entities.

This clustering behaviour may shed some light to the phenomenology observed in the power Vs time pattern in figure 6. There we have two power maxima, which correspond to the two stronger clusters at the edges of the lattice. The big power drop, which coincides with the weaker cluster, reflects a region of oscillation death. Thus the units in the middle of the lattice are dynamically 'pulled' towards the frequencies of the two edge clusters (which introduces an ever growing phase difference between the edge elements of the middle cluster, units 4 and 6) but the presence of the diffusive coupling tends to reduce this phase difference. As a result the amplitude has to decrease, so that the phase difference can be reset. Thus oscillation death here marks the cluster boundaries: as a consequence the synchronization processes in the two main clusters become more distinct.

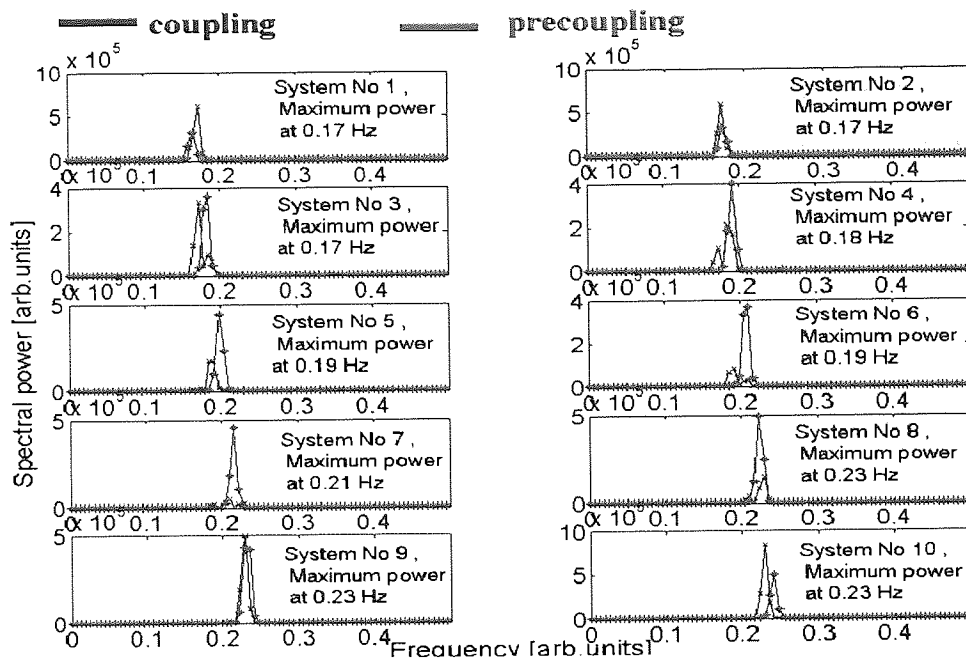


Figure 11. Power spectra of the χ variables of the individual units in the lattice of locally coupled oscillators defined in [4-5]. The power is plotted in blue for the coupling time and red for the precoupling time. See text for details.

In terms of synergetics we arrive at the following generalization. The collective variable, the one that specifies the interactions of the elements in the system, at the *mesoscopic* level is the *phase difference*. The emergent *macroscopic* order parameter is the *frequency difference* of the synchronization process *between* the clusters. Note how the order parameters in both mesoscopic and macroscopic levels are *relational* rather than physical observables. This is the hallmark of synergetic systems. The frequency difference of the synchronization process between the clusters keeps the cluster elements segregated by continually accelerating their phase difference. This is another typical example of synergetic behaviour, once a macroscopic order parameter is formed; it in turn specifies the behaviour of the system and constrains the behaviour of the individual units. However, if the frequency difference (the order parameter at a macroscopic level) changes, then the phase difference (the order parameter at the mesoscopic level) between elements originally placed in different clusters may stabilize and thus the clusters can change or entirely new clusters may emerge. Such changes in the collective variables are expected whenever a control parameter (here either the coupling strength or the distribution of characteristic time scales) changes and may give rise to a phase transition. Another possibility for change in the clustering is intermittent behaviour in the presence of fixed control parameters. In that case we would observe an intermittent behaviour in the order parameters of the system, thus either the phase difference of the individual elements at a mesoscopic level or the order parameter at a mesoscopic level. In the simulation shown here the clusters are fairly stable for the entire duration of the coupling.

In many experimental cases, we do not have access to the mesoscopic level and only macroscopic system observables are available. In this simulation the parameter of interest (the macroscopic order parameter) would be the frequency difference of the clusters. This brings us back to central question, we attempt to address here. Can we use the mean field signal to learn something about the underlying collective process? We should look for the answer by observing the macroscopic order parameter, which is in the frequency domain. The mean field signal for this simulation is computed according to equation [3] and displayed in figure 12.

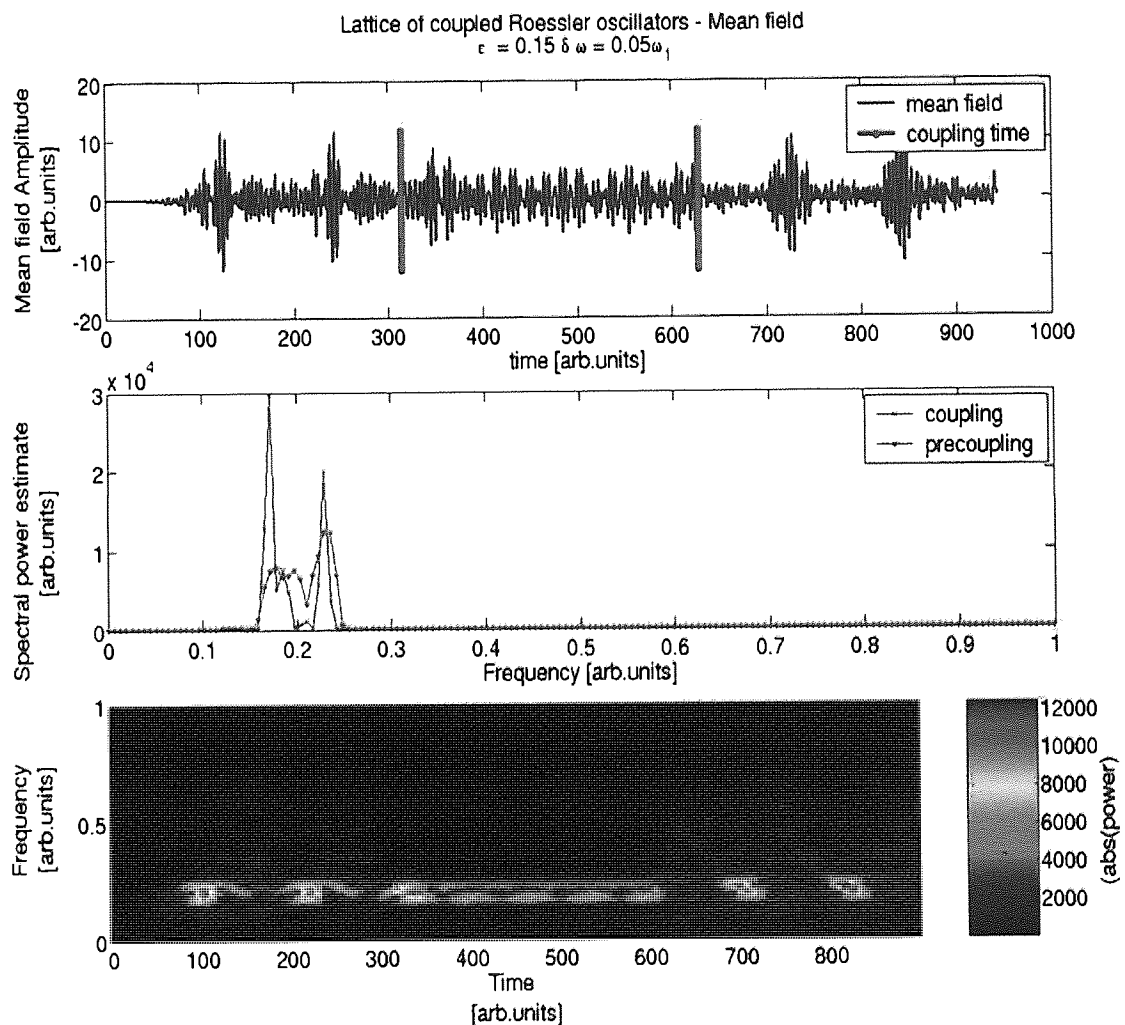


Figure 12. Mean field signal of the lattice of coupled oscillators in [4-5]. On the top panel the time course of the mean field signal is plotted. The coupling time is indicated by red bars (roughly between 300- 600 time units). The middle panel shows the power spectra for the signal before (red) and during (blue) the coupling. In the bottom panel a moving window FFT spectrogram is shown. The x and y axis depict time and frequency respectively and power is indicated by the colour bar. Note the emergence of 3 distinct power peaks in the spectrum during coupling and the marked power drop in the middle. These correspond to the emergent clusters shown in figures 7 and 10 and the drop reflects the oscillation death at the cluster boundaries. The time course of the clusters can be seen in the spectrogram of the mean field signal, and suggests that they are stable. The mean field signal captures the essential coordination phenomena occurring in the array.

The signal appears more structured during the coupling and on the whole does not seem to increase in amplitude as we had seen in the case of the globally coupled array. The transition from no coupling to coupling is accompanied by the emergence of three accentuated peaks in the spectrum of the signal (plotted in the middle panel of the figure) and a marked power drop between the two main peaks. The power drop here is highly frequency specific and reflects the boundary between the clusters shown in figure 7 and 11, whereas the discrete peaks correspond to the 3 synchronized clusters. The bottom panel shows a spectrogram of the signal, which exhibits two clear peaks during the coupling. The lower frequency component shows a somewhat periodic fluctuation in its power but remains discrete in frequency, whereas the higher frequency component is fairly sustained in time. The frequency difference between the components seems fairly stable. Hence, the mean field signal captures the essential coordination phenomena occurring in the array, the formation of synchronized clusters and oscillation death occurring at the boundary. The order parameters for the array emerge in the frequency domain and can thus be extracted from the mean field using standard spectral methods

4.4 Discussion

Some remarks are in order here with respect to the relation of synchronization processes and macroscopic power changes. As we have seen in the simulation above, the power of the array does not *increase* during the coupling, despite the presence of *synchronization* between the units. Quite on the contrary, a fairly significant power drop occurs, which is evident as a broadband *power decrease* in the spectrum of the mean field signal. This power drop is due to spatial clustering and reflects the boundary of the synchronized clusters, which are evident as distinct and fairly discrete power increases in the spectrum of the mean field signal. However, the clustering process is in essence *partial* and *specific* synchronization, with the emergent formation of simultaneously active alliances of interacting units, which become however themselves segregated through the emergence of a collective order parameter, the frequency difference. This kind of process is typical for complex systems in terms of an interplay between functional integration and segregation. Here we used a simple, abstract model, which only vaguely resembles the characteristics of cortical connectivity; nevertheless such complex behaviour was spontaneously generated.

Furthermore, even in this simple model the relation between synchronization processes occurring at lower levels of description and the macroscopic power changes in the mean field signal is not straightforward. Most of all we have seen that *power decreases* are *not*

necessarily due to *desynchronization*; quite on the contrary they may well reflect the 'boundary' of highly specific and complex synchronization phenomena. Such synchronization phenomena do not necessarily result to marked power increases but can give rise to accentuations of very discrete power peaks, which are clearly distinct for the different clusters. Thus the claim implicit in the ERD/ERS nomenclature (Pfurtscheller and Lopes Da Silva, 1999) that power increases are due to synchronization and decreases are due to desynchronization cannot be supported even in this simple model. This may help reconcile some of the discrepancies, found in the neuroscience literature. At microscopic levels of description, synchronization processes have been documented to underlie task-related integration of information (for a review Singer, 1999). According to the ERD/ERS model (Pfurtscheller and Lopes Da Silva, 1999), *increases* in power in the mean field are to be expected, if microscopic synchronization is to occur. However, at the macroscopic level for similar tasks very often *decreases* in power are reported and interpreted as desynchronization. If one follows, the two literatures one gets the impression that at a microscopic level, *synchronization* is a synonym for *activation*, while in the literature dealing with the macroscopic level synchronization is a synonym for *idling* while *desynchronization* is a synonym for *activation*.

The critical point is that power increases are synonymous to synchronization *only if* the underlying network is a globally coupled network of identical elements, as we have seen in the previous section. However, this assumption may only be realistic when considering microscopic scales in the brain. For the spatial scale at which macroscopic signals are generated in the brain this assumption is violated: the functional units are inhomogeneous and (predominantly) locally coupled. Even the simplest possible model allowing for diversity of the units and local coupling such as the one presented here, does not allow the direct mapping of a power increase to synchronization and a power decrease to desynchronization.

Furthermore, using this simple model we have seen that power increases and decreases in the mean field can be found in quite neighbouring frequencies; explicitly power drops 'surround' the peaks. This may shed some light on another intriguing phenomenon in the literature, the existence of concurrent ERD and ERS in the same cortical rhythm, typically reported for the broad alpha band (Klimesch *et al.*, 2000). The typical findings are alpha power increases in very circumscribed frequencies, embedded in a broadband power decrease. These findings are deemed paradoxical because of the assumptions implicit in the ERD/ERS model, which interprets the concurrent power changes of opposite sign as simultaneous synchronizations

and desynchronizations. In our simple model such patterns of power changes emerge as a signature of specific functional clustering processes.

The formation of frequency specific clusters marked by oscillation death is an intriguing possibility for macroscopic spatiotemporal brain dynamics. The number and the size of the synchronized clusters may vary dynamically, especially if the control parameters are themselves time varying. According to Breakspear, Terry and Friston, 2003, ascending and diffuse neuromodulatory systems are consistent with this role in the brain, namely acting as dynamic coupling parameters. These when incorporated in a biologically plausible network of cortical columns give rise to intermittent phase synchronization and desynchronization, which leads to a dynamic reshaping of the form and size of the clusters. The latter is synonymous to a dynamic modulation of the effective dimensionality of the global system. The line of work presented here may eventually help to extend some of these observations with respect to the phenomenology observed at the macroscopic level and thus facilitate the connection to the EEG/MEG literature. Here we have seen that synchronized clusters may give rise to discrete spectral components and may be surrounded by large boundaries, where oscillation quenching is observed.

The first consequence is that distinct functional clusters may be sought in the frequency domain. Thus if a power increase in the mean field signal is observed, this may be the result of the formation of synchronized clusters, perhaps governed by an order parameter in the frequency domain. Such power increases will be most likely in neighbouring networks with close characteristic frequencies and thus in networks with dense intermediate range connections and synchronized input. This maybe particularly relevant for early visual processing. A vast amount of literature suggests that the perception of holistic stimuli is related to oscillations of increasing power, which are however *confined* in the gamma frequency range (Gray and Singer, 1989, Koenig, Engel and Singer 1995, Tallon-Baudry *et al.*, 1996, Tallon-Baudry and Bertrand, 1999). This seems to be particularly relevant for primary visual cortex. Thus crudely put, for different stimuli or tasks requiring task specific integration of information, one should expect clustering at different frequencies, evident as peaks in the spectrum the mean field signal. This simple line of reasoning is followed in chapter 6, where experiments in the visual system are performed and the data seem to support this idea.

The second consequence relates to the origin of power decrease in complex perceptual and cognitive tasks. It is possible that several synchronization processes may simultaneously

occur in *very different* frequency ranges in the same *local* network. One may speculate about the following constellation: the more specific the synchronization process is, thus the more the need for functional segregation is pronounced in a certain area (for instance by virtue of spatially and temporally discrete input to a given network), the smaller the functional clusters will be. If the clusters are small they will give rise to small but discrete peaks in the mean field signal. However, the cluster boundaries may be large, in order to enhance the separation of the clusters. This may be instantiated by synchronized clusters whose emergent frequencies are quite distant in the presence of strong coupling. Such strong coupling in the brain is however local. Thus in a certain large-scale network, such a constellation may produce a very pronounced power decrease and distinctive and highly frequency specific power increases. The latter would have been interpreted as a prevailing ERD in the presence of ‘paradoxical’ ERS’s, implying that desynchronization had occurred. However, the underlying collective process would have been a complex spatiotemporal dynamic process with formation of highly specific functional clusters.

In biologically plausible, multiscale models such as in Breakspear, Terry and Friston, 2003, transient synchronization results in dimensional reduction. Desynchronization results in short-lived dimensional explosion and is subsequently followed by a rearrangement of the spatial pattern of synchronization into different clusters. The model presented here suggests that intermittent dynamics in larger spatial scales may produce oscillation death, which as we have seen is a mechanism of contrast enhancement but also may contribute substantially to a ‘resetting’ of the system by abruptly minimizing the input to the neighbouring collective modes. Thus oscillation death on a global scale may contribute to the ‘updating’ of the clustering process. This is a role very much consistent with the demands of complex cognitive tasks, where marked power decreases are indeed often observed.

Finally, we are fully aware of the limitations of the simple models presented here. These are very abstract and thus potentially important details of the biological systems are not considered. Furthermore, the basic constituent unit used in this work exhibits very discrete and sustained oscillatory behaviour, which may not be the case for many cortical networks, which may consequently not exhibit discrete spectral peaks. The latter may question the validity of the emergent order parameters. However, many of the synchronization phenomena and fundamental mechanisms encountered in such simple models are universal and can be demonstrated in realistic brain models (Breakspear, Terry and Friston, 2003, Breakspear and Stam, 2004). Thus whether or not the predictions of these models will be useful for real neurophysiological data is ultimately an empirical question. The generality of the predictions

may contribute to their experimental testability, which is explored in chapter 6. Most importantly, although models such as the ones described here are not biologically plausible, they may provide us with general but helpful insights about the relationship of the mean field signal to the underlying coordination phenomena and thus inform about the relation between scales. The latter is extremely important for unifying large bodies of literature in neuroscience. We have attempted to show that even such simple models help to disambiguate pronounced discrepancies and paradoxes arising through a mere difference in the scale of observation.

Chapter 5: Quantifying local and global nonlinear neural interactions from magnetoencephalographic data: application to an auditory AM task.

5.1 Background and rationale

The steady-state auditory-evoked potential (SSAEP) (Rees *et al.*, 1986, Kuwada *et al.*, 1986, Picton *et al.*, 1987) is the response to a periodic stimulus such as an amplitude modulation (AM) that closely follows the frequency of the driving stimulus. The magnitude of the AM- following SSAEP is proportional to the level of the stimulus, and this level-dependency has led to its use as an index of hearing threshold in the calculation of “physiological audiograms”, used clinically (John *et al.*, 1998, John and Picton, 2000). The SSAEP magnitude is also proportional to the modulation depth of the driving AM stimulus, and mirrors the psychophysically-defined temporal modulation transfer function for AM, implying that it reflects the processes underlying AM perception (Rees *et al.*, 1986, Picton *et al.*, 1987). Despite its proven clinical utility, the periodic locking behaviour of the auditory cortex to the AM stimulus implied in the SSAEP concept is distinctly unfavourable in terms of information processing. Any integrative information processing, which is to be expected at the level of auditory cortex, would inevitably require some form of signal transformation/modulation.

The classical method of measuring the SSAEP is by averaging responses over a large number of very short epochs, usually the length of the period of the driving AM waveform, to maximise the signal-to-noise ratio of the response (Picton *et al.*, 1987, Ross *et al.*, 2003, Pantev *et al.*, 1996). The assumptions behind averaging (and steady state techniques in general) are that the underlying neural signal is stationary, time-locked to the stimulus and superimposed on white noise. In this study we set out to test these assumptions by examining the continuous temporal dynamics of dipole moments computed over a series of epochs. We investigate these dynamics both in terms of the relative phase and amplitude relationships between the auditory cortices across hemispheres and within hemispheres but across frequency bands.

The central query in this study relates to whether the AM following response indeed merely entails a steady state response, both at intrahemispheric and interhemispheric levels. The concept of the steady state response essentially implies an additive signal plus noise model, in which a periodic response at the frequency of the AM stimulus is superimposed on a white noise

background. Therefore, there shouldn't be any interactions between the ongoing rhythms (considered as independent additive noise) and the AM following response (considered as the signal). In the case of binaural stimulation one would *additionally* expect, crosscorrelated periodic activity in the two hemispheres due to the common driving signal (and thus at the AM frequency) but no nonlinearities and no cross frequency interactions, which would imply a genuine interaction between the two sites.

Thus testing these hypotheses is synonymous with detecting (or not) the presence of a nonlinear structure in both local and global amplitude and phase dynamics. This is not a trivial undertaking, since the nonstationarity the presence of instrument noise, finite data length and filtering are factors often associated with the detection of spurious nonlinearity (Rapp *et al.*, 1993, Breakspear, 2002). We use two metrics based on mutual information to capture the interactions in the slow amplitude and phase dynamics. Since mutual information is sensitive to both linear and nonlinear interactions, the issue of detecting nonlinearity can be reduced to identifying *components* of the interactions that cannot be explained by solely linear, stochastic processes.

5.2 Methods

5.2.1 Experimental Design

Participants

Three listeners (age range 25 – 49 years; two males) participated in the study. All were right handed and none reported any hearing loss or neurological disorder.

Stimuli

MEG data were collected while listeners were presented with three different auditory stimuli. The stimuli could be either a pure tone at 500 Hz, or a 500-Hz pure tone that was sinusoidally amplitude-modulated with a modulation rate of 32 Hz. The amplitude modulation could be presented to each ear identically (*diotic AM*) or with a 180-degree phase lag (3.14 radians) between the modulation waveforms (*dichotic AM*). All stimuli had a duration of 4000 ms and were gated on and off with 20 ms linear rise and fall times. The sounds were presented at a comfortable hearing level, through echoless plastic tubing fitted with foam ear tips. Each stimulus type was repeated 25 times, and the order of presentation was pseudo-random. During stimulus presentation, subjects were asked to listen to the stimuli (although they were not required to complete any task) and to fixate on a visual fixation point.

5.2.2. Recordings, Dipole Analysis

Data collection was carried out using a CTF Omega 151 Channel MEG system (CTF Systems Inc., Port Coquitlam, Canada). Participants wore an inflatable head cuff to minimise movement during recording. Reference coils localised before and after the recording session enabled the measurement of any head movement that occurred during recording; no subject moved more than 5 mm.

The data were recorded in 3rd order gradiometer mode (Vrba *et al.*, 1999), sampled at 625Hz and low-pass filtered at 100Hz. A 50Hz comb filter was applied to remove the power line interference and its harmonics. Recording epochs were 5.8 seconds in duration, with the onset of the stimulus occurring 1.5 second after the start of the epoch. Stimulus duration was 4s and the inter-stimulus interval was 2 s. The data were DC corrected based on the pre-trigger period within each epoch and then averaged according to stimulus type. Digitised head shapes were co-registered onto structural T1 MRI scans using surface matching techniques described elsewhere (Adjamian *et al.*, 2004b).

The averaged data for diotic 32-Hz AM were filtered with a 4-Hz band-pass filter centred on 32 Hz. The filtered data were then modelled, using a reduced chi-square goodness of fit (Supek and Aine, 1997), with two unconstrained spatiotemporal dipoles over the 4 second stimulus duration, each manually seeded close to auditory cortex in the left or right hemisphere. Monte-Carlo analysis was performed by fixing each dipole in turn and re-fitting the remaining dipole to the averaged data with added noise (estimated from the anti-average).

We then projected the unaveraged data through these dipole models to give epoch-by-epoch time-series estimates of the response to both the diotic and dichotic stimulus types. Therefore, for each subject, with both diotic and dichotic AM, there were 25 x 5.8 second epochs of un-averaged data for each dipole model.

5.2.3 Time frequency analyses

In order to observe time-frequency components not reflected in the time-domain average we performed multiresolution wavelet analysis using Morlet wavelets on an epoch-by-epoch basis. Mann-Whitney z-scores were computed for the epochwise differences in the two dimensional (time, frequency) wavelet coefficients between pre-stimulus and stimulus states. For instance, a z-score of 3 for a given time-frequency voxel in the stimulus phase would indicate that wavelet

power was larger by 3 standard deviations than the average wavelet power of all the voxels in the same frequency bin during the prestimulus phase.

5.2.4 Detection of signal interdependencies using the Hilbert transform.

The analysis described below was conducted on the epoch-by-epoch unaveraged data projected through the dipole models as described in the previous section.

We were interested in the following cases:

1. the interactions of the AM following response with the ongoing rhythms at all possible frequencies in the same hemisphere
2. the interactions of the AM following response between hemispheres
3. the interactions of the AM following response in one hemisphere with ongoing rhythms in at all possible frequencies *in the other hemisphere*
4. the interactions of ongoing rhythms between hemispheres but in the same frequency

The raw dipole data were narrow band pass filtered between 30-34 Hz to extract the following AM response. In order to extract all possible frequency components a 4Hz wide bandpass filter was applied to the raw data stemming from the same or the contra lateral dipole data for a frequency range between 2-62Hz in steps of 2 Hz.

The narrow band pass filtered data were convolved with the Hilbert transform to obtain uniquely defined estimates of the *instantaneous* amplitude and phases of the signals. This approach is based on the analytic signal concept (Gabor, 1946). The analytic signal $\psi(t)$ is a complex function of time:

$$\psi(t) = s(t) + j\tilde{s}(t) = A(t) e^{j\phi(t)} \quad [1]$$

where $s(t)$ is an arbitrary signal where the function $\tilde{s}(t)$ is the Hilbert transform of $s(t)$:

$$\tilde{s}(t) = \frac{1}{\pi} P.V. \int_{-\infty}^{\infty} \frac{s(\tau)}{\tau - t} d\tau \quad [2]$$

and P.V means that the integral is taken in the sense of the Cauchy principal value. The instantaneous amplitude $A(t)$ and phase $\phi(t)$ are uniquely defined by [1].

The instantaneous amplitude $A(t)$ is given by :

$$A(t) = \sqrt{\Re(\tilde{s}(t))^2 + \Im(\tilde{s}(t))^2} \quad [3]$$

and the instantaneous phase $\phi(t)$:

$$\phi(t) = \arctan \frac{\tilde{s}(t)}{s(t)} \quad [4]$$

The instantaneous amplitudes and phases obtained in [3] and [4] can be used to examine possible signal interdependencies.

5.2.5 Detection of phase synchronization

In the case of the instantaneous phase, the coordination phenomenon of interest is phase synchronization. The sufficient condition for the latter is that the *instantaneous* phase difference of two synchronized systems remains bounded (see Rosenblum *et al.*, 1996, Pikovsky, Rosenblum and Kurths, 2001 and Tass *et al.* 1998). In the general case of unequal frequencies we have:

$$|n\phi_k - m\phi_l| \leq c \quad [5]$$

where ϕ_k, ϕ_l are the *instantaneous* phases of two systems k and l , c is a constant and n, m are integers defining the frequency ratio of the systems. The instantaneous phase difference $\delta\phi$ is wrapped in the interval $[0, 2\pi]$.

$$\delta\phi = [n\phi_k - m\phi_l] \bmod 2\pi \quad [6]$$

In the special case of an equality, [5] states that the phase difference will be constant. In the more general case, the phase difference will not exceed a given value and will hence remain bounded. This corresponds to synchronization in a statistical sense and can be visualized by means of a histogram of the phase difference. If the distribution of the instantaneous phase difference is flat, there is no preferred value for the phase difference, which is thus unbounded in the interval $[0, 2\pi]$. If the distribution has a preferred (modal) value, this corresponds to synchronization in statistical sense. The degree of synchronization in terms of a synchronization index can be quantified by the entropy of the distribution of the instantaneous phase differences as in Tass *et al.*, 1998. Thus the broader the distribution is, the larger the entropy and the weaker the observed synchronization. Although, this approach is very intuitive and efficient when dealing with detection of synchronization between processes of the same frequency (thus when $n=m$), it is

somewhat impractical when dealing with cross frequency n:m synchronization. In such a case, the n:m ratio has to be picked up by trial and error (Tass *et al.*, 1998). In this study we adopted a very similar approach but we treated the bivariate *instantaneous* phases of paired signals (ϕ_k and ϕ_l) as the variables of interest and calculated a phase synchrony index based on Mutual Information (see Hadjipapas *et al.*, 2005 and chapter 2). The advantage of this method is that it can be directly applied to all possible combinations of frequency ranges in the data, without having to arbitrarily choose an n:m ratio. The procedure for calculating the synchronization index (SI) follows:

The Shannon Entropy of a given univariate probability of a distribution of the phase angle in a given time series can be easily estimated using histogram based methods (Van Quyen *et al.*, 2001) according to:

$$H(\phi_k) = - \sum_{k=1}^{Nbins} p(\phi_k) \ln p(\phi_k) \quad [7]$$

where *Nbins* is the number of bins in the histogram and $p(\phi_k)$ is the relative frequency of finding the phase in the k-th bin. The number of bins was determined as the cubic root of the number of data points in the distribution. The binned distribution was then evenly spaced between its maximum and minimum.

The joint entropy can be estimated analogously as:

$$H(\phi_k, \phi_l) = - \sum_{k=1}^{Nbins} \sum_{l=1}^{Mbins} p(\phi_k, \phi_l) \ln p(\phi_k, \phi_l), \quad [8]$$

where *Nbins* and *Mbins* are the number of bins in the univariate phase distributions ϕ_k, ϕ_l respectively and $p(\phi_k, \phi_l)$ is the relative joint frequency of finding the phase ϕ_k and phase ϕ_l in the k-th and l-th bin respectively.

Mutual Information (MI) between the instantaneous phases of two signals is then:

$$MI(\phi_k, \phi_l) = H(\phi_k) + H(\phi_l) - H(\phi_k, \phi_l) \quad [9]$$

and is a measure of the statistical (linear and nonlinear) dependence between the two variables. We used a histogram-based method to assess Mutual Information. With this method the maximal MI is a function of the number of chosen histogram bins. The MI measures we present here have been normalized by the maximal possible MI.

Explicitly:

$$SI = \frac{MI}{MI_{\max}}, \quad SI \in [0, 1] \quad [10]$$

where MI is the observed Mutual Information and $MI_{\max} = \ln(Nbins)$.

In this way we obtain a synchronization index, SI , between 0 and 1, where $SI = 0$ represents no synchronization and $SI = 1$ represents perfect synchronization.

An important feature of the synchronization index based on MI is that it can identify interdependence between phase at different frequencies and thus $n:m$ phase locking according to:

$$|n\phi_k - m\phi_l| \leq c \quad [11]$$

where ϕ_k, ϕ_l are the instantaneous phases of the two frequency signals, c is a constant and n, m are integers defining the frequency ratio of the signals. If the analysis is done across the entire combination space in terms of all possible cross frequency interactions, n and m can be explicitly set to the mean frequency of the frequency range on which the analysis is being conducted.

Explicitly, if two signals of interest are narrow band filtered at two different frequency ranges, say $range_1 = f_1$ to f_2 for signal 1 and $range_2 = f_3$ to f_4 for signal 2 and ϕ_k and ϕ_l are the instantaneous phases of the narrow band filtered signals 1 and 2 respectively, then [10] can be used in the following way:

$$\left| \frac{f_3 + f_4}{2} \phi_k - \frac{f_1 + f_2}{2} \phi_l \right| \leq c \quad [12]$$

That is, $n = \frac{f_3 + f_4}{2}$ and $m = \frac{f_1 + f_2}{2}$.

The products $n\phi_k$ and $m\phi_l$ are then substituted in place of the instantaneous phase angle values (ϕ_k and ϕ_l) in equations [7]- [10] and then the cross frequency, high-order synchronization index SI is computed for every possible frequency combination.

5.2.6 Detection of interdependencies between instantaneous amplitudes.

The instantaneous amplitudes obtained from [3] are often also referred to as envelopes. These two terms will be used interchangeably in the context of this paper. The approach followed for detecting interdependencies between the instantaneous amplitudes of a given pair of signals was essentially the same as with instantaneous phases and thus using a metric based on MI. The instantaneous amplitudes obtained from [3] were substituted in equations [7] - [10], in place of the instantaneous phases to yield as a normalized measure of mutual information (MIenv).

5.2.7 Envelope versus phase interdependence

It should be noted, that although the same statistical metric (Mutual Information) was applied to both instantaneous phases and amplitudes, the two respective normalized indices SI and MIenv reflect very different properties of signal interdependency. The SI reflects a statistically stable relationship between the phases of given signals at a certain frequency (or a pair of frequencies). Thus, the SI can essentially capture the phase dynamics at a *discrete* time scales, namely the ones that corresponds to the frequencies of the synchronization process. The SI is therefore (largely) independent of any modulations in the signal amplitude. The envelope of a signal in contrast, reflects amplitude modulations of the signal that occur at a *range* of slower time scales. Thus the MIenv can reflect a common modulation of the *slow* amplitude dynamics in two signals. Note, that in contrast to the phase, the amplitude dynamics is not strictly restricted to a discrete frequency range. Consequently, apart from the obvious distinction of measuring interactions either in the phase or amplitude domain the two metrics also reflect *different* characteristic time scales.

It should be also noted that amplitude and phase are treated as independent entities from a general statistical signal processing point of view and thus *without* an explicit model of the process generating the signals. This distinction is strictly speaking only true in the case of linear stochastic processes. However, in many chaotic systems, frequency (corresponding to the mean velocity of the phase rotation) and amplitude are interdependent (see Rosenlum *et al.*, 1996, Pikovsky, Rosenblum and Kurths, 2001 and chapter 3). The consequence of this is that the phase is dependent on the amplitude and cannot be therefore clearly defined in the sense of the Hilbert transform, which assumes a more or less uniform rotation of the phase (see Boccaletti *et al.*, 2002). This becomes particularly important in systems, which exhibit multiple interrelated frequencies. Two such systems can exhibit a form of synchronization, which does not involve

adjustment of their frequencies and phases but instead occurs in the form of a deterministic mapping between their (combined amplitude and phase) dynamics. This phenomenon is referred to as generalized synchronization (Rulkov *et al.*, 1995) and methods based on explicit nonlinear models of interaction have been proposed for its detection in experimental data, such as the synchronization likelihood (see Stam and Van Dijk, 2002). Even though, the MI_{env} metric is not explicitly based on a model of the underlying data, it is likely that it will be sensitive to at least a proportion of these generalized nonlinear interdependencies.

5.2.8. Detection of nonlinearity in signal interdependencies using surrogate data.

In order to detect nonlinear structure in the interaction metrics one can compare the observed experimental data to surrogate data, in which possible nonlinear structure is fully destroyed, whereas linear structure is preserved. In the case of testing for interactions in the same frequency range but in different hemispheres we employed a multivariate algorithm for generating surrogate data, which is based on randomisation of the phase of the Fourier transformed data (Prichard and Theiler, 1994). Hence, for a given pair of experimentally observed time series, which are to be tested for interdependence, the algorithm preserves *both* the auto and cross correlation functions in the time domain (corresponding to the spectral and cross spectral density functions in the frequency domain) but destroys any higher order moments. Thus the surrogate data exhibit the *same* auto and cross correlations, the same spectra and crossspectra as the original data and can be therefore used to formulate the null hypothesis of a multivariate purely stochastic process. Briefly, the algorithm is as follows: a given pair of experimental signals is transformed in the Fourier domain using the discrete Fourier operator. Then for *both* Fourier transformed signals the phase at each frequency is rotated by the *same* random value drawn from a uniform distribution in the interval $[0, 2\pi]$. Finally, the data is transformed back to the time domain using the inverse Fourier transform. Rotating the phases by the same random variable essentially destroys possible interdependencies between different frequencies both within and between signals. Thus in operational terms, in case of the SI, the surrogate data stand for the null hypothesis of a purely linear stochastic (resonance-like) synchronization process and in terms of the MI_{env} they represent the hypothesis of a linear correlation of the envelopes. In the case of testing interactions between the two dipolar time series at *different frequency* ranges, there is no requirement to preserve the crosscorrelation function. Hence, in these cases the phases of the two Fourier-transformed dipole time series were rotated by *different* random numbers at each frequency bin yielding (after applying the inverse FFT operator) two surrogate time series. These were then filtered in two different frequency ranges and further processed in the same way as the real data.

In order to test for interactions between different frequencies in the same dipole time series we just rotated the phase of the Fourier-transformed dipole time series *once* for every frequency bin, which yielded a single surrogate time series. The latter was then filtered in two different frequency ranges and then processed in the same way as the real data.

Finally, one should consider the reliability of the procedure for generating surrogate data. It has been shown that the FFT-based surrogate methods can lead to false positive rejections of the null hypothesis when a non-gaussian amplitude distribution is not corrected for (Rapp *et al.*, 1994). Some numerical studies have shown that metrics of generalized synchronization were not affected by non-gaussian amplitude distributions and thus did not result to false positive detections of nonlinearity (Stam *et al.*, 2003). However, whether or not a non-gaussian distribution of amplitudes can give spurious detections of nonlinearity (assessed using different signal statistics) has not yet been studied systematically. Therefore, employing conservative inferential statistics over many experimental realizations is essential in order to detect any nonlinear effects, genuinely due to the experimental paradigm.

5.2.9 Statistical comparison of signal interaction metrics between observed and surrogate data

For each experimental trial and thus for any given pair of experimental signals of interest (inter or intrahemispheric), 100 surrogates were constructed. Then both the true (observed) and surrogate time series were band passed filtered and analysed in exactly the same way, to obtain SI and MI_{env} indices. This yielded a one-dimensional distribution of true SI and MI_{env} values across experimental trials and a two dimensional distribution (thus including the values for each surrogate and epoch) of surrogate SI and MI_{env} values. We wanted to test the hypothesis that *additional* nonlinear interactions occur, which are not present in the surrogate data. This was achieved by comparing the central tendency (mean/median) of the real with the surrogate distribution. Thus the null hypothesis would be that the *mean/median* of the real data distribution could in fact be drawn from a distribution of *means/medians* of the surrogate data. The latter distribution was generated as follows: for each real epoch of data 100 surrogate epochs were generated resulting in a *two dimensional* distribution of size equal to the number of epochs for the first dimension and to the number of surrogates for the second dimension. Next a random index was assigned to the surrogate dimension and the mean/median across the epoch dimension was taken. For instance a random index of 3 would mean that the 3rd surrogate of each epoch was chosen and the mean/median across all the epochs was computed. This was repeated 1000 times giving rise to a randomised distribution of the means/medians. The latter served as a null

distribution, whose one-tailed 95th confidence interval served as a significance level. Thus if the true mean/median of the observed data was larger than the 95th percentile of the random distribution of means/medians it was deemed significant.

5.2.10 Quantifying nonlinear interactions of envelope and phase dynamics in simulated datasets

In order to test the methodology described in the previous sections we used it on interactions in the phase and envelope domain, which were known to be nonlinear.

In order to test the phase synchronization metric we used two coupled Rössler systems:

$$\begin{aligned}
 \dot{\chi}_{1,2} &= -\omega_{1,2}\psi_{1,2} - z_{1,2} + \xi_{1,2} + \varepsilon (\chi_{2,1} - \chi_{1,2}), \\
 \dot{\psi}_{1,2} &= \omega_{1,2} \chi_{1,2} + 0.15 \psi_{1,2}, \\
 \dot{z}_{1,2} &= 0.2 + z_{1,2}(\chi_{1,2} - 10).
 \end{aligned} \tag{13}$$

where the parameters $\omega_1 = 1.00$, $\omega_2 = 0.7 \omega_1$ represent the natural frequencies of the two systems and govern their initial frequency mismatch ($\delta\omega = |\omega_1 - \omega_2|$); $\varepsilon = 0.18$ is the parameter governing the coupling strength of the two systems and $\xi_{1,2}$ are two Gaussian delta correlated noise processes.

The χ variables of the Rössler systems are shown in figure 1, panel A. Although the systems are diffusively coupled their interaction is not entirely linear, since the dynamics of the systems are locally chaotic and *nonidentical* (the two systems are frequency detuned). Some evidence for possible nonlinearity can be observed in the plot of the instantaneous phase difference in panel B. The latter exhibits periods of stability, which irregularly alternate with periods of acceleration and deceleration of the phase difference. Two distinct main plateaus indicating the presence of synchronization are observed: early one occurring around 1.4 radians and a later one around 1.2 radians. The distribution of the phase difference shown in panel C is indeed not uniform but indeed exhibits a bounded distribution with these two main peaks. The nonlinear nature of this phase interdependence is quantified using the methodology described in the previous sections. The results for the synchronization index (SI) analysis are shown in panel D. The observed SI between the two systems, indicated by the red line is clearly larger than the 95 % confidence interval of the distribution of mean SI in the surrogate data. In fact the true mean SI lies well

outside the null distribution, which means that there is a nonlinear component in the phase interdependence, which can not be explained by a purely linear cross correlation.

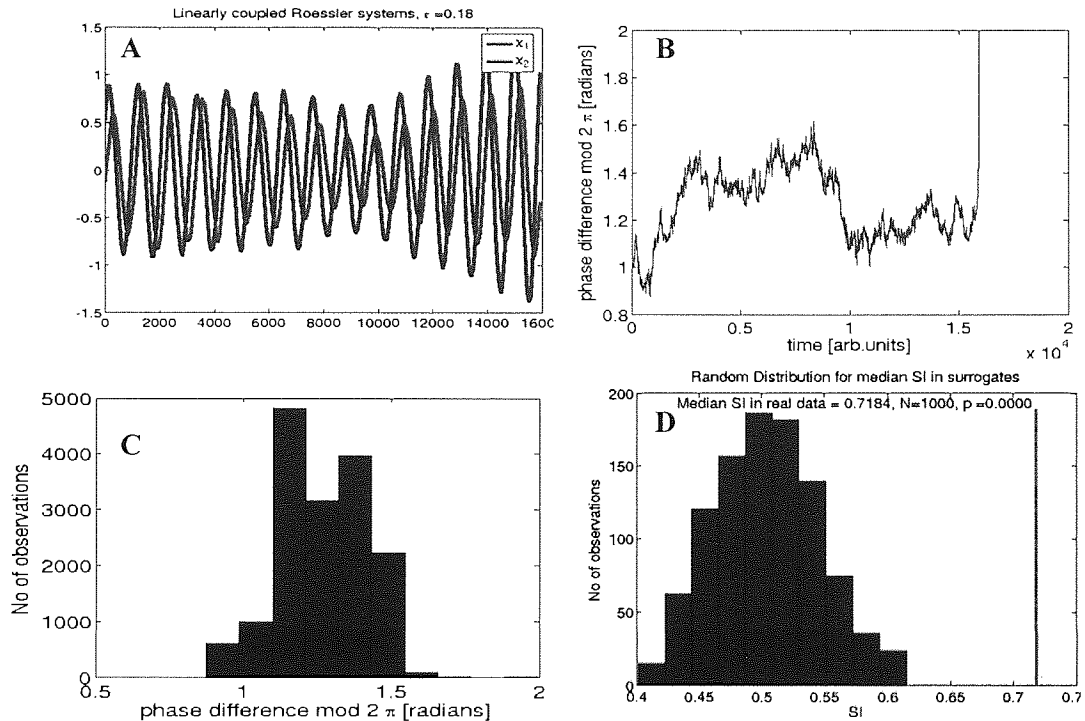


Figure 1. Quantification of nonlinear phase synchronization. Panel A. Time courses of two interacting Rössler systems, see text for details. Panel B. Time course of the phase difference of the systems in A. The phase difference is bounded denoting synchronization. Note the existence of two distinct plateaus, which are interrupted by periods of phase acceleration and deceleration. Panel C. Histogram of the phase difference shown in B. Note the bounded distribution and the existence of two modal responses. Panel D. Distribution of mean SI for the surrogate data. The 95th percentile serves as a confidence interval. The true mean is shown by the red line. Note that the true mean lies well outside the null distribution

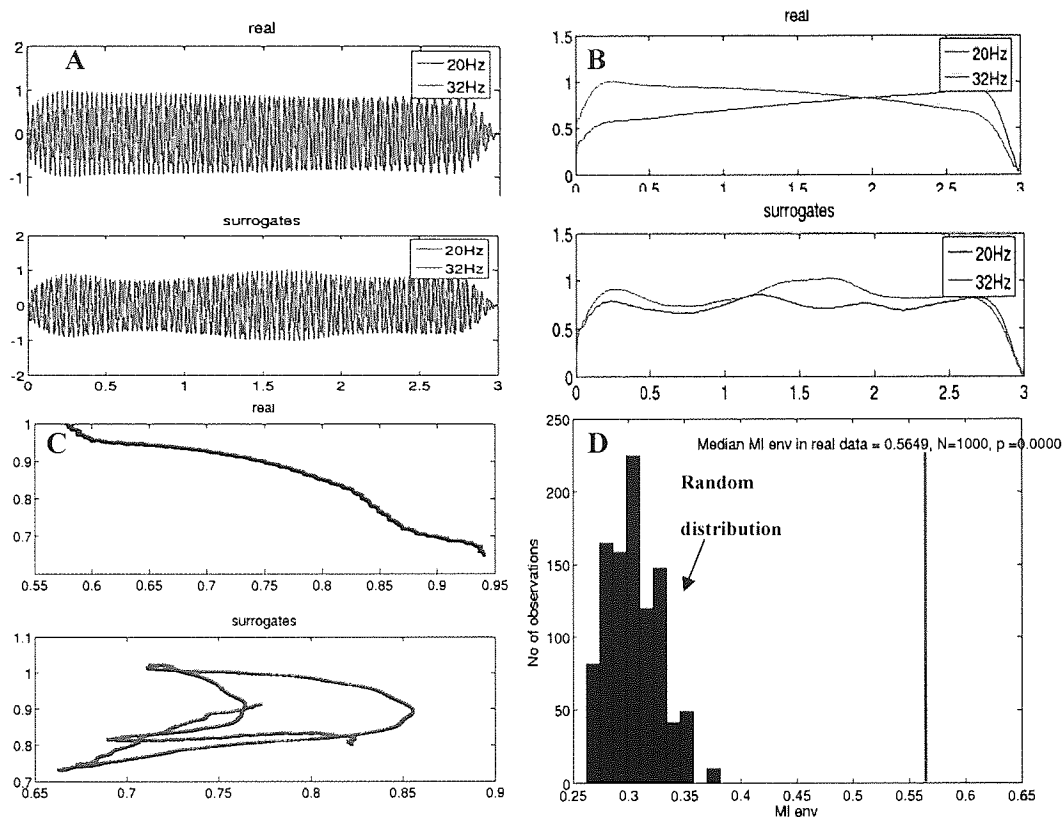


Figure 2. Quantification of nonlinear envelope interactions. Panel A shows the two signals and the corresponding surrogate data. Panel B shows the envelopes of the signals shown in A. Note the exponential damping and amplification present in the real data but not in the surrogates. Panel C shows a scatterplot of the envelopes of the signals plotted against each other. Note the clear nonlinear relationship present between the envelopes of the signals and the random scatter plot of the surrogate data. Panel D show the results of the analysis of the mutual information between the envelopes. The true median MI_{env} shown as a red line lies well outside the distribution of the medians in the surrogate data. This indicates that a truly nonlinear relationship between the envelopes of the signals exists.

In order to test for nonlinear interactions in the envelope domain we used a somewhat more artificial example. Two sinusoidal signals at different frequencies (20 and 32 Hz) were created. The signals were modulated by either an exponential damping or an exponential amplification function. The signals are shown in figure 2, panel A. For comparison surrogate data are plotted below. Panel B shows the envelopes of the signals as extracted by the Hilbert transform. Notably the exponential damping and amplification is present in the real data but not in the surrogates. Panel C shows scatterplot of the envelopes of the signals shown in B plotted against each other. A negative nonlinear relationship is clearly present between the envelopes of the true signals whereas the scatter plot of the surrogate data appears to be random. Panel D shows the results of the analysis of the mutual information between the envelopes. The true median MI_{env} lies well

outside the null distribution. This indicates that a part of the mutual information between the envelopes cannot be explained by a purely linear Gaussian process.

The above give us some confidence that the methodology applied is indeed sensitive to nonlinear interactions. The methodology was also tested against Gaussian noise to make sure that it is specific to nonlinear interactions. The analysis was performed 1000 times and the rate of false positive results was less than 5%.

5.3 Results

5.3.1 Results of dipole analysis for the time averaged AM following response.

The moments of the spatiotemporal dipole models of the averaged and band-pass filtered data for the 32-Hz diotic AM stimulus are shown in Figure 3. For all participants, dipoles localized on, or just superior to the STP, in the region of primary auditory cortex. For all participants, the magnitude of the dipole moment increases after the onset of the AM stimulus, reflecting the increased power from the steady-state evoked response within the band-pass filter centred on 32Hz. This increase in magnitude fluctuates over the duration of the stimulus epoch reflecting the influence of measurement system noise and possibly a non-stationary neuronal following response. We used the same dipole locations for both conditions because similar magnitude fluctuations are also seen in the dichotic condition. The same respective dipole location is used for both the diotic and dichotic AM.

5.3.2 Time-frequency analysis of the response to an AM stimulus and interhemispheric phase synchronization of the responses at the frequency of the stimulus

Figure 6 shows a time frequency plot of the signal arising from a source in auditory cortex for a representative participant. The presentation of the AM stimulus (at time 0) is followed by a power increase in the signal centred on the frequency of the AM stimulus (32 Hz), which constitutes the following AM response. Additionally, stimulus-related increases in power also occur at frequencies other than the ones inherent in the stimulus itself. These stimulus related power changes in ongoing cortical rhythms are most apparent in the beta and (to a lesser extent) alpha frequency bands.

In figure 4, a 500-ms portion of the narrow band filtered (30-34 Hz), but un-averaged, dipole time-series in each hemisphere is shown. The two traces show the phase of the response for diotic AM (top panel), and dichotic IAM (bottom panel). The phase difference is shifted by 180 degrees between the AM and IAM conditions. Figure 5 shows the distributions of instantaneous

phase differences between the narrow band filtered dipole time-series shown in figure 4. The 0 and 180 degree modal responses in the interhemispheric phase difference distribution closely reflect the intra-ear phase differences between the diotic and dichotic auditory stimuli respectively.

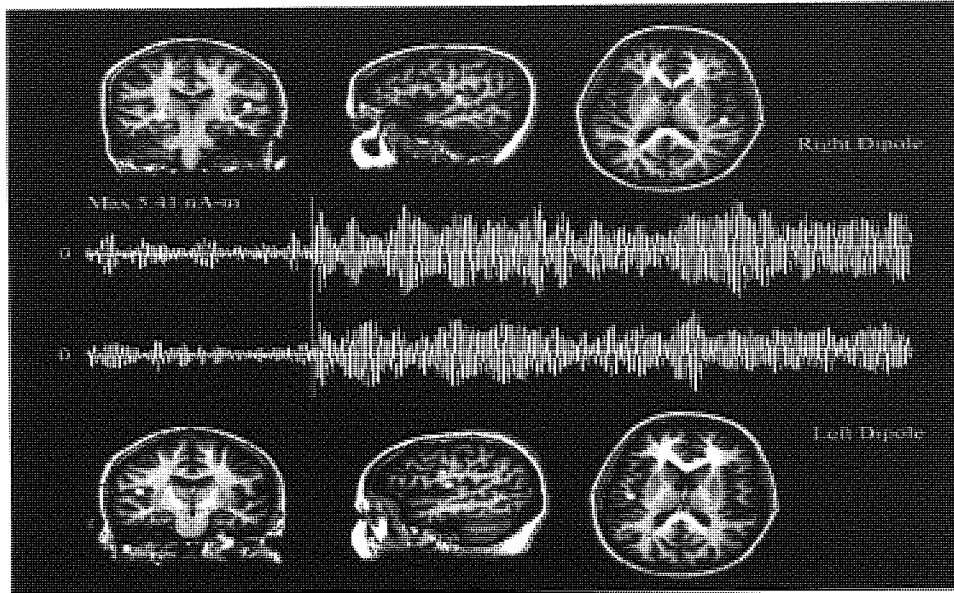


Figure 3. Spatiotemporal dipoles for participant S. The top MRI images show the location of the dipole in the right superior temporal plane, and the bottom MRI images the location of the dipole in the left superior temporal plane. The moments of the dipoles are shown next to the respective hemisphere. The onset of the sound is denoted by the vertical white bar. Note the difference in dipole magnitude before and after the stimulus onset.

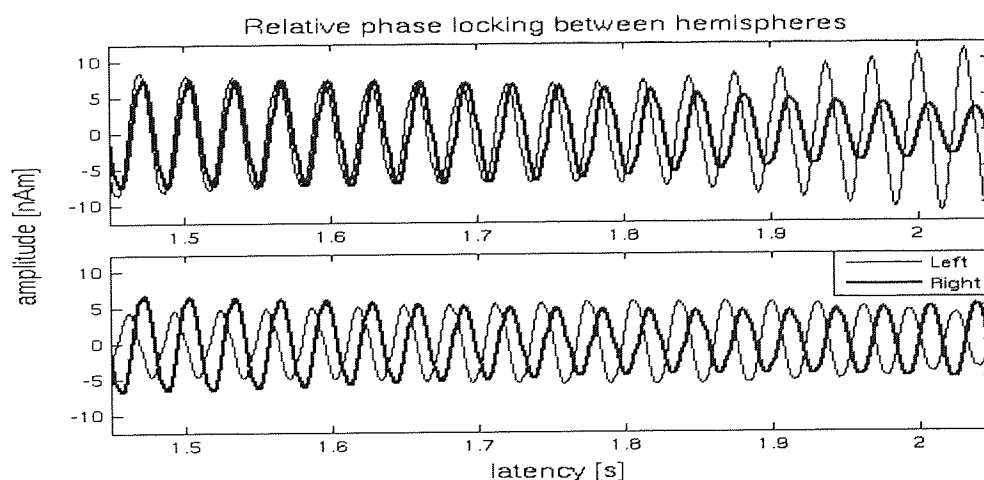


Figure 4. Non time-averaged narrow band filtered (30-34 Hz) responses to the AM stimulus in both dipoles. The top panel shows responses from each hemisphere in the diotic AM condition, and the bottom panel shows responses from each hemisphere in the dichotic AM condition. The phase locking to the AM stimulus is constant.

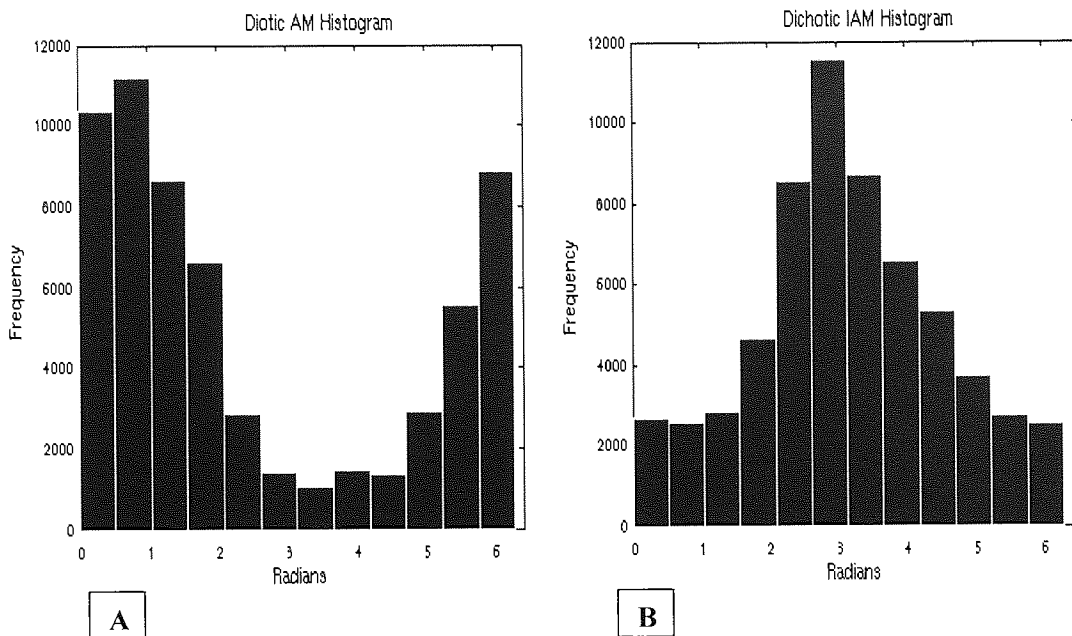


Figure 5. Distributions of relative phase differences wrapped in the interval $[0, 2\pi]$ between the responses in Figure 4. Panel A shows the diotic stimulation condition and panel B shows the dichotic condition. In Figure 2, responses for participant KDS are shown for 500 ms of the first epoch. The above histograms however are calculated the phase difference for the whole 4 seconds of the modulation. The distributions of the phase difference are consistent with phase synchronization in a statistical sense. Note that the phase synchronization occurs at different phase lags for the diotic and dichotic case. The modal responses of the interhemispheric phase difference at the frequency of the AM strongly reflect the phase differences inherent in the auditory stimulation.

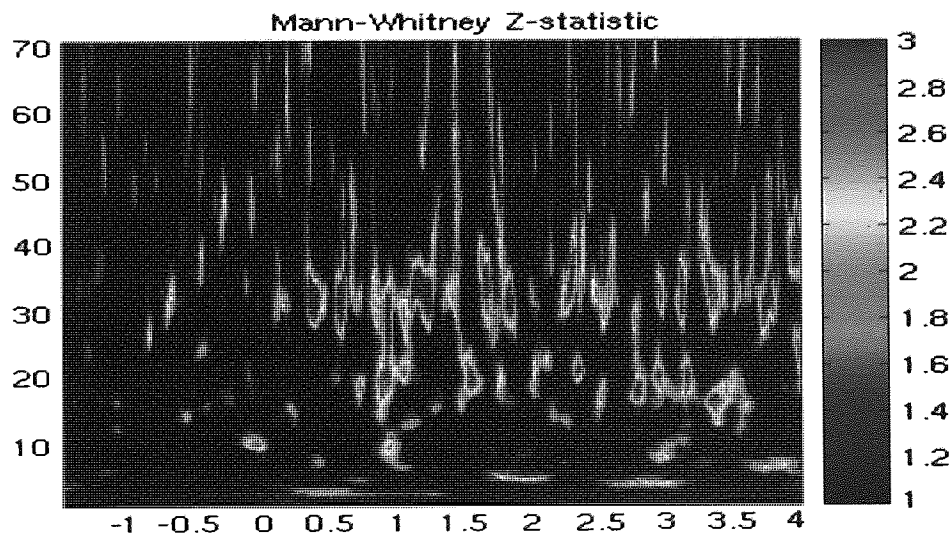


Figure 6. Time frequency analysis (participant JS) in a virtual electrode at the source of the AM following response, which is localised with Synthetic Aperture Magnetometry (SAM, see Robinson and Vrba 1999, Barnes and Hillebrand, 2003), a beamformer method for localising the source of M&acti activity that is complimentary to dipole modelling. SAM provides a power-based metric of oscillatory change, rather than amplitude change, thus permitting the additional observation of stimulus induced neuronal activity which is not necessarily phase locked to the stimulus onset and therefore not observed in averaged data sets. SAM

weights were derived for data in a 2-Hz wide frequency band centred on 32 Hz. The responses in the 'active' 32 Hz epochs, and 'passive' Pure Tone epochs were calculated with Morlet Gaussian wavelets, and compared using a Mann Whitney statistic (see methods). The Mann Whitney Z is shown on a colour scale, and displayed in the colour bar. Note that the power of the signal increases at the frequency of the AM stimulus (around 32 Hz- the following AM response). Additionally, stimulus related increases in power occur are also seen in the alpha and beta frequency ranges. These responses occur at frequencies, which are not inherent in the auditory AM stimulation and therefore correspond to stimulus-induced power changes of the ongoing cortical rhythms.

5.3.3. Quantifying the variance of instantaneous envelopes in the AM following response

As it is evident in figures 2 and 3, the AM following response seems to exhibit variations in its amplitude. These are best described as fluctuations in the instantaneous envelope of the signal. The signal plus noise model inherent in the SSAEP literature assumes that these fluctuations are purely due to superimposed Gaussian noise. Thus according to that data model, the envelope of the AM following response should be flat and any fluctuations would just be due to random noise. Thus the first step for examining this hypothesis will be to compare the variability of the instantaneous envelopes of the following AM response against those arising from system noise alone. The system noise condition essentially involved data acquisition identical to the experimental condition but without a participant in the scanner. The system noise data was subsequently treated in the exact same way as the experimental data. This enables to quantify fluctuations in the envelope in the same frequency band as the AM following response, which are merely due to system noise.

Both experimental and system noise data were filtered between 30-34 Hz (the frequency range for the AM following response). Then the instantaneous envelopes were extracted using the Hilbert transform. The standard deviation of the envelopes was computed for each epoch in each dipole time series.

Figure 7 shows the results for participant IEH (top panel) and system noise recording (bottom

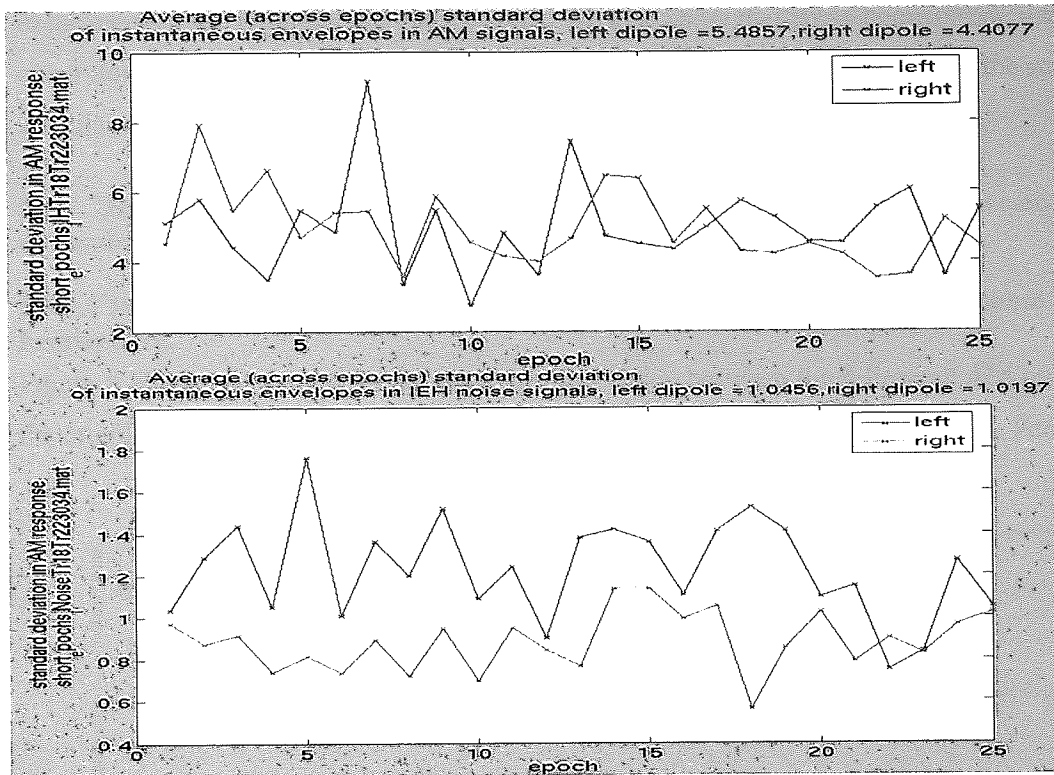


Figure 7. Epochwise standard deviations of instantaneous envelopes in 30-34 Hz narrow band filtered signals for the two spatiotemporal dipoles for participant IEH (top panel) and system noise (bottom panel) in nAm. The average variability of the envelopes in the following AM response is four times larger than the one in system noise.

panel). The average (across epochs) standard deviations for the following response for the left and right dipole in participant IEH is 5.48 nAm and 4.4 nAm respectively. However, the corresponding metrics for the system noise are only 1.04 and 1.01 nAm. Squaring the average standard deviations for the AM following response gives the total variance of the envelope. The ratio of the variances in the system noise condition and the following AM response gives us the amount of envelope in the following AM response that can be explained merely by system noise. In the case shown here only 3% of the variance of the instantaneous envelopes can be explained by system noise for the left dipole and 5% for the right dipole. Thus more than 90% of the variability in the instantaneous envelope of the following AM response cannot be explained by the noise. Very similar results were observed for the two other participants; for participant KDS the variance explained by system noise was less than 0.5%. The latter result suggests that the signal plus noise model for the AM response clearly does not explain the observed data. Over 90% of the variance in the continuous envelope dynamics are not due to system noise and must be due to some neuronal process in the brain. In the next section we show that some of this

variability may be due to interactions between the AM following response with ongoing rhythms in the same or the contralateral hemispheres. We also show that cross-hemispheric interactions occur during the presentation of the AM stimulus at frequencies independent of the sensory stimulation.

5.3.4. Detection of local and global nonlinear interactions in continuous phase and envelope dynamics

5.3.4.1 Interactions of following AM response with ongoing rhythms in the same hemisphere.

Figure 8, shows the results for the envelope interaction between the following AM response and the ongoing rhythms for the right hemispheric dipole time series, participant IEH. Panel A

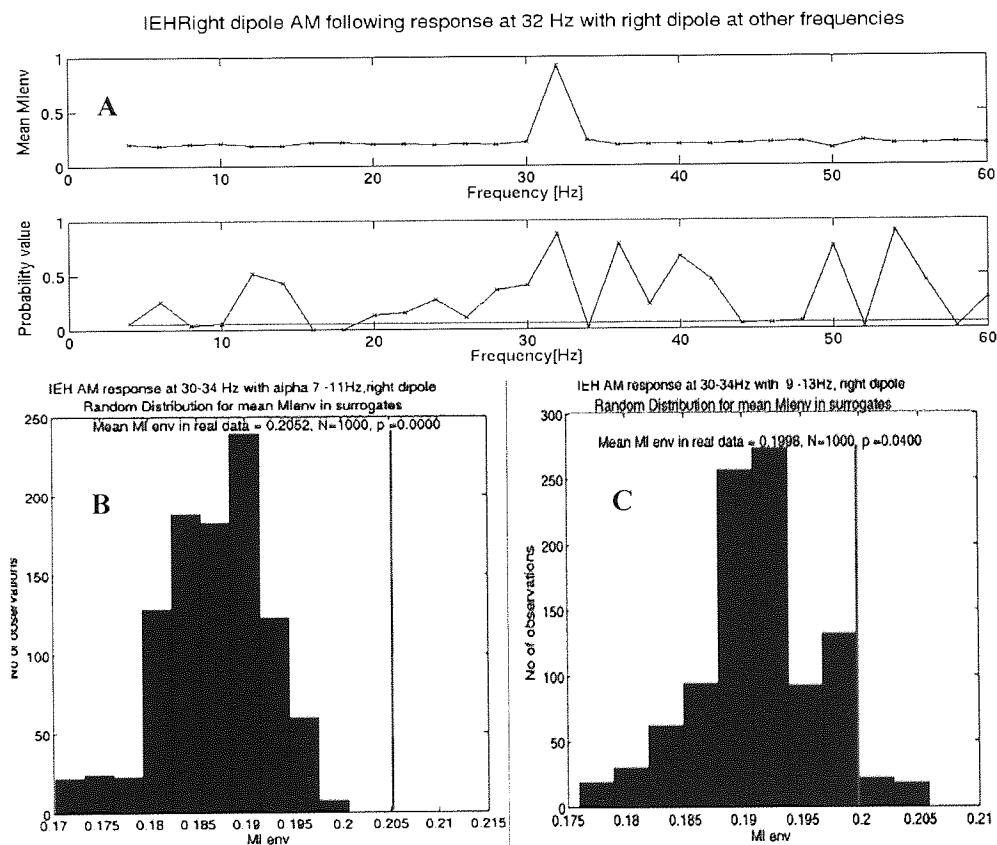


Figure 8. Results for the interaction between the instantaneous envelopes between the AM following response and the ongoing rhythms in the right dipole time series, participant IEH. Panel A shows the summary of the testing for interaction of the AM following response (30-34 Hz) with other frequencies in the same dipole time series. The top plot corresponds to the mean MIenv statistic across epochs and the bottom plot to the associated p-value obtained from the null distribution of means in the surrogate data. The red horizontal line indicates the p=0.05 threshold. Note that each point in the summary graph was collected independently. Significant interactions with the AM following response can be observed in the alpha and beta range. Panels B and C show details for the interaction of the following AM response with the alpha band. Panel B shows the random distribution of means in the surrogate data for the interaction of the following AM response with the lower alpha band (7-11Hz). The red line indicates the true mean. Note that the true mean is well outside the null distribution. Panel C shows the corresponding result for the higher alpha band (9-13Hz).

shows the summary of envelope interactions of the following AM response(30-34Hz) with the other frequencies in the same time series. The top plot in panel A corresponds to the true mean MI_{env} and the bottom plot corresponds to the probability value that the true mean could be obtained from the null distribution of means in the surrogate data. The results from testing of the median MI_{env} were generally consistent with the results for the mean, so that these are not shown here. Note that each probability point in the summary plot was collected independently, since the mean value for that particular interaction was tested against a random distribution of mean MI_{env} in the surrogate data. Significant interactions of the following AM response in the alpha and beta band are observed. Panels B and C show details of the interaction of the following AM response with the alpha rhythm in two subsequent frequency ranges in the alpha band, namely 7-11 and 9-13 Hz. The results are deemed significant implying a nonlinear envelope interaction. However testing the same frequency bands in the other two participants did not yield significant results. The latter taken together with the fact that multiple comparisons are made suggest that any conclusions based on such pattern of results should be drawn with great caution. Nevertheless, the fact that subsequent frequency bins show similar behaviour and the fact that the results for the lower alpha band (7-11Hz) are highly significant suggest that a type 1 error is rather unlikely. In addition the fact that the analysis was conducted across epochs suggests a systematic nonlinear effect.

Similar behaviour was observed for local interactions of the following AM response with ongoing rhythms in the *left* hemisphere. Figure 9 shows the summary of results for participants IEH and JS. The figure is formatted in the same way as figure 8A. Panels A and B show the results for participants IEH and JS respectively. In both participants an interaction of the following AM response with the ongoing alpha rhythm can be observed. In participant IEH there is an additional interaction of the following AM response with the ongoing beta rhythm.

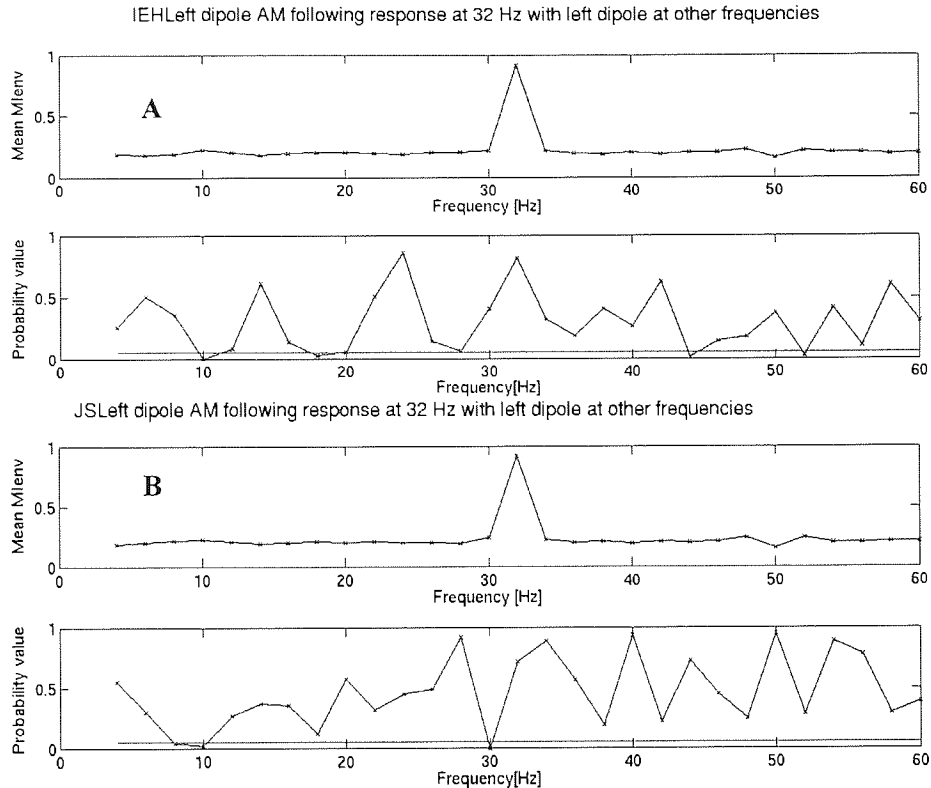


Figure 9. Summary of results for the interaction of the left following AM response (30-34Hz) with ongoing rhythms in the same dipole for participants IEH (panel A) and JS (panel B). The figure is formatted exactly as figure 8A. The top plots show the mean Mlenv for the interaction and the bottom plots the associated p-value. Note that in both participants a significant interaction of the following AM response with the ongoing alpha rhythm can be observed. This result is consistent with the interactions in the right hemispheric dipole. In participant IEH there is an additional interaction of the following AM response with the beta band.

5.3.4.2 Interactions of following AM response with ongoing rhythms in the contralateral hemisphere.

Figure 10 shows significant envelope interactions between the following AM response in the right dipole time series and the ongoing beta rhythms in the left hemisphere for participants KDS and IEH. Note that the interactions occur at somewhat different frequencies for the two participants. For participant IEH there are additional interactions of the following AM response with the beta rhythm. Interestingly, the beta rhythms in the two hemispheres are also mutually interactive (next section).

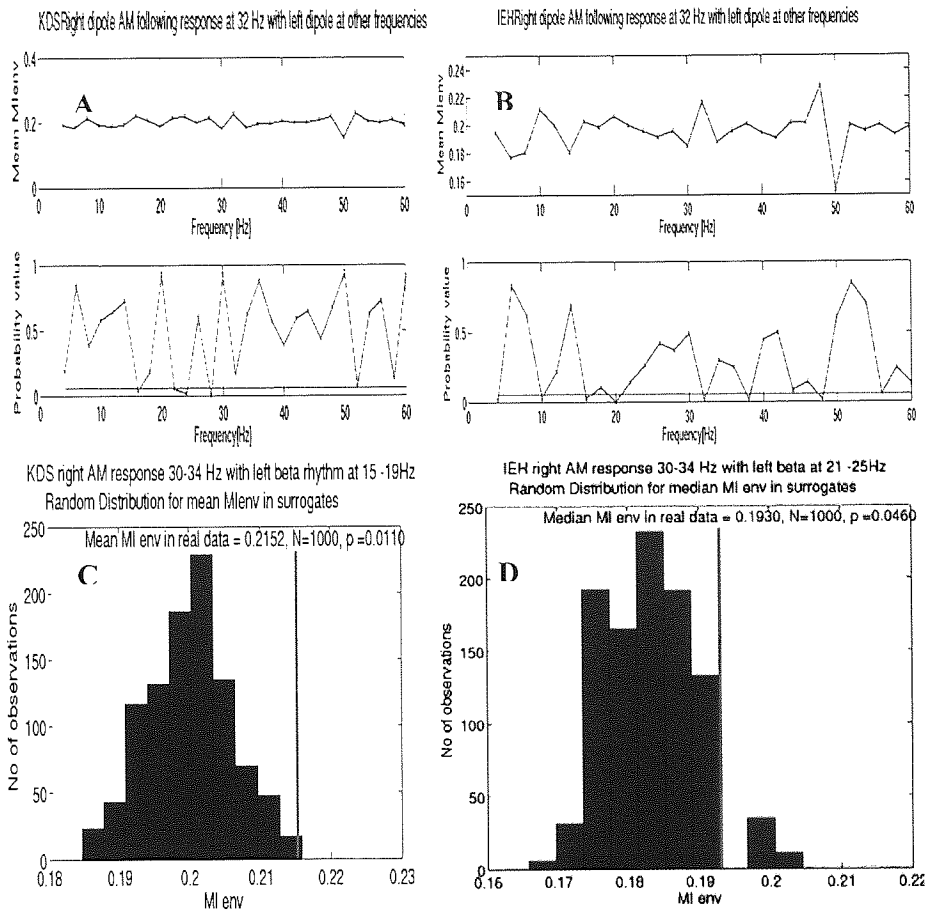


Figure 10. Interactions of the following AM response in the right dipole time series with the ongoing rhythms in the left dipole time series. Panel A and B summarize results for participant KDS and IEH respectively. These panels are formatted in the same way as figure 8A. Note that in both participants there is a significant crosshemispheric interaction of the following AM response with ongoing beta rhythms, however this occurs at somewhat different frequencies for each participant. Panels C and D show details of these interactions for participant KDS and IEH respectively. Panel C: there is a significant interaction of the AM following response in the right dipole with the ongoing beta rhythm in the left hemispheric dipole (15-19Hz). Panel D, participant IEH: a marginally significant interaction of the AM following response in the right dipole with the ongoing beta rhythm in the left hemispheric dipole at a somewhat higher frequency (21-25Hz).

Notably, for participant IEH nonlinear $n:m$ phase synchronization could be observed between the AM following response and alpha and beta ongoing rhythms in the *contralateral* dipole (figure 11). The same participant also showed crosshemispheric envelope interactions. However, for the other two participants no such (phase-domain) interactions could be detected.

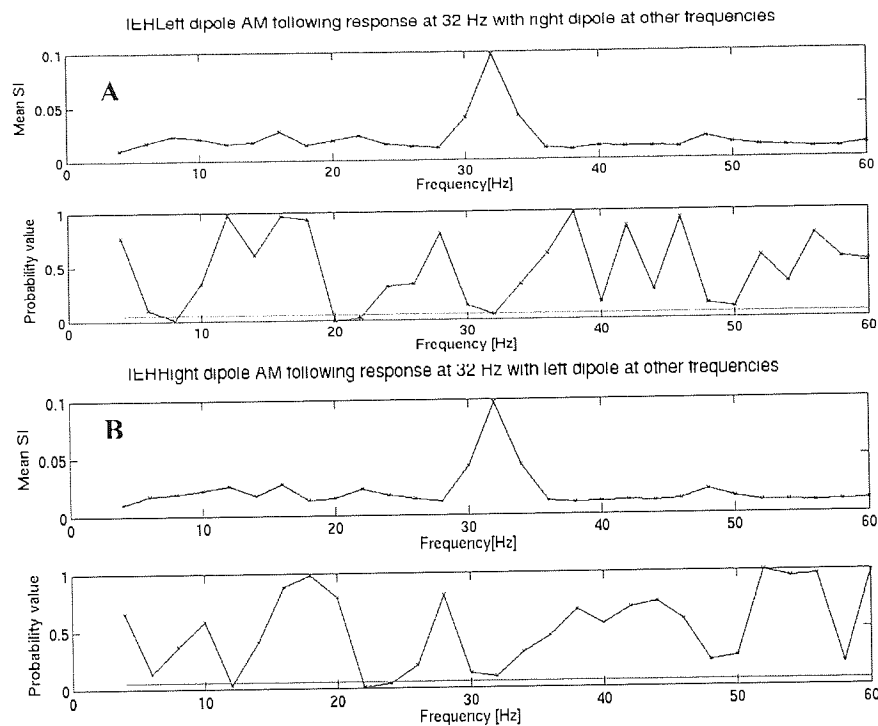


Figure 11. Nonlinear, crosshemispheric, n:m phase synchronization between the AM following response and ongoing rhythms in the contralateral hemisphere (participant IEH). Panel A shows the interactions of the right hemispheric AM following response with the ongoing rhythms on the left. Panel B shows the interactions of the left hemispheric following AM response with ongoing rhythms in the right hemispheric dipole. 'Mean SI' indicates the mean synchronization index across epochs for each frequency bin. The plot below indicates the associated probability value. The red line indicates the $p < 0.05$ threshold. Significant results are found between the beta band and the following AM response suggesting nonlinear n:m phase synchronization.

5.3.4.3 Interhemispheric interactions between ongoing rhythms in the same frequency range.

Figure 12 shows the summary of results for envelope interactions in the *same* frequency ranges between the two hemispheres. For all participants interactions of the ongoing rhythms in the alpha and/or the beta band can be observed. These interactions occur *during* the presentation of the AM stimulus. Details of some of these interactions are shown in Figure 13. Participant IEH shows significant crosshemispheric envelope interactions in the alpha band. Recall that the alpha rhythm in the right dipole was found to be nonlinearly interacting with the AM following response in the same hemisphere.

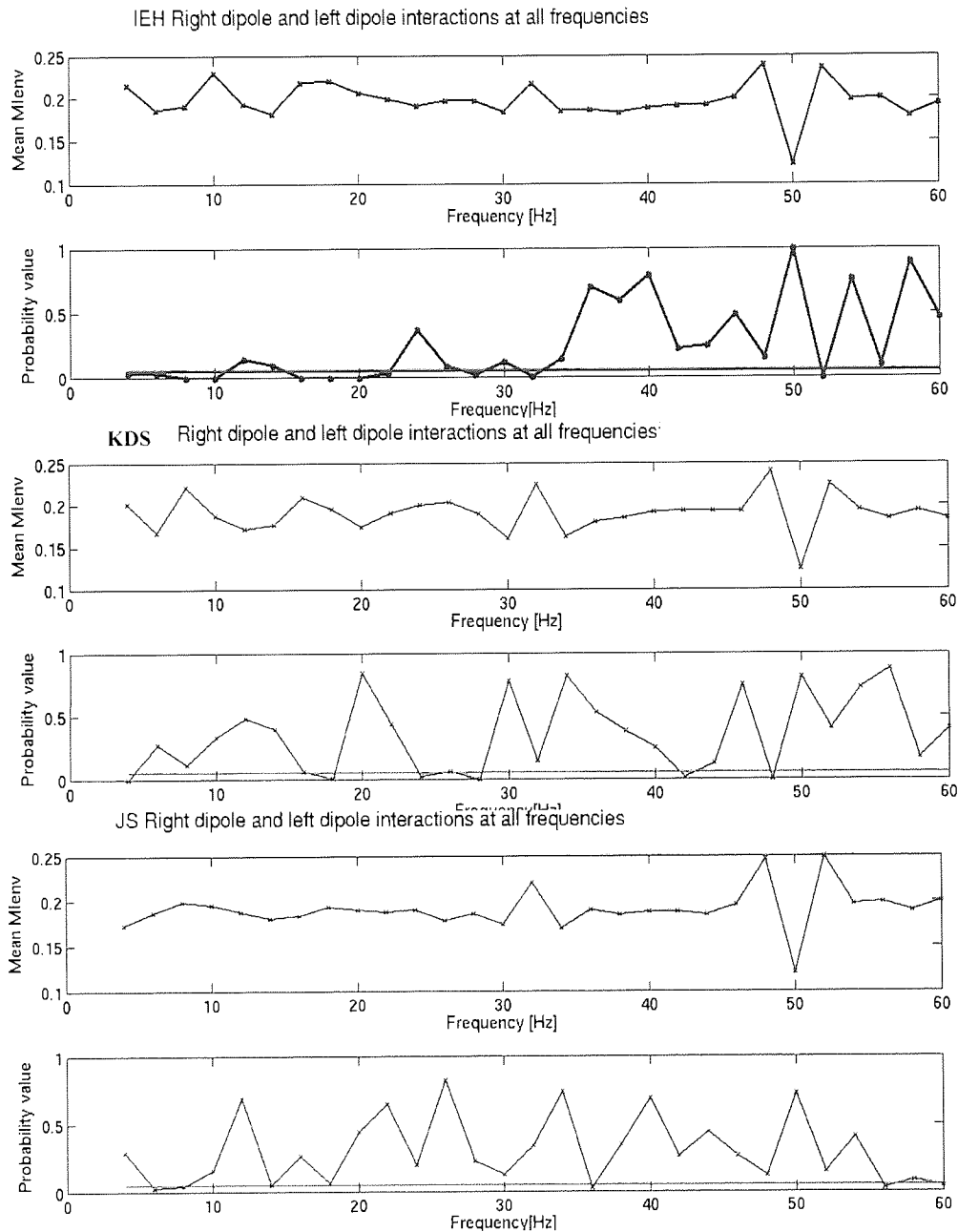


Figure 12. Summary results for crosshemispheric envelope interactions in the same frequency for participants IEH, KDS and JS (from top to bottom). The format of the plots is the same as in figure 8A. For all participants interactions of the ongoing rhythms (concurrent with the AM stimulus) in the alpha and/or beta band are observed.

Thus alpha and beta rhythms cannot be considered as simple 'brain' noise, since they are not only mutually interactive but also *modulate* the AM following responses both in terms of its slow amplitude and phase dynamics. Furthermore in participant KDS the following AM response at

30-34 Hz was found to exhibit distinctly nonlinear phase synchronization as shown in figure 14. This would not be expected if the two auditory cortices were simply driven by the periodic AM stimulus. The latter scenario would only give rise to a linear crosscorrelation. The finding of a nonlinear phase synchronization taken together with the nonlinear envelope interdependencies in the beta rhythm seems to reinforce the notion, that there is a genuine interaction between the two auditory cortices during the presentation of the AM stimulus. However, such nonlinear phase synchronization was not observed for the other two participants.

Although the data was not corrected for multiple comparisons, which may have introduced type I errors, the pattern of the observed interactions, the fact that the statistics were conducted across all experimental epochs and the extremely low probability values make the case that the particular interactions illustrated here were genuine.

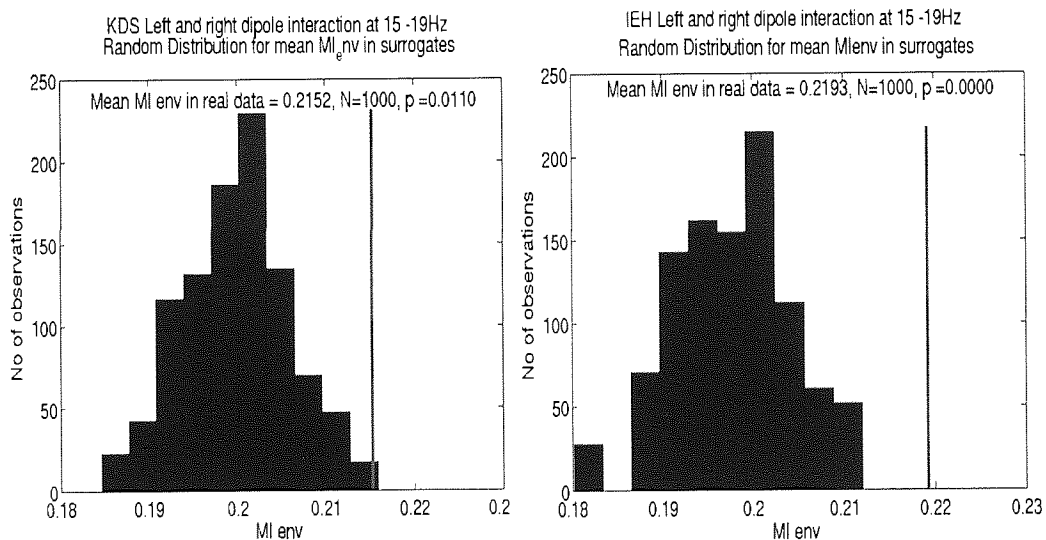


Figure 13. Significant cross-hemispheric interactions in the envelope dynamics of the ongoing beta rhythms during the presentation of the AM stimulus for participants KDS (left) and IEH (right).

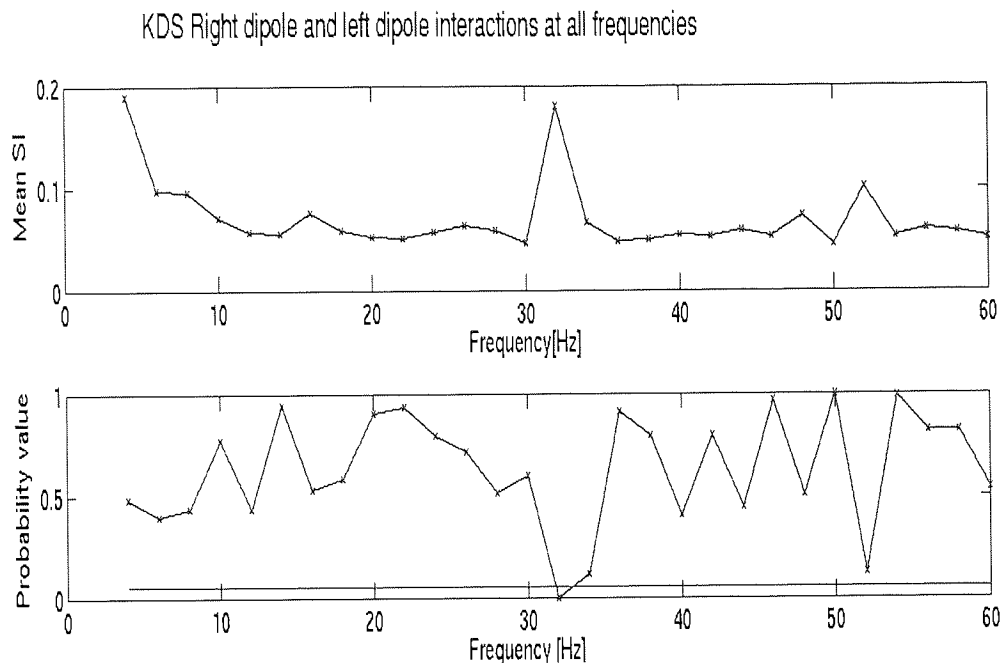


Figure 14. Participant KDS. Summary of interhemispheric phase synchronization analysis. The top plot shows the mean synchronization index across epochs for each frequency bin. The bottom plot indicates the associated probability value. The red line indicates the $p=0.05$ threshold. Note the significant result at the frequencies close to the frequency of the AM stimulation. This indicates the presence of nonlinear phase synchronization between the two hemispheres.

5.4 Discussion

In this study we set out to test the concept of the steady state response following an AM stimulus. The latter implies that a constant and invariant signal response follows the stimulus and any variations in that response are due to noise, irrelevant to the processing of the stimulus (Picton *et al.*, 1987, Ross *et al.*, 2003, Pantev *et al.*, 1996). However, from information theoretical point of view the concept of a steady state response of the auditory cortex to an AM stimulus is not efficient, since a rigid, stable and periodic response that closely follows the stimulus simply corresponds to signal transmission. Yet, accurate signal transmission is known to already occur at the level of the inferior colliculus (Rees and Moller, 1987) and it is not consistent with the putative role of the auditory cortex, which presumably involves some kind of integrative process.

Investigation of the instantaneous (non time- averaged) envelope dynamics of the following AM response strongly suggested that the variability in the following AM response cannot be simply due to noise. In fact system noise could only explain 3-5% of the total variance in the

instantaneous envelopes. This indicated that the rest of the variance must be entailed in neuronal processes, which somehow modulate the following AM response.

We found that the instantaneous *phase* dynamics of the AM following response were overall indeed consistent with periodic locking to the stimulus. This was further supported by the fact, that the modal response in the distribution of the interhemispheric phase difference (of the AM following responses) strongly reflected the nature of the intraaural phase difference inherent in the stimulus. Nevertheless, in one of the three participants (KDS) *nonlinear phase synchronization* was observed indicating a genuine interaction between the two hemispheres, which could not be simply due to common driving from the brainstem.

Further, we found instantaneous *envelope* interactions of the AM following response with the ongoing alpha and beta rhythms in the same and the contralateral hemisphere. Interestingly, alpha and beta rhythms in the two hemispheres were also found to be nonlinearly interactive in the envelope domain. For one participant (IEH), additional nonlinear, high-order ($n:m$) phase synchronization of the AM following response and the ongoing alpha and beta rhythms could be detected. The crosshemispheric interactions of the ongoing rhythms during the presentation of the AM stimulus, strongly suggest that both alpha and beta ongoing rhythms cannot be considered simply as crosscorellated noise processes and thus discarded by means of signal averaging. In addition, the fact that these ongoing rhythms *modulate* the AM following response in the same or the contralateral hemisphere strongly suggests that they are relevant for the processing of the AM stimulus.

The effects described above were not generally consistent across participants. One reason for this may be the individual variability of the ongoing rhythms. The small number of participants and the fact that the analysis was conducted in terms of partitioning the signal in predetermined frequency bands may have contributed for the lack of consistency. Moreover, the presence of strong nonlinear *envelope* interactions taken together with *lack* of strong nonlinear *phase* synchronization is very intriguing and points to a potentially crucial fact about macroscopic brain interactions. The instantaneous envelopes reflect slow amplitude dynamics across a range of time scales and their interactions are not strictly confined to the time scale imposed by the narrow band filter. Thus metrics of envelope interaction may reflect generalized interdependencies in the signal, which are not confined to the frequency or phase domain. Such generalized synchronization phenomena (Rulkov *et al.*, 1995) are not only of particular theoretical interest

but also methods exploiting this concept (for instance Breakspear and Terry, 2002a and Stam and Van Dijk, 2002) have been successfully utilized to characterize brain coordination in health (Breakspear and Terry 2002a, Stam, van Walsum and Micheloyannis 2002, Stam *et al.*, 2003) and disease (Stam *et al.*, 2002, Altenburg *et al.*, 2003). The main advantage of these methods is that they do not necessarily depend on narrow band filtering and thus the arbitrary partitioning of the signal in to frequency bands can be avoided; the latter may indeed remove undesired individual variability in the frequency domain. The fact that the most pronounced interactions reported here occur in the envelope domain may also advocate the notion that long-range interactions between brain areas may not strictly occur at given frequencies and thus methods based on generalized synchronization may prove more appropriate for their study. However, the approach followed here is also justified when distinct frequency components are present in the signal. These often indeed reflect ongoing brain rhythms, which can be considered as separate semiautonomous entities. Nevertheless, narrow band filtering can attenuate otherwise present interdependencies between frequencies. The latter may to some degree explain why we did not find pronounced nonlinear phase synchronization.

Our results suggest that detections of nonlinear structure were rather rare. Some remarks for possible causes for such rare detections are in order. In the study presented here we adopted an approach to quantify nonlinear interactions specific to the experimental paradigm. Therefore the inferential statistics were conducted across experimental epochs. We were testing that the mean metric of interdependence across epochs could be distinguished from the distributions of means in surrogate data. The latter were however constructed on the basis of all the experimental epochs. Thus in order to be able to reject the null hypothesis nonlinear interdependence should have been present in the majority of experimental epochs. Although this approach of testing across experimental epochs is perfectly justified for the particular task, where experimental epochs are expected to be homogeneous (and indeed there is evidence for stimulus specific spectral changes, which are consistent across epochs), it may prove too rigorous for the detection of nonlinear interdependence. The latter is supported by the literature, which suggests that nonlinear interdependence occurs only in a very small number of epochs (Breakspear and Terry, 2002a). Breakspear and Terry (2002a) adopted an epoch-wise approach for detecting nonlinear interdependence. The latter enables for the identification of 'nonlinear' epochs. These epochs can then be further studied in more detail. This epoch-wise approach is entirely justified for the study of spontaneous brain rhythms, where individual data epochs are not expected to be homogeneous and such studies have indeed yielded some fruitful insights in the phenomenology of the human

alpha rhythm (Breakspear and Terry, 2002a). However, in our study we were interested to quantify nonlinear interactions, which were strictly related to the particular stimulus. In this case an epoch-wise approach may help identifying a higher proportion of nonlinear interactions otherwise obscured by the epoch average. Nevertheless, such an approach will inevitably reduce the task /stimulus specificity of the results.

Finally, an important conceptual issue has to be discussed in relation to the predominantly linear patterns of interaction associated with the AM stimulus. The AM stimulus imposes a strong periodic driving in the early auditory pathways. This has been well documented at the level of the brain stem (Rees and Moller, 1987). Neurons in the inferior colliculus have been found to strictly phase lock to the stimulus. These neurons however provide the main input to the auditory cortex. The latter can be viewed abstractly as strong periodic forcing on the dynamics of the auditory cortex, which may be abstractly conceptualized as a nonlinear oscillator. Such dynamic scenarios often result in a regularization of the otherwise nonlinear dynamics. The latter become entrained through the periodic driving and undergo a global bifurcation resulting to low dimensional periodic dynamics. This phenomenon is known as chaos destroying synchronization (Pikovsky, Rosenblum and Kurths, 2001, Boccaletti *et al.*, 2002 and chapter 3). The latter may be indeed the case for the AM following response. This is particularly obvious in the phase dynamics, which seem to generally conform to periodic entrainment. However, the driving may not be strong enough to completely entrain the amplitude dynamics, which may be captured in the instantaneous envelopes. This effect reflects a fundamental property of oscillators: the phase of an oscillator is much easier to adjust (it requires considerably less forcing) than the amplitude (Pikovsky, Rosenblum and Kurths, 2001). The latter may explain why the slow amplitude dynamics as reflected in the instantaneous envelopes exhibit nonlinear structure more frequently than phase dynamics in the context of the particular task. The main consequence of the above is that the overall periodic behaviour of the following AM response observed in this paradigm may not be characteristic for the activity of the auditory cortex in real life situations but may instead result purely as a consequence of strong forcing by an artificial, overly periodic stimulus. Such stimuli however have limited ecological validity, since they are infrequent in the environment and are even less characteristic for speech signals, which on the contrary exhibit complex spectral and temporal structure.

In conclusion, we set to examine the concept of the steady state response following an AM stimulus by studying the continuous phase and amplitude dynamics. We argued that the signal

plus noise concept of the AM following response may be very unfavourable in terms of information theory. We showed that only 3-5% of the variability of the AM following response can be attributed to system noise. We presented a methodology for detecting local and global nonlinear interactions in order to account for the residual variability. We found some evidence for envelope interactions of the ongoing alpha and beta rhythms and the following AM response within the same and the contralateral hemisphere. Furthermore, we found crosshemispheric interactions of the ongoing alpha and beta rhythms, which were *concurrent* with the stimulus. This strongly suggests that ongoing rhythms *modulate* the following AM response and are therefore relevant for the processing of the stimulus. The results presented here, namely the presence of nonlinear interdependencies in macroscopic brain signals are in agreement with existing literature (Breakspear and Terry, 2002a, Stam *et al.*, 2003), despite the fact that very different metrics of nonlinear interaction were employed. The findings presented here may extend this literature by virtue of the fact that the nonlinear interactions reported in this study occur between well-defined neuronal *sources* and within the context of a *specific* experimental paradigm.

Chapter 6: The functional role of gamma oscillations in sensory coding- A complex systems approach.

6.1 Background and objectives

The abstract models presented in chapter 4 suggested that functional clusters may be defined in terms of *phase synchronization* between cortical columns at mesoscopic scales.

Furthermore, the synchronization processes in separate clusters occurred at different frequency ranges, giving rise to *frequency-specific* power changes in the macroscopic mean field signal. Therefore we hypothesize that spatial stimuli, which require integration of activity across distributed cortical columns in primary visual cortex, would be accompanied by the emergence of frequency-specific mean field oscillations.

Several authors have demonstrated a close relationship between neuronal spike synchronization and induced *gamma oscillations* (30-60Hz) in the Local Field Potential (LFP), which records the collective activity of thousands of neurons, and is often referred to as the mean field (Gray and Singer, 1995, Koenig, Engel, Singer 1995, Traub *et al.*, 1996, Nase *et al.*, 2003). Consequently, if synchronization acts as a grouping mechanism at the neuronal level, then we should expect a coherent mean field gamma oscillation in macroscopic brain signals when encoding a global coherent pattern. The spatial frequency (SF) of full-field gratings is such a holistic feature, since information from different parts of the visual field, which is retinotopically represented in primary visual cortex, is needed to infer the SF of the stimulus. Spatial frequency is fundamental feature of natural objects and scenes since it captures the scale of contours. Thus one may expect that neurons coding for contours of the same spatial frequency may synchronize their responses resulting in a mean field oscillation in the gamma frequency range. However, the problem remains of how distinct global neuronal representations of such patterns are distinguished assuming that neuronal synchronization is always involved in their formation. The frequency of the mean

field oscillation, that is the frequency (or frequency range) of the collective synchronization process occurring at the microscopic neuronal level might provide such a differentiating feature. In a complex system such as the visual brain, which potentially requires spatially overlapping networks to be simultaneously active and thus synchronized in order to encode a visual scene (Engel, Konig, Singer, 1991), network frequency could act as a highly effective segregating variable. This idea is also consistent with the modelling work presented in chapter 4.

In order to test these hypotheses we reanalysed previously recorded MEG data during an experimental paradigm, where the spatial frequency of the stimuli was parametrically varied (Adjamian *et al.*, 2004a).

6.2 Methods

6.2.1 Subjects/Materials and Experimental procedures

Details of the methods employed were reported in an earlier paper (Adjamian *et al.*, 2004a). In short, seven subjects (three males, four females, aged (24–47 years) participated in the study after giving their informed consent. Subjects viewed a set of static horizontal black/white square-wave grating patterns for 5 s (experimental condition or active period) followed by 5 s of a uniform field of the same mean luminance (control condition or passive period). Each sequence of active and passive states was repeated 20 times for each grating SF, starting from 0.5 c.p.d., with increments of 1 c.p.d. up to 6 c.p.d. Each SF of the grating was presented in separate recording sessions. The presentation of gratings was randomized in order to avoid task familiarity and habituation of cortical neurons.

6.2.2 Recordings

MEG data were recorded using a 151-channel system, (CTF Systems Inc., a subsidiary of VSM MedTech Ltd) using 3rd order gradiometer configuration. The data were sampled offline at 625 Hz and anti alias filtered at 100Hz. A 50Hz comb filter was applied to remove the power line interference and its harmonics. Individual MEG data were then coregistered with

each subjects anatomical MRI (Adjamian *et al.*, 2004b), to prepare them for source reconstruction procedures.

6.2.3 Source Reconstruction

We used synthetic aperture magnetometry (SAM, chapter 2, Van Veen *et al.*, 1997, Robinson and Vrba, 1999, Singh *et al.*, 2002, Barnes and Hillebrand 2003, Singh, Barnes and Hillebrand, 2003) to generate statistical parametric maps (SPMs') of stimulus or event-related changes in cortical oscillatory power (Pfurtscheller and Lopes Da Silva, 1999). We obtained locations for region of interest, or virtual electrode, analysis (Barnes and Hillebrand 2003, Singh, Barnes and Hillebrand, 2003) by looking at images of spectral power change between active and passive states within the gamma band.

6.2.4 Analysis of the frequency response in the primary visual cortex

6.2.4.1 Induced response

The first step was to estimate the stimulus-related change in induced spectral power for a given discrete frequency range (5 sec pattern vs. 5 sec blank). Here we used three frequency ranges, gamma (30 to 60 Hz), lower frequency range (0 to 20Hz) and higher beta (20-30 Hz) with a frequency bin size of about 2.5Hz. For each epoch the frequency bins were ranked in terms of power change from active to passive state. These ranks were summed across epochs to give a ranked distribution of power change for each stimulus. These rank distributions for all possible pairs of different SF pattern stimuli were then compared by means of a chi-square test.

The significance of the chi-square value was assessed by means of randomization testing. Briefly, the true chi-square is computed once for any pair of experimental conditions, for example 2 Vs 3 c.p.d. Then epochs from both conditions are pooled together in a large distribution and random indices are assigned to obtain paired comparisons. This procedure is repeated 1000 times resulting in distributions of chi-square values of these random comparisons. This random distribution of chi-squared values gives the 95 % confidence interval (one-tailed) from which the significance of the true chi-square value can be assessed.

6.2.4.2 Evoked response

The virtual electrode time series was averaged across trials to give us the evoked response time series for the pattern. Then the spectral analysis and the ranking method were applied as described above with the sole difference that the rank distribution here just reflected a single trial. For the randomisation testing we pooled the epochs of virtual electrode data from both conditions into a large distribution and assigned random indices to make new pairs of random conditions. The data was then averaged across trials for each condition, yielding two averaged time series for each randomisation trial, on which the spectral and ranking procedure was conducted in the same way as in true data. This procedure was repeated 1000 times to give a chi-square distribution of the randomized data.

6.3 Results and Discussion

Detailed results of the source localization and time- frequency analysis were reported previously (Adjajian *et al.*, 2004a). The main findings relevant to the current paper can be summarized as follows. Gamma oscillatory power change in primary visual cortex was the most robust finding being consistent across all subjects and all experimental conditions (see figure 1 for 3 c.p.d. pattern), although the recordings and the coregistration procedures were conducted at different times.

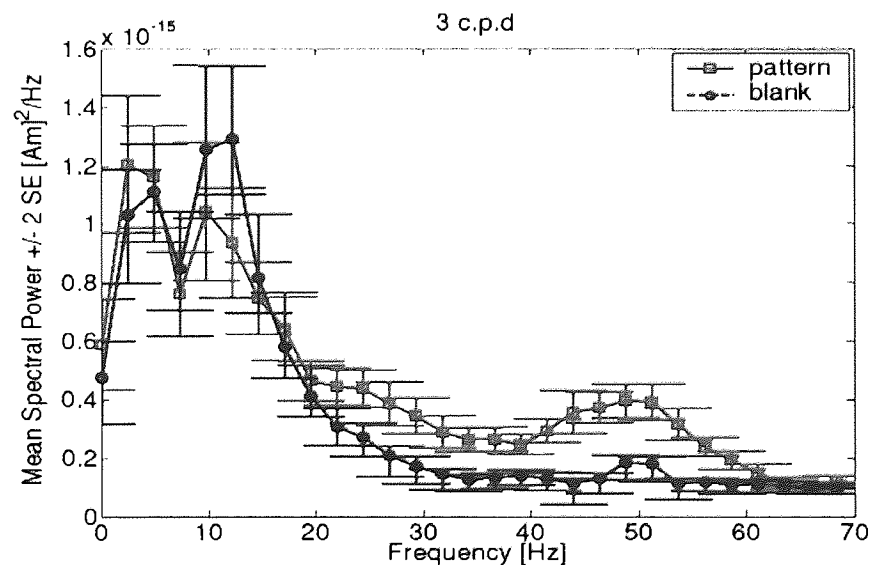


Figure 1. Example of induced oscillatory change of the signal arising from the SPM peak voxel located in primary visual cortex (V1) for one subject at 3 c.p.d. (S.W.). Mean spectral power across experimental trials as a function of temporal frequency in the passive period (blank screen), is indicated by blue circles; for the 3 c.p.d. pattern mean spectral power across trials is indicated by red squares, bars indicate ± 2 standard errors of the mean. Note the marked broadband increase in power in the gamma range, which ranges from 20-60Hz.

Oscillatory power in the gamma frequency range was clearly modulated by stimulus spatial frequency. Stimuli with spatial frequencies of 2-3 c.p.d. consistently exhibited higher power than stimuli of 0.5, 4, 5, 6 c.p.d. (see figure 2).

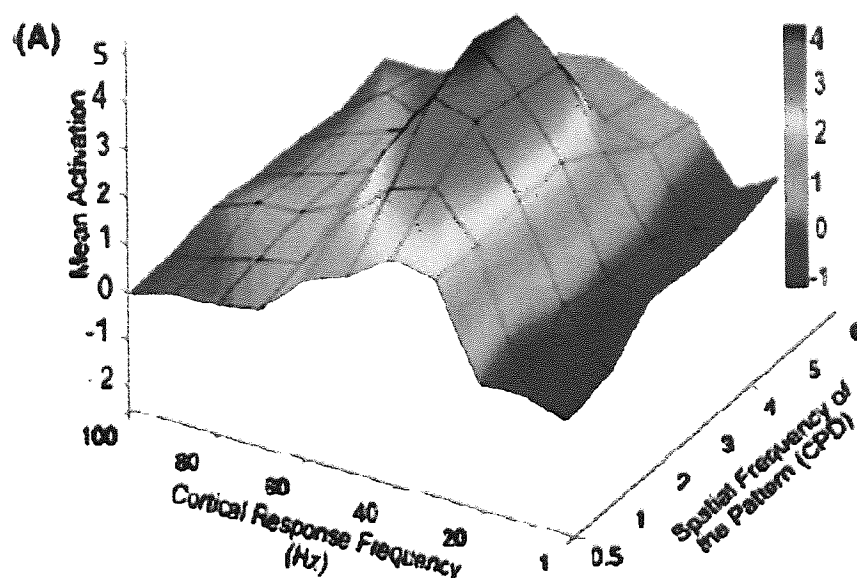


Figure 2. Adapted from Adjamian *et al.*, 2004a. (A) Up-average ($n=7$) magnitude (in arbitrary units) of oscillatory power in primary visual cortex as a function of stimulus SF and cortical response frequency. The total amount of stimulus related power change in each frequency band was measured within an anatomically defined region of interest encompassing the primary visual cortex. Maximal activity occurred within the gamma band (30–60 Hz) and when the static grating has a SF of 3 c.p.d.

From our time frequency analyses we noticed additional variation in the frequency range of the gamma response with respect to different gratings, with stimuli of 2-3 c.p.d. exhibiting a seemingly broadband response and 0.5-1 c.p.d. 5-6 c.p.d. exhibiting a more sharply tuned response. A reasonable question, given the synchronization literature in animals, was whether or not the different SF stimuli could be distinguished in terms of the frequency composition of the induced response. Further, we were interested in whether the well-studied visual evoked response [the response that is strictly time locked to the stimulus and is obtained through signal averaging across experimental trials] would exhibit the same behaviour as the induced response.

We looked at the stimulus related spectral change in the signal arising from primary visual cortex and tested, for each possible stimulus pair, whether these changes arose from the same or different distributions (see methods and figure 3).

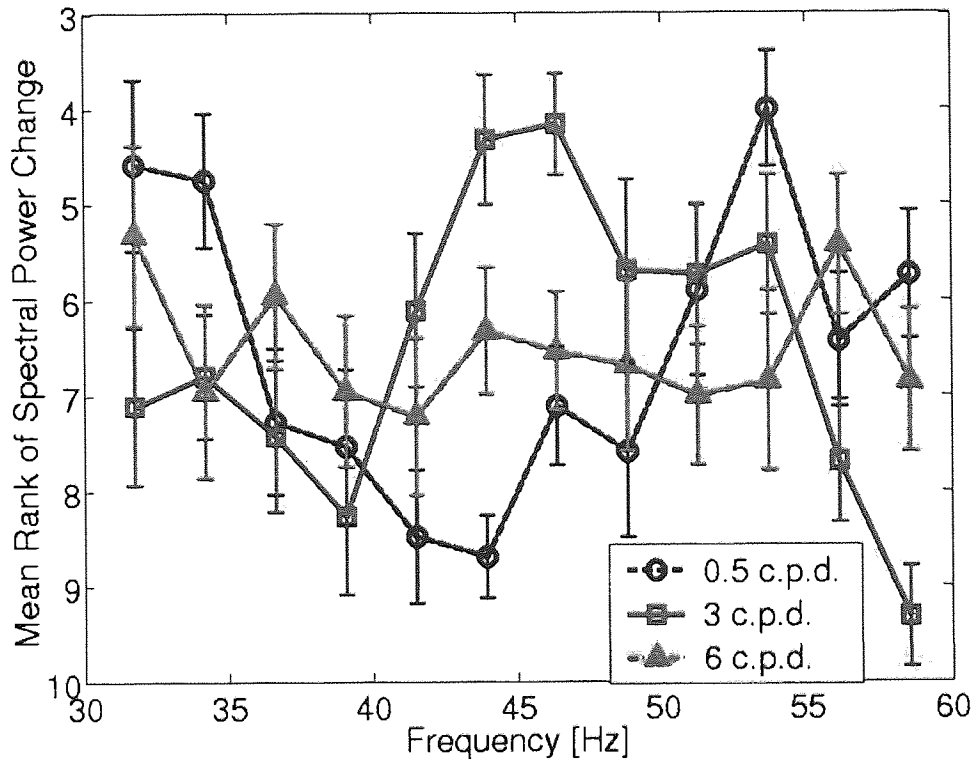


Figure 3. Stimulus-related changes in the spectral distribution as a function of temporal frequency for 0.5 (blue circles), 3 (red squares) and 6 c.p.d. (green triangles) patterns for participant S.W. The x-axis depicts the temporal frequency of the signal, the y-axis shows the rank for a given frequency bin, in terms of the stimulus related spectral power change. Low ranks indicate larger changes and high ranks indicate smaller changes. The bars indicate ± 1 standard error of the mean. Note the sharply tuned response for the 0.5 c.p.d. pattern peaking at 30-40 and 50- 55 Hz as opposed to a fairly broadband response for the 3 c.p.d., which peaks at 40-55 Hz.

Although the rank distributions of the frequencies of power change were variable across the subjects, the significant differences in the gamma band (30-60Hz) between experimental conditions involving different grating stimuli were consistent between subjects (figure 4A). In contrast, frequency analysis of the evoked response showed no significant differences between most of the experimental conditions (figure 4B). Neither did we find changes in other frequency bands tested (20-30Hz and 0-20Hz) in either the evoked or induced responses. The fact that we found minimal differences between the evoked responses across runs, nor any differences in the other frequency bands also gave us confidence that the

changes we observed had real functional relevance and were not simply due to inter-session variability.

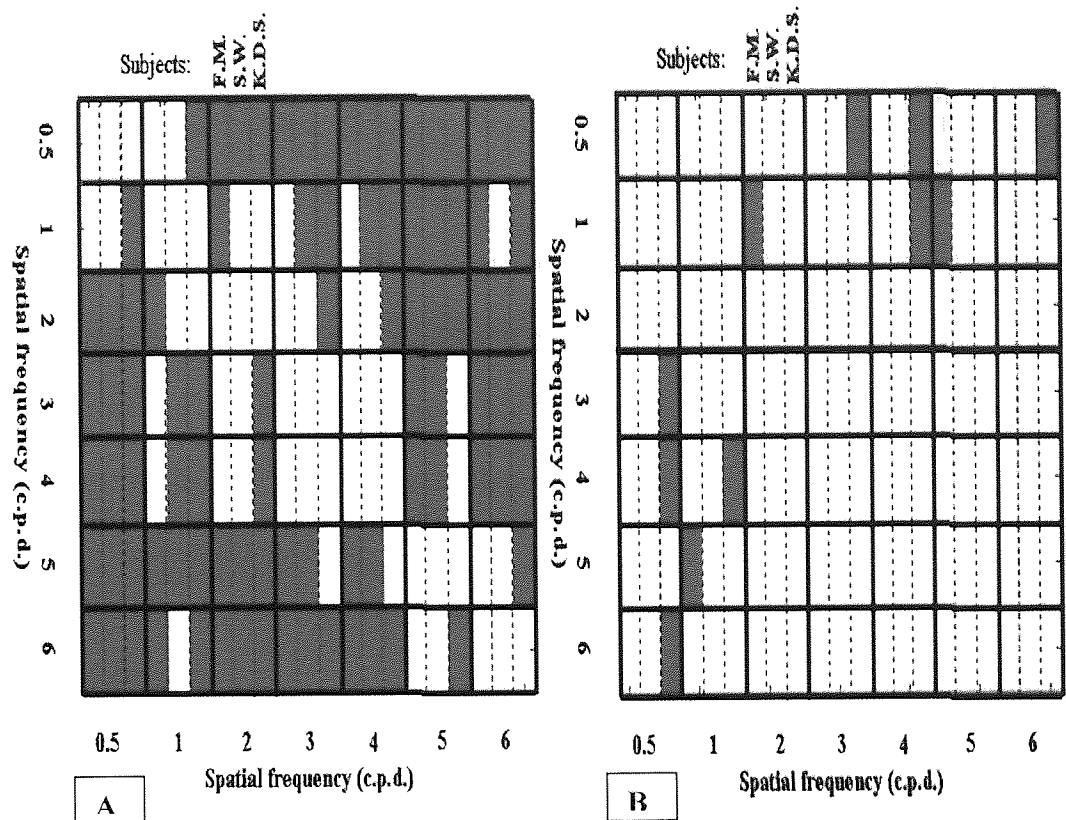


Figure 4A. Significant differences between stimulus-related changes in the gamma frequency range (30-60 Hz) for 3 subjects. Each large cell depicts a comparison between the gamma spectra due to two spatial frequencies (x and y axes), filled in cells indicate a difference at the $p < 0.05$ level. The 3 elements within each cell represent each of 3 subjects (FM, SW and KDS respectively). Note that the significant differences tend to be concentrated to comparisons between patterns of non-adjacent SF. Also note the consistency between participants. Figure 4B. Significant differences between the evoked responses in the gamma range (30-60 Hz), same scheme as 3A. Note, the infrequent significant differences, which are not consistent between participants.

Interestingly, gamma power was higher for psychophysically more salient stimuli, 2-3 c.p.d. (Adjamian *et al.*, 2004a), strongly suggesting larger-scale synchronization with the recruitment of more neurons. However, as evident in figures 1 and 3, this increase in power was also concomitant with a widened frequency range, a broadband response as opposed to 0.5 c.p.d., where the response seems to be fairly sharp tuned. This suggests that the underlying synchronization is not homogeneous and smooth, as in the case of global coupling of identical entities; this would give rise to cumulating power with increasing number of

neurons at a *discrete frequency*. The presence of several concurrent modes in the frequency spectrum rather suggests a more complex dynamic process, namely the interaction of distinct already frequency locked processes. This would be consistent with the notion of overlapping receptive fields of visual neurons (De Valois, Albrecht and Thorell, 1982 , Foster *et al.*, 1985, Bredfeldt and Ringach ,2002) whose degree of overlap may be higher at the peak of the contrast sensitivity function , that is at 2-3 c.p.d. and lower at the side lobes of the function (Campbell and Robson, 1958) . The scenario of synchronization between inhomogeneous frequency modes would also be in agreement with the phenomenology, namely the marked bursting behaviour of these oscillations, since such a dynamic scenario often results in dynamic intermittency (Pikovsky, Rosenblum and Kurths, 2001, Rim *et al.*, 2002). These questions are addressed in chapter 7.

In conclusion, we found that induced gamma oscillations in primary visual cortex seem to differentiate between different SF grating stimuli both in terms of their power and most importantly in terms of their frequency composition. Interestingly, the evoked response did not show the same behaviour. The stimulus-specific information was lost by signal averaging. This implies a clear dissociation of evoked and induced gamma response. These results are also consistent with predictions arising from the synchronization hypothesis (Gray, Koenig, Engel and Singer, 1989, Engel, Konig and Singer, 1991, Engel *et al.*, 1992, Singer and Gray, 1995, Neuenschwander and Singer, 1996) and with experimental data from invasive neurophysiology suggesting that induced gamma oscillations are related to neuronal synchronization in perceptual processes involving feature binding (Gray and Singer, 1995, Koenig, Engel, Singer 1995, Traub *et al.*, 1996, Nase *et al.*, 2003). Our results suggest that magnetoencephalography can be potentially utilized for directly testing experimental hypotheses, which are motivated by invasive animal neurophysiology, in human participants using entirely non-invasive methodologies.

Chapter 7. Quantitative investigation of the bursting behaviour of visually induced gamma oscillations.

7.1 Rationale

In this chapter we set out to investigate the bursting character of visually induced gamma oscillations in the datasets analysed in chapter 6. Time frequency analyses of the signal arising from primary visual cortex revealed marked bursting behaviour in the gamma range during the presentation of the spatial pattern. This is illustrated with the example of the response to a 3 c.p.d grating in figure 1.

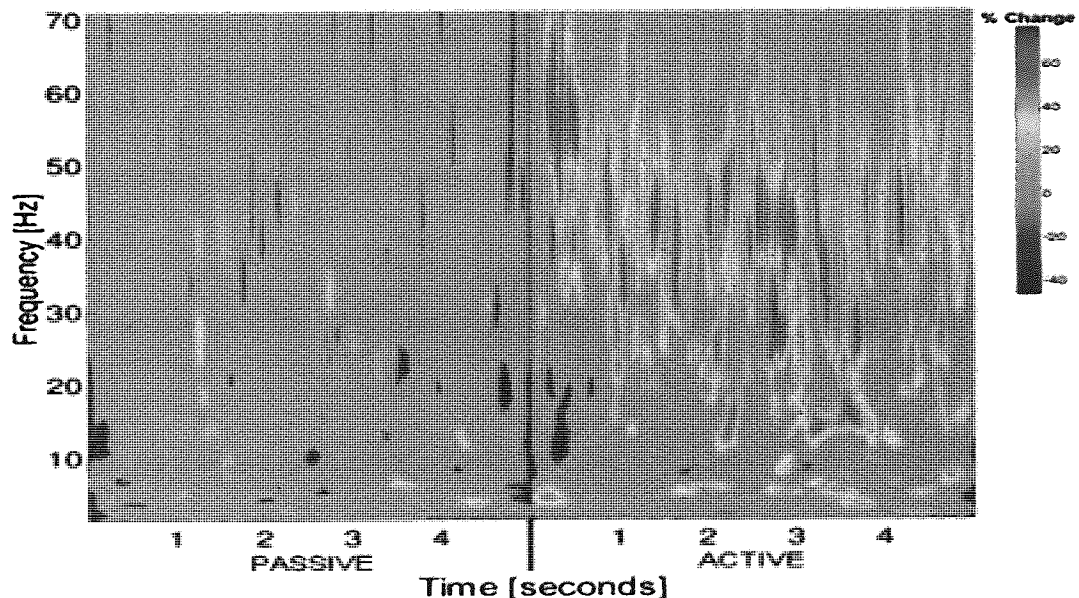


Figure 1. Adapted from Adjarian *et al.*, 2004a. Wavelet time–frequency analysis of the activity in the SPM maximum located in primary visual cortex (participant SW). Statistically significant (bootstrapped at $P < 0.05$) average (across trials) power increases and decreases are shown between the passive (left panel) and active (right panel) states. Left panel indicates cortical activity during passive viewing of the control stimulus and is used as the baseline for comparison of the active period (right panel). The stimulus was a static grating with a SF of 3 c.p.d. Non-significant power changes are shown as zero values (cyan). Power increases are mostly in the 20–60 Hz range and are bursting across the active period.

This apparent bursting behaviour seemed to be consistent across subjects and experimental conditions but was particularly pronounced in the case of a 3 c.p.d. stimulus (Adjarian *et al.*, 2004a). For the 3 c.p.d stimulus, both the spectral power and the frequency spread of the

spectral distribution in the response signal seemed to increase with respect to the responses to the other stimuli (chapter 6). This may reflect a more pronounced overlap of the receptive fields of visual neurons for 3 c.p.d. stimuli and suggests that the underlying synchronization process might not simply correspond to frequency locking (see chapter 6 and references therein). From a dynamical perspective, such behaviour may be conceptualised as an interaction between inhomogeneous frequency modes (nonidentical oscillators). Such interactions often result in dynamic intermittency (Pikovsky, Rosenblum and Kurths, 2001, Rim *et al.*, 2002). In chapters 3 and 4 we have seen, that often interactions of inherently dissimilar oscillating systems exhibit a dynamic regime referred to as modulational or on-off intermittency (Platt, Spiegel and Tresser, 1993). Qualitatively, the time frequency data (see figure 1) seem to support this idea. However, as always under realistic measurement conditions, with several and often unidentified noise sources one has to reject the hypothesis that these stimulus induced modulations of the amplitude (or power) of the gamma oscillations are just due to a noisy linear process. In other words we wanted to test whether the slow modulations in the amplitude of the gamma oscillations in primary visual cortex had a dynamical deterministic structure or alternatively if they just reflected random, noisy fluctuations. As we have suggested in chapters 3 and 4, the former case, namely intermittent dynamics arising through complex interactions may be adaptive in terms of metastability and may reflect perceptual updating processes. In the next section we briefly present the phenomenon of on-off intermittency and then we describe a method for testing the hypothesis of deterministic bursting behaviour in noisy, experimental data. Finally, results are presented for the data set under consideration.

7.2 On-off intermittency: phenomenology and quantification in abstract model systems

This phenomenon was first described in one-dimensional maps coupled to either chaotic or noisy signals (Platt, Spiegel and Tresser, 1993). In essence this phenomenon reflects an irregular behaviour that seems to switch between relatively long-lived, low signal-variability periods of often-small amplitude (referred to as laminar phases) and relatively short-lived periods of bursting oscillations of higher-signal amplitude and variability (Platt, Spiegel and

Tresser, 1993, Platt, Hammel and Heagy, 1994 and Heagy, Platt and Hammel, 1994). Such phenomena seem to abundant in nature, some examples involve solar cycles exhibiting turbulent convection, stock market crashes, species that become almost extinct but yet survive (Platt, Spiegel and Tresser, 1993) and earthquakes (Platt, Hammel and Heagy, 1994). It has been suggested that in many cases such phenomena maybe observed in systems, where only a few variables are measurable but many other ‘hidden’ variables may be implicated (Platt, Spiegel and Tresser, 1993). Hence, such phenomena may be expected in macroscopic systems composed of interacting subsystems. A good example comes from (Zhan, Wei, and Lai, 2002), where two coupled nonidentical (somewhat detuned) Rössler systems exhibiting lag synchronization were studied. The transition to lag synchronization was characterized by a transition from *on-off intermittency* to *periodicity* of the collective variable, which in this case was the time-shifted difference of two corresponding system observables. This illustrated in Figure 2 (adapted from Zhan, Wei, and Lai, 2002). As we have seen in chapter 3, lag synchronization (Rosenblum *et al.*, 1997) occurs when the coupling is relatively strong but is not sufficient to instate generalized or identical synchronization. This can be considered as a compromise situation between phase and identical synchronization. Essentially, in lag synchronization a signal $x_1(t)$ is approximately equal to a shifted version of another signal x_2 with some time lag φ :

$$x_2(t + \varphi) \approx x_1(t)$$

Plotting the raw (non time-shifted) signals $x_2(t)$, $x_1(t)$ would result in an ellipsoid distribution around the straight line. If one plots the signals $x_2(t + \varphi)$ and $x_1(t)$ against each other one will obtain concentration along a straight line as in the case of identical synchronization. This corresponds to panel b in figure 2 for the simulation concerned. We see that the points are concentrated mainly on the main diagonal but large deviations (wings) seem to exist as well. The instantaneous difference between two systems operating in a regime of lag synchronization is the relevant collective variable (Rosenblum *et al.*, 1997) and should be zero or at least constant. Thus if one plots the difference $x_1(t) - x_2(t + \varphi)$, one should obtain a straight line. The corresponding plot in figure 2 is shown in panel c. We see that long periods of zero difference are alternated with periods of marked excursions of the instantaneous difference in a seemingly irregular manner. Thus here the coupling between the two systems

is not sufficient to achieve perfect lag synchronization and the dynamics observed corresponds to intermittent lag synchronization. The hallmarks of on-off intermittency can be seen in panel c. The instantaneous difference of the relevant system observables is concentrated mainly around zero and remains there for long periods of time, indicating that the systems are in lag synchronization. However, in a seemingly random way, large bursts of oscillation of the instantaneous difference arise, indicating desynchronization of the coupled systems. The intervals of constant difference and thus the intervals between subsequent bursts are referred to as laminar phases and their duration is of particular importance. Thus the essence of intermittent dynamics for a given observable can be captured by quantifying the duration of these interburst intervals. This can be quantified by setting an arbitrary threshold and considering everything above that threshold to be a 'burst' and everything below to be an interburst interval. Intermittency can be characterized by examining the shape of the distribution of these interburst intervals. If there is a regular switching between lag synchronization and desynchronization one should expect only one additional time scale, thus there should be modal responses at one frequency and its harmonics. If however the switching is irregular the durations of the interburst intervals will stretch across several time scales. Heagy, Platt and Hammel, 1994 have shown that for a range of systems exhibiting on-off intermittency the distribution of laminar phases has a typical $-3/2$ power law scaling. This is consistent with panel d in figure 2, which show the log-log plot of the distribution of laminar phases for the coupled Rössler systems. The power law distribution of the laminar phases means that the switching of the interacting systems on and off lag synchronization occurs across a *range of interrelated time scales*.

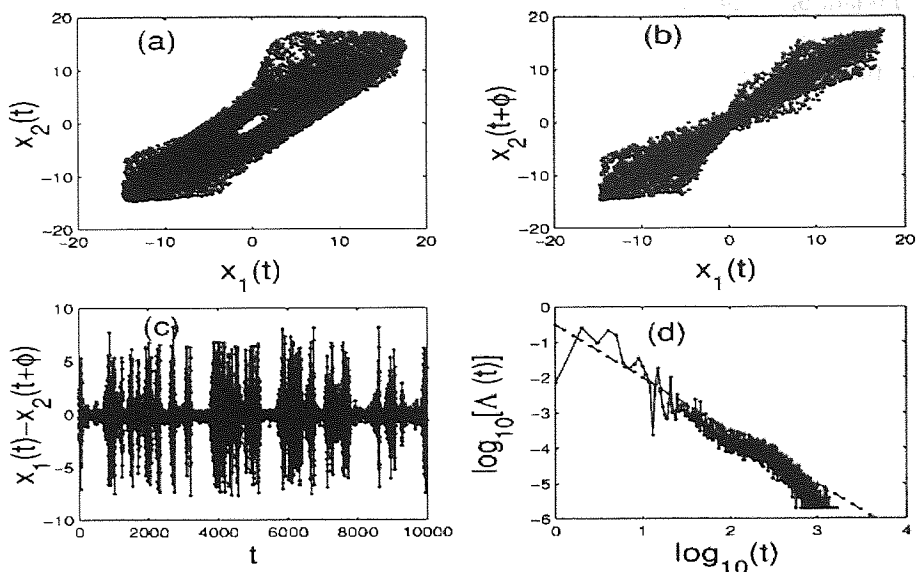


Figure 2. Adapted from Zhan, Wei, and Lai, 2002. Intermittent lag synchronization of coupled nonidentical Rössler systems, the coupling parameter is below the threshold for onset of lag synchronization, see text for details. Panel a shows a scatter plot of the x observables of the two systems. Panel b shows the scatter plot of x_1 vs a time-shifted version of x_2 . Note that the distribution is not entirely confined on the main diagonal. Panel c shows the time course of the amplitude difference between x_1 and a time shifted version of x_2 . Note that the difference irregularly switches between longer periods of almost zero difference (laminar phases) and shorter bursts of departures from zero. This is characteristic of on-off intermittency. Panel d shows a log-log plot of the distribution of the duration of the laminar phases (interburst intervals in panel c). A typical $-3/2$ power scaling is observed.

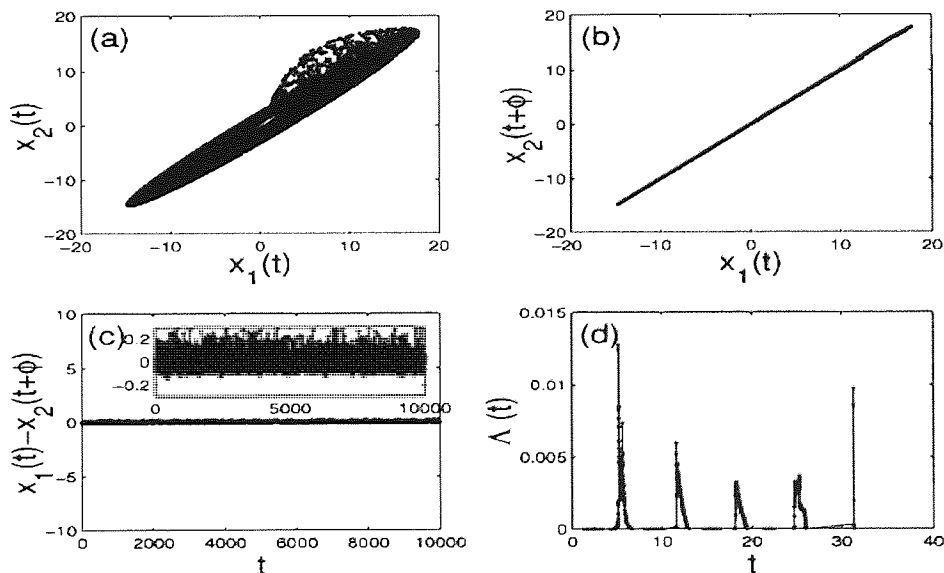


Figure 3. Adapted from Zhan, Wei, and Lai, 2002. Lag synchronization of coupled nonidentical Rössler systems, the coupling parameter is above the threshold for onset of lag synchronization, see text for details. Same format as figure 2. From panels b we observe that the systems are in lag synchronization, the distribution is confined on the main diagonal (compare panel b in figure 2). In panel c we observe that the amplitude difference does not deviate much from zero (compare panel c in figure 2). However, there are smaller fluctuations shown in the inset. The distribution of laminar phases shown in panel d is periodic corresponding to the rotational period of a single Rössler system indicating lag synchronization (compare panel d, figure 2).

In figure 3, similar plots are shown for a higher value of the coupling parameter and thus when lag synchronization sets in between the interacting systems. The latter is evident in

panel b where the scatter plot is confined on the main diagonal. The instantaneous difference in panel c shows very little departure from zero but on a smaller amplitude scale there are small and seemingly regular fluctuations. This is in contrast with the irregular high amplitude bursts in figure 2, panel c. The distribution of laminar phases has a periodic structure with peaks corresponding to a single rotational period of one system and its harmonics. This is again to be contrasted with the power law distribution in the case of intermittent lag synchronization (figure 2, panel d).

To conclude, on-off intermittency is characterized by modulations of the switching times between low variability laminar phases and high variability bursts, which stretch across a range of time scales. The distribution of the laminar phases follows a typical $-3/2$ power scaling law. Thus if one wishes to infer the presence of on-off intermittency, one needs to study the distribution of experimentally observed laminar phases. However, the latter is the case when the system under study is formally described as in the numerical examples of coupled oscillators shown in the previous section. In noisy experimental data the system generating the observed signal is not known and therefore a certain power law distribution of interburst intervals is *not sufficient* to infer intermittency. This is further supported by theoretical studies, which have shown that the presence of additive noise (as it is expected in any realistic experimental situation) introduces ‘shoulders’ in the power law distribution and can somewhat obscure the $-3/2$ scaling law (Platt, Hammel and Heagy, 1994). Nonetheless, one can test the hypothesis that the distribution of interburst intervals observed in experimental data cannot be explained by a solely linear, Gaussian process but may be of some deterministic origin. The latter can be addressed by performing comparisons of the distributions of the interburst intervals with surrogate data, where possible nonlinear structure and therefore cross frequency interdependencies are explicitly destroyed (Theiler et al, 1992). Our approach to this issue is illustrated in the next section.

7.3 Detection of deterministic bursting in noisy magnetoencephalographic data

The time series of the peak SPM voxels located in primary visual cortex were first band pass filtered in the gamma frequency range (30-60 Hz) for a number of epochs collected during the presentation of the pattern stimulus. Prior to filtering for each epoch phase shifted FFT surrogates were constructed (Theiler *et al.*, 1992). This approach was illustrated in greater detail in chapter 5. The surrogate data have the same autocorrelation and spectral properties as the real data but possible nonlinear structure is destroyed. This effectively removes possible interdependencies between frequencies. The latter however is the main characteristic of on-off intermittency: a power law distribution of time scales. Thus the phase shifted FFT surrogates have the same autocorrelation functions and power spectra as the real data but lack any nonlinear structure. Therefore they are used as a null hypothesis in which the fluctuations of the interburst intervals of the gamma oscillations are due to linear, noisy processes. The surrogate data were band pass filtered and processed further in the exact same way as the real data.

An exemplar epoch is shown in figure 4. The top panel shows the real data filtered between 30 and 60 Hz, whereas the bottom panel shows the corresponding surrogate data. The typical bursting behaviour of gamma oscillations is evident in the top panel with periods of high amplitude bursts ('on' phases) irregularly interrupted by periods of low amplitude oscillation ('off' or laminar phases). Nevertheless, the comparison with the surrogate data plotted in the bottom panel is compelling: the surrogate data also apparently exhibit 'bursting' behaviour. We were interested to quantify the duration of the 'off' phases or the interburst intervals.

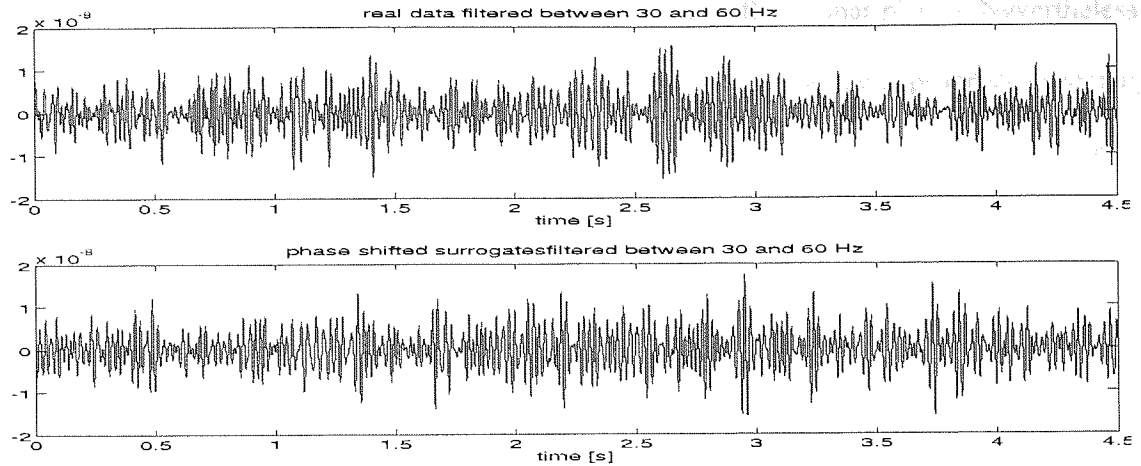


Figure 4. The top panel shows the band pass filtered time series of the SPM peak voxel located in the primary visual cortex for participant F.M after the appearance of a 3 c.p.d pattern at time 0. The gamma oscillations show typical bursting behaviour. The bottom panel shows the phase shifted FFT surrogate time series filtered in the same range as the real data. Note the similarity of the real and surrogate time series, which also appears as ‘bursting’.

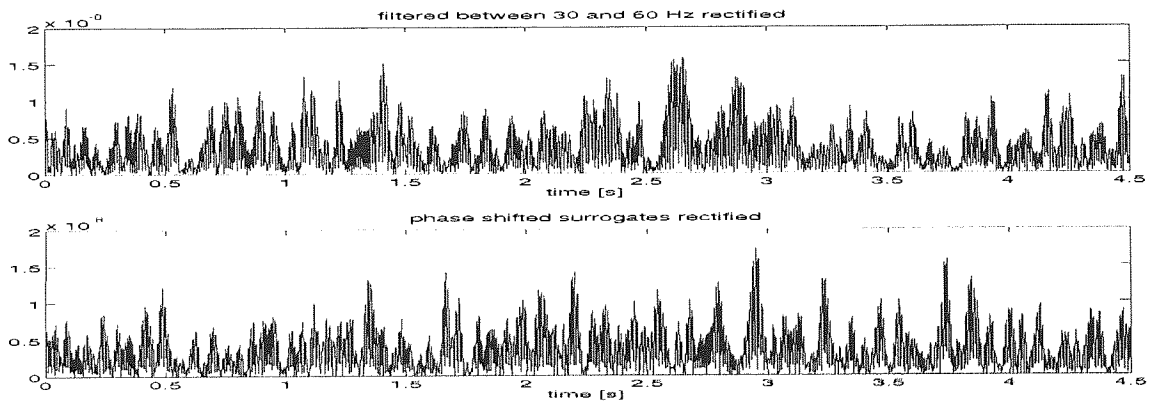


Figure 5. The data in figure 4 were rectified by taking the absolute values.

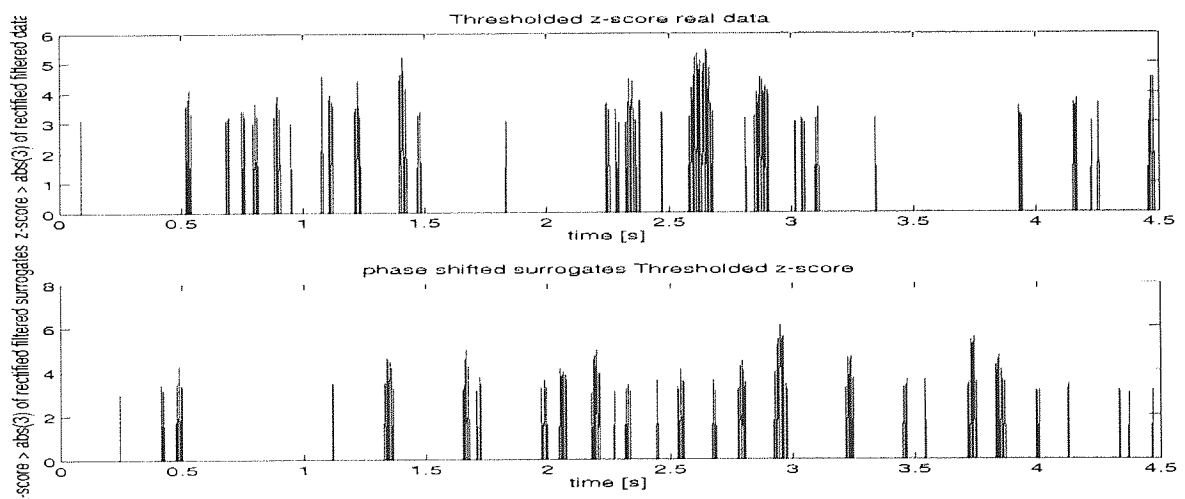


Figure 6. The rectified data in figure 5 were transformed to z-scores (see text) and thresholded at $z > 3$. The thresholded z-scores are plotted here for the real data (top) and surrogate data (bottom). These analysis aims to locate the local maxima in the signal and thus the ‘on’ bursting phases. The ‘off’ phases are the intervals between the maxima.

Therefore the data were first rectified by taking the absolute value of the time series (figure 5). The approach illustrated in the previous section, would suggest implementing an absolute

threshold and consider everything below the threshold as ‘off’ laminar phases. Nevertheless, in a noisy and nonstationary signal an absolute threshold would not be appropriate especially when multiple trials are to be used. Therefore we utilized a threshold in a statistical sense: for every trial z-scores of the rectified data were computed based on the mean and the standard deviation of the epoch time series. This would then help identifying local maxima in the signal corresponding to ‘bursts’ or ‘on phases’. The threshold for a ‘burst’ was set to 3 standard deviations of the mean signal amplitude for each experimental epoch. Figure 6, shows the thresholded data for an experimental epoch. Note that this signal begins to resemble the one in figure 2, panel c. The intervals between the local maxima ($z > 3$ standard deviations of the mean) correspond to the ‘off’ or laminar phases. One can see that the on and off phases seem to switch irregularly. However, the surrogate data shown in the bottom panel look surprisingly similar.

Finally, in order to quantify the duration of the ‘off’ laminar phases, the time between subsequent local maxima were calculated. Because we were primarily interested in the bursting behaviour of *gamma oscillations (30-60Hz)*, only durations longer than the lower boundary of the gamma frequency range (here we used $1/30\text{Hz} = 0.0333\text{s}$) were considered. This is because durations smaller than 0.0333 s would essentially denote laminar phases between adjacent signal maxima in the gamma frequency range itself (within the ‘bursts’) rather than laminar phases between subsequent gamma ‘bursts’.

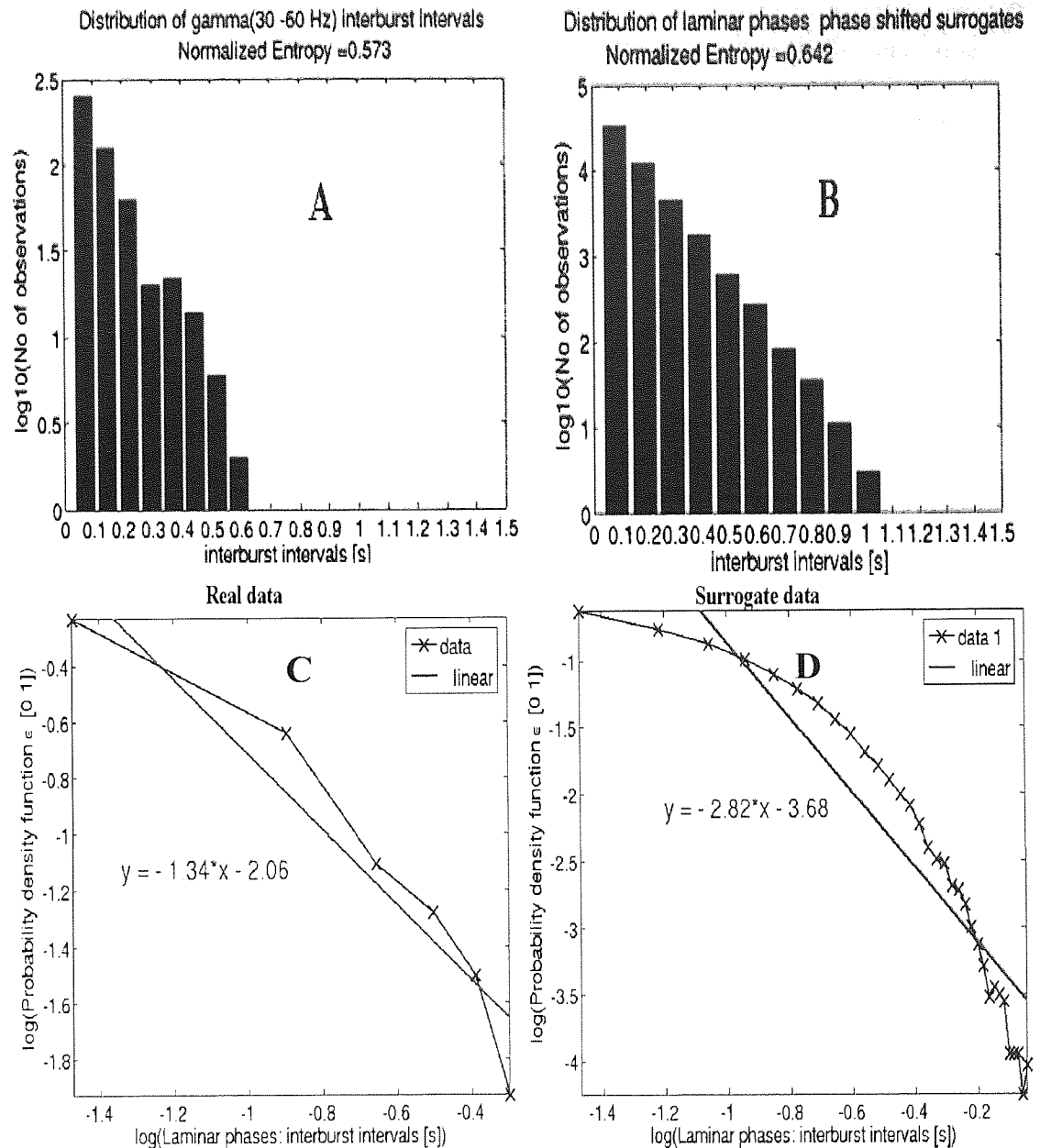


Figure 7. Distributions of gamma interburst intervals pooled over all experimental trials for participant F.M. viewing a 3 c.p.d. grating. Panel A shows the distribution of interburst intervals for the real data on log-linear axes. Panel B shows the respective distribution for the surrogate data. The two distributions look similar however note the roughly bimodal response in the real data, which is absent in the surrogates. Also note that the real distribution has an upper limit of 0.6s corresponding to roughly 1.6 Hz. Further note the difference in the normalized entropy of the two distributions. Panels C and show a log-log plot of the probability density functions Vs the duration of the interburst intervals. Nearly linear relationship can be observed for both the real and surrogate data, suggesting power law scaling of the laminar phases distributions. The gradient of a linear least squares fit indicates different slopes for the real and surrogate data distributions. The slope for the real data is -1.34 and thus consistent with observations of on-off intermittency scaling in noisy data.

The interburst intervals (which were computed epoch wise) were then pooled in a large distribution for all experimental epochs. The Shannon entropy of the distribution was calculated for real and surrogate data according to:

$$H(t_{\text{laminar}}) = - \sum_{k=1}^{N_{\text{bins}}} p(t_{\text{laminar}}) \ln p(t_{\text{laminar}})$$

where the t_{laminar} denotes the laminar phases, N_{bins} is the number of bins in the histogram and $p(\phi_k)$ is the relative frequency of finding the given laminar phase in the k-th bin. The number of bins was determined as the cubic root of the number of data points in the distribution. The binned distribution was then evenly spaced between its maximum and minimum. The entropy of a binned distribution increases with the number of bins. Therefore the entropy needs to be normalized. Here we used a fraction of the observed entropy with respect to the maximally possible entropy given the number of bins:

$$H_{\text{norm}} = \frac{H(t_{\text{laminar}})}{H_{\text{max}}}, \quad H_{\text{norm}} \in [0, 1],$$

where $H_{\text{max}} = \ln(N_{\text{bins}})$.

Figure 7 shows the distributions of the interburst intervals (laminar phases) for both real and surrogate data. Panel A shows the distribution of interburst intervals for the real data on log-linear axes. And panel B shows the respective distribution for the surrogate data. Note that the distributions are bounded from the left hand side, as values smaller than 0.033s are not considered. The distributions are also bounded from the right hand side by the virtue of finite data samples: here the largest possible lag must be smaller than 4.5s (the time of an experimental trial). The seemingly exponential distributions observed are due to the fact that, for a limited number of data samples, shorter intervals are more likely to be observed than longer ones. The two distributions look similar at first glance; however note the roughly bimodal response in the real data, which is absent in the surrogates. This suggests that the gamma oscillations exhibit *stronger modulations* at mainly *theta* (periods around 0.15-0.25s) and *delta* frequencies (periods around 0.4-0.5s) than the expected distribution presented by the surrogate data. Also, the real data distribution shows a higher limit of about 0.6s (1.67 Hz)

where as the surrogate distribution has a much higher limit. Thus although interburst intervals longer than 0.6s are expected and indeed observed in the surrogate data distribution, they are completely absent in the real data. This implies that modulations of gamma at very low frequencies (lower delta range) do not occur for this dataset. Further note the marked difference in the normalized entropy of the two distributions. Here the entropy is lower in the real than in the surrogate data.

The probability density functions for both real and surrogate data were calculated and then plotted as a function of the interburst intervals in terms of a log-log plot. In case of a power law scaling this should yield a straight line, whose gradient would denote the power. A least squares linear fit was performed on the logarithmic data. Panels C and D shows a log-log plot of the probability density functions (PDF) Vs the duration of the interburst intervals for the real and surrogate data respectively. No linear relationships could be observed for the real data, a finding which is not consistent with power law scaling of the laminar phases distributions. The surrogate data also exhibit a curvilinear relationship and a steeper fall off of the PDF as a function of the duration of laminar phases. The gradient of a linear least squares fit indeed indicates *different* slopes for the real and surrogate data distributions. The slope is steeper for the surrogate data distribution and is estimated at -2.82 as opposed to -1.34 for the real data. Figure 8 shows the PDF's for real and surrogate data for another participant (K.D.S.) and a 3 c.p.d. stimulus. The results are again inconsistent with power law scaling, nevertheless there are differences in the real and surrogate data distributions. This suggests that the interburst intervals of gamma oscillations may not be purely due to noise.

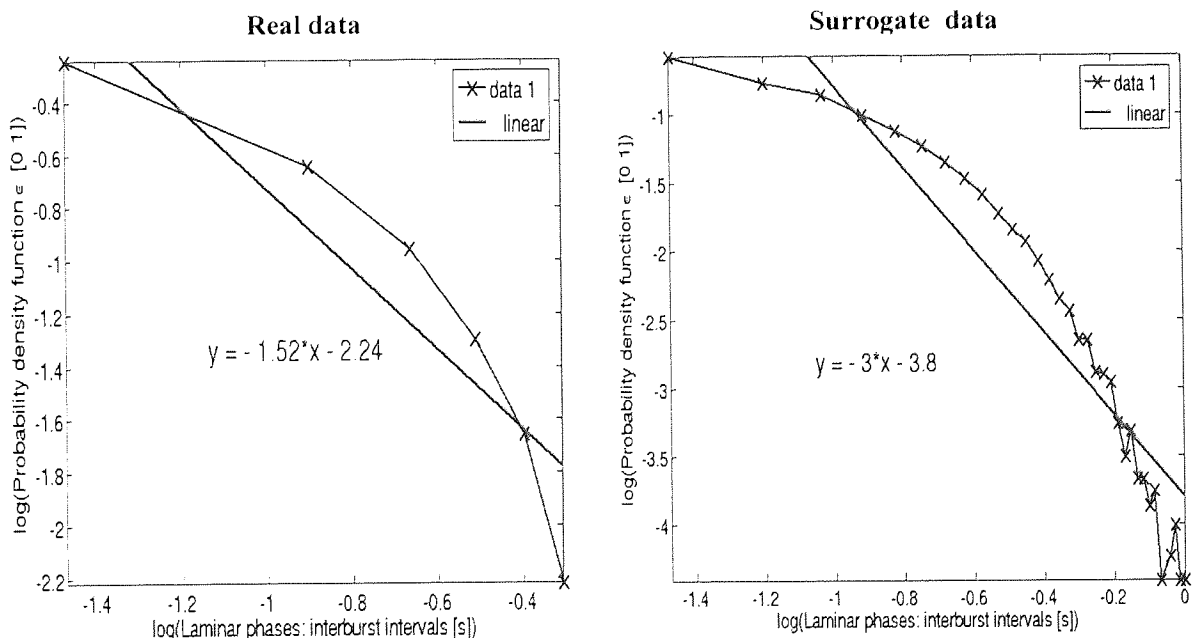


Figure 8. Log-log plots of the PDF's (probability density function) Vs the duration of interburst intervals for participant KDS and a 3 c.p.d. stimulus. The left panel shows the results for the real data and the right panel shows the surrogate data. Note that the slopes of the linear fit are very different for the real data and surrogate data and that the slope for the real data is close to $-3/2$. This is furthermore consistent with the results for participant F.M. for the same stimulus.

7.4 Statistical comparisons between distributions of interburst intervals in the real and surrogate data

We should note that the method described here is (at present) merely semi quantitative. This is because it lacks a rigorous statistical inference of whether the distributions of interburst intervals in real and surrogate data are different. However the latter is not a trivial question. Current methods for the detection of on-off intermittency are based on a $-3/2$ power law scaling of the distribution of laminar phases (Heagy, Platt and Hammel, 1994). The exact exponent of the power law may be influenced by the presence of noise (Platt, Hammel and Heagy, 1994). Given the fact that the experimentally observed distributions are inconsistent with such a power law scaling, the only null hypothesis that remains to be tested is that the observed interburst intervals can be entirely explained by a purely linear random process and are thus purely due to noise. Thus the problem may be reduced to a deviation of the distribution of the real data from the one obtained using surrogate data (Theiler et al, 1992). For a given epoch of real data many samples of surrogate data can be generated and thus facilitate the construction of a null-distribution. In chapter 5 we used this approach to test the hypothesis that additional nonlinear interactions occur, which are not present in the null distributions. The metric used there however, was exploiting the central tendency (mean/median) of the distribution. In the case of the distributions of laminar phases, this approach is possibly not adequate, since it is the whole *shape* of the distribution that is different and not merely its central tendency. Approaches based on a chi-square comparison of surrogate and real data may be more fruitful, since they quantify deviations of the real data distribution from the expected surrogate data distribution. This is an explicit test of whether the observed distribution of laminar phases significantly deviates from the one expected in a signal with exactly the same linear statistics but where the phase relationships between frequencies have been randomized.

For each experimental trial and thus for any given pair of experimental signals of interest, 100 surrogate data epochs were constructed. Then both the true (observed) and surrogate time series were band passed filtered and analysed in exactly the same way, to obtain distributions of laminar phases pooled across experimental epochs. This yields a distribution of truly observed laminar phases *across* experimental trials and a 100 times larger distribution of

laminar phases in surrogate data. The true and the surrogate distributions were then compared by means of a chi square test adjusted for unequal sample size yielding a chi square value χ_{true}^2 (Teukolsky, Vetterling, and Flannery, 1992).

$$\chi_{true}^2 = \frac{\sum_{i=1}^k (K_1 T_i - K_2 S_i)^2}{T_i + S_i}$$

where the summation is for bin $i=1..k$, T_i is the observed frequency of the true data for bin i , S_i is the observed frequency of the surrogate data for bin i (both surrogate and true data distributions were binned in the same way) and K_1 and K_2 are scaling coefficients to adjust for unequal sample size:

$$K_1 = \sqrt{\frac{\sum_{i=1}^k T_i}{\sum_{i=1}^k S_i}}$$

$$K_2 = \sqrt{\frac{\sum_{i=1}^k S_i}{\sum_{i=1}^k T_i}}$$

In this way, we are essentially testing the null hypothesis, that the true and surrogate distributions could have been drawn from a common distribution. To assess the statistical significance of the chi square test a randomisation procedure was undertaken: A randomly assigned *subsample* of the *same* sample size as the true data was drawn from the surrogate distribution and this was compared to the whole surrogate distribution to yield a chi square value, χ_{random}^2 . This was repeated 1000 times to give a randomised distribution of chi square values. The 95th percentile of this randomised distribution served as a (one-tailed) confidence interval. Thus χ_{true}^2 was deemed significant if it was larger than the 95th percentile of the randomized distribution.

7.5 Results of statistical testing and discussion

Figure 9 shows the results for participant F.M. and a 3 c.p.d stimulus. The true chi-square χ_{true}^2 was larger than 95 % of the chi-square values obtained by comparing a random subsample of the surrogate distribution with the entire distribution. This implies that the apparent bursting of the visually induced gamma oscillation for this particular stimulus may not be entirely explained by a noisy Gaussian process and may be of a deterministic nonlinear

nature. In participant S.W. for the same stimulus a trend was observed ($p=0.09$, see table1), however the latter was absent in participant K.D.S.

The analysis of the datasets for the signals associated with the other stimuli and participants suggests that nonlinear bursting phenomena are rather infrequent. The results are summarized in table 1. The results suggest that the hypothesis that the bursting behaviour of gamma oscillations is purely due to a noisy linear process cannot be generally rejected; on the contrary detections of nonlinear structure were rather rare. However, these findings are consistent with previous observations that nonlinear phenomena can seldom be detected in macroscopic brain signals such as the EEG (Breakspear and Terry, 2002a and references therein). The approaches followed in Breakspear and Terry, 2002a is based on rejecting the null hypothesis of a purely linear Gaussian process on an epoch-by-epoch basis. In that way the percentage of ‘nonlinear’ epochs can be assessed. In the case of spontaneous rhythms (in the absence of an experimental task) such as the ones studied in the above reference, there is no reason why one should expect that individual epochs should be homogeneous. However in our study a very specific stimulus was presented and the data also suggested that the experimental epochs were homogeneous. Therefore all the epoch data were pooled in a large distribution and the latter was then tested for nonlinearity. In addition, the statistics used here, both the chi square comparisons and the randomisation testing are nonparametric and thus fairly conservative. Although this approach is sensible for assessment of task related nonlinear behaviour, it is statistically speaking very rigorous. Taken together with the fact that nonlinear structure in brain signals seems to be infrequent (Breakspear and Terry, 2002a) the latter may explain why most of the comparisons were deemed insignificant. Current work focuses on developing an epochwise test for detecting nonlinear bursting phenomena. This will enable to isolate nonlinear epochs and study them in greater detail.

Stimulus	Participant F.M.	Participant S.W.	Participant K.D.S
0.5 c.p.d.	$\chi^2 = 3.193, p=0.88$	$\chi^2 = 6.178, p=0.52$	$\chi^2 = 27.759, p=0.03$
1 c.p.d.	$\chi^2 = 18.73, p=0.07$	$\chi^2 = 2.87, p=0.81$	$\chi^2 = 13.4, p=0.14$
2 c.p.d.	$\chi^2 = 15.76, p=0.11$	$\chi^2 = 7.42, p=0.45$	$\chi^2 = 16.69, p=0.06$
3 c.p.d.	$\chi^2 = 21.68, p=0.04$	$\chi^2 = 13.79, p=0.09$	$\chi^2 = 2.378, p=0.93$
4 c.p.d.	$\chi^2 = 3.30, p=0.71$	$\chi^2 = 12.45, p=0.18$	$\chi^2 = 5.66, p=0.56$
5 c.p.d.	$\chi^2 = 3.26, p=0.84$	$\chi^2 = 11.9, p=0.11$	$\chi^2 = 10.29, p=0.13$
6 c.p.d.	$\chi^2 = 5.19, p=0.52$	$\chi^2 = 4.90, p=0.68$	$\chi^2 = 18.47, p=0.07$

Table 1. Results of the chi-square statistical analysis for all stimuli conditions and all participants. χ^2 stands for the true χ^2 comparison and p is the probability value of χ^2 with respect to the random χ^2 distribution.

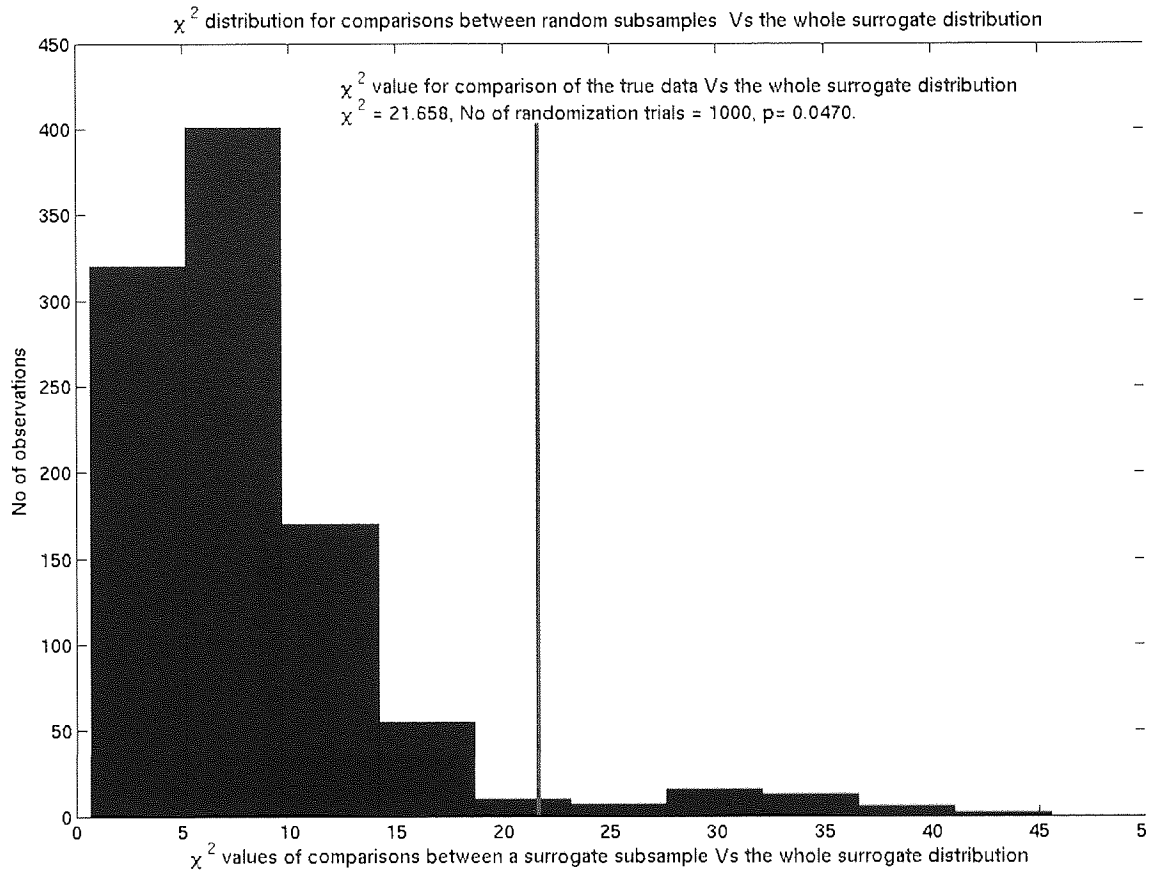


Figure 9. Results of chi-squared test between the real distribution of laminar phases and the distribution in surrogate data (red line and text) for participant F.M viewing a 3 c.p.d. stimulus. The significance of the chi square test was assessed using a randomisation procedure (see methods for details). A random subsample of the surrogate data was taken 1000 times and compared with the whole surrogate distribution. This yields a null distribution of chi-square values χ^2_{random} shown in the histogram. The 95th percentile is utilized as a significance level for the true chi square value χ^2_{true} (corresponding to the comparison of the true distribution with the whole distribution of surrogates) shown as red line.

In conclusion, we examined the bursting behaviour of stimulus-induced oscillations in the gamma range (30-60Hz). Motivated by the phenomenology of the data and the modelling work presented in chapters 3 and 4 we wanted to test the hypothesis that this apparent bursting behaviour may be a reflection of dynamic intermittency arising from interactions between nonlinear subentities contributing to the same macroscopic signals. We presented a quantitative approach for constructing the distribution of the interburst intervals based on

identifying local maxima in the signal. The temporal structure of these signal maxima strongly resembled the dynamic phenomenon of on-off intermittency (Platt, Spiegel and Tresser, 1993). However, the distribution of these interburst intervals did *not* generally conform to the $-3/2$ power law scaling characteristic for on-off intermittency (Platt, Spiegel and Tresser, 1993). Inferential statistics utilized to compare the distribution of interburst intervals in real and surrogate data indicated that the null hypothesis, namely that the bursting behaviour of gamma oscillations is purely due to a noisy linear process could not be generally rejected. On the contrary, rejections of the null hypothesis were the exception rather than the rule. Therefore we have *not* found evidence in support of deterministic nonlinear dynamics underlying the bursting character of visually induced gamma oscillations

Chapter 8. Synopsis and general conclusions

8.1 Synopsis

The work presented in this thesis was centred on describing, quantifying and modelling large scale coordination phenomena in the brain. The main ideological foundation was that information processing and thus brain function crucially depends on complex coordination phenomena at several spatial and temporal scales and the emergence of particular forms of macroscopic order.

In chapter 1 we presented the most eminent theoretical approaches to the binding problem. We adopted the view that the most promising approach rests within the field of coordination dynamics in complex systems (Kelso, 1995, Friston, 2000 a,b,c Bressler and Kelso 2001). The dynamical approach is naturally concordant with the inherently dynamic, context-sensitive and flexible nature of the brain (Kelso, 1995). This approach uses the powerful geometric formalisms of dynamical systems and deterministic chaos theories. The quintessence of the approach is in the view of the brain as a global dynamical system, which is comprised of sparsely connected, interacting nonlinear subsystems (Friston 2000a,b, Sporns and Tononi, 2002). The complexity of the brain is a reflection of a constant interplay between opponent forces subserving functional integration on one hand and functional segregation on the other (Friston, 2000 b, c). The interplay of these opponent gradients gives rise to a self-organized global coordination state, which consists of multiple simultaneously active separate coordination entities, the *functional clusters* (Sporns and Tononi, 2002). The global state is however inherently unstable (*metastable*) because of complex pattern of interactions between the subsystems (Bressler and Kelso, 2001). These global states, which subsume several functional clusters, are sufficiently complex entities to facilitate efficient information processing. Furthermore, the temporal instability of the global and local coordination states facilitates flexible switching to subsequent states (Friston, 2000b, Bressler and Kelso, 2001). Although this approach provides very powerful concepts and formalisms, they may prove too abstract to be utilized for the formulation of experimental hypotheses in functional neuroimaging. Explicitly, the particular nature of interactions in the brain, the collective variables of interest at different spatial scales and finally their relation to the macroscopically measured signals such as the EEG and MEG are still largely unknown. These topics are central to the rest of the thesis.

In chapter 2 we examined methods for assessing interactions between macroscopic brain sources using non-invasive functional neuroimaging techniques such as the MEG. We argued that it is perhaps equally important to know both, the location of the sources that generate these macroscopic signals but also how these interact with each other in a given experimental setting in real time. The knowledge of both the location and the pattern of interactions of brain sources are vital if we want to employ the theoretical framework described above in order to characterize the neural substrates of information processing. We showed that under realistic measurement conditions the assessment of the location, the time courses and most importantly the interactions between linear and nonlinear sources is possible within reasonable limitations imposed by the beamformer methodology.

In chapter 3 we examined the nature of synchronization phenomena arising from the interaction of low dimensional nonlinear systems in greater detail. Synchronization phenomena have been observed at all levels of description in the brain and are empirically closely linked to integrative and highly specific information processing (Varela et al., 2001). The study of synchronization phenomena in simpler systems was centred on the idea that the mechanisms and the dynamics of the collective coordination process will be *universal* and also *primarily causal* for the appearance of macroscopic order in the brain (or in fact any other complex system). In other words, we were looking for specific dynamical substrates for the key concepts of functional integration, segregation and metastability in terms of synchronization and desynchronization processes. It had been previously suggested that synchronization is synonymous to stable linear resonance (or crosscorrelation) and thus cannot possibly facilitate information processing (Friston, 2000a). We have argued that this is not the case. On the contrary, a multitude of synchronization phenomena arise through the interaction of merely two coupled nonlinear systems. These phenomena are highly dynamic and can be distinctly unstable and in fact, for a range of parameters, the collective dynamics are intermittent (*metastable*). Furthermore, we have demonstrated that the introduction of strong coupling between dissimilar chaotic systems or strong periodic forcing may lead to low dimensional periodic behaviour in the previously chaotic systems.

The latter phenomenon, known as *chaos destroying synchronization* may be relevant in the context of strong driving sensory inputs of a periodic nature, widely used in sensory paradigms. Thus the periodic structure of the stimulus may be reflected in the sensory input of subcortical structures to the cortex and subsequently enforce low dimensional periodic behaviour. This may however not be typical of the activity of the cortex in the absence of

such strong and regular stimuli, which are also seldom found in the environment. We tested these ideas explicitly in chapter 5 using the steady state auditory evoked response.

We were mainly interested in two cases, that of identical (*symmetry* condition) and that of nonidentical (*broken symmetry* condition) interacting systems. In the first case we observed the emergence of *identical synchronization* (Pecora and Carroll, 1990) or strong *generalized synchronization* (Pyragas, 1996). The dynamics in the coupled systems remained chaotic but were nearly identical. Thus the synchronization dynamics were confined to a subpartition of the state space, the symmetry manifold (a hyperplane). We speculated that this extreme dimensional reduction might play a role in enhancement of signal to noise ratio and hence facilitate secure message transmission. This could be particularly useful for neuronal interactions at microscopic levels and in particular in the context of early sensory processing. However, this kind of interaction is not truly adaptive, since the synchronization dynamics are confined on the symmetry manifold; for this reason there is no creation of information given that the coupled system does not undergo a bifurcation (this kind of interaction corresponds to total *integration* in the sense of Sporns and Tononi, 2002). In the case of nonidentical systems, we observed two main classes of dynamic regimes that of *phase synchronization* (Rosenblum *et al.*, 1996) and *generalized synchronization* (Rulkov *et al.*, 1995, Pyragas, 1996). These interactions do not constrain the coordination dynamics in a simple (hyper) plane but exhibit more geometrically complex manifolds, which essentially comprise a *mixture* of the dynamics in the interacting systems and consequently the synchronization manifolds often become unstable. Hence in these cases there is true integration (this corresponds to the notion of *complexity* (Sporns and Tononi, 2002), in the sense that the systems preserve some autonomy despite their interaction. This kind of interaction may be important for information processing at mesoscopic and macroscopic scales in the brain, where dissimilar modular structures need to transiently interact but still need to preserve their autonomy. *Phase synchronization* occurred for lower coupling strengths. Inherently dissimilar systems, could exhibit synchronization but they required higher coupling strengths and dissipated more energy to do so; crucially this phenomenon, often referred to as *oscillation death*, occurred for an entire range of parameters. The latter is due to the tendency of interacting systems to preserve their autonomous dynamics despite the presence of relatively strong coupling. The coordination scenarios, which arose in the case of coupled dissimilar systems, were likely to involve relative coordination dynamics such as intermittent and/or imperfect phase synchronization. The metastable coordination dynamics in this case often came about in the form of *on-off intermittency* (Platt, Spiegel and Tresser, 1993) of the phase difference (the collective variable). Perhaps the most important consequence of the

observations above is that if such processes were to occur in the brain, they would concur with energy dissipation and could be thus captured as amplitude changes in metabolic and electric measures of mean neuronal activity. Oscillation death when occurring on the basis of intermittent phase dynamics may be related to resetting the subtle equilibrium (*metastable*) dynamics between different oscillatory processes (segregation) and inherent structural coupling (functional integration).

In chapter 4 we extended the study to multidimensional nonlinear systems with an explicit spatial structure. Such systems exhibit interactions between their subcomponents, which result in the emergence of macroscopic order. The scope of this work was to explore, potential scale-specific collective variables (that determine macroscopic pattern formation) and how these change with respect to system control parameters such as the connectivity and homogeneity of constituent units. Above all we were interested in the inverse problem: Can the changes in a gross macroscopic observable such as the mean field signal tell us anything about the coordination processes occurring in the underlying network? This issue is extremely important for the analysis and interpretation of phenomenological patterns observed in macroscopic MEG/EEG signals such as task-related power changes (ERD/ERS, Pfurtscheller and Lopes Da Silva, 1999). We postulated that at least two levels of brain organization are indispensable for the generation of a macroscopic brain signal: a *microscopic* level, subsuming interactions of neurons (or minicolumns) *within* a cortical column, where the connectivity is global and the constituent units are nearly identical and a *mesoscopic* level, encompassing interactions of neurons *between* cortical columns, where the connectivity is local and the units are dissimilar. The mesoscopic level is more likely to contribute to the mean field signal; however it may itself be considered 'emergent' upon the interactions at the microscopic level. The microscopic level was abstractly modelled as an array of nearly identical, globally coupled oscillators and the mesoscopic level was abstractly modelled as a lattice of locally coupled oscillators. In the case of the globally coupled network of nearly identical elements (an abstract model of the interactions within a cortical column) introducing the coupling resulted to the emergence of almost complete array synchronization. The latter was consistent with the Kuramoto transition (Kuramoto, 1974 and 1985). The mean field signal exhibited an amplitude enhancement, which was mainly due to a power increase at a *discrete* frequency, the frequency of the collective synchronization occurring within the array. The latter was consistent with an increase of the 'signal to noise' ratio of the entire array through the onset of synchronization. In this case a microscopic synchronization process mapped directly to a specific power increase at a discrete frequency range perhaps analogous to the empirically observed ERS (Pfurtscheller and Lopes Da Silva, 1999). However, we

pointed out that the core assumptions of the model: the *homogeneity* of the units and the *global* nature of the coupling could be only justified for the microscopic and not the mesoscopic level of description. Nevertheless, this result suggested, that at the level of the cortical column, global synchronization processes may occur. These would result to the emergence of a mean field existent at well-defined frequency ranges; the latter seems to be supported by invasive neurophysiological data (Gray and Singer, 1995, Koenig, Engel, Singer 1995, Traub, Whittington, Stanford, and Jefferys, 1996). As a consequence, cortical columns could be abstractly modelled as oscillators exhibiting characteristic frequencies.

We then looked at an array of locally coupled nonidentical oscillators. The latter was conceived as an abstract model of a mesoscopic level, mainly pertaining to the interactions *between* cortical columns. Introducing the coupling resulted in partial synchronization in the array, with the formation of several synchronized clusters. The relevant collective variable at the mesoscopic level was the *phase difference* between the units, since the coordinative phenomenon that occurred was *phase synchronization*. The strength of the synchronization in fact defined the clusters. Nevertheless, these clusters exhibited distinct frequencies, and in effect the *frequency difference* between the clusters was the collective variable (the order parameter) at a macroscopic level of description. That is, these clusters were detectable in the mean field signal, in the form of *distinct* spectral peaks. Interestingly, the array as a whole did *not* exhibit a marked *power increase* after the onset of synchronization; on the contrary a *power decrease* was evident in the units, which were situated between the two stronger clusters. This relatively broadband power decrease was also evident in the power spectrum of the mean field signal and occurred at the boundary of the spectral peaks corresponding to the synchronized clusters in the array. Closer inspection of this phenomenon revealed the emergence of auxiliary frequency modes, intermittent phase synchronization between the units concerned and *oscillation death*. We suggested that oscillation death contributed to the separation of the clusters by minimizing their 'extrinsic' input and thus decreasing their effective interaction. We suggested that this may be a generic contrast enhancement mechanism. The presence of intermittent phase dynamics suggested that the form and number of the clusters may (under circumstances) change *without* any change in the control parameters. Thus intermittency in such models with a spatial domain implies the spontaneous formation and dissolution of functional clusters. Recent work on realistic, multiscale models of interacting cortical columns suggested that this is possible and furthermore made the case for the adaptive role of intermittent phase synchronization and desynchronization (Breakspear, Terry and Friston, 2003). Oscillation death in the presence of intermittent phase dynamics can hence be conceived as a fundamental resetting (updating) mechanism. In terms

of synergetics (Haken, 1983) such spatiotemporal intermittency should be evident in the macroscopic order parameter. In our array this was the frequency difference of the clusters, which could be inspected through time frequency analyses of the mean field signal.

Studying these abstract and rather simplistic models lead to somewhat general but still important conclusions. Firstly, the mapping between synchronization occurring at microscopic and mesoscopic levels of description to macroscopic power changes in the mean field signal is not straightforward. Synchronization does not always imply power increase (an ERS according to the classical definition by Pfurtscheller and Lopes Da Silva, 1999). Actually the adaptive form of synchronization involving the formation of functional clusters in terms of the complexity framework (Sporns and Tononi, 2002, Breakspear, Terry and Friston, 2003) may well be accompanied by specific power increases and decreases, where the power decrease may be marked and of a broader frequency range, whereas the power increases maybe fairly sharp. This may shed some light on the empirical observations of marked power decreases (ERD's) when integrative information processing is required. Secondly, these results may also contribute to the understanding of concurrent power increases and decreases that are common in the alpha frequency band, which is often conceived as a unitary cortical rhythm (Klimesch *et al.*, 2000). Finally, these very simple models may provide a way to explore the relation between coordination processes occurring at smaller scales and integral macroscopic observables.

In chapter 5, we used a dynamical systems approach and applied it to analyze MEG steady state auditory evoked response data. The classical method of measuring the steady state response, the response that follows a periodic AM stimulus, is by averaging responses over a large number of very short epochs, usually the length of the period of the driving AM waveform, to maximise the signal-to-noise ratio of the response (Picton *et al.*, 1987, Ross *et al.*, 2000, Pantev *et al.*, 1996). The assumptions behind averaging in the temporal domain (and steady state techniques in general) are that the underlying neural signal is stationary, time-locked to the stimulus and superimposed on white noise. Therefore any variation in the envelope of the steady state response should be just due to effects of additive noise that is irrelevant to the processing of the stimulus. We tested this hypothesis by measuring the variability of the envelope of the (non time-averaged) following AM response and comparing it to the variability of a system noise recording. We showed that only 3-5% of the variability in the envelopes of the AM following response can be attributed to system noise. The rest of the variability remained unaccounted for and had to arise from neuronal processes occurring during the presentation of the stimulus. We suggested that inter and intra hemispheric

interactions between the AM following response and ongoing brain rhythms may explain some of the variability. The analysis of the phase and envelope interdependencies within the same hemisphere but across frequencies provided some evidence for *nonlinear envelope interactions* between the ongoing alpha and beta rhythms and the following AM response and additional crosshemispheric interactions of the alpha and beta rhythms concurrent with the stimulus. There was also some evidence for crosshemispheric nonlinear phase synchronization at the frequency of the AM stimulation signifying a genuine crosshemispheric interaction. These results strongly suggested that ongoing cortical rhythms *modulate* the following AM response and are therefore relevant for the processing of the stimulus and should not be therefore discarded by means of signal averaging. Furthermore, the presence of nonlinear interactions in macroscopic brain signals is in agreement with the literature (Breakspear and Terry, 2002a, Stam *et al.*, 2003). These results may extend this literature by virtue of the fact that the nonlinear interactions reported here occur at the *source (and not the sensor) level* and within the context of a *specific* experimental paradigm.

In chapter 6, we tested the hypothesis that distinct holistic stimuli, requiring the integration of activity in distributed neurons, would crucially depend on the formation of measurable functional clusters. The abstract models presented in chapter 4 suggested that the clusters would be defined as mutual synchronization of cortical columns at mesoscopic levels. The synchronization process however should express distinct characteristic frequencies for each stimulus pattern, so that distinct stimuli can be disambiguated. These emergent characteristic frequencies should be apparent as distinct spectral characteristics in the macroscopic mean field signal. Gamma oscillations (30-60Hz) have been suggested as mechanism for binding together information from specialized neurons that code for specific stimulus features. While the magnitude of gamma oscillations was found to increase in a multitude of tasks that require feature binding both in animals and humans, their temporal dynamics, which are probably closely linked to their function, have remained largely unexplained. We tested the hypothesis whether the temporal frequency of these oscillations may facilitate differential coding of distinct spatial stimuli. Using Magnetoencephalography (MEG) we studied responses to full-field square-wave patterns of varying spatial frequency.

We used a nonparametric ranking method to assess stimulus related changes in the spectral distributions across frequencies in the signal arising from a source located in primary visual cortex. The analysis performed in both the induced and the evoked response in the following three frequency ranges: gamma (30-60Hz), beta (20-30 Hz) and lower frequency range (0-20Hz). By doing this we were explicitly testing the null hypothesis of whether the rank

distributions of the stimulus related power changes may have arisen from the same distributions for the different spatial stimuli. Stimulus related increases in gamma oscillatory power in primary visual cortex was the most robust finding being consistent across all subjects and all experimental conditions. For different spatial frequencies we found significant differences in the spectral distribution of signal change in the induced (not strictly time-locked to stimulus) gamma band (30-60Hz) oscillations arising from primary visual cortex. Thus different spatial stimuli were accompanied by different temporal frequency distributions in the signal. We did not however observe similar changes in the evoked (time-locked) response or in induced frequency ranges outside the gamma band. These findings are consistent with invasive animal neurophysiology relating microscopic neuronal synchronization to mean field gamma oscillations. We showed for the first time that the frequency distribution of gamma oscillations in the human brain is governed by the spatial structure of visual stimuli. We speculated that the coding of spatial stimuli might be a process of competition of coarsely tuned receptive fields instantiated by synchronized processes at different frequencies.

Closer inspection of the temporal dynamics of the signal arising from primary visual cortex revealed bursting oscillations in the gamma range (30-60Hz). Motivated by the results of the modelling work (chapters 3 and 4), in chapter 7 we set out to test the hypothesis that this apparent bursting behaviour may be a reflection of dynamic intermittency arising from interactions between nonlinear subentities contributing to the same macroscopic signals. Although the presence of dynamic intermittency can not be inferred from noisy signal observables generated by a largely unknown system, we argued that one can test the operational hypothesis, of whether the slow modulations in the amplitude of the oscillation exhibited a deterministic nonlinear structure or alternatively they just reflected random, noisy fluctuations. We presented a technique for assessing the distribution of the interburst intervals based on identifying local maxima in the signal. For salient 3 c.p.d. stimuli the temporal structure of these signal maxima strongly resembled the dynamic phenomenon of on-off intermittency (Platt, Spiegel and Tresser, 1993). However, the distribution of these interburst intervals did *not* conform to the $-3/2$ power law scaling characteristic for on-off intermittency (Platt, Spiegel and Tresser, 1993). Further, this distribution was only seldom different to the one obtained by phase randomized FFT surrogates (Theiler *et al.*, 1992), where possible nonlinear structure was destroyed. Thus rejections of the null hypothesis of a purely linear noisy process underlying the bursting behaviour of gamma oscillations were rather rare. Consequently, we could not provide support for deterministic nonlinear dynamics underlying the bursting behaviour of these visually induced gamma oscillations

8.2 General conclusions and implications

The work presented in this thesis examined collective coordination phenomena and their relation to macroscopic neuroimaging signals such as the MEG recorded during sensory paradigms. We adopted a theoretical framework based on dynamical systems theory. The latter proved to be extremely valuable not only by providing novel conceptual insights and motivating testable experimental hypotheses but also in the process of devising appropriate methodology and interpreting experimental neuroimaging data.

The application of the dynamical approach to neuroimaging data discloses novel perspectives, as it facilitates a direct link between microscopic, intermediate and macroscopic measures of neuronal function, which are generally studied in isolation by distinct disciplines.

Furthermore, the findings presented here, when interpreted within the framework of a general coordination theory of brain function, have direct implications for further research in a range of diverse fields both in empirical and theoretical neuroscience. The main implication to be drawn from this research is the following: predictions of the neuronal synchronization hypothesis (with support from invasive studies in animals with intracellular and local field recordings) in combination with predictions from the theory of coordination in nonlinear systems can be used to formulate testable operational hypotheses considering the macroscopic level of description of neuronal networks. These predictions are specific as to *which patterns* can be expected in macroscopic brain signals and therefore have direct implications for *which* variables would be of interest in these complex, integral measurements. These hypotheses can be tested in human participants using non-invasive neuroimaging techniques in conjunction with sophisticated signal processing methodologies. These predictions seem to be confirmed by the *phenomenological patterns* observed in the experimental results. These seem to be in accordance with well-documented findings regarding neuronal *function*, as studied in terms of perception (visual psychophysics), neuronal receptive fields (single and multi unit recordings) and networks of coupled neurons/dynamical systems (theoretical and computational neuroscience). These results indicate not only, that new experimental possibilities arise for functional neuroimaging but also that the relation between different levels of description in the brain can be investigated by integrating all these related literatures. Functional neuroimaging methodologies have the major advantage of directly studying brain function in humans and not inferring it through animal models. Also they allow for complex behavioural experimentation and accurate behavioural measurement (an objective 'functional' measurement of the brain), which is not possible in animal experiments. The latter nevertheless, enable direct measurement of neuronal network function, which can then be

modelled mathematically to illuminate possible mechanisms at work. Moreover large-scale neural network modelling in conjunction with experimental data from neuronal, intermediate and integral brain measurements can inform the relation between observed phenomenology and function. Experimental data such as these presented here can help in both evaluating and providing physiological constraints for such models and furthermore relating them to behavioural or perceptual processes. We argue that the approach of combining these diverse bodies of research is not only extremely useful but also seems to be technically feasible with the methods available to us today. We consider that, the possible link that can be created between invasive animal and non-invasive human literatures by application of these concepts and the related methodologies may represent a major advancement in neuroscience.

Finally, we acknowledge that we are still far from a general and widely accepted theory of coordination in the brain. In fact, still little is known about large-scale coordination dynamics in the brain and their role in information processing. We are fully aware of the fact that the work presented in this thesis is merely scratching the surface. However, the theoretical and empirical studies presented here suggest that developments in the theory of synchronization in complex nonlinear systems in conjunction with advancements in magnetoencephalography can potentially provide powerful insights into brain function. Similar approaches may contribute to extending the interpretation of neuroimaging data beyond phenomenology and hence eventually justify the term 'functional' in functional neuroimaging.

References

- Adjamian,P., Holliday,I.E., Barnes,G.R., Hillebrand,A., Hadjipapas,A., and Singh,K.D. (2004a). Induced visual illusions and gamma oscillations in human primary visual cortex. *European Journal of Neuroscience* 20, 587-592.
- Adjamian,P., Barnes,G.R., Hillebrand,A., Holliday,I.E., Singh,K.D., Furlong,P.L., Harrington,E., Barclay,C.W., and Route,P.J.G. (2004b). Co-registration of magnetoencephalography with magnetic resonance imaging using bite-bar-based fiducials and surface- matching. *Clinical Neurophysiology* 115, 691-698.
- Altenburg,J., Vermeulen,R.J., Strijers,R.L.M., Fetter,W.R., and Stam,C.J. (2003). Seizure detection in the neonatal EEG with synchronization likelihood. *Clinical Neurophysiology* 114, 50-55.
- Ashwin,P. and Breakspear,M. (2001). Anisotropic properties of riddled basins. *Physics Letters A* 280, 139-145.
- Barnes,G.R. and Hillebrand,A. (2003). Statistical flattening of MEG beamformer images. *Human Brain Mapping* 18, 1-12.
- Barnes,G.R., Singh,K.D., Fawcett,I., Hadjipapas,A., and Hillebrand,A. Quantification of the relationship between magnetoencephalographic (MEG) and blood oxygenation level dependent (BOLD) images of brain function. Workshop on Statistical Signal Processing, Sept.28 – Oct.1, 2003, St.Louis, Missouri, U.S.A. 2003.
- Basar, E., 1980. EEG-Brain dynamics. Relation between EEG and Brain Evoked Potentials. (Amsterdam.:Elsevier).
- Basar, E., Bullock TH. 1992. Induced Rhythms in the Brain. (Boston: Birkhauser).
- Basar,E., Schurmann,M., BasarEroglu,C., and Karakas,S. (1997). Alpha oscillations in brain functioning: An integrative theory. *International Journal of Psychophysiology* 26, 5-29.
- Basar,E., Basar-Eroglu,C., Karakas,S., and Schurmann,M. (2001). Gamma, alpha, delta, and theta oscillations govern cognitive processes. *International Journal of Psychophysiology* 39, 241-248.
- Boccaletti,S., Kurths,J., Osipov,G., Valladares,D.L., and Zhou,C.S. (2002). The synchronization of chaotic systems. *Physics Reports-Review Section of Physics Letters* 366, 1-101.
- Braitenberg V.,S.A. (1998). CORTEX: Statistics and Geometry of Neuronal Connectivity. Second Edition. (Berlin: Springer).

- Breakspear, M. (2002). Nonlinear phase desynchronization in human electroencephalographic data. *Human Brain Mapping* 15, 175-198.
- Breakspear, M. and Terry, J.R. (2002a). Detection and description of non-linear interdependence in normal multichannel human EEG data. *Clinical Neurophysiology* 113, 735-753.
- Breakspear, M. and Terry, J.R. (2002b). Topographic organization of nonlinear interdependence in multichannel human EEG. *Neuroimage* 16, 822-835.
- Breakspear, M., Terry, J.R., and Friston, K.J. (2003). Modulation of excitatory synaptic coupling facilitates synchronization and complex dynamics in a nonlinear model of neuronal dynamics. *Neurocomputing* 52-4, 151-158.
- Breakspear, M. (2004). "Dynamic" connectivity in neural systems - Theoretical and empirical considerations. *Neuroinformatics* 2, 205-225.
- Breakspear M. and Stam C.J. (2004). Dynamics of a neural system with a multiscale architecture. *Proceedings of the Brain Connectivity Workshop, Havana-Cuba, 26-29 April, 2004*
- Breakspear, M., Williams, L.M., and Stam, C.J. (2004). A novel method for the topographic analysis of neural activity reveals formation and dissolution of 'dynamic cell assemblies'. *Journal of Computational Neuroscience* 16, 49-68.
- Bredfeldt, C.E. and Ringach, D.L. (2002). Dynamics of spatial frequency tuning in macaque V1. *Journal of Neuroscience* 22, 1976-1984.
- Bressler, S.L. and Kelso, J.A.S. (2001). Cortical coordination dynamics and cognition. *Trends in Cognitive Sciences* 5, 26-36.
- Burgess, A.P. and Gruzelier, J.H. (2000). Short duration power changes in the EEG during recognition memory for words and faces. *Psychophysiology* 37, 596-606.
- Campbell, F.W. a. R.J.G. (1957). Moving Visual Images Produced by Regular Stationary Patterns. *Nature*. 180, 849-850.
- Curuklu, B. and Lansner, A. (2001). Spike and burst synchronization in a detailed cortical network model with I-F neurons. *Artificial Neural Networks-Icann 2001, Proceedings* 2130, 1095-1102.
- David, O., Cosmelli, D., and Friston, K.J. (2004). Evaluation of different measures of functional connectivity using a neural mass model. *Neuroimage* 21, 659-673.
- Descartes C. (1972). *Treatise on Man (1644)*. Trans. by T.S.Hall. Harvard University Press, 1972.

- Devalois,R.L., Yund,E.W., and Hepler,N. (1982). The orientation and direction selectivity of cells in macaque visual-cortex. *Vision Research* 22, 531-544.
- Devalois,R.L., Albrecht,D.G., and Thorell,L.G. (1982). Spatial-frequency selectivity of cells in macaque visual-cortex. *Vision Research* 22, 545-559.
- Engel,A.K., Konig,P., and Singer,W. (1991). Direct physiological evidence for scene segmentation by temporal coding. *Proceedings of the National Academy of Sciences of the United States of America* 88, 9136-9140.
- Engel,A.K., Konig,P., Kreiter,A.K., Schillen,T.B., and Singer,W. (1992). Temporal coding in the visual-cortex - new vistas on integration in the nervous-system. *Trends in Neurosciences* 15, 218-226.
- Engel,A.K. and Singer,W. (2001). Temporal binding and the neural correlates of sensory awareness. *Trends in Cognitive Sciences* 5, 16-25.
- Ermentrout,G.B. and Kopell,N. (1984). Frequency plateaus in a chain of weakly coupled oscillators .1. *Siam Journal on Mathematical Analysis* 15, 215-237.
- Fell,J., Fernandez,G., Klaver,P., Elger,C.E., and Fries,P. (2003). Is synchronized neuronal gamma activity relevant for selective attention? *Brain Research Reviews* 42, 265-272.
- Felleman,D.J. and Van.Essen, D.C. (1991). Distributed hierarchical processing in the primate cerebral cortex. *Cereb Cortex*.1991 1, 1-47.
- Foster,K.H., Gaska,J.P., Nagler,M., and Pollen,D.A. (1985). Spatial and temporal frequency-selectivity of neurons in visual cortical areas v1 and v2 of the macaque monkey. *Journal of Physiology-London* 365, 331-363.
- Földiák,P.and Young, .M.P. (1995). Sparse coding in the primate cortex. In *Handbook of Brain Theory and Neural Networks*, (Cambridge: MIT Press), pp. 895-898.
- Freeman, W.J. (1975) *Mass Action in the Nervous System*.(New York: Academic Press).
- Freeman W.J.,Barry .J.M. (1994). Chaotic oscillations and the genesis of meaning in cerebral cortex. In *Temporal Coding in the Brain*, Buzsaki G., Llinas R., Singer W., Berthoz A., Christen Y., ed. (Berlin: Springer-Verlag), pp. 13-37.
- Freeman,W.J. (1992). Tutorial on Neurobiology: From Single Neurons to Brain Chaos. *International Journal of Bifurcation and Chaos* 2, 451-482.
- Friston,K.J. (1997). Transients, metastability, and neuronal dynamics. *Neuroimage* 5, 164-171.

- Friston, K.J. (2000a). The labile brain. I. Neuronal transients and nonlinear coupling. *Philosophical Transactions of the Royal Society of London Series B-Biological Sciences* 355, 215-236.
- Friston, K.J. (2000b). The labile brain. II. Transients, complexity and selection. *Philosophical Transactions of the Royal Society of London Series B-Biological Sciences* 355, 237-252.
- Friston, K.J. (2000c). The labile brain. III. Transients and spatio-temporal receptive fields. *Philosophical Transactions of the Royal Society of London Series B-Biological Sciences* 355, 253-265.
- Gabor D. (1946). Theory of Communication. *J EE Lond* 93, 429-457.
- Gatlin L. (1972). *Information Theory and the Living System*. (New York: Columbia University Press).
- Goldman-Rakic, P.S. (1995). Cellular basis of working-memory. *Neuron* 14, 477-485.
- Gray, C.M. and Singer, W. (1989). Stimulus-specific neuronal oscillations in orientation columns of cat visual-cortex. *Proceedings of the National Academy of Sciences of the United States of America* 86, 1698-1702.
- Gray, C.M., Konig, P., Engel, A.K., and Singer, W. (1989). Oscillatory responses in cat visual-cortex exhibit inter-columnar synchronization, which reflects global stimulus properties. *Nature* 338, 334-337.
- Gross, J., Kujala, J., Hamalainen, M., Timmermann, L., Schnitzler, A., and Salmelin, R. (2001). Dynamic imaging of coherent sources: Studying neural interactions in the human brain. *Proceedings of the National Academy of Sciences of the United States of America* 98, 694-699.
- Hadjipapas A., Hillebrand A, Holliday I.E., Singh K.D., and Barnes G.R (2005). Assessing interactions of linear and nonlinear neuronal sources: a proof of concept. In press, *Clinical Neurophysiology*.
- Haken, H. (1983). *Synergetics: an introduction: nonequilibrium phase transitions and self-organization in physics, chemistry, and biology*. (Berlin: Springer).
- Haken, H., Kelso, J.A.S., and Bunz, H. (1985). A theoretical-model of phase-transitions in human hand movements. *Biological Cybernetics* 51, 347-356.
- Hall, S.D., Holliday, I.E., Hillebrand, A., Singh, K.D., Furlong, P.L., Hadjipapas, A. and Barnes, G.R (2005). The missing link: concurrent human and primate cortical gamma oscillations. In Press, *NeuroImage*.
- Heagy, J.F., Platt, N., and Hammel, S.M. (1994). Characterization of on-off intermittency. *physical review e* 49, 1140-1150.

Heagy, J.F., Carroll, T.L., and Pecora, L.M. (1995). Desynchronization by periodic-orbits. *Physical Review E* 52, r1253-r1256.

Hellwig, B. (2000). A quantitative analysis of the local connectivity between pyramidal neurons in layers 2/3 of the rat visual cortex. *Biological Cybernetics* 82, 111-121.

Hillebrand, A., Singh, K.D., Holliday, I.E., Furlong, P.L., Barnes, G.R. (2005). A new approach to neuroimaging with magnetoencephalography. In press, *Human Brain Mapping*.

Hubel D.H. and Wiesel, T.N. (1962). Receptive fields, binocular interaction and functional architecture in the cat's visual cortex. *J Physiol* 160, 106-154.

Hubel D.H. and Wiesel, T.N. (1968). Receptive fields and functional architecture of the monkey striate cortex. *J Physiol* 195, 215-243.

Hubel D.H., Wiesel, T.N. (1972). Laminar and columnar distribution of geniculocortical fibers in the macaque monkey. *J Comp Neurol* 146, 421-450.

Hubel, D.H. (1982). Exploration of the primary visual-cortex, 1955-78. *Nature* 299, 515-524.

Hunt, B.R., Ott, E., and Yorke, J.A. (1997). Differentiable generalized synchronization of chaos. *Physical Review E* 55, 4029-4034.

Ioannides, A.A., Bolton, J.P.R., and Clarke, C.J.S. (1990). Continuous probabilistic solutions to the biomagnetic inverse problem. *Inverse Problems* 6, 523-542.

Jensen, O. and Tesche, C.D. (2002). Frontal theta activity in humans increases with memory load in a working memory task. *European Journal of Neuroscience* 15, 1395-1399.

Jirsa, V.K. and Haken, H. (1996). Field theory of electromagnetic brain activity. *Physical Review Letters* 77, 960-963.

Jirsa, V.K., Jantzen, K.J., Fuchs, A., and Kelso, J.A.S. (2002). Spatiotemporal forward solution of the EEG and MEG using network modeling. *IEEE Transactions on Medical Imaging* 21, 493-504.

John, M.S., Lins, O.G., Boucher, B.L., and Picton, T.W. (1998). Multiple auditory steady-state responses (MASTER): Stimulus and recording parameters. *Audiology* 37, 59-82.

John, M.S. and Picton, T.W. (2000). MASTER: a Windows program for recording multiple auditory steady-state responses. *Computer Methods and Programs in Biomedicine* 61, 125-150.

- Josic, K. (1998). Invariant manifolds and synchronization of coupled dynamical systems. *Physical Review Letters* 80, 3053-3056.
- Kaneko, K. (1990). Clustering, coding, switching, hierarchical ordering, and control in a network of chaotic elements. *Physica D* 41, 137-172.
- Kaneko, K. and Tsuda, I. (2003). Chaotic itinerancy. *Chaos* 13, 926-936.
- Karrasch, M., Krause, C.M., Laine, M., Lang, A.H., and Lehto, M. (1998). Event-related desynchronization and synchronization during an auditory lexical matching task. *Electroencephalography and Clinical Neurophysiology* 107, 112-121.
- Keil, A., Müller, M.M., Ray, W.J., Gruber, T., and Elbert, T. (1999). Human gamma band activity and perception of a gestalt. *Journal of Neuroscience* 19, 7152-7161.
- Kelso, J.S.A. (1995). *Dynamic patterns: The self-organization of brain and behavior*. (Cambridge, Massachusetts, London, England.: MIT Press).
- Klimesch, W. (1996). Memory processes, brain oscillations and EEG synchronization. *International Journal of Psychophysiology* 24, 61-100.
- Klimesch, W., Doppelmayr, M., Rohm, D., Pollhuber, D., and Stadler, W. (2000). Simultaneous desynchronization and synchronization of different alpha responses in the human electroencephalograph: a neglected paradox? *Neuroscience Letters* 284, 97-100.
- Klimesch, W., Doppelmayr, M., Stadler, W., Pollhuber, D., Sauseng, P., and Rohm, D. (2001). Episodic retrieval is reflected by a process specific increase in human electroencephalographic theta activity. *Neuroscience Letters* 302, 49-52.
- Kobatake, E. and Tanaka, K. (1994). Neuronal selectivities to complex object features in the ventral visual pathway of the macaque cerebral cortex. *Journal of Neurophysiology* 71, 856-867.
- Kocarev, L., Parlitz, U., and Brown, R. (2000). Robust synchronization of chaotic systems. *Physical Review E* 61, 3716-3720.
- König, P., Engel, A.K., and Singer, W. (1995). Relation between oscillatory activity and long-range synchronization in cat visual cortex. *Proceedings of the National Academy of Sciences of the United States of America* 92, 290-294.
- Kotter, R. and Stephan, M.E. (2003). Network participation indices: characterizing component roles for information processing in neural networks. *Neural Networks* 16, 1261-1275.
- Krause, C.M., Lang, A.H., Laine, M., Kuusisto, M., and Porn, B. (1996). Event-related EEG desynchronization and synchronization during an auditory memory task. *Electroencephalography and Clinical Neurophysiology* 98, 319-326.

- Krause, C.M., Porn, B., Lang, A.H., and Laine, M. (1997). Relative alpha desynchronization and synchronization during speech perception. *Cognitive Brain Research* 5, 295-299.
- Krause, C.M., Astrom, T., Karrasch, M., Laine, M., and Sillanmaki, L. (1999). Cortical activation related to auditory semantic matching of concrete versus abstract words. *Clinical Neurophysiology* 110, 1371-1377.
- Kuramoto Y. (1975). Self-entrainment of a population of coupled nonlinear oscillators. In *International Symposium on Mathematical Problems in Theoretical Physics*, In H. Araki, ed. (New York: Springer).
- Kuramoto Y. (1984). *Chemical Oscillations Waves and Turbulence*. (Berlin: Springer).
- Kuwada, S., Batra, R., and Maher, V.L. (1986). Scalp potentials of normal and hearing-impaired subjects in response to sinusoidally amplitude-modulated tones. *Hearing Research* 21, 179-192.
- Lachaux, J.P., Rodriguez, E., Martinerie, J., and Varela, F.J. (1999). Measuring phase synchrony in brain signals. *Human Brain Mapping* 8, 194-208.
- Leocani, L., Magnani, G., Comi, G. (1999). Event-related desynchronization during execution, imagination and withholding of movement. In: Pfurtscheller, G., Lopes da Silva, F.H. Eds., *Event-Related Desynchronization. Handbook of Electroencephalography and Clinical Neurophysiology*, 6, Revised ed Elsevier, Amsterdam, pp. 291-301.
- Livingstone, M.S. (1998). Mechanisms of direction selectivity in macaque V1. *Neuron* 20, 509-526.
- Lopes da Silva, F.H. and Pfurtscheller, G. (1999). Basic concepts on EEG synchronization and desynchronization. Event-related desynchronization and related oscillatory phenomena of the brain. In: Pfurtscheller, G. and Lopes da Silva, F.H. Editors, 1999. *Handbook of electroencephalography and clinical neurophysiology vol. 6*, revised edition Elsevier, Amsterdam, pp. 3-11.
- Maistrenko, Y.L., Maistrenko, V.L., Popovich, A., and Mosekilde, E. (1998). Transverse instability and riddled basins in a system of two coupled logistic maps. *Physical Review* e 57, 2713-2724.
- Makeig, S., Westerfield, M., Jung, T.P., Enghoff, S., Townsend, J., Courchesne, E., and Sejnowski, T.J. (2002). Dynamic brain sources of visual evoked responses. *Science* 295, 690-694.
- Manneville, P. & P.Y. (1979). Intermittency and the Lorenz Model. *Phys. Lett. A* 75, 1-2.
- May, R. M. (1974). Biological populations with nonoverlapping generations: stable points, stable cycles and chaos. *Science* 186, 645-647.

- May, R. M. (1976). Simple mathematical models with very complicated dynamics. *Nature*. 261, 459-467.
- Meijs, J.W.H., Weier, O.W., Peters, M.J., and Vanoosterom, A. (1989). On the numerical accuracy of the boundary element method. *Ieee Transactions on Biomedical Engineering* 36, 1038-1049.
- Mountcastle, V.B. (1997). The columnar organization of the neocortex. *Brain* 120, 701-722.
- Mountcastle, V.B. (2003). Untitled - Introduction. *Cerebral Cortex* 13, 2-4.
- Nase, G., Singer, W., Monyer, H., and Engel, A.K. (2003). Features of neuronal synchrony in mouse visual cortex. *Journal of Neurophysiology* 90, 1115-1123.
- Neuenschwander, S. and Singer, W. (1996). Long-range synchronization of oscillatory light responses in the cat retina and lateral geniculate nucleus. *Nature* 379, 728-733.
- Neuper, C. and Pfurtscheller, G. (1996). Post-movement-synchronization of beta rhythms in the EEG over the cortical foot area in man. *Neuroscience Letters* 216, 17-20.
- Neuper, C. and Pfurtscheller, G. (2001). Evidence for distinct beta resonance frequencies in human EEG related to specific sensorimotor cortical areas. *Clinical Neurophysiology* 112, 2084-2097.
- Nunez, P.L., Srinivasan, R., Westdorp, A.F., Wijesinghe, R.S., Tucker, D.M., Silberstein, R.B., and Cadusch, P.J. (1997). EEG coherency .I. Statistics, reference electrode, volume conduction, Laplacians, cortical imaging, and interpretation at multiple scales. *Electroencephalography and Clinical Neurophysiology* 103, 499-515.
- Nunez, P.L., Silberstein, R.B., Shi, Z.P., Carpenter, M.R., Srinivasan, R., Tucker, D.M., Doran, S.M., Cadusch, P.J., and Wijesinghe, R.S. (1999). EEG coherency II: experimental comparisons of multiple measures. *Clinical Neurophysiology* 110, 469-486.
- Nunez, P.L., Wingeier, B.M., and Silberstein, R.B. (2001). Spatial-temporal structures of human alpha rhythms: Theory, microcurrent sources, multiscale measurements, and global binding of local networks. *Human Brain Mapping* 13, 125-164.
- Osipov, G.V., Pikovsky, A.S., Rosenblum, M.G., and Kurths, J. (1997). Phase synchronization effects in a lattice of nonidentical Rossler oscillators. *Physical Review e* 55, 2353-2361.
- Ott, E. and Sommerer, J.C. (1994). Blowout bifurcations - the occurrence of riddled basins and on off intermittency. *Physics Letters A* 188, 39-47.
- Palus, M. (1997). Detecting phase synchronization in noisy systems. *Physics Letters A* 235, 341-351.

- Pantev,C., Roberts,L.E., Elbert,T., Ross,B., and Wienbruch,C. (1996). Tonotopic organization of the sources of human auditory steady- state responses. *Hearing Research* 101, 62-74.
- Pecora,L.M. and Carroll,T.L. (1990). Synchronization in chaotic systems. *Physical Review Letters* 64, 821-824.
- Pecora,L.M. and Carroll,T.L. (1998). Master stability functions for synchronized coupled systems. *Physical Review Letters* 80, 2109-2112.
- Perrett,D.I., Rolls,E.T., and Caan,W. (1982). Visual neurones responsive to faces in the monkey temporal cortex. *Experimental Brain Research* 47, 329-342.
- Pfurtscheller,G., Stancak,A., and Neuper,C. (1996). Post-movement beta synchronization. A correlate of an idling motor area? *Electroencephalography and Clinical Neurophysiology* 98, 281-293.
- Pfurtscheller,G. and da Silva,F.H.L. (1999). Event-related EEG/MEG synchronization and desynchronization: basic principles. *Clinical Neurophysiology* 110, 1842-1857.
- Pfurtscheller,G., Neuper,C., and Krausz,G. (2000). Functional dissociation of lower and upper frequency mu rhythms in relation to voluntary limb movement. *Clinical Neurophysiology* 111, 1873-1879.
- Pfurtscheller,G. (2001). Functional brain imaging based on ERD/ERS. *Vision Research* 41, 1257-1260.
- Picton,T.W., Skinner,C.R., Champagne,S.C., Kellett,A.J.C., and Maiste,A.C. (1987). Potentials-evoked by the sinusoidal modulation of the amplitude or frequency of a tone. *Journal of the Acoustical Society of America* 82, 165-178.
- Pijnenburg,Y.A.L., Made,Y.V., van Walsum,A.M.V., Knol,D.L., Scheltens,P., and Stam,C.J. (2004). EEG synchronization likelihood in mild cognitive impairment and Alzheimer's disease during a working memory task. *Clinical Neurophysiology* 115, 1332-1339.
- Pikovsky,A.S. and Grassberger,P. (1991). Symmetry-breaking bifurcation for coupled chaotic attractors. *Journal of Physics A-Mathematical and General* 24, 4587-4597.
- Pikovsky,A., Rosenblum, M.G., Zaks, M.A., Kurths, J. (1999). Phase Synchronization of Regular and Chaotic oscillators. In *Handbook of Chaos Control*, H.G.Schuster, ed. Weinheim: Wiley-VCH, pp. 305-328.
- Pikovsky,A., Rosenblum,M., and Kurths,J. (2000). Phase synchronization in regular and chaotic systems. *International Journal of Bifurcation and Chaos* 10, 2291-2305.
- Pikovsky,A., Rosenblum,M.G., and Kurths,J. (2001). *Synchronization. A Universal Concept in Nonlinear Sciences.* (Cambridge, UK: Cambridge University Press).

Platt, N., Spiegel, E.A., and Tresser, C. (1993). On-off intermittency - a mechanism for bursting. *Physical Review Letters* 70, 279-282.

Platt, N., Hammel, S.M., and Heagy, J.F. (1994). Effects of additive noise on on-off intermittency. *Physical Review Letters* 72, 3498-3501.

Press, W.H., Teukolsky, S.A., Vetterling, W.T., Flannery, B.P. (1992). *Numerical Recipes: The Art of Scientific Computing*. Cambridge: Cambridge Press, pp. 614-622.

Prichard, D. and Theiler, J. (1994). Generating surrogate data for time-series with several simultaneously measured variables. *Physical Review Letters* 73, 951-954.

Pulvermuller, F., Lutzenberger, W., Preissl, H., and Birbaumer, N. (1995). Spectral responses in the gamma-band - physiological signs of higher cognitive-processes. *Neuroreport* 6, 2059-2064.

Pulvermuller, F., Birbaumer, N., Lutzenberger, W., and Mohr, B. (1997). High-frequency brain activity: Its possible role in attention, perception and language processing. *Progress in Neurobiology* 52, 427-445.

Pyragas, K. (1996). Weak and strong synchronization of chaos. *Physical Review e* 54, R4508-R4511.

Quiroga R., Basar E and Schurmann M. (2000). *Phase locking of event related alpha oscillations*. In: *Chaos in brain?* K Lehnertz, CE Elger, J Arnhold and P Grassberger (eds). World Scientific, pp:301-304.

Quiroga, R., Kraskov, A., Kreuz, T., and Grassberger, P. (2002). Performance of different synchronization measures in real data: A case study on electroencephalographic signals. *Physical Review e* 65, art-041903.

Raghavachari, S., Kahana, M.J., Rizzuto, D.S., Caplan, J.B., Kirschen, M.P., Bourgeois, B., Madsen, J.R., and Lisman, J.E. (2001). Gating of human theta oscillations by a working memory task. *Journal of Neuroscience* 21, 3175-3183.

Rapp, P.E., Albano, A.M., Schmah, T.I., and Farwell, L.A. (1993). Filtered noise can mimic low-dimensional chaotic attractors. *Physical Review e* 47, 2289-2297.

Rapp P. E., Albano A. M., Zimmerman I. D. Jimenez-Montano M. A. (1994), Phase-randomized surrogates can produce spurious identifications of non-random structure. *Physics Letters A*. Vol. 192: 27-33

Rees, A., Green, G.G.R., and Kay, R.H. (1986). Steady-state evoked-responses to sinusoidally amplitude-modulated sounds recorded in man. *Hearing Research* 23, 123-133.

Rees, A. and Moller, A.R. (1987). Stimulus properties influencing the responses of inferior colliculus neurons to amplitude-modulated sounds. *Hearing Research* 27, 129-143.

- Rim,S., Kim,I., Kang,P., Park,Y.J., and Kim,C.M. (2002). Routes to complete synchronization via phase synchronization in coupled nonidentical chaotic oscillators. *Physical Review e* 66, art-015205.
- Robinson,S.E. and Vrba,J. (1999). Functional neuroimaging by synthetic aperture magnetometry (SAM). In *Recent Advances in Biomagnetism*, Sendai, Tohoku Univ. Press), pp. 302-305.
- Rodriguez,E., George,N., Lachaux,J.P., Martinerie,J., Renault,B., and Varela,F.J. (1999). Perception's shadow: long-distance synchronization of human brain activity. *Nature* 397, 430-433.
- Roelfsema,P.R., Engel,A.K., Konig,P., and Singer,W. (1997). Visuomotor integration is associated with zero time-lag synchronization among cortical areas. *Nature* 385, 157-161.
- Rohm,D., Klimesch,W., Haider,H., and Doppelmayr,M. (2001). The role of theta and alpha oscillations for language comprehension in the human electroencephalogram. *Neuroscience Letters* 310, 137-140.
- Rolls,E.T. and Tovee,M.J. (1995). Sparseness of the neuronal representation of stimuli in the primate temporal visual-cortex. *Journal of Neurophysiology* 73, 713-726.
- Rosenblum,M.G., Pikovsky,A.S., and Kurths,J. (1996). Phase synchronization of chaotic oscillators. *Physical Review Letters* 76, 1804-1807.
- Rosenblum,M.G., Pikovsky,A.S., and Kurths,J. (1997). From phase to lag synchronization in coupled chaotic oscillators. *Physical Review Letters* 78, 4193-4196.
- Ross,B., Draganova,R., Picton,T.W., and Pantev,C. (2003). Frequency specificity of 40-Hz auditory steady-state responses. *Hearing Research* 186, 57-68.
- Rulkov,N.F., Sushchik,M.M., Tsimring,L.S., and Abarbanel,H.D.I. (1995). Generalized synchronization of chaos in directionally coupled chaotic systems. *Physical Review e* 51, 980-994.
- Rulkov,N.F. and Sushchik,M.M. (1997). Robustness of synchronized chaotic oscillations. *International Journal of Bifurcation and Chaos* 7, 625-643.
- Sakurai,Y. (1996). Population coding by cell assemblies - What it really is in the brain. *Neuroscience Research* 26, 1-16.
- Sakurai,Y. (1998). The search for cell assemblies in the working brain. *Behavioural Brain Research* 91, 1-13.
- Sakurai,Y. (1999). How do cell assemblies encode information in the brain? *Neuroscience and Biobehavioral Reviews* 23, 785-796.

Sarnthein, J., Petsche, H., Rappelsberger, P., Shaw, G.L., and von Stein, A. (1998). Synchronization between prefrontal and posterior association cortex during human working memory. *Proceedings of the National Academy of Sciences of the United States of America* 95, 7092-7096.

Sarvas, J. (1987). Basic mathematical and electromagnetic concepts of the biomagnetic inverse problem. *Physics in Medicine and Biology* 32, 11-22.

Sauseng, P., Klimesch, W., Gruber, W., Doppelmayr, M., Stadler, W., and Schabus, M. (2002). The interplay between theta and alpha oscillations in the human electroencephalogram reflects the transfer of information between memory systems. *Neuroscience Letters* 324, 121-124.

Schack, B., Vath, N., Petsche, H., Geissler, H.G., and Moller, E. (2002). Phase-coupling of theta-gamma EEG rhythms during short-term memory processing. *International Journal of Psychophysiology* 44, 143-163.

Schiff, S.J., So, P., Chang, T., Burke, R.E., and Sauer, T. (1996). Detecting dynamical interdependence and generalized synchrony through mutual prediction in a neural ensemble. *Physical Review E* 54, 6708-6724.

Schurmann, M. and Basar, E. (2001). Functional aspects of alpha oscillations in the EEG. *International Journal of Psychophysiology* 39, 151-158.

Sekihara, K., Nagarajan, S.S., Poeppel, D., and Marantz, A. (2002). Performance of an MEG adaptive-beamformer technique in the presence of correlated neural activities: Effects on signal intensity and time-course estimates. *Ieee Transactions on Biomedical Engineering* 49, 1534-1546.

Singer, W. and Gray, C.M. (1995). Visual feature integration and the temporal correlation hypothesis. *Annual Review of Neuroscience* 18, 555-586.

Singer, W. (1999). Neuronal synchrony: A versatile code for the definition of relations? *Neuron* 24, 49-65.

Singer, W. (2001). Consciousness and the binding problem. *Cajal and Consciousness* 929, 123-146.

Singh, K.D., Barnes, G.R., Hillebrand, A., Forde, E.M.E., and Williams, A.L. (2002). Task-related changes in cortical synchronization are spatially coincident with the hemodynamic response. *Neuroimage* 16, 103-114.

Singh, K.D., Barnes, G.R., and Hillebrand, A. (2003). Group imaging of task-related changes in cortical synchronisation using nonparametric permutation testing. *Neuroimage* 19, 1589-1601.

Sporns, O. a. T.G. (2002). Classes of network connectivity and dynamics. *Complexity* 7, 28-38.

Stam,C.J., van Walsum,A.M.V., Pijnenburg,Y.A.L., Berendse,H.W., de Munck,J.C., Scheltens,P., and van Dijk,B.W. (2002). Generalized synchronization of MEG recordings in Alzheimer's disease: Evidence for involvement of the gamma band. *Journal of Clinical Neurophysiology* 19, 562-574.

Stam,C.J., van Walsum,A.M.V., and Micheloyannis,S. (2002). Variability of EEG synchronization during a working memory task in healthy subjects. *International Journal of Psychophysiology* 46, 53-66.

Stam,C.J. and van Dijk,B.W. (2002). Synchronization likelihood: an unbiased measure of generalized synchronization in multivariate data sets. *Physica D* 163, 236-251.

Stam,C.J., Breakspear,M., van Walsum,A.M.V., and van Dijk,B.W. (2003). Nonlinear synchronization in EEG and whole-head MEG recordings of healthy subjects. *Human Brain Mapping* 19, 63-78.

Strogatz,S.H. (2000). From Kuramoto to Crawford: exploring the onset of synchronization in populations of coupled oscillators. *Physica D* 143, 1-20.

Supek S. and Aine C.J (1997). Spatio-temporal modeling of neuromagnetic data: I. Multi-source location vs. timecourse estimation accuracy, *Human Brain Mapping* 5, 139-153.

Tallon-Baudry,C., Bertrand,O., Peronnet,F., and Pernier,J. (1998). Induced gamma-band activity during the delay of a visual short- term memory task in humans. *Journal of Neuroscience* 18, 4244-4254.

Tallon-Baudry,C. and Bertrand,O. (1999). Oscillatory gamma activity in humans and its role in object representation. *Trends in Cognitive Sciences* 3, 151-162.

Tallon-Baudry,C., Bertrand,O., and Fischer,C. (2001). Oscillatory synchrony between human extrastriate areas during visual short-term memory maintenance. *Journal of Neuroscience* 21, art-RC177.

TallonBaudry,C., Bertrand,O., Delpuech,C., and Pernier,J. (1996). Stimulus specificity of phase-locked and non-phase-locked 40 Hz visual responses in human. *Journal of Neuroscience* 16, 4240-4249.

Tass,P., Rosenblum,M.G., Weule,J., Kurths,J., Pikovsky,A., Volkman,J., Schnitzler,A., and Freund,H.J. (1998). Detection of n : m phase locking from noisy data: Application to magnetoencephalography. *Physical Review Letters* 81, 3291-3294.

Tass,P.A., Fieseler,T., Dammers,J., Dolan,K., Morosan,P., Majtanik,M., Boers,F., Muren,A., Zilles,K., and Fink,G.R. (2003). Synchronization tomography: A method for three-dimensional localization of phase synchronized neuronal populations in the human brain using magnetoencephalography. *Physical Review Letters* 90, art-088101.

Tesche,C.D. and Karhu,J. (2000). Theta oscillations index human hippocampal activation during a working memory task. *Proceedings of the National Academy of Sciences of the United States of America* 97, 919-924.

Theiler,J., Eubank,S., Longtin,A., Galdrikian,B., and Farmer,J.D. (1992). Testing for nonlinearity in time-series - the method of surrogate data. *Physica D* 58, 77-94.

Tononi,G., Sporns,O., and Edelman,G.M. (1994). A measure for brain complexity - relating functional segregation and integration in the nervous-system. *Proceedings of the National Academy of Sciences of the United States of America* 91, 5033-5037.

Tononi,G., Sporns,O., and Edelman,G.M. (1996). A complexity measure for selective matching of signals by the brain. *Proceedings of the National Academy of Sciences of the United States of America* 93, 3422-3427.

Traub,R.D., Whittington,M.A., Stanford,I.M., and Jefferys,J.G.R. (1996). A mechanism for generation of long-range synchronous fast oscillations in the cortex. *Nature* 383, 621-624.

Tsuda,I. (1991). Chaotic itinerancy as a dynamical basis of hermeneutics in brain and mind. *World Futures* 32, 167-184.

Tsuda,I. and Umemura,T. (2003). Chaotic itinerancy generated by coupling of Milnor attractors. *Chaos* 13, 937-946.

Van Quyen,M., Foucher,J., Lachaux,J.P., Rodriguez,E., Lutz,A., Martinerie,J., and Varela,F.J. (2001). Comparison of Hilbert transform and wavelet methods for the analysis of neuronal synchrony. *Journal of Neuroscience Methods* 111, 83-98.

VanVeen,B.D., vanDrongelen,W., Yuchtman,M., and Suzuki,A. (1997). Localization of brain electrical activity via linearly constrained minimum variance spatial filtering. *Ieee Transactions on Biomedical Engineering* 44, 867-880.

Varela,F., Lachaux,J.P., Rodriguez,E., and Martinerie,J. (2001). The brainweb: Phase synchronization and large-scale integration. *Nature Reviews Neuroscience* 2, 229-239.

Von der Malsburg,C. (1981). *The Correlation Theory of Brain Function*. Technical Report 81-2, Biophysical Chemistry, MPI. 81.

Von der Malsburg,C. (1999). The what and why of binding: The modeler's perspective. *Neuron* 24, 95-104.

von Stein,A., Chiang,C., and Konig,P. (2000). Top-down processing mediated by interareal synchronization. *Proceedings of the National Academy of Sciences of the United States of America* 97, 14748-14753.

Vrba, J., Anderson, G., Betts, K., Burbank, M. B., Cheung, T., Cheyne, D., Fife, A. A., Govorkov, S., Habib, F., Haid, V., Hoang, T., Hunter, C., KubiK, P. R., Lee, S.,

McCubbin, J., McKay, J., McKenzie, D., Nonis, D., Paz, J., Reichl, E., Ressler, D., Robinson, S. E., Schroyen, C., Sekatchev, I., Spear, P., Taylor, B., Tillotson, M., and Sutherling, W. (1999). 151-Channel whole-cortex MEG system for seated or supine positions. In Yoshimoto, T., Kotani, M., Kuriki, S., Karibe, H., and Nakasato, N. eds. *Recent Advances in Biomagnetism*. Sendai, Tohoku University Press. 1999, pp.93-96.

Vrba, J. and Robinson, S.E. (2001). Signal processing in magnetoencephalography. *Methods* 25, 249-271.

Wickelgren, W.A. (1999). Webs, cell assemblies, and chunking in neural nets: Introduction. *Canadian Journal of Experimental Psychology-Revue Canadienne de Psychologie Experimentale* 53, 118-131.

Wright, J.J., Rennie, C.J., Lees, G.J., Robinson, P.A., Bourke, P.D., Chapman, C.L., Gordon, E., and Rowe, D.L. (2003). Simulated electrocortical activity at microscopic, mesoscopic, and global scales. *Neuropsychopharmacology* 28, S80-S93.

Young, M.P. and Yamane, S. (1992). Sparse population coding of faces in the inferotemporal cortex. *Science* 256, 1327-1331.

Young, M.P. (1992). Objective analysis of the topological organization of the primate cortical visual-system. *Nature* 358, 152-155.

Zhan, M., Wei, G.W., and Lai, C.H. (2002). Transition from intermittency to periodicity in lag synchronization in coupled Rossler oscillators. *Physical Review e* 65, art-036202.

Appendix 1: Linear stability analysis and Lyapunov exponents

Linear stability analysis

The notions of attractors, repellers and saddles are derived from the classical notion of (temporal) stability, as originally introduced by Lyapunov, and can be rigorously classified by means of a methodological framework referred to as linear stability analysis. The latter is described very briefly below in the simple cases of 1 and 2-D to introduce the basic concepts.

Essentially, the notion of stability in the simplest case of a one-dimensional system is related to behaviour of the time derivative. Thus, given the one dimensional dynamical system:

$$\dot{y}=f(x,t). \quad [1]$$

the state equation will be a 1-D ordinary differential equation of the form:

$$\frac{dx}{dt} = f(x). \quad [2]$$

Equilibria can be found where the time derivative is zero and thus

$$f(x) = 0 \implies x^*. \quad [3]$$

where x^* is the value of x where the time derivative $f(x)$ is zero.

x^* here corresponds to an *equilibrium* or a *fixed point*. This just implies that this point in state space is invariant in time.

Stability is then determined by the sign of $df(x)/dx$ evaluated at x^* . The system y , is said to be stable if $df(x)/dx < 0$, unstable if $df(x)/dx > 0$ (evaluated at x^*).

Stable fixed points are also called point attractors, this essentially means that a trajectory visiting this point will remain trapped in there for an infinite time, unless a bifurcation takes place due to a change in system parameters. An unstable fixed point, also called a repeller, means that a visiting trajectory will be almost instantaneously repelled. System behaviour near such equilibria is generally given by:

$$x = x^* + (x_0 - x^*)e^{\lambda t}. \quad [4]$$

where x_0 , is the initial condition of state variable x , and x^* is the value of x near equilibrium as in equation [3] and

$$\lambda = df/dx \text{ (at } x = x^*). \quad [5]$$

is the growth rate.

This general result is very informative because it captures the essence of chaotic dynamics. The system which is initiated at x_0 , will (after initial transients have died off) reach a certain equilibrium point x^* . Depending on the sign of λ , the growth rate, the system will either exponentially move away from equilibrium (in case λ is positive indicating an unstable point) or it will exponentially move closer to equilibrium (indicating a stable point).

It is easy to see, how this result may be extended to a 2-D system, e.g.

$$dx/dt = f(x). \quad [6]$$

$$dy/dt = g(y).$$

Equilibrium points will be respectively at $f = g = 0 \implies x^*, y^*$. We can then calculate the Jacobian matrix J (the matrix of partial derivatives) at x^*, y^* .

The general form of the Jacobian matrix for an n - dimensional system (where n is the number of differential equations and thus state variables) is:

$$J(x_1, \dots, x_n) = \begin{bmatrix} \frac{\partial y_1}{\partial x_1} & \dots & \frac{\partial y_1}{\partial x_n} \\ \vdots & \ddots & \vdots \\ \frac{\partial y_n}{\partial x_1} & \dots & \frac{\partial y_n}{\partial x_n} \end{bmatrix} \quad [7]$$

where $\frac{\partial y_1}{\partial x_1}$ is the partial derivative of y_1 with respect to x_1 , and $\frac{\partial y_n}{\partial x_n}$ is the partial derivative of y_n with respect to x_n . The Jacobian is very useful, when dealing with multidimensional systems, in terms of an estimation of Lyapunov exponents.

In the case of a two dimensional system we only have two partial derivatives. Let f_x be the partial derivative of f with respect to x , and f_y the partial derivative of f with respect to y .

A useful matrix characteristic of the Jacobian is its determinant. In this case we have:

$$\det J = f_x g_y - f_y g_x = \lambda_1 \lambda_2 \quad (\text{determinant of } J) \quad [8]$$

The determinant is useful for formulating the so-called *characteristic equation*, which is generally of the form $\det(J - \lambda) = 0$, where \det denotes the determinant of the matrix). In this case we have:

$$(f_x - \lambda_1)(g_y - \lambda_2) = f_y g_x. \quad [9]$$

λ_1, λ_2 denote the eigenvalues. Solutions are of the form: $x = x_0 e^{\lambda_1 t}, y = y_0 e^{\lambda_2 t}$.

What we can see again is that if the eigenvalues are positive, the solutions of the system are bound to diverge from the initial conditions in an exponential way in two directions corresponding to the two state variables x and y . As we shall see below, this is a very useful concept, with respect to the quantification of chaos using Lyapunov exponents. The Lyapunov exponent is essentially a generalization of an eigenvalue to a multidimensional system. For a multidimensional system Lyapunov exponents can be estimated using its characteristic equation.

In the case where we have the simplest 2-D system:

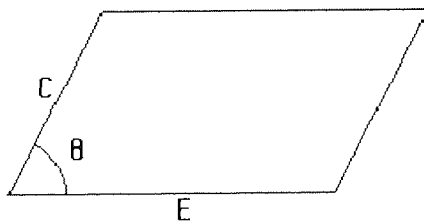
$$dx/dt = y.$$

$$dy/dt = -x.$$

This yields the eigenvalues $\lambda_1 = 1$, $\lambda_2 = -1$, corresponding to a saddle point. This means that the system will expand in the y direction but it will contract in the x direction.

Volume expansion and contraction in chaotic systems

One of the core characteristics of chaotic systems is their ability to expand or contract simultaneously in different directions in state space. This is the basis of the typical stretching and folding behaviour. This behaviour can be quantified or indeed predicted in terms of the eigenvalues or their generalizations the Lyapunov exponents, which forecast not only whether the system will expand or contract on average but also in which directions it will do so. This is illustrated in a simple case where we only have a 2-D system, with state variables C and E , as shown in the figure below. For simplicity let's consider that the system is expanding in direction E and contracting in direction C .



Schematic representation of the area involved in contraction and expansion in a 2 D system.

The rate of change, i.e. the time derivative in the expanding direction is given by $dE/dt = \lambda_1 E$, where $\lambda_1 > 0$. [10]

In the contracting direction we can write in a similar way:

$dC/dt = \lambda_2 C$, where $\lambda_2 < 0$. [11]

The state space area is simply given by:

$A = CE \sin \theta$. [12]

The rate of change in state space area per time unit is thus:

$dA/dt = C dE/dt \sin \theta + E dC/dt \sin \theta = CE(\lambda_1 + \lambda_2) \sin \theta$ [13]

The normalized quantity, and thus the fraction of the rate of change (*fractional rate of area expansion*) in state space area divided by the total area is given by the sum of the eigenvalues:

$$dA/dt / A = \lambda_1 + \lambda_2 \quad [14]$$

Elegantly, the *sum* of the eigenvalues corresponds to the *trace* of the Jacobian. Thus according to equation [9] in a 2-d system, we will have

$$\text{trace}J = f_x + g_y = \lambda_1 + \lambda_2 \quad [15]$$

This result can be generalized to higher dimensions in terms of the fractional rate of volume expansion/ contraction, which will be generally of the form:

$$dV/dt / V = \lambda_1 + \lambda_2 + \dots + \lambda_n = \sum_{i=1}^n \lambda_n \quad [16]$$

where V is the state -space volume of initial conditions, $i = 1..n$, is the number of the eigenvalues $\lambda_1, \dots, \lambda_n$.

From [16] it becomes clear that the sum of the eigenvalues must be negative for an attractor, as this would lead to a negative fractional rate of expansion (and thus a contraction). For a conservative (non dissipative, Hamiltonian) system the sum of eigenvalues should be zero. Note that the fractional rates are *instantaneous* quantities.

Lyapunov exponents

The above can be generalized to many dimensions using the Lyapunov exponents. However, in many multidimensional chaotic systems, one observes a geometrically non-uniform dimensional reduction: generally one can say that (hyper) spheres –as initial conditions- evolve into (hyper) ellipsoids- as attractors-. Hence, trajectories in such systems change both their direction and their magnitude continuously. Thus, a fractional measure of expansion can only be predictive, when we *average* along the trajectory. Thus Lyapunov exponents (LE) can be considered as *time averages* of the instantaneous eigenvalues and are always real; the units of LE for continuous systems such as multidimensional flows are thus inverse seconds. As with eigenvalues, the

volume expansion fractional rate (as in equation [16]) corresponds to the sum of the (time averaged) Lyapunov exponents. There is one Lyapunov exponent per dimension. The collection of all LE for a given system is referred to as spectrum of Lyapunov exponents or simply Lyapunov spectrum. By convention, LEs are ordered from largest to smallest, i.e. $\lambda_1 > \lambda_2 > \lambda_3 > \dots \lambda_n$. The requirement for chaos is that at least one Lyapunov exponent is positive. This practically implies that $\lambda_1 > 0$, and thus at least the Largest Lyapunov exponent (LLE) should be positive.

In summary, Lyapunov exponents allow a quantification of chaos, based on the notion that trajectories initiated in nearby points in state space will diverge exponentially on the long term. Furthermore, Lyapunov exponents allow for predictions of the nature of long-term system dynamics. In multidimensional space, additional information is given by the spectrum of the Lyapunov exponents. These specify, the geometry of system dynamics and can therefore predict the long-term behaviour of the flow (see table below for an example in 3-D) in terms of point attractors, limit cycles, tori, strange attractors and so on. Therefore Lyapunov exponents are extremely useful for the study of chaotic systems.

Spectrum of Lyapunov exponents in 3-D flows (e.g Rössler and Lorenz models) and resultant long term dynamics (attractors).

λ_1	λ_2	λ_3	Attractor
Neg	neg	neg	equilibrium point (point attractor)
0	neg	neg	Limit cycle (stable period-1 oscillation)
0	0	neg	2-torus (two frequency periodicity)
Pos	0	neg	strange (chaotic)